BRNO UNIVERSITY OF TECHNOLOGY
VYSOKÉ UČENÍ TECHNICKÉ V BRNĚ

FACULTY OF MECHANICAL ENGINEERING
FAKULTA STROJNÍHO INŽENÝRSTVÍ

INSTITUTE OF SOLID MECHANICS, MECHATRONICS AND BIOMECHANICS
ÚSTAV MECHANIKY TĚLES, MECHATRONIKY A BIOMECHANIKY

EVALUATION OF FRACTURE MECHANICAL PARAMETERS FOR BI-PIEZO-MATERIAL NOTCH
STANOVENÍ LOMOVĚ MECHANICKÝCH PARAMETRŮ PRO BI-PIEZO- MATERIÁLOVÝ VRUB

DOCTORAL THESIS
DIZERTAČNÍ PRÁCE

AUTHOR
AUTOR PRÁCE

Ing. Miroslav Hrstka

SUPERVISOR
ŠKOLITEL

doc. Ing. Tomáš Profant, Ph.D.

BRNO 2019

Abstract

The presented dissertation thesis deals with evaluation of the leading terms of the Williams asymptotic expansion describing an in-plane electro-elastic field at the tip of piezoelectric bi-material notches and interface cracks using the expanded Lekhnitskii-Eshelby-Stroh formalism in connection to the pure anisotropic elasticity. It is demonstrated that the expanded Lekhnitskii-Eshelby-Stroh formalism with modern Python programming concepts represents an effective theoretical as well as a practical tool for the fracture analysis of piezoelectric bi-materials. The theoretical part of the thesis outlines aspects of anisotropic elasticity and their connection with piezoelectric materials. The governing equations focused on special types of monoclinic piezoelectric materials, which enable decoupling to the in-plane and anti-plane problem, are introduced via the complex potentials. In the practical part of the thesis, the eigenvalue problem of a bi-material notch is proposed in order to determine the singularity exponents as well as the generalized stress intensity factors by application of the two-state Ψ-integral. All relations and numerical procedures are applied to the pure anisotropic and subsequently expanded to the piezoelectric fracture problem of bi-material notches and deeply investigated in the numerical examples. A special attention is paid to the change of the asymptotic solution connected with the transition of a very closed notch into an interface crack. Also the influence of arbitrary oriented poling directions upon asymptotic solution is investigated. The accuracy of calculations of the generalised stress intensity factors is tested by comparing the asymptotic solutions with results obtained by the finite element method using a very fine mesh. Finally, the formalism is modified for non-piezoelectric media such as conductors and insulators.

Keywords

Bi-material notch, interface crack, monoclinic material, expanded Lekhnitskii-Eshelby-Stroh formalism, piezoelectricity, Ψ-integral, singularity exponent, generalized stress intensity factor

Abstrakt

Předkládaná dizertační práce se zabývá stanovením hlavních členů Williamsova asymptotického rozvoje popisujícího rovinné elektro-elastické pole v okolí piezoelektrických bi-materiálových vrubů a trhlin na rozhraní za použití rozšířeného Lechnického-Eshelbyho-Strohova formalismu v návaznosti na čistě anizotropní pružnost. Je ukázáno, že rozšířený Lechnického-Eshelbyho-Strohův formalismus představuje spolu s moderními programovacími koncepty v jazyku Python efektivní a také praktický nástroj pro lomovou analýzu piezoelektrických bi-materiálů. Teoretická část práce popisuje aspekty anizotropní pružnosti a její návaznost na piezoelektrické materiály. Základní rovnice zaměřené na speciální typy monoklinických materiálů, které umožňují oddělení rovinného a anti-rovinného problému, jsou vyjádřeny pomocí komplexních potenciálů. V praktické části práce je sestaven problém vlastního hodnot pro bi-materiálový vrub, na jehož základě jsou stanoveny exponenty singularity a pomocí dvoustavového Ψ-integrálu také zobecněné faktory intenzity napětí. Veškeré vztahy a numerické procedury jsou následně rozšířeny na problém piezoelektrických bi-materiálových vrubů a podrobně prozkoumány v uvedených příkladech. Zvláštní pozornost je věnována přechodu asymptotického řešení téměř zavřených vrubů a trhlin na rozhraní. Vliv směru polarizace na asymptotické řešení je také zkoumán. Přesnost stanovení zobecněných faktorů intenzity napětí je testována srovnáním asymptotického řešení a řešení získaného pomocí metody konečných prvků s velmi jemnou sítí konečných prvků. Na závěr je formalismus modifikován pro nepiezoelektrické materiály.

Klíčová slova

Bi-materiálový vrub, trhlina na rozhraní, monoklinický materiál, rozšířený Lechnického-Eshelbyho-Strohův formalismus, piezoelektřina, Ψ-integrál, exponent singularity, zobecněný faktor intenzity napětí

Bibliographic citation

HRSTKA, M. *Evaluation of Fracture Mechanical Parameters for Bi-Piezo-Material Notch.* Brno, 2019. 168 p. Dissertation thesis. Brno University of Technology, Faculty of Mechanical Engineering, Institute of Solid Mechanics, Mechatronics and Biomechanics. Supervisor doc. Ing. Tomáš Profant, Ph.D.

Bibliografická citace

HRSTKA, M. *Stanovení lomově mechanických parametrů pro bi-piezo- materiálový vrub.* Brno, 2019. 168 s. Dizertační práce. Vysoké učení technické v Brně, Fakulta strojního inženýrství, Ústav mechaniky těles, mechatroniky a biomechaniky. Vedoucí práce doc. Ing. Tomáš Profant, Ph.D.

Sworn statement

I state that I am the only author of this work, which I elaborated based on the discussions with my supervisor doc. Ing. Tomáš Profant, Ph.D. and by the use of the referenced literature.

Čestné prohlášení

Prohlašuji, že jsem tuto disertační práci zpracoval samostatně na základě konzultací se svým školitelem doc. Ing. Tomášem Profantem, Ph.D. a s použitím uvedené literatury.

In Brno, 06/05/2019

_____

Ing. Miroslav Hrstka

Acknowledgements

Contents

1 Introduction

Piezoelectric materials have been extensively used as sensors or actuators in smart advanced structure design, as well as in many branches of technology. It is well known that piezoelectric materials produce an electric field when deformed and undergo deformation when subjected to an electric field. This is so called intrinsic electromechanical coupling phenomenon. Commonly used piezoelectric materials are ceramics manufactured by conventional ceramic processing. In order to insure the reliability and structural integrity of electromechanical devices made from these materials, it is necessary to understand their mechanical behaviour. There has been a lot of research dealing with behaviour of piezoelectric ceramics. The introduction of the Pak's paper [1] is a vignette of primary scientific researches in the field of piezoelectricity, such as [2, 3, 4, 5]. Nevertheless, these studies were limited to the linear elastic fracture mechanics without taking the electrical effects into account. Modelling of the electro-elastic coupling in combination with anisotropic behaviour requires a different approach.

Firstly, the computational model for general elastic anisotropic bi-materials is investigated. The constitutive laws for generally anisotropic materials involve 21 independent elastic constants. Stress and displacement fields are described by using two well-known formalisms, based on the complex potential theory. The Lekhnitskii formalism [6] starts from expressions for stresses in terms of stress functions that satisfy equilibrium and provides a compatibility condition decomposed into six operators of the first order. Alternatively, the Stroh formalism [7, 8] shows that particular solutions can be found in the form of a certain complex combination of x_1 and x_2 coordinate axes. More detailed exposition of the Stroh's solution including numerous examples can be seen in [9]. Both the Stroh and Lekhnitskii methods are based on the appropriate linear transformation of the in-plane coordinates x_1, x_2. This approach requires special solution methods, limited only to plane elasticity problems.

Many researchers have investigated singular stress fields around a sharp notch in homogeneous materials or interface corners [1, 10, 11, 12]. Williams introduced an eigenvector approach to examine sharp notches in homogeneous media [13]. Based on this studies, Labossiere and Dunn [14], Carpenter [15] and Sinclair et al. [16] used the Betti's reciprocal principle to derive the path-independent Ψ-integral to obtain the stress intensity factors of interface corners between dissimilar anisotropic materials by using the Stroh formalism. The general solution for eigenvalues of anisotropic multi-wedges has been provided by Hwu [17].

Stress field in the closed vicinity of multi-material joints has a singular character and stress singularity exponents differ from $1/2$, a characteristic value for cracks. The degree of anisotropy of many advanced materials is lower than the general anisotropy [9]. These materials possess one or more symmetry planes, e.g. orthotropic materials with three symmetry planes or transversally isotropic materials. In such cases, in-plane and anti-plane strains can be decoupled, which allows these cases to have counterparts for plane analysis of cracks in isotropic materials [18]. To avoid the difficulty with handling the large number of material constants, the so-called Lekhnitskii-Eshelby-Stroh (LES) formalism can be implemented [9, 17, 19].

Based on the above mentioned anisotropic theories, piezoelectric continuum is governed by the expanded equations of linear electromechanical statics. The anisotropy of piezoelectric materials requires usage of suitable mathematical tools and numerical methods. The expanded Stroh formalism has been developed for this purpose, as can be seen in [20, 21, 22]. A detailed study was done by Hirai et al. [23] and Abe et al. [24] for bi-material corners including determination of the stress intensity factors by using the Ψ-integral. However, the correspondence with other approaches, such as in Ou and Wu [25] or Ou and Chen [26], has not been pointed out.

In the beginning of the presented thesis, basics of the linear fracture mechanics and its generalization to the case of the piezoelectric materials are briefly summarized. The thesis is

focused on the Irwin's concept of the stress intensity factors and its generalized form for bi-material notches. Their evaluation combines analytical and numerical methods, which are put together in the so-called Ψ-integral. The main goal is the deep investigation of the present LES formalism for pure anisotropic elasticity and its expansion for problems of piezoelectric materials and a subsequent implementation to the eigenvalue problem of the bi-material notches and interface cracks. Equivalence of the formalism for the limit case of the geometry – an interface crack and the Hilbert problem will be also proved.

In spite of a large number of studies related to the interface corners and interface cracks in jointed dissimilar piezoelectric materials there are only limited data concerning the asymptotic solutions around these concentrators. In particular, a transition between the oscillatory and non-oscillatory singularity as a function of the notch geometry and poling orientation for various dissimilar bi-materials has not been investigated yet. Hence, a wide range of notch geometries, material combinations, and poling orientations is considered here to shed some light on these problems.
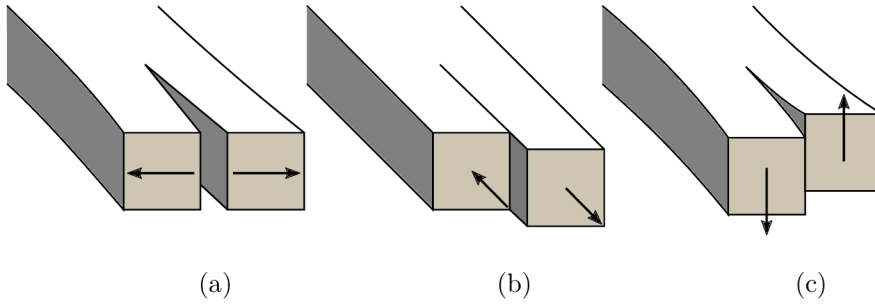
Fig. 2.1: Three symmetry modes, (a) in-plane opening mode, (b) in-plane shearing mode, (c) anti-plane shearing mode.

2 Linear elastic fracture mechanics

The theory of fracture mechanics is based on stress distribution and stability criterion assessment of a crack in a homogeneous isotropic material. For description of a stress distribution in the vicinity of a bi-material notch, we proceed from concepts describing crack properties, because the basic type of a failure is the unstable crack propagation. Subsequent relations for a simple crack can be then generalized to notches or wedges. The linear elastic fracture mechanics (LEFM) can be applied, if the relation between stress and deformation is linear, i.e. the material follows the Hooke's law [27]. There are two basic approaches for a crack assessment: the Griffith's principle of energetic balance and the Irwin's principle of the stress intensity factor (K-conception) [18, 27].

2.1 Symmetry modes

In 1960, Irwin introduced so-called symmetry modes describing the fundamental crack loading states, as illustrates Fig. 2.1. This specification does not impose a limitation on the non-uniform loaded notches, because such problems can be solved as a superposition of the three symmetry modes [27]:

1. The opening mode is referred as mode I. The principal load is applied normal to the crack plane and tends to open it (Fig. 2.1(a)).
2. The in-plane shearing mode is referred as mode II. This mode tends to slide one crack face with respect to the other (Fig. 2.1(b)).
3. The anti-plane shearing or sliding mode is referred as mode III. The stresses are parallel both with the plane of a crack and with a crack front (Fig. 2.1(c)).

2.2 Stress and displacement distribution in the vicinity of a crack

The K-conception, based on the works of Westergaard [28] and Williams [29], is the historically oldest method for description of a singularity ahead of the crack front. However, it is practically usable if the plastic zone at the crack tip is small. This is called the small-scale yielding concept.

Let us assume a crack in a continuous linear elastic medium. The crack has a sharp tip (the crack tip radius $\to \infty$), see Fig. 2.2. The stress and displacement ahead of a crack tip can be then described as

$$\sigma_{ij} = \frac{K_k}{\sqrt{2\pi r}} f_{ijk}(\theta), \quad k = \mathrm{I}, \mathrm{II}, \mathrm{III}, \tag{2.1a}$$
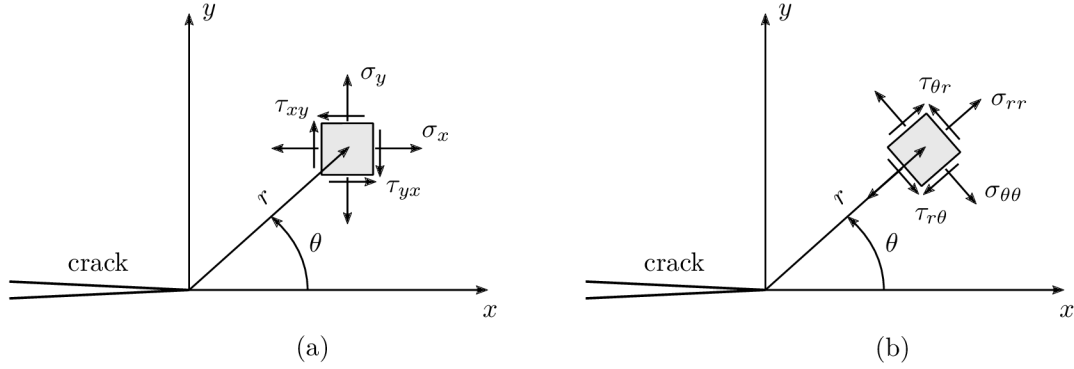
Fig. 2.2: Definition of the (a) Cartesian and (b) polar coordinate system ahead of a crack tip, the z direction is normal to xy-plane.

$$u_i = \frac{2K_k(1+\nu)}{E}\sqrt{\frac{r}{2\pi}}g_i(\theta,\nu), \quad k = \text{I}, \text{II}, \text{III}, \tag{2.1b}$$

where K_k, $k = \text{I}, \text{II}, \text{III}$ is defined as the stress intensity factor [18]. The functions f_{ijk} and g_i depend only on the polar coordinate θ and Poisson's ratio ν. The relations (2.1a) and (2.1b) represent the classical formulation of fracture mechanics problems, where functions describing the stress or displacement development are expressed in the form of the product of the normalized shape function and the stress intensity amplitude. The amplitude is characterised by the stress intensity factor K_k. In practice, the mode I is often considered as the most dangerous case. The equations (2.1) only for mode I can be then expressed in the form of [30]

$$\begin{Bmatrix} \sigma_x \\ \sigma_y \\ \tau_{xy} \end{Bmatrix} = \frac{K_{\text{I}}}{\sqrt{2\pi r}}\cos\left(\frac{\theta}{2}\right)\begin{Bmatrix} 1 - \sin\frac{\theta}{2}\sin\frac{3\theta}{2} \\ 1 + \sin\frac{\theta}{2}\sin\frac{3\theta}{2} \\ \sin\frac{\theta}{2}\cos\frac{3\theta}{2} \end{Bmatrix}, \tag{2.2a}$$

$$\begin{Bmatrix} u_x \\ u_y \end{Bmatrix} = \frac{K_{\text{I}}}{2G}\sqrt{\frac{r}{2\pi}}\left(\kappa - \cos\theta\right)\begin{Bmatrix} \cos\frac{\theta}{2} \\ \sin\frac{\theta}{2} \end{Bmatrix}, \tag{2.2b}$$

where for

$$\begin{aligned} \text{plane strain}: \quad &\kappa = 3 - 4\nu, &\sigma_z &= \nu\left(\sigma_x + \sigma_y\right), \\ \text{plane stress}: \quad &\kappa = (3 - \nu)/(1 + \nu), &\sigma_z &= 0. \end{aligned} \tag{2.3}$$

The solution for stresses has the singularity type $\frac{1}{\sqrt{r}}$, which approaches infinity for $r \to 0$. The amplitude of the crack-tip field is characterised by the above mentioned stress intensity factor K_{I}, which can be determined from the stresses in (2.2) by setting $\theta = 0$ [30]:

$$K_{\text{I}} = \lim_{r \to 0}\sqrt{2\pi r}\sigma_y(\theta = 0). \tag{2.4}$$

For larger distances r from the crack tip, higher (non-singular) terms have to be taken into account, as reported in [31, 32, 33].
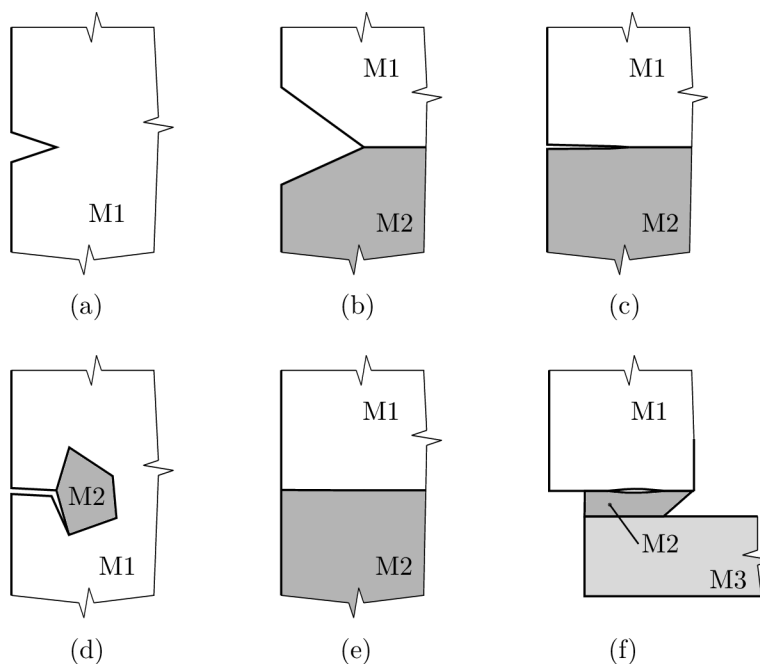
Fig. 2.3: Typical examples of general singular stress concentrators: (a) V-notch in a homogeneous material, (b) bi-material V-notch, (c) interface crack or very closed bi-material notch, (d) crack terminating at the inclusion surface (e) free edge singularity, (f) example with multiple stress singularity concentrators.

2.3 General singular stress concentrator

Modern material constructions require application of components with a complicated geometry including also a combination of different materials whose presence is generally connected with existence of singular stress concentration. There are many types of singularities such as cracks with the tip at the bi-material interface, a bi-material laminate, bi-material notches and wedges [34], as is schematically shown in Fig. 2.3.

The stress near the tip of a singular stress concentrator has a singular character, but the type of singularity differs from this of cracks. Hence, the standard approach of fracture mechanics cannot be applied directly. To establish fracture parameters, the asymptotic analysis of the stress and strain fields has been introduced. Considering n singular terms only, the stress distribution in the vicinity of a general singular stress concentrator (GSSC) is generally expressed in the form of

$$\sigma_{ij} = \sum_{k=1}^{n} \frac{H_k}{\sqrt{2\pi}} r^{-p_k} F_{ijk}, \tag{2.5}$$

where r, θ are polar coordinates with the origin at the tip of the concentrator, see Fig. 2.4, and F_{ijk} are the functions of a material and geometry. H_k ($k = 1, 2, \ldots, n$) are the generalized stress intensity factors (GSIF), which determine the amplitude of the stress distribution and are dependent on the external loading. p_k is the stress singularity exponent and it can be determined on the basis of boundary conditions prevailing at the notch tip [34]. The value of p_k is generally complex and since the stress field and strain energy cannot be unbounded, only values located in the range of $0 < \Re(p_k) < 1$ are considered.

In the case of a transversally isotropic bi-material notch, which is the subject of the study,
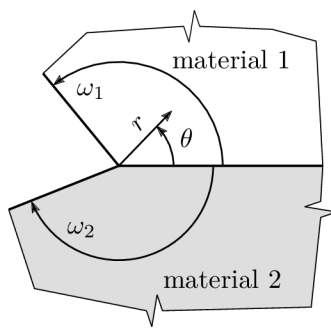
Fig. 2.4: Bi-material notch as a special case of the general singular stress concentrator. The stress and
displacement field is described by polar coordinate system with the origin in the notch tip.

the value $k = 2$ is taken into consideration. The stress singularity exponent p_k is given by

$$p_k = 1 - \delta_k, \tag{2.6}$$

in which δ_k is the kth eigenvalue (exponent) of the eigenvalue problem established from the
boundary conditions at the bi-material notch tip. Note that the physical unit of the GSIF is
$[H_k] = \mathrm{MPa} \cdot \mathrm{m}^{1-\delta_k}$.

The electro-mechanical coupling and anisotropy of piezoelectric materials make the stress
distribution near a general singular concentrator more complex. The singularity exponent need
not to be necessary simple root of the corresponding eigenproblem. Moreover, it can be accom-
panied with the logarithmic type of singularity $(\ln r) \, r^{1-\delta}$. Omitting this kind of solution, the
stress field can be written as (2.5), but supplemented with the electric displacement field. The
stress tensor σ_{ij} is extended with

$$D_j = \sigma_{4j} = \sum_{k=1}^{n} \frac{H_k}{\sqrt{2\pi}} r^{p_k} F_{4jk}. \tag{2.7}$$

2.3.1 Conditions of stability

The classical approach of the linear elastic fracture mechanics (the K-conception) says that an
unstable fracture occurs if the stress intensity factor reaches its critical value K_{Icrit}, which is
represented for brittle materials by the fracture toughness K_{IC}. In other words, a crack will
propagate under the pure mode I whenever the stress intensity factor K_{I} reaches the material
constant K_{IC} [18, 27]. A similar situation comes about fatigue crack growth where the range of
the stress intensity factor ΔK is lower than the fatigue crack growth threshold ΔK_{th} [27]. The
stability criterion for a crack has the following form

$$K_{\mathrm{I}} < K_{\mathrm{Icrit}}. \tag{2.8}$$

Analogically to cracks, a condition for a general singular stress concentrator can be establish.
This value expresses circumstances under which no crack is initiated from the GSSC tip. A
general principle of the stability assessment has been introduced in [34]. Equivalently to (2.8),
the stability condition for such concentrators can be expressed by means of its critical value
$H_{k\mathrm{crit}}$, that is [34, 35, 36]

$$H_k \left(\sigma_{\mathrm{appl}} \right) < H_{k\mathrm{crit}}. \tag{2.9}$$

In practice, there is sometimes a requirement to express the relation between K_{Icrit} and
$H_{k\mathrm{crit}}$. We assume that the mechanism of the crack propagation from the tip in a generally

anisotropic material is the same as in the case of a crack in a homogeneous media. New control variable L with the clear physical meaning is introduced. The second assumption is based on the condition that instability (i.e. K_{Icrit} and $H_{k\mathrm{crit}}$) occurs when the variable L reaches its critical value $L = L_{\mathrm{C}}$, which is identical for both critical parameters [34]. For the bi-material notch stability assessment, we proceed from relations derived for cracks.

2.3.2 Maximal tangential stress criterion (MTS)

The stability condition for a crack with the singularity exponent different from $1/2$ is related to the average stress $\overline{\sigma}$ calculated across a critical distance d ahead of the crack tip [37]. It is expected that the crack will initiate from the notch tip when the average stress achieves its critical value σ_{C}, i.e. [19]

$$\overline{\sigma}_{\theta\theta} = \sigma_{\mathrm{C}}(\theta_0), \tag{2.10}$$

where the averaged stress on the left-hand side is expressed as

$$\overline{\sigma}_{\theta\theta} = \frac{1}{d} \int_0^d \sigma_{\theta\theta}\,(r, \theta_0)\;\mathrm{d}r. \tag{2.11}$$

2.3.3 Criterion of strain energy density factor (SEDF)

The strain energy density factor criterion is based upon the work of Erdogan and Sih [38]. The modified criterion was introduced for example in [39] or [40]. The stress field around a bi-material notch inherently combines the normal and shear mode of loading. Additionally, under an assumption that both materials are perfectly bonded, the crack propagation into either material 1 or 2 is supposed. The strain energy density is defined as

$$\Sigma\,(r,\theta) = r\frac{\mathrm{d}W}{\mathrm{d}V} = r\int_0^{\varepsilon_{pq}} \sigma_{ij}\,\mathrm{d}\varepsilon_{ij}, \tag{2.12}$$

where W is the strain energy, $\mathrm{d}V$ is a differential volume and ε_{ij} is a strain. The integrand in (2.12) has to be the total differential to provide the integral path-independent. The strain energy density depends on the distance r from the notch tip. To avoid this dependence, it is convenient to introduce a mean value of the SEDF over some distance d, which is defined by the relation

$$\overline{\Sigma}\,(r,\theta) = \frac{1}{d}\int_0^d \Sigma\,(r,\theta)\;\mathrm{d}r, \tag{2.13}$$

from which the resulting direction is determined and subsequently used for the stability criterion estimation defined in Eq. (2.9). A detailed study was reported in [39, 41].

2.4 Determination of the singularity exponent

Let us consider a bi-material notch composed of two generally anisotropic materials. An ideal adhesion along the interface is assumed. The most effective tool for describing problems of plane elasticity are methods based on the complex variable theory. Isotropic plane elasticity is dominantly treated by employing the Muskhelischvili complex potential theory [17, 42]. But, for dealing with generally anisotropic materials, there are two major approaches implementing complex potential methods: the Lekhnitskii [6] and Stroh [7] formalism. The expanded Stroh formalism for piezoelectric media developed by Barber and Ting [43], Pak [1], Suo et al. [10] and Hwu [20, 22], includes both in-plane and anti-plane fields. But, within the dissertation, an expansion of the LES formalism presented by Suo [44] is introduced, based on works [45, 46, 47,

48, 49, 50, 51, 52, 53]. The principle of the expanded LES formalism will be described below in section 4.2.8 after introducing the linear theory of piezoelectricity.

2.5 Determination of the generalized stress intensity factor

Methods for a stress intensity factor determination of a crack has been well examined and they are also available in the commercial FEM software. Determination of the GSIF requires more sophisticated methods, such as the direct or integral method implemented for example in [32, 54, 55]. The latter group involves one special and robust tool for the GSIF computation – the two state path-independent Ψ-integral (in the literature also known as the H-integral), which is based on the Betti's reciprocal theorem. The method of the Ψ-integral enables determination of the local stress field in the vicinity of the crack or notch tip by using the real deformation and stress field in the remote points, where the numerical results are more accurate [19]. Neglecting the body forces and residual stresses, the Ψ-integral is expressed in the following form:

$$\Psi\left(\mathbf{u}, \hat{\mathbf{u}}\right) = \int_{\Gamma} \left(\mathbf{u}^{\mathsf{T}}\hat{\mathbf{t}} - \hat{\mathbf{u}}^{\mathsf{T}}\mathbf{t}\right) \mathrm{d}s. \tag{2.14}$$

It is path-independent for free-free multi-material wedges when the path Γ emanates from one notch face to the second one in the counter-clockwise direction [17]. The GSIF is then determined by virtue of the FEM, regular and auxiliary solutions.

3 Aims of the thesis

On the basis of the literature survey, the aims of the research conducted within the dissertation can be proposed as:

- Determination of the stress singularity exponents of a sharp piezoelectric bi-material notch using the expanded Lekhnitskii-Eshelby-Stroh formalism.

- Establishing the path-independent Ψ-integral to determine the generalized stress intensity factors. The method of the Ψ-integral enables to define the local stress field parameters, i.e. the generalized stress intensity factors, in the vicinity of the crack or notch tip by using a displacement and stress field obtained by the finite element analysis in the remote points.

- Parametric studies of a dependence of the fracture-mechanical parameters on the material parameters and boundary conditions.

One of the goals is to introduce and describe theories in the most general way and after that to give simplified relations that often occur in published papers.

4 Overview to references relating to the solved problems

4.1 Two-dimensional anisotropic elasticity

A bi-material notch composed of two generally anisotropic materials covers a group of special configurations such as orthotropic and isotropic materials or their combinations. Before introducing the complex potential theories describing stress singularity, some restrictions of material symmetry have to be defined. The equilibrium equations can be then simplified and decoupled to in-plane and anti-plane counterparts.

4.1.1 Generalized Hooke's law

Let us assume an elastic material. Additionally, if the relationship between stresses and strains is linear, it is usually called the generalized Hooke's law and written as [17]

$$\sigma_{ij} = C_{ijkl}\varepsilon_{kl}, \tag{4.1}$$

where C_{ijkl} is the fourth rank tensor characterising elastic behaviour of the solid with 81 independent constants and $i,j,k,l = 1,2,3$. Employing the stress tensor properties and material symmetry leads to reduction of the independent material constants.

Since the stress and strain tensor components are symmetric, it implies that [17]

$$C_{ijkl} = C_{jikl}, \qquad C_{ijkl} = C_{ijlk}, \qquad C_{ijkl} = C_{klij}. \tag{4.2}$$

Foregoing symmetry restrictions lead to 21 independent elastic constants for the most general case of anisotropy.

4.1.2 Contracted notation

It is more convenient to express the generalized Hooke's law by using the contracted notation of strains and stresses as

$$\sigma_p = C_{pq}\varepsilon_q, \quad C_{pq} = C_{qp} \qquad p,q = 1,2,\ldots,6, \tag{4.3a}$$

where the indices shrink according to Tab. 4.1. In engineering applications, σ_i and ε_i are usually replaced by the engineering stress τ_{ij} and engineering strain γ_{ij}. The definition (4.3a) can be expressed in the matrix form as

$$\boldsymbol{\sigma} = \mathbf{C}\boldsymbol{\varepsilon}. \tag{4.3b}$$

It is necessary to point out that the quantities σ_p, C_{pq}, ε_q are not tensors[1] and their transformation cannot be treated as by tensors. In the literature, C_{pq} is sometimes called stiffness matrix. Its transformation to a new coordinate system will be described in the section 4.1.4.

The inverse Hooke's law is defined as

$$\varepsilon_{ij} = S_{ijkl}\sigma_{kl}, \tag{4.4}$$

---

[1] Note that the material properties written down in the component form C_{ijkl} are called elastic constants. A bold symbol $\mathbf{C}$ is usually called elastic tensor.

index ij or kl	index p or q
11	1
22	2
33	3
23 or 32	4
31 or 13	5
12 or 21	6

Tab. 4.1: Contraction of the individual tensor component indices.

in which S_{ijkl} are the compliances, also components of a four rank tensor. The symmetry conditions and contracted notation can be specified in the same manner of the previous relations (4.2) and (4.3a), i.e.

$$S_{ijkl} = S_{jikl}, \qquad S_{ijkl} = S_{ijlk}, \qquad S_{ijkl} = S_{klij}. \tag{4.5}$$

The contracted notation can be also introduced, nevertheless, some additional rules have to be added [9]:

$$\begin{aligned} S_{ijkl} &= S_{pq}, & \text{if both } p,q \leq 3, \\ 2S_{ijkl} &= S_{pq}, & \text{if either } p \text{ or } q \leq 3, \\ 4S_{ijkl} &= S_{pq}, & \text{if both } p,q > 3. \end{aligned} \tag{4.6}$$

Using the above-stated conditions, it is also possible to express the inverse Hooke's law in the contracted form as

$$\varepsilon_p = S_{pq}\sigma_q, \quad S_{pq} = S_{qp} \qquad p,q = 1,2,\ldots,6 \tag{4.7a}$$

and in the matrix form:

$$\boldsymbol{\varepsilon} = \mathbf{S}\boldsymbol{\sigma}. \tag{4.7b}$$

Substituting (4.7b) into (4.3b) yields to the important relation

$$\mathbf{CS} = \mathbf{SC} = \mathbf{I}, \tag{4.8}$$

where $\mathbf{I}$ is the unit matrix of the shape 6×6.

4.1.3 Material symmetry

Due to the symmetry of the elastic tensor, it is possible to express the relation (4.3b) as

$$\begin{Bmatrix} \sigma_1 \\ \sigma_2 \\ \sigma_3 \\ \sigma_4 \\ \sigma_5 \\ \sigma_6 \end{Bmatrix} = \begin{bmatrix} C_{11} & C_{12} & C_{13} & C_{14} & C_{15} & C_{16} \\ C_{12} & C_{22} & C_{23} & C_{24} & C_{25} & C_{26} \\ C_{13} & C_{23} & C_{33} & C_{34} & C_{35} & C_{36} \\ C_{14} & C_{24} & C_{34} & C_{44} & C_{45} & C_{46} \\ C_{15} & C_{25} & C_{35} & C_{45} & C_{55} & C_{56} \\ C_{16} & C_{26} & C_{36} & C_{46} & C_{56} & C_{66} \end{bmatrix} \begin{Bmatrix} \varepsilon_1 \\ \varepsilon_2 \\ \varepsilon_3 \\ \varepsilon_4 \\ \varepsilon_5 \\ \varepsilon_6 \end{Bmatrix}. \tag{4.9}$$

The stiffness matrix in Eq. (4.9) has the form characterising the most general anisotropic material with no planes of symmetry of the material properties, usually called triclinic material.

If a material has some symmetry planes, the number of independent constants will be reduced. Without loss of generality, let the symmetry planes coincide with the global coordinate planes defined by the Cartesian coordinate system x_1, x_2, x_3. If a material has one symmetry plane defined by $x_3 = 0$, the stiffness matrix in (4.9) reduces to

$$\mathbf{C} = \begin{bmatrix} C_{11} & C_{12} & C_{13} & 0 & 0 & C_{16} \\ C_{12} & C_{22} & C_{23} & 0 & 0 & C_{26} \\ C_{13} & C_{23} & C_{33} & 0 & 0 & C_{36} \\ 0 & 0 & 0 & C_{44} & C_{45} & 0 \\ 0 & 0 & 0 & C_{45} & C_{55} & 0 \\ C_{16} & C_{26} & C_{36} & 0 & 0 & C_{66} \end{bmatrix} \tag{4.10}$$

and such material is called monoclinic and has 13 independent elastic constants.

If a material has three mutually orthogonal planes [9], we call it orthotropic (or rhombic) material. With the above introduced condition of principal axes and coordinate system coincidence, the matrix of elastic constants has the following form:

$$\mathbf{C} = \begin{bmatrix} C_{11} & C_{12} & C_{13} & 0 & 0 & 0 \\ C_{12} & C_{22} & C_{23} & 0 & 0 & 0 \\ C_{13} & C_{23} & C_{33} & 0 & 0 & 0 \\ 0 & 0 & 0 & C_{44} & 0 & 0 \\ 0 & 0 & 0 & 0 & C_{55} & 0 \\ 0 & 0 & 0 & 0 & 0 & C_{66} \end{bmatrix}, \tag{4.11}$$

which has 9 independent elastic constants.

An orthotropic material with one certain plane in which the material is isotropic, is called transversally isotropic. If the plane $x_1 = 0$ is the plane of isotropy, the stiffness matrix is

$$\mathbf{C} = \begin{bmatrix} C_{11} & C_{12} & C_{12} & 0 & 0 & 0 \\ C_{12} & C_{22} & C_{23} & 0 & 0 & 0 \\ C_{12} & C_{23} & C_{22} & 0 & 0 & 0 \\ 0 & 0 & 0 & \frac{C_{22}-C_{23}}{2} & 0 & 0 \\ 0 & 0 & 0 & 0 & C_{44} & 0 \\ 0 & 0 & 0 & 0 & 0 & C_{44} \end{bmatrix}, \tag{4.12}$$

with 5 independent constants. A material with elastic constants symmetric to any axis, or in other words, material properties are identical in all directions, is called isotropic and the stiffness matrix structure is

$$\mathbf{C} = \begin{bmatrix} C_{11} & C_{12} & C_{12} & 0 & 0 & 0 \\ C_{12} & C_{11} & C_{12} & 0 & 0 & 0 \\ C_{12} & C_{12} & C_{11} & 0 & 0 & 0 \\ 0 & 0 & 0 & \frac{C_{11}-C_{12}}{2} & 0 & 0 \\ 0 & 0 & 0 & 0 & \frac{C_{11}-C_{12}}{2} & 0 \\ 0 & 0 & 0 & 0 & 0 & \frac{C_{11}-C_{12}}{2} \end{bmatrix}. \tag{4.13}$$

Such material is characterised by 2 independent Lamé constants λ and μ defined from Eq. (4.13) by [17]

$$\lambda = C_{12}, \qquad \mu = \frac{C_{11} - C_{12}}{2}. \tag{4.14}$$

The generalized Hooke's law for an isotropic material can be written as

$$\sigma_{ij} = \lambda \delta_{ij} \varepsilon_{kk} + 2\mu \varepsilon_{ij}, \quad i,j = 1,2,3, \tag{4.15}$$
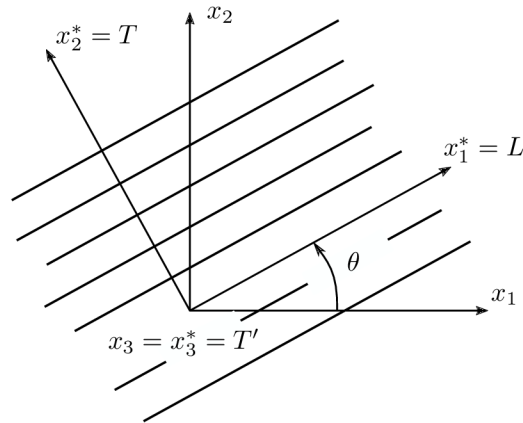
Fig. 4.1: Transformation between L-T and x_1-x_2 coordinate systems.

where δ_{ij} is the Kronecker delta.

Considering an orthotropic or an isotropic material in engineering applications, material constants are usually defined, unlike elastic properties of piezoelectric materials, by the Young's moduli, Poisson's ratios and shear moduli. They are measured by uniaxial tension and shear tests. The structure of the compliance matrix $\mathbf{S}$ composed of these engineering constants for a general anisotropic material is stated in [17], by using the Chentsov coefficients that have to be additionally defined.

In the following chapters, a bi-material notch composed of at least one transversally isotropic solids with fibres parallel to the plane $x_3 = 0$ is considered. Such properties can have for example unidirectional fibre-reinforced composites consisted of parallel fibres embedded in the matrix. The direction parallel to the fibres is generally called longitudinal, referred as L, the perpendicular is called transverse direction, referred as T or T'. Note that TT' is the plane where the material has isotropic properties, from which it follows that $E_T = E_{T'}$. Let us designate a coordinate system LTT' in these principal material directions. The compliance matrix $\mathbf{S}$ is defined in the principal material axes by using the engineering constants as

$$\mathbf{S} = \begin{bmatrix} \frac{1}{E_L} & \frac{-\nu_{LT}}{E_L} & \frac{-\nu_{LT}}{E_L} & 0 & 0 & 0 \\ \frac{-\nu_{TL}}{E_T} & \frac{1}{E_T} & \frac{-\nu_{TT'}}{E_T} & 0 & 0 & 0 \\ \frac{-\nu_{TL}}{E_{T'}} & \frac{-\nu_{T'T}}{E_{T'}} & \frac{1}{E_{T'}} & 0 & 0 & 0 \\ 0 & 0 & 0 & \frac{2(1+\nu_{TT'})}{E_T} & 0 & 0 \\ 0 & 0 & 0 & 0 & \frac{1}{G_{LT}} & 0 \\ 0 & 0 & 0 & 0 & 0 & \frac{1}{G_{LT}} \end{bmatrix}, \tag{4.16}$$

where the components of the lower triangular matrix have to be recomputed by using the symmetry conditions

$$\frac{\nu_{ij}}{E_i} = \frac{\nu_{ji}}{E_j}, \quad i,j = L,T,T'. \tag{4.17}$$

Assuming an arbitrary fibre orientation defined by the angle θ (see Fig 4.1), the stiffness, or the compliance matrix, respectively, has the form described in Eq. (4.10) for a monoclinic material. Let us consider that fibres are oriented so that the principal axes go along with the global Cartesian coordinate system defined by the axes x_1, x_2, x_3. To avoid a mismatch in the directional indices, we establish that the longitudinal direction L coincides with x_1 and the transversal direction T with x_2, i.e. $\alpha = 0$. Then the stiffness matrix attains the form (4.11),

e.g. the components C_{16}, C_{26}, C_{36} and C_{45} vanish.

The most convenient approach to compose the compliance matrix of a transversally isotropic material with an arbitrary fibre orientation in the plane $x_1 x_2$ can be divided into the following steps:

1. Assembly of the compliance matrix $\mathbf{S}$ (4.16) by using the engineering constants in the principal material coordinate system LTT'.
2. Rotation of the L-T axes to the global x_1-x_2 axes about x_3 axis by an angle θ. Note that the arrow of the angle determines the positive direction of rotation (counter-clockwise). The sign of the angle will be negative when transforming in the opposite direction (clockwise).

4.1.4 Transformation of the coordinate system

Before we introduce the conditions for a two-dimensional analysis, an orthogonal transformation of the reference coordinate system has to be defined. Transformation of the principal fibre directions discussed in the previous section stands for a rigid body rotation about the x_3 axis by the angle θ. The orthogonal transformation matrix $\mathbf{\Omega}$ is defined as

$$\mathbf{\Omega} = \begin{bmatrix} \cos\theta & \sin\theta & 0 \\ -\sin\theta & \cos\theta & 0 \\ 0 & 0 & 1 \end{bmatrix}. \tag{4.18}$$

Let us pronounce the principal material coordinate system LTT' as x_i^*. Four rank tensor of the elastic constants referred to a new coordinate system x_i is expressed under the orthogonal transformation $x_i = \Omega_{ij} x_j^*$ as [9]

$$C_{ijkl} = \Omega_{ip}\Omega_{jq}\Omega_{kr}\Omega_{ls}C_{pqrs}^*. \tag{4.19}$$

The identical relation can be written for S_{ijkl}. If we introduce the contracted notation (4.3a) or (4.7a), using of Eq. (4.19) is not convenient. The stresses and strains in (4.9) are transformed according to

$$\boldsymbol{\sigma} = \mathbf{K}\boldsymbol{\sigma}^*, \tag{4.20a}$$

$$\boldsymbol{\varepsilon} = \left(\mathbf{K}^{-1}\right)^{\mathsf{T}} \boldsymbol{\varepsilon}^*, \tag{4.20b}$$

where the matrix

$$\mathbf{K} = \begin{bmatrix} \cos^2\theta & \sin^2\theta & 0 & 0 & 0 & 2\cos\theta\sin\theta \\ \sin^2\theta & \cos^2\theta & 0 & 0 & 0 & -2\cos\theta\sin\theta \\ 0 & 0 & 1 & 0 & 0 & 0 \\ 0 & 0 & 0 & \cos\theta & -\sin\theta & 0 \\ 0 & 0 & 0 & \sin\theta & \cos\theta & 0 \\ -\cos\theta\sin\theta & \cos\theta\sin\theta & 0 & 0 & 0 & \cos^2\theta - \sin^2\theta \end{bmatrix} \tag{4.21}$$

defines a rotation about x_3 axis by the angle θ (positive in counter-clockwise direction). The Hooke's law (4.3b) in the coordinate system x_i^* is expressed as

$$\boldsymbol{\sigma}^* = \mathbf{C}^*\boldsymbol{\varepsilon}^*. \tag{4.22}$$

Substituting inverse relations (4.20) into (4.22) we get

$$\mathbf{K}^{-1}\boldsymbol{\sigma} = \mathbf{C}^*\mathbf{K}^{\mathsf{T}}\boldsymbol{\varepsilon}. \tag{4.23}$$

Multiplying by $\mathbf{K}$ from the left side, the stress-strain relations in the new coordinate system are obtained:

$$\boldsymbol{\sigma} = \mathbf{K}\mathbf{C}^*\mathbf{K}^\mathsf{T}\boldsymbol{\varepsilon}, \tag{4.24}$$

where

$$\mathbf{C} = \mathbf{K}\mathbf{C}^*\mathbf{K}^\mathsf{T} \tag{4.25}$$

defines the stiffness matrix transformation from the coordinate system x_i^* to x_i. Analogically, one can derive a relation for transformation of the compliance matrix:

$$\mathbf{S} = \left(\mathbf{K}^{-1}\right)^\mathsf{T}\mathbf{S}^*\mathbf{K}^{-1}. \tag{4.26}$$

4.1.5 Generalized plane deformation

In a body with general anisotropic properties, plane deformation is usually not possible. Considering a transversely isotropic material enables to solve the problem as two-dimensional (plane) problem by asserting that all stress and displacement components depend only on x_1 and x_2 [17]. By satisfying this conditions, behaviour of such body is called generalized plane stress or generalized plane strain. This state corresponds to given plane state in an isotropic material.

The state of generalized plane strain is characterised by

$$\varepsilon_3 = 0. \tag{4.27}$$

Under this condition, the third row of (4.7a) is rewritten as

$$\sigma_3 = -\sum_{q\neq 3}\frac{S_{3q}\sigma_q}{S_{33}}. \tag{4.28}$$

Substituting this relation back into (4.7a), we obtain

$$\boldsymbol{\varepsilon}^0 = \hat{\mathbf{S}}\boldsymbol{\sigma}^0, \tag{4.29}$$

where

$$\boldsymbol{\sigma}^0 = \begin{Bmatrix} \sigma_1 \\ \sigma_2 \\ \sigma_4 \\ \sigma_5 \\ \sigma_6 \end{Bmatrix}, \qquad \boldsymbol{\varepsilon}^0 = \begin{Bmatrix} \varepsilon_1 \\ \varepsilon_2 \\ \varepsilon_4 \\ \varepsilon_5 \\ \varepsilon_6 \end{Bmatrix} \qquad \hat{\mathbf{S}} = \begin{bmatrix} \hat{S}_{11} & \hat{S}_{12} & \hat{S}_{14} & \hat{S}_{15} & \hat{S}_{16} \\ \hat{S}_{12} & \hat{S}_{22} & \hat{S}_{24} & \hat{S}_{25} & \hat{S}_{26} \\ \hat{S}_{14} & \hat{S}_{24} & \hat{S}_{44} & \hat{S}_{45} & \hat{S}_{46} \\ \hat{S}_{15} & \hat{S}_{25} & \hat{S}_{45} & \hat{S}_{55} & \hat{S}_{56} \\ \hat{S}_{16} & \hat{S}_{26} & \hat{S}_{46} & \hat{S}_{56} & \hat{S}_{66} \end{bmatrix}. \tag{4.30}$$

Components $\hat{S}_{pq}$ are the reduced elastic compliances defined as

$$\hat{S}_{pq} = S_{pq} - \frac{S_{p3}S_{3q}}{S_{33}}, \quad \hat{S}_{pq} = \hat{S}_{qp}. \tag{4.31}$$

Similarly, the relation (4.3a) under the condition (4.27) leads to

$$\boldsymbol{\sigma}^0 = \mathbf{C}^0\boldsymbol{\varepsilon}^0, \tag{4.32}$$

where

$$\mathbf{C}^0 = \begin{bmatrix} C_{11} & C_{12} & C_{14} & C_{15} & C_{16} \\ C_{12} & C_{22} & C_{24} & C_{25} & C_{26} \\ C_{14} & C_{24} & C_{44} & C_{45} & C_{46} \\ C_{15} & C_{25} & C_{45} & C_{55} & C_{56} \\ C_{16} & C_{26} & C_{46} & C_{56} & C_{66} \end{bmatrix} \tag{4.33}$$

is created from (4.9) simply by deleting the third row and the third column.

Analogically, the generalized plane stress is defined by

$$\sigma_3 = 0. \tag{4.34}$$

The equations (4.29) and (4.32) are rewritten as follows:

$$\varepsilon^0 = \mathbf{S}^0 \boldsymbol{\sigma}^0, \qquad \boldsymbol{\sigma}^0 = \hat{\mathbf{C}}^0 \varepsilon^0, \tag{4.35}$$

where the components of $\mathbf{S}^0$ are established by eliminating the third row and the third column of (4.7). $\hat{\mathbf{C}}^0$ is the reduced stiffness matrix, which components are defined by

$$\hat{C}_{pq} = C_{pq} - \frac{C_{p3} C_{3q}}{C_{33}}, \quad \hat{C}_{pq} = \hat{C}_{qp}. \tag{4.36}$$

Similarly to (4.8), it can be proved that

$$\mathbf{C}^0 \hat{\mathbf{S}} = \mathbf{I} \qquad \mathbf{S}^0 \hat{\mathbf{C}} = \mathbf{I}. \tag{4.37}$$

4.1.6 Decoupling of in-plane and anti-plane relations

Let us consider a monoclinic material with symmetry plane parallel to x_3 and generalized plane strain. The constitutive equation (4.9) for (4.10) comes into the shape of

$$\begin{Bmatrix} \sigma_1 \\ \sigma_2 \\ \sigma_4 \\ \sigma_5 \\ \sigma_6 \end{Bmatrix} = \begin{bmatrix} C_{11} & C_{12} & 0 & 0 & C_{16} \\ C_{12} & C_{22} & 0 & 0 & C_{26} \\ 0 & 0 & C_{44} & C_{45} & 0 \\ 0 & 0 & C_{45} & C_{55} & 0 \\ C_{16} & C_{26} & 0 & 0 & C_{66} \end{bmatrix} \begin{Bmatrix} \varepsilon_1 \\ \varepsilon_2 \\ \varepsilon_4 \\ \varepsilon_5 \\ \varepsilon_6 \end{Bmatrix}, \tag{4.38}$$

in which the in-plane and anti-plane relations are decoupled. Eqs. (4.38) can be written in the decomposed form as

$$\begin{Bmatrix} \sigma_1 \\ \sigma_2 \\ \sigma_6 \end{Bmatrix} = \begin{bmatrix} C_{11} & C_{12} & C_{16} \\ C_{12} & C_{22} & C_{26} \\ C_{16} & C_{26} & C_{66} \end{bmatrix} \begin{Bmatrix} \varepsilon_1 \\ \varepsilon_2 \\ \varepsilon_6 \end{Bmatrix} \tag{4.39a}$$

and

$$\begin{Bmatrix} \sigma_4 \\ \sigma_5 \end{Bmatrix} = \begin{bmatrix} C_{44} & C_{45} \\ C_{45} & C_{55} \end{bmatrix} \begin{Bmatrix} \varepsilon_4 \\ \varepsilon_5 \end{Bmatrix}. \tag{4.39b}$$

The above stated assumptions allow solving the in-plane and anti-plane problem separately. This relations can be analogically written for generalized plane stress.

Most approaches analysing stress singularities are derived for certain singular stress concentrators. Bi-material or multi-material anisotropic wedges are modelled by using plane elasticity theories based on the Stroh and Lekhnitskii formalism, such as for example [56, 57]. By exceeding a certain wedge angle, the singularity exponent becomes complex-valued, just as the resulting stress intensity factors. The aim of the following paragraphs is to derive an universal formalism that would not distinguish whether the singularity exponents are real or complex.

4.1.7 Complex potential method – Lekhnitskii-Eshelby-Stroh formalism

In the second half of the last century, plane anisotropic elasticity theory based on complex variable functions had been formulated. Lekhnitskii [6] and Stroh [8] presented pioneering works for a stress description near singular stress concentrators, which employs advantages of complex variable functions. At the beginning, the Lekhnitskii formalism considers two-dimensional stresses, whereas Stroh starts with two-dimensional displacements [17]. The application suitability of the individual approaches depends on the type and degree of the problem.

Hwu employed the Stroh formalism [8, 9] in his extensive research and introduced the Key matrix [58] and the unified definition [59] for stress intensity factors of interface corners and cracks. This theory represents a strong mathematical tool for dealing with anisotropic singular concentrator. Considering a combination of an orthotropic and isotropic material, the relations for complex potentials violate the key matrix. However, Hwu presented a study in [60] that concerns with these configurations.

Besides that, Suo [44] introduced the Lekhnitskii-Eshelby-Stroh formalism (LES). It was also based on the studies of Ting [61, 62], where the modified Lekhnitskii formalism was introduced, which was in fact the same principle. When a monoclinic material defined in (4.38) is considered, the Lekhnitskii and Stroh formalism are formally indistinguishable. The equivalence allows to take an advantage of the clear algebraic results as well as the explicit solutions derived from Lekhnitskii's relations. There have been two reasons to use these basic characteristics of complex variable functions. Firstly, differentiation in the complex domain can be treated as an equivalent of harmoniousness, i.e. when a function has its derivative in a complex domain (in the complex theory they are called analytical functions), it fulfils the so called biharmonic equation automatically and thus it can be used for an expression of the Airy stress function. Another advantage is a complex variable application, which leads to simplification of the elastic variable description. In the LES formalism, material properties of a monoclinic material are characterized only by three material eigenvalues μ_i ($i = 1,2,3$), when both in-plane and anti-plane fields are taking into account. When only in-plane fields are considered, material eigenvalues are reduced to two. Their definition will be shown in the following paragraphs.

Governing differential equations

The basic equations for anisotropic elasticity are the equilibrium equations for static loading conditions (4.40), the strain-displacement relations (4.40b) and the Hooke's law for linear anisotropic elastic solids (4.40c). That is

$$\frac{\partial \sigma_{ij}}{\partial x_j} + \hat{f}_i = 0\,, \tag{4.40a}$$

$$\varepsilon_{ij} = \frac{1}{2}\left(\frac{\partial u_i}{\partial x_j} + \frac{\partial u_j}{\partial x_i}\right)\,, \tag{4.40b}$$

$$\sigma_{ij} = C_{ijkl}\varepsilon_{kl}\,, \tag{4.40c}$$

where indices $i,j,k,l = 1,2,3$, $\hat{f}_i$ designates body forces referred to a unit volume. In order to conform with the Lekhnitskii's nomenclature, all parameters will be written out according to the conventional notation instead of the contracted notation, i.e. $x_1 \to x$, $x_2 \to y$, $\sigma_1 \to \sigma_x$, $\sigma_2 \to \sigma_y$, $\sigma_{12} \to \tau_{xy}$, $\sigma_{13} \to \tau_{xz}$, $\sigma_{23} \to \tau_{yz}$. On the basis of two Airy functions $\varphi(x,y)$ and $\psi(x,y)$, the stresses are expressed as

$$\sigma_x = \frac{\partial^2 \varphi}{\partial y^2} + \hat{F}, \quad \sigma_y = \frac{\partial^2 \varphi}{\partial x^2} + \hat{F}, \quad \tau_{xy} = -\frac{\partial^2 \varphi}{\partial x \partial y}, \quad \tau_{xz} = \frac{\partial \psi}{\partial y}, \quad \tau_{yz} = -\frac{\partial \psi}{\partial x}, \tag{4.41}$$

where $\hat{F}$ is the potential of the body forces $\hat{f}_x$ and $\hat{f}_y$, for which it holds

$$\hat{f}_x = -\frac{\partial \hat{F}}{\partial x}, \quad \hat{f}_y = -\frac{\partial \hat{F}}{\partial y}. \tag{4.42}$$

By employing the inverse stress-strain relation (4.40c) and strain-displacement relation (4.40b), strain and displacement components can also be written out in terms of the Airy stress function.

For the sake of brevity, only relevant equations of the formalism will be stated, the reader is referred to [17, p. 34] for the detailed derivation. When the displacement compatibility is satisfied, the problem leads to a homogeneous system of differential equations:

$$L_4\varphi + L_3\psi = -(\hat{S}_{12} + \hat{S}_{22})\frac{\partial^2 \hat{F}}{\partial x^2} + (\hat{S}_{16} + \hat{S}_{26})\frac{\partial^2 \hat{F}}{\partial x \partial y} - (\hat{S}_{11} + \hat{S}_{12})\frac{\partial^2 \hat{F}}{\partial y^2},$$

$$L_3\varphi + L_2\psi = -2\alpha + AS_{34} - BS_{35} + (\hat{S}_{14} + \hat{S}_{24})\frac{\partial \hat{F}}{\partial x} + (\hat{S}_{15} + \hat{S}_{25})\frac{\partial \hat{F}}{\partial y}, \tag{4.43a}$$

where L_2, L_3, L_4 are differential operators of the second, third and fourth order:

$$L_2 = \hat{S}_{44}\frac{\partial^2}{\partial x^2} - 2\hat{S}_{45}\frac{\partial^2}{\partial x \partial y} + \hat{S}_{55}\frac{\partial^2}{\partial y^2},$$

$$L_3 = -\hat{S}_{24}\frac{\partial^3}{\partial x^3} + (\hat{S}_{25} + \hat{S}_{46})\frac{\partial^3}{\partial x^2 \partial y} - (\hat{S}_{14} + \hat{S}_{56})\frac{\partial^3}{\partial x \partial y^2} + \hat{S}_{15}\frac{\partial^3}{\partial y^3}, \tag{4.43b}$$

$$L_4 = \hat{S}_{22}\frac{\partial^4}{\partial x^4} - 2\hat{S}_{26}\frac{\partial^4}{\partial x^3 \partial y} + (2\hat{S}_{12} + \hat{S}_{66})\frac{\partial^4}{\partial x^2 \partial y^2} - 2\hat{S}_{16}\frac{\partial^4}{\partial x \partial y^3} + \hat{S}_{11}\frac{\partial^4}{\partial y^4},$$

where $\hat{S}_{ij}$ are the reduced elastic compliances defined in (4.31). A, B, α are the arbitrary constants associated with the rigid body motion.

General solution

Lekhnitskii [6] assumed the solution in the form

$$\varphi = \varphi^{(h)} + \varphi^{(p)}, \quad \psi = \psi^{(h)} + \psi^{(p)}, \tag{4.44}$$

where $\varphi^{(p)}$, $\psi^{(p)}$ are the particular solutions of the non-homogeneous system (4.43a). Let us first find a solution of the homogeneous system

$$L_4\varphi^{(h)} + L_3\psi^{(h)} = 0,$$

$$L_3\varphi^{(h)} + L_2\psi^{(h)} = 0, \tag{4.45}$$

where $\varphi^{(h)}$, $\psi^{(h)}$ are the homogeneous solutions of the Airy stress functions. Eliminating $\psi^{(h)}$ from both equations in (4.43a), we get an equation of the sixth order:

$$\left(L_4 L_2 - L_3^2\right)\varphi^{(h)} = 0. \tag{4.46}$$

The sixth order operator $L_4 L_2 - L_3^2$ can be decomposed into six operators of the first order, i.e.

$$D_6 D_5 D_4 D_3 D_2 D_1 \varphi^{(h)} = 0, \tag{4.47}$$

where

$$D_k = \frac{\partial}{\partial y} - \mu_k \frac{\partial}{\partial x}, \quad k = 1, 2, \ldots 6 \tag{4.48}$$

and μ_k are the roots of the characteristic algebraic equation associated with the differential equation (4.46), i.e. [62]

$$l_4(\mu)l_2(\mu) - l_3^2(\mu) = 0, \tag{4.49a}$$

where

$$
\begin{aligned}
l_2(\mu) &= \hat{S}_{55}\mu^2 - 2\hat{S}_{45}\mu + \hat{S}_{44}, \\
l_3(\mu) &= \hat{S}_{15}\mu^3 - (\hat{S}_{14} + \hat{S}_{56})\mu^2 + (\hat{S}_{25} + \hat{S}_{46})\mu - \hat{S}_{24}, \\
l_4(\mu) &= \hat{S}_{11}\mu^4 - 2\hat{S}_{16}\mu^3 + (2\hat{S}_{12} + \hat{S}_{66})\mu^2 - 2\hat{S}_{26}\mu + \hat{S}_{22}.
\end{aligned}
\tag{4.49b}
$$

For an anisotropic material and by considering both in-plane and anti-plane stress components, there are always three pair of complex conjugate roots of the characteristic equation (4.49a). For the subsequent computations, let us arrange the roots μ_k in the following order:

$$\mu_{k+3} = \overline{\mu}_k, \qquad \Im\mu_k > 0, \quad k = 1,2,3. \tag{4.50}$$

Solving the problem (4.47) by successive integration, we obtain the stress functions in the form

$$\varphi^{(h)} = 2\Re \sum_{k=1}^{3} \varphi_k(z_k), \quad z_k = x + \mu_k y \tag{4.51}$$

or

$$\psi^{(h)} = 2\Re \sum_{k=1}^{3} \psi_k(z_k), \tag{4.52}$$

when Eq. (4.46) is expressed in terms of $\psi^{(h)}$.

At this point, it is convenient to introduce a material assumption which will lead to simplification of the governing equations. Firstly, for a monoclinic material with the symmetry plane at $z = 0$ (see (4.10)), the elastic compliances in $l_3(\mu)$ all vanish. The sextic equation (4.49a) is then reduced to two equations: $l_4(\mu) = 0$ for the in-plane field and $l_2(\mu) = 0$ for the anti-plane field. Three distinct material eigenvalues split up into μ_1, μ_2 as the roots of $l_4(\mu) = 0$ and μ_3 of $l_2(\mu) = 0$. Secondly, when the problem is treated as two-dimensional, with the monoclinic material assumption and neglecting of the body forces, the particular solution is zero including the arbitrary constants A, B and α. The relation between φ_k and ψ_k is

$$\psi_k(z_k) = \eta_k \varphi_k'(z_k), \quad k = 1,2,3, \tag{4.53}$$

where

$$\eta_k = \frac{-l_3(\mu_k)}{l_2(\mu_k)} = \frac{-l_4(\mu_k)}{l_3(\mu_k)}. \tag{4.54}$$

As $l_4(\mu_1) = l_4(\mu_2) = l_2(\mu_3) = 0$, relations (4.54) will lead to be divided by zero or infinity. To get non-zero expressions, we use $l_4(\mu_3) = l_2(\mu_1) = l_2(\mu_2) \neq 0$. To avoid of using coefficients that approach zero or infinity due to the $l_3(\mu_k) = 0$, the expressions for stress functions are defined as

$$
\begin{aligned}
\varphi &= 2\Re\left\{\varphi_1(z_1) + \varphi_2(z_2) + \varphi_3(z_3)\right\}, \\
\psi &= 2\Re\left\{\lambda_1\varphi_1'(z_1) + \lambda_2\varphi_2'(z_2) + \frac{1}{\lambda_3}\varphi_3'(z_3)\right\},
\end{aligned}
\tag{4.55}
$$

in which

$$\lambda_1 = \eta_1 = \frac{-l_3(\mu_1)}{l_2(\mu_1)}, \quad \lambda_2 = \eta_2 = \frac{-l_3(\mu_2)}{l_2(\mu_2)}, \quad \lambda_3 = \frac{1}{\eta_3} = \frac{-l_3(\mu_k)}{l_4(\mu_k)}. \tag{4.56}$$

Since the terms λ_1, λ_2 and λ_3 become zero for a monoclinic material and φ_3 is an arbitrary function, we introduce the new stress functions $f_k(z_k)$ that absorb the coefficients as follows:

$$f_1(z_1) = \varphi_1'(z_1), \quad f_2(z_2) = \varphi_2'(z_2), \quad f_3(z_3) = \frac{1}{\lambda_3}\varphi_3'(z_3). \tag{4.57}$$

Inserting Eq. (4.55) into (4.41) with the new functions (4.57) leads to the following expressions for stresses:

$$\begin{aligned}
\sigma_x &= 2\Re\left\{\mu_1^2 f_1'(z_1) + \mu_2^2 f_2'(z_2)\right\}, \\
\sigma_y &= 2\Re\left\{f_1'(z_1) + f_2'(z_2)\right\}, \\
\tau_{xy} &= -2\Re\left\{\mu_1 f_1'(z_1) + \mu_2 f_2'(z_2)\right\}, \\
\tau_{xz} &= 2\Re\left\{\mu_3 f_3'(z_3)\right\}, \\
\tau_{yz} &= -2\Re\left\{f_3'(z_3)\right\}.
\end{aligned} \tag{4.58}$$

The displacements are expressed by inserting Eq. (4.58) into the inverse stress-strain relation (4.29) and consequently to (4.40b), which leads to

$$\begin{aligned}
\frac{\partial u}{\partial x} &= \hat{S}_{11}\sigma_x + \hat{S}_{12}\sigma_y + \hat{S}_{14}\tau_{yz} + \hat{S}_{15}\tau_{xz} + \hat{S}_{16}\tau_{xy}, \\[4pt]
\frac{\partial v}{\partial y} &= \hat{S}_{12}\sigma_x + \hat{S}_{22}\sigma_y + \hat{S}_{24}\tau_{yz} + \hat{S}_{25}\tau_{xz} + \hat{S}_{26}\tau_{xy}, \\[4pt]
\frac{\partial w}{\partial y} &= \hat{S}_{14}\sigma_x + \hat{S}_{24}\sigma_y + \hat{S}_{44}\tau_{yz} + \hat{S}_{45}\tau_{xz} + \hat{S}_{46}\tau_{xy}, \\[4pt]
\frac{\partial w}{\partial x} &= \hat{S}_{15}\sigma_x + \hat{S}_{25}\sigma_y + \hat{S}_{45}\tau_{yz} + \hat{S}_{55}\tau_{xz} + \hat{S}_{56}\tau_{xy}, \\[4pt]
\frac{\partial u}{\partial y} + \frac{\partial v}{\partial x} &= \hat{S}_{16}\sigma_x + \hat{S}_{26}\sigma_y + \hat{S}_{46}\tau_{yz} + \hat{S}_{56}\tau_{xz} + \hat{S}_{66}\tau_{xy},
\end{aligned} \tag{4.59}$$

where the contracted notation $u_1 \equiv u$, $u_2 \equiv v$, $u_3 \equiv w$ was implemented. Considering a monoclinic material and generalized plane strain, the reduced elastic compliances vanish, i.e. $\hat{S}_{14} = \hat{S}_{15} = \hat{S}_{24} = \hat{S}_{25} = \hat{S}_{46} = \hat{S}_{56} = 0$. By integration of these resulting equations, we can find the displacements functions as

$$\begin{aligned}
u &= 2\Re\left\{\sum_{k=1}^{3} a_{1k}f_k(z_k)\right\}, \\[4pt]
v &= 2\Re\left\{\sum_{k=1}^{3} a_{2k}f_k(z_k)\right\}, \\[4pt]
w &= 2\Re\left\{\sum_{k=1}^{3} a_{3k}f_k(z_k)\right\},
\end{aligned} \tag{4.60a}$$

where

$$\begin{aligned}
a_{1k} &= \mu_k^2 \hat{S}_{11} + \hat{S}_{12} - \mu_k \hat{S}_{16}, \\
a_{2k} &= \left(\mu_k^2 \hat{S}_{21} + \hat{S}_{22} - \mu_k \hat{S}_{26}\right)/\mu_k, \\
a_{3k} &= 0, \quad k = 1,2, \\
a_{13} &= 0, \\
a_{23} &= 0, \\
a_{33} &= \left(\mu_3 \hat{S}_{45} - \hat{S}_{44}\right)/\mu_3,
\end{aligned} \tag{4.60b}$$

Eshleby et al. [63] presented a similar representation based on the Navier-Cauchy equations. It has the same structure as Eqs. (4.60) and (4.58) and it is written in more elegant form as

$$u_i = 2\Re\left\{\sum_{k=1}^{3} A_{ik} f_k(z_k)\right\}, \tag{4.61a}$$

$$T_i = -2\Re\left\{\sum_{k=1}^{3} L_{ik} f_k(z_k)\right\}, \tag{4.61b}$$

$$\sigma_{1i} = -2\Re\left\{\sum_{k=1}^{3} L_{ik}\mu_k f_j'(z_k)\right\}, \quad \sigma_{2i} = 2\Re\left\{\sum_{k=1}^{3} L_{ik} f_k'(z_k)\right\}, \tag{4.61c}$$

where T_i are the components of the stress function vector along the semi-infinite line passing through the origin of the coordinate system $x_1 x_2$. It is convenient to adopt the matrix convention from the Stroh formalism. Let us write the complex potentials into a vector as

$$\mathbf{f}(z) = \begin{Bmatrix} f_1(z_1) \\ f_2(z_2) \\ f_3(z_3) \end{Bmatrix}, \quad z_k = x + \mu_k y, \quad k = 1,2,3. \tag{4.62}$$

Then, the equations (4.61a) and (4.61b) can be written as

$$\mathbf{u}(z) = 2\Re\left\{\mathbf{A}\mathbf{f}(z)\right\}, \tag{4.63a}$$

$$\mathbf{T}(z) = 2\Re\left\{\mathbf{L}\mathbf{f}(z)\right\}. \tag{4.63b}$$

The displacements and stress function vectors have the form:

$$\mathbf{u}(z) = \begin{Bmatrix} u_1 \\ u_2 \\ u_3 \end{Bmatrix}, \quad \mathbf{T}(z) = \begin{Bmatrix} T_1 \\ T_2 \\ T_3 \end{Bmatrix}, \tag{4.64}$$

where $u \equiv u_1$, $v \equiv u_2$, $u \equiv u_3$. The matrices $\mathbf{A}$ and $\mathbf{L}$ have then the following structure:

$$\mathbf{A} = \begin{bmatrix} a_{11} & a_{12} & a_{13} \\ a_{21} & a_{22} & a_{23} \\ a_{31} & a_{32} & a_{33} \end{bmatrix}, \quad \mathbf{L} = \begin{bmatrix} -\mu_1 & -\mu_2 & 0 \\ 1 & 1 & 0 \\ 0 & 0 & -1 \end{bmatrix}. \tag{4.65}$$

The matrix elements a_{ik} are defined in (4.60b). Assuming plane strain, each of the characteristic roots μ_k and each corresponding column of $\mathbf{A}$ are solved from the eigenvalue problem from the Stroh formalism [7], [44]

$$\left[\mathbf{Q} + \mu_k\left(\mathbf{R} + \mathbf{R}^\mathsf{T}\right) + \mu_k^2\mathbf{T}\right]\mathbf{a} = 0, \tag{4.66}$$

where

$$Q_{ik} = C_{i1k1}, \quad R_{ik} = C_{i1k2}, \quad T_{ik} = C_{i2k2}, \quad i,k = 1,2,3. \tag{4.67}$$

Each column of $\mathbf{A}$ is multiplied by the arbitrary normalization coefficient, i.e.

$$\mathbf{A} = \begin{bmatrix} c_1 a_{11} & c_2 a_{12} & c_3 a_{13} \\ c_1 a_{21} & c_2 a_{22} & c_3 a_{23} \\ c_1 a_{31} & c_2 a_{32} & c_3 a_{33} \end{bmatrix}, \quad \mathbf{L} = \begin{bmatrix} -c_1\mu_1 & -c_2\mu_2 & 0 \\ c_1 & c_2 & 0 \\ 0 & 0 & -c_3 \end{bmatrix}. \tag{4.68}$$
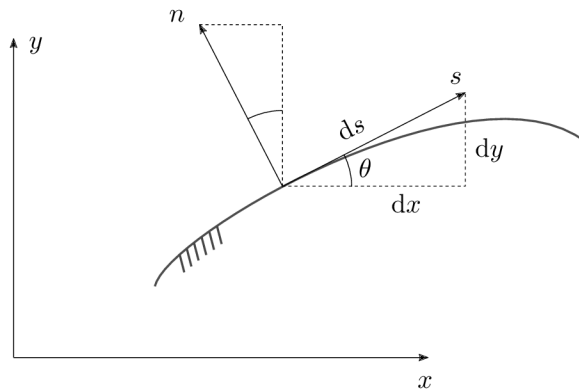
Fig. 4.2: Normal and tangent directions of a boundary surface.

Thus, μ_k are the roots of the characteristic sixth-order polynomial

$$\left| \mathbf{Q} + \mu_k \left(\mathbf{R} + \mathbf{R}^\mathsf{T} \right) + \mu_k^2 \mathbf{T} \right| = 0. \tag{4.69}$$

The matrix $\mathbf{L}$ is associated with $\mathbf{A}$ as

$$L_{ij} = \sum_{k=1}^{3} \left[R_{ik} + \mu_j T_{ik} \right] a_{kj} = 0. \tag{4.70}$$

This relation shows that by comparing the uniquely normalized Lekhnistkii matrices (4.65) with those in (4.68) derived by Stroh [7], the normalization coefficients are eliminated by using Eq. (4.70) and Eshelby's [63] representation (4.61) is uniquely determined by the elastic constants of the considered material.

Boundary conditions

The arbitrary complex functions $f_k(z_k)$ are determined through the satisfaction of the boundary conditions on the lateral surface. The first fundamental problem resides in prescribing the tractions $\hat{t}_x$, $\hat{t}_y$ and $\hat{t}_z = 0$ along the boundary by

$$\sigma_x n_1 + \tau_{xy} n_2 = \hat{t}_x, \quad \tau_{xy} n_1 + \sigma_y n_2 = \hat{t}_y, \quad \tau_{xz} n_1 + \tau_{yz} n_2 = 0. \tag{4.71}$$

The normal vector $\mathbf{n}$ of the boundary is defined by

$$n_1 = -\sin\theta = -\frac{\mathrm{d}y}{\mathrm{d}s}, \quad n_2 = \cos\theta = \frac{\mathrm{d}x}{\mathrm{d}s}. \tag{4.72}$$

The tangential direction s is chosen so that when we face the direction of the increasing s, the material lies on the right side (see Fig. 4.2). Inserting (4.41) and (4.72) into (4.71) and integrating with respect to s, we get

$$\frac{\partial \varphi}{\partial y} = \hat{T}_x(s) + c_1, \quad \frac{\partial \varphi}{\partial x} = \hat{T}_y(s) + c_2, \quad \psi = c_3, \tag{4.73a}$$

where c_1, c_2, c_3 are the integration constants and

$$\hat{T}_x(s) = -\int_0^s \hat{t}_x \, \mathrm{d}s,$$
$$\hat{T}_y(s) = \int_0^s \hat{t}_y \, \mathrm{d}s. \tag{4.73b}$$

Substituting (4.55) and (4.57) into (4.73a), we obtain

$$
\begin{aligned}
2\Re\left\{\mu_1 f_1 + \mu_1 f_1\right\} &= \hat{T}_x(s) + c_1, \\
2\Re\left\{f_1 + f_1\right\} &= \hat{T}_y(s) + c_2, \\
2\Re\left\{f_3\right\} &= c_3.
\end{aligned}
\tag{4.74}
$$

The second fundamental problem is represented by the displacements prescribed along the boundary:

$$
u = \hat{u}, \quad v = \hat{v}, \quad w = \hat{w}.
\tag{4.75}
$$

Using (4.59), (4.60) and (4.75), one gets

$$
\begin{aligned}
2\Re\left\{\sum_{k=1}^{3} a_{1k} f_k(z_k)\right\} &= \hat{u}, \\
2\Re\left\{\sum_{k=1}^{3} a_{2k} f_k(z_k)\right\} &= \hat{v}, \\
2\Re\left\{\sum_{k=1}^{3} a_{3k} f_k(z_k)\right\} &= \hat{w}.
\end{aligned}
\tag{4.76}
$$

4.2 Two-dimensional piezoelectric elasticity

4.2.1 Background

Piezoelectricity was discovered by the brothers Jacques and Pierre Curie in 1880. Piezoelectric materials possess a property that an electric field is induced when it is subjected to pressure, i.e. direct piezoelectric effect. The effect is also reversible, i.e. deformations occur due to the applied electric field, which is known as the converse piezoelectric effect predicted by Gabriel Lippmann in 1881. The piezoelectric effect can be manifested only when materials have a non-centrosymmetric crystal structure, represented by 21 crystal classes. Ten of them exhibit spontaneous polarization without mechanical stress due to the permanent dipole moment [64]. Such materials are called pyroelectric [65]. If the polarization can be reversed, the material is denoted as ferroelectric. Their relations can be seen in Fig. 4.3. Anther non-ferroelectric piezoelectric classes do not have a spontaneous polarization, such as quartz, which has a trigonal crystal lattice. The piezoelectric effect is then caused by polarization due to the distortion on the crystal lattice and creating electrical dipoles, which dismiss during unloading. However, the effect is not very strong. In the case of ferroelectric solids, the piezoelectric effect is caused by changing the magnitude of polarization also by the lattice distortion, but it is stronger and proportional to the initial polarization. These materials are not spontaneously polarized, but the polarization can be induced through so called poling [66, p. 27], [67, p. 16]. Ferroelectric materials can be crystals, ceramics or polymers.

Within the dissertation, we introduce a simplification that when we speak about piezoelectric materials, we mean a group of ferroelectric piezoelectric materials, i.e. spontaneous polarization exists in their structure even in the absence of an electrical field. We focus on piezoelectric ceramics whose physical properties are suitable for a wide range of smart technical applications, namely zirconate titanate (PZT) series, potassium sodium niobate (PSN) series or perovkites characterized by the chemical formula ABO_3, where A is a mono- or divalent alkaline earth metal and B is a tetra- or pentavalent metal [65, 68]. These materials exhibit good strength and stiffness and excellent piezoelectricity [69]. Piezoelectric ceramics are produced by pressing
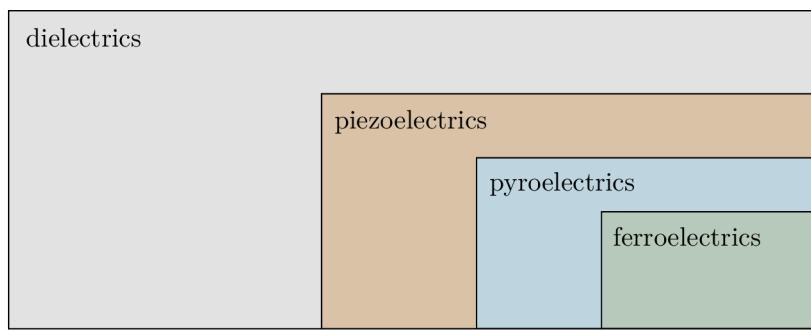
Fig. 4.3: Sorting of dielectric materials [66].

(a)   (b)
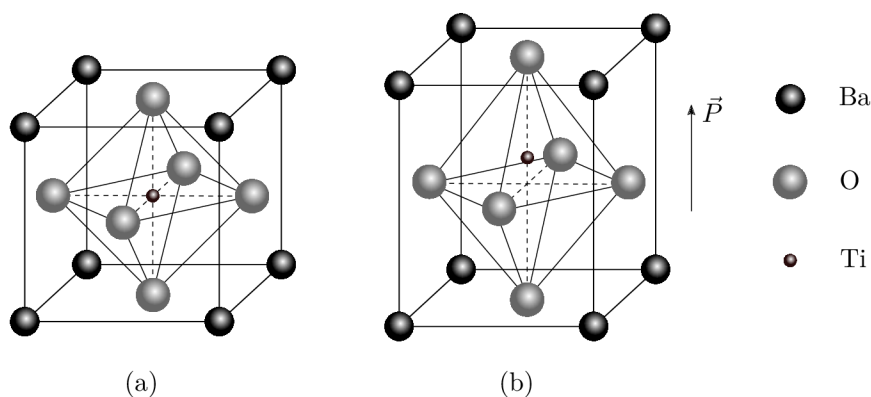
Fig. 4.4: Perovskite crystal structure of BaTiO$_3$ (a) above the Curie temperature with cubic lattice, (b) below the Curie temperature with tetragonal lattice (Curie temperature $\sim 130\,°$C).

ferroelectric grains, which are provided in a form of a fine powder. During the fabrication process, the powder is sintered above the Curie temperature. Over this point, the crystal has a cubic symmetry (such materials are called paraelectrics), with no dipole moments. As it cools down, it undergoes a phase transformation to the ferroelectric state with a tetragonal or rhomboedral crystal symmetry [70]. The process can be illustrated on the barium titanate (BaTiO$_3$) in Fig. 4.4. The phase transformation at about $130\,°$C involves movement of the Ba^{2+} ions to the off-centre position, which initiates a dipole moment. The electric domains are randomly oriented, which leads to zero macroscopic net polarization and all piezoelectric constants would be zero (Fig. 4.5(a)). Exposing the ceramic element to a sufficiently strong uni-direction electric field usually at the temperature slightly below the Curie temperature causes reorientation of domains in the direction of the applied field (Fig. 4.5(b)). After this poling process, domains do not return to their initial positions and most nearly remain in alignment with the direction of the applied electric field, which is called the poling direction (Fig. 4.5(c)). Now, it is able to induce the piezoelectric effect by applying an appropriate electric field, which results to the domain motion and consequent lattice deformation [71]. Hence, the poling direction is a significant material parameter which plays an important role in a design of piezoelectric devices. Note that the above described transformation phase is not the only one. For example, at $0\,°$C (the second transition temperature) or at $-90\,°$C the ferroelectric to ferroelectric phase transformation occurs.
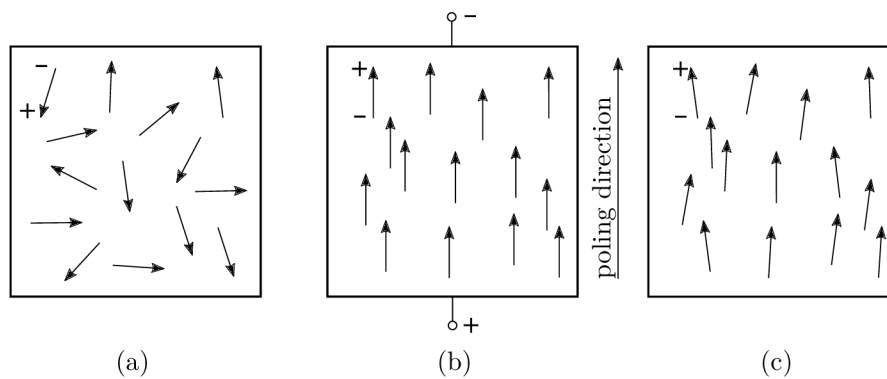
Fig. 4.5: Poling of a piezoelectric element: (a) prior to polarization, domains are oriented randomly, (b) exposing to large uni-direction electric field, (c) state after polarization, almost unidirectional polarization of domains.

4.2.2 Piezoelectric constitutive equations

In the following paragraphs, the governing equations and boundary conditions for piezoelectric materials by considering the variation principle and thermodynamics are introduced. The internal energy stored in any linear-elastic dielectric can be written as [1]

$$U = \frac{1}{2}\sigma_{ij}\varepsilon_{ij} + \frac{1}{2}E_iD_i, \tag{4.77}$$

where U is the internal energy density, σ_{ij} is the stress tensor, ε_{ij} is the strain tensor, D_i is the electric displacement (in the literature also called induction) and E_i is the electric field. The internal energy U can be considered as the thermodynamic potential with respect to charges on a dielectric. To derive the governing equations with E_i (related to the electric potential ϕ) instead of D_i (related to the electric charge q) as an independent variable, we need to introduce another thermodynamic potential with respect to the electric potential. Therefore, the electric enthalpy density is defined as [72]

$$H = U - D_iE_i, \tag{4.78}$$

where the second term $-D_iE_i$ has an importance due to the energy variation [1]. Therefore, H is the thermodynamic potential when the mechanical displacement and the electric potential are taken to be the independent variables.

To derive the governing equations and boundary conditions for a piezoelectric material, we need to employ the following variational form of the relation between the enthalpy (4.78) and the work of the external mechanical and electric loads [73]:

$$\delta \int_V H \, \mathrm{d}V - \int_V (f_i\delta u_i - q_b\delta\phi) \, \mathrm{d}V - \int_S (t_i\delta u_i - q_s\delta\phi) \, \mathrm{d}S = 0, \tag{4.79}$$

where f_i is the body force, u_i is the displacement, q_b or q_s is the body or applied surface charge, which is usually zero, t_i is the applied surface traction, ϕ is the electric potential, V is the volume of the material and S is the material boundary. The electric enthalpy density in the first integral of (4.79) for a linear elastic piezoelectric material follows from Eq. (4.78) and according to [72] it is defined as

$$H\left(\varepsilon_{ij}, E_i\right) = \frac{1}{2}C_{ijkl}\varepsilon_{ij}\varepsilon_{kl} - \frac{1}{2}\omega_{ij}E_iE_j - e_{ikl}\varepsilon_{kl}E_i, \tag{4.80}$$

where C_{ijkl} is the elastic stiffness at constant electric field, ω_{ij} is the dielectric permittivity at constant strains and e_{ikl} is piezoelectric stress/charge tensors [20]. The strain and electric field tensors are expressed by

$$\varepsilon_{ij} = \frac{1}{2}\left(u_{i,j} + u_{j,i}\right),$$
$$E_k = -\phi_{,k}, \tag{4.81}$$

where the comma denotes differentiation with respect to k. By substitution (4.80), (4.81) into (4.79) we get the the variational form

$$\int_V C_{ijkl}\varepsilon_{kl}\delta u_{i,j}\mathrm{d}V - \int_V \omega_{ik}E_k\delta\phi_{,i}\mathrm{d}V - \int_V e_{ikl}\left(\varepsilon_{kl}\delta\phi_{,i} + \delta u_{k,l}E_i\right)\mathrm{d}V -$$
$$- \int_V \left(f_i\delta u_i - q_b\delta\phi\right)\mathrm{d}V - \int_S \left(t_i\delta u_i - q_S\delta\phi\right)\mathrm{d}S = 0, \tag{4.82}$$

from which, after the integration by parts, one can deduce equilibrium equations:

$$\sigma_{ij,j} + f_i = 0$$
$$D_{i,i} = q_b, \tag{4.83}$$

and boundary conditions:

$$\sigma_{ij}n_j = t_i$$
$$D_i n_i = -q_s, \tag{4.84}$$

where n_i is the outer unit normal vector to the boundary S and the stress and electric displacement are defined by

$$\sigma_{ij} = \frac{\partial H}{\partial \varepsilon_{ij}} = C_{ijkl}\varepsilon_{ij} + e_{kij}E_k,$$
$$-D_i = \frac{\partial H}{\partial E_i} = e_{ikl}\varepsilon_{kl} - \omega_{ij}E_k. \tag{4.85}$$

4.2.3 Constitutive laws for piezoelectric materials in three-dimensional state

There are natural crystals such as quartz that exhibit piezoelectricity. Much more stronger piezoelectric coupling exhibit man-made piezoelectric materials, for example barium titanate or lead zirconate ceramics. These materials are implicitly in isotropic and non-piezoelectric state. Piezoelectric properties can be induced in these ceramics through a process called poling [1], during which their mechanical properties change to generally anisotropic. However, most poled material become transversally isotropic.

For an anisotropic and linearly electro-elastic solid, the constitutive laws between the elastic field tensors (σ_{ij} and ε_{ij}) and electric field vectors (induction D_j and electric field E_j) are represented by four equally important equation systems. They can be written in a tensor notation as [20, 74]

$$\begin{cases}\sigma_{ij} = C^E_{ijkl}\varepsilon_{kl} - e_{kij}E_k, \\ D_j = e_{jkl}\varepsilon_{kl} + \omega^\varepsilon_{jk}E_k,\end{cases} \quad \begin{cases}\varepsilon_{ij} = S^E_{ijkl}\sigma_{kl} - d_{kij}E_k, \\ D_j = d_{jkl}\sigma_{kl} + \omega^\sigma_{jk}E_k,\end{cases}$$
$$\begin{cases}\sigma_{ij} = C^D_{ijkl}\varepsilon_{kl} - h_{kij}D_k, \\ E_j = -h_{jkl}\varepsilon_{kl} + \beta^\varepsilon_{jk}D_k,\end{cases} \quad \begin{cases}\varepsilon_{ij} = S^D_{ijkl}\sigma_{kl} - g_{kij}D_k, \\ E_j = -g_{jkl}\sigma_{kl} + \beta^\sigma_{jk}D_k,\end{cases} \tag{4.86}$$

where S_{ijkl}^E and S_{ijkl}^D are elastic compliances at constant electric field and induction; C_{ijkl}^E and C_{ijkl}^D are elastic stiffnesses at constant electric field and induction; ω_{jk}^ε, ω_{jk}^σ and β_{jk}^ε, β_{jk}^σ are dielectric permittivities on non-permittivities at constant strains and stresses; d_{kij}, e_{kij}, g_{kij} and h_{kij} are piezoelectric strain/charge, stress/charge, strain/voltage and stress/voltage tensors, respectively. Due to the symmetry of the stresses and strains and the path-independence of the elastic strain energy, the electro-mechanical material constants have the following symmetry properties:

$$
\begin{aligned}
C_{ijkl}^E &= C_{jikl}^E = C_{klij}^E, & e_{kij} &= e_{kji}, & \omega_{jk}^\varepsilon &= \omega_{kj}^\varepsilon, \\
S_{ijkl}^E &= S_{jikl}^E = S_{klij}^E, & d_{kij} &= d_{kji}, & \omega_{jk}^\sigma &= \omega_{kj}^\sigma, \\
C_{ijkl}^D &= C_{jikl}^D = C_{klij}^D, & h_{kij} &= h_{kji}, & \beta_{jk}^\varepsilon &= \beta_{kj}^\varepsilon, \\
S_{ijkl}^D &= S_{jikl}^D = S_{klij}^D, & g_{kij} &= g_{kji}, & \beta_{jk}^\sigma &= \beta_{kj}^\sigma.
\end{aligned}
\tag{4.87}
$$

4.2.4 Contracted notation

In order to determine the solution of piezoelectric problems, it is suitable to transform the extended tensor notation to the matrices by using the contracted matrix notation introduced in section 4.1.1 for pure elastic anisotropic materials. This simplification consists in replacing ij or kl by p or q, where i, j, k and l take the values 1, 2 and 3 and p and q take the values 1, 2,..., 6. The parameters are transformed by the following prescription:

- if $i = j$ or $k = l$, then $p = i$ and $q = k$, for example $C_{1122} = C_{12}$

- if $i \neq j$ or $k \neq l$, then p or q is equal to the remaining number from the progression 1, 2, 3 increased of 3, for example $C_{3123} = C_{54}$.

With this assignment and the symmetry properties (4.87), certain transformation rules have to be added:

$$
\begin{aligned}
2S_{ijkl} &= S_{pq}, & &\text{if either } p \text{ or } q > 3, \\
4S_{ijkl} &= S_{pq}, & &\text{if both } p \text{ and } q > 3, \\
2\varepsilon_{ij} &= \varepsilon_p, \quad 2d_{kij} = d_{kp}, \quad 2g_{kij} = g_{kp} & &\text{if } p > 3.
\end{aligned}
\tag{4.88}
$$

Using the contracted notation, the constitutive laws (4.86) can be then rewritten in the matrix form as [20]

$$
\begin{Bmatrix} \boldsymbol{\sigma} \\ \mathbf{D} \end{Bmatrix} = \begin{bmatrix} \mathbf{C}_E & \mathbf{e}^\mathsf{T} \\ \mathbf{e} & -\boldsymbol{\omega}_\varepsilon \end{bmatrix} \begin{Bmatrix} \boldsymbol{\varepsilon} \\ -\mathbf{E} \end{Bmatrix}, \quad
\begin{Bmatrix} \boldsymbol{\varepsilon} \\ \mathbf{D} \end{Bmatrix} = \begin{bmatrix} \mathbf{S}_E & -\mathbf{d}^\mathsf{T} \\ \mathbf{d} & -\boldsymbol{\omega}_\sigma \end{bmatrix} \begin{Bmatrix} \boldsymbol{\sigma} \\ -\mathbf{E} \end{Bmatrix},
$$

$$
\begin{Bmatrix} \boldsymbol{\sigma} \\ -\mathbf{E} \end{Bmatrix} = \begin{bmatrix} \mathbf{C}_D & -\mathbf{h}^\mathsf{T} \\ \mathbf{h} & -\boldsymbol{\beta}_\varepsilon \end{bmatrix} \begin{Bmatrix} \boldsymbol{\varepsilon} \\ \mathbf{D} \end{Bmatrix}, \quad
\begin{Bmatrix} \boldsymbol{\varepsilon} \\ -\mathbf{E} \end{Bmatrix} = \begin{bmatrix} \mathbf{S}_D & \mathbf{g}^\mathsf{T} \\ \mathbf{g} & -\boldsymbol{\beta}_\sigma \end{bmatrix} \begin{Bmatrix} \boldsymbol{\sigma} \\ \mathbf{D} \end{Bmatrix},
\tag{4.89}
$$

where

$$\boldsymbol{\sigma} = \begin{Bmatrix} \sigma_1 \\ \sigma_2 \\ \sigma_3 \\ \sigma_4 \\ \sigma_5 \\ \sigma_6 \end{Bmatrix} = \begin{Bmatrix} \sigma_{11} \\ \sigma_{22} \\ \sigma_{33} \\ \sigma_{23} \\ \sigma_{13} \\ \sigma_{12} \end{Bmatrix}, \quad \boldsymbol{\varepsilon} = \begin{Bmatrix} \varepsilon_1 \\ \varepsilon_2 \\ \varepsilon_3 \\ \varepsilon_4 \\ \varepsilon_5 \\ \varepsilon_6 \end{Bmatrix} = \begin{Bmatrix} \varepsilon_{11} \\ \varepsilon_{22} \\ \varepsilon_{33} \\ 2\varepsilon_{23} \\ 2\varepsilon_{13} \\ 2\varepsilon_{12} \end{Bmatrix},$$

$$\mathbf{C}_E = \begin{bmatrix} C_{11}^E & C_{12}^E & C_{13}^E & C_{14}^E & C_{15}^E & C_{16}^E \\ C_{12}^E & C_{22}^E & C_{23}^E & C_{24}^E & C_{25}^E & C_{26}^E \\ C_{13}^E & C_{23}^E & C_{33}^E & C_{34}^E & C_{35}^E & C_{36}^E \\ C_{14}^E & C_{24}^E & C_{34}^E & C_{44}^E & C_{45}^E & C_{46}^E \\ C_{15}^E & C_{25}^E & C_{35}^E & C_{45}^E & C_{55}^E & C_{56}^E \\ C_{16}^E & C_{26}^E & C_{36}^E & C_{46}^E & C_{56}^E & C_{66}^E \end{bmatrix}, \tag{4.90}$$

$$\mathbf{E} = \begin{Bmatrix} E_1 \\ E_2 \\ E_3 \end{Bmatrix}, \quad \mathbf{D} = \begin{Bmatrix} D_1 \\ D_2 \\ D_3 \end{Bmatrix}, \quad \mathbf{e} = \begin{bmatrix} e_{11} & e_{12} & e_{13} & e_{14} & e_{15} & e_{16} \\ e_{21} & e_{22} & e_{23} & e_{24} & e_{25} & e_{26} \\ e_{31} & e_{32} & e_{33} & e_{34} & e_{35} & e_{36} \end{bmatrix},$$

$$\boldsymbol{\omega}_\varepsilon = \begin{bmatrix} \omega_{11}^\varepsilon & \omega_{12}^\varepsilon & \omega_{13}^\varepsilon \\ \omega_{12}^\varepsilon & \omega_{22}^\varepsilon & \omega_{23}^\varepsilon \\ \omega_{13}^\varepsilon & \omega_{23}^\varepsilon & \omega_{33}^\varepsilon \end{bmatrix}.$$

Expressions for the matrices $\mathbf{S}_E$, $\mathbf{S}_D$, $\mathbf{C}_D$, $\mathbf{d}$, $\mathbf{g}$, $\mathbf{h}$, $\boldsymbol{\omega}_\sigma$, $\boldsymbol{\beta}_\sigma$ $\boldsymbol{\beta}_\varepsilon$ are similar. The superscript T denotes a matrix transposition. One set can be recomputed from the other by the following equations:

$$\mathbf{C}_E = \mathbf{S}_E^{-1}, \quad \mathbf{C}_D = \mathbf{S}_D^{-1}, \quad \boldsymbol{\beta}_\varepsilon = \boldsymbol{\omega}_\varepsilon^{-1}, \quad \boldsymbol{\beta}_\sigma = \boldsymbol{\omega}_\sigma^{-1},$$

$$\mathbf{d} = \mathbf{e}\mathbf{S}_E = \boldsymbol{\omega}_\sigma\mathbf{g}, \quad \mathbf{e} = \mathbf{d}\mathbf{C}_E = \boldsymbol{\omega}_\varepsilon\mathbf{h},$$

$$\mathbf{g} = \mathbf{h}\mathbf{S}_D = \boldsymbol{\beta}_\sigma\mathbf{d}, \quad \mathbf{h} = \mathbf{g}\mathbf{C}_D = \boldsymbol{\beta}_\varepsilon\mathbf{e},$$

$$\boldsymbol{\omega}_\sigma - \boldsymbol{\omega}_\varepsilon = \mathbf{d}\mathbf{C}_E\mathbf{d}^\mathsf{T} = \mathbf{e}\mathbf{S}_E\mathbf{e}^\mathsf{T} = \mathbf{d}\mathbf{e}^\mathsf{T}, \tag{4.91}$$

$$\boldsymbol{\beta}_\varepsilon - \boldsymbol{\beta}_\sigma = \mathbf{h}\mathbf{S}_D\mathbf{h}^\mathsf{T} = \mathbf{g}\mathbf{C}_D\mathbf{g}^\mathsf{T} = \mathbf{h}\mathbf{g}^\mathsf{T},$$

$$\mathbf{C}_D - \mathbf{C}_E = \mathbf{e}^\mathsf{T}\boldsymbol{\beta}_\varepsilon\mathbf{e} = \mathbf{h}^\mathsf{T}\boldsymbol{\omega}_\varepsilon\mathbf{h} = \mathbf{h}^\mathsf{T}\mathbf{e},$$

$$\mathbf{S}_E - \mathbf{S}_D = \mathbf{g}^\mathsf{T}\boldsymbol{\omega}_\sigma\mathbf{g} = \mathbf{d}^\mathsf{T}\boldsymbol{\beta}_\sigma\mathbf{d} = \mathbf{d}^\mathsf{T}\mathbf{g}.$$

An inversion of the material characteristics can be also performed by using the matrix identities

$$\begin{bmatrix} \mathbf{C}_E & \mathbf{e}^\mathsf{T} \\ \mathbf{e} & -\boldsymbol{\omega}_\varepsilon \end{bmatrix}\begin{bmatrix} \mathbf{S}_D & \mathbf{g}^\mathsf{T} \\ \mathbf{g} & -\boldsymbol{\beta}_\sigma \end{bmatrix} = \mathbf{I}, \quad \begin{bmatrix} \mathbf{C}_D & -\mathbf{h}^\mathsf{T} \\ \mathbf{h} & -\boldsymbol{\beta}_\varepsilon \end{bmatrix}\begin{bmatrix} \mathbf{S}_E & -\mathbf{d}^\mathsf{T} \\ \mathbf{d} & -\boldsymbol{\omega}_\sigma \end{bmatrix} = \mathbf{I}, \tag{4.92}$$

where $\mathbf{I}$ is the unit matrix of a shape 9×9.

4.2.5 Material symmetry

Material characteristics of piezoelectric materials are predominantly provided by the elastic stiffnesses C_{ij}^E, piezoelectric constants e_{ij} and dielectric permitivities ω_{ij}^ε. The inverse forms can be determined by the transformation relations (4.91), or the elastic, piezoelectric and electric constants can be merged into a compact matrix as in (4.89) and use the identities (4.92) to get the inverse constants. Both operations lead to the same result.

The stiffness, piezoelectric and permittivity matrices $\mathbf{C}_E$, $\mathbf{e}$ and $\boldsymbol{\omega}_\varepsilon$ in (4.90) characterise the most general form of an anisotropic material with piezoelectric properties. We make the same deliberation as for the pure anisotropic elasticity in section 4.1.3. The symmetry planes

coincide with the global coordinate planes in the Cartesian coordinate system x_1, x_2, x_3. The matrix structure of the monoclinic piezoelectric material, i.e. when the material has only one symmetry plane defined by $x_3 = 0$, is

$$
\mathbf{C}_E = \begin{bmatrix} C_{11}^E & C_{12}^E & C_{13}^E & 0 & 0 & C_{16}^E \\ C_{12}^E & C_{22}^E & C_{23}^E & 0 & 0 & C_{26}^E \\ C_{13}^E & C_{23}^E & C_{33}^E & 0 & 0 & C_{36}^E \\ 0 & 0 & 0 & C_{44}^E & C_{45}^E & 0 \\ 0 & 0 & 0 & C_{45}^E & C_{55}^E & 0 \\ C_{16}^E & C_{26}^E & C_{36}^E & 0 & 0 & C_{66}^E \end{bmatrix},
\tag{4.93}
$$

$$
\mathbf{e} = \begin{bmatrix} e_{11} & e_{12} & e_{13} & 0 & 0 & e_{16} \\ e_{21} & e_{22} & e_{23} & 0 & 0 & e_{26} \\ 0 & 0 & 0 & e_{34} & e_{35} & 0 \end{bmatrix}, \quad \boldsymbol{\omega}_\varepsilon = \begin{bmatrix} \omega_{11}^\varepsilon & \omega_{12}^\varepsilon & 0 \\ \omega_{12}^\varepsilon & \omega_{22}^\varepsilon & 0 \\ 0 & 0 & \omega_{33}^\varepsilon \end{bmatrix}.
$$

It is worth noticing that the stiffness and permittivity matrices are symmetric, but the piezo-electric matrix is not.

An orthotropic material has three mutually orthogonal symmetry planes. Considering a poling direction parallel to x_1-axis, the material matrices reduce to [75]

$$
\mathbf{C}_E = \begin{bmatrix} C_{11}^E & C_{12}^E & C_{13}^E & 0 & 0 & 0 \\ C_{12}^E & C_{22}^E & C_{23}^E & 0 & 0 & 0 \\ C_{13}^E & C_{23}^E & C_{33}^E & 0 & 0 & 0 \\ 0 & 0 & 0 & C_{44}^E & 0 & 0 \\ 0 & 0 & 0 & 0 & C_{55}^E & 0 \\ 0 & 0 & 0 & 0 & 0 & C_{66}^E \end{bmatrix},
\tag{4.94}
$$

$$
\mathbf{e} = \begin{bmatrix} e_{11} & e_{12} & e_{13} & 0 & 0 & 0 \\ 0 & 0 & 0 & 0 & 0 & e_{26} \\ 0 & 0 & 0 & 0 & e_{35} & 0 \end{bmatrix}, \quad \boldsymbol{\omega}_\varepsilon = \begin{bmatrix} \omega_{11}^\varepsilon & 0 & 0 \\ 0 & \omega_{22}^\varepsilon & 0 \\ 0 & 0 & \omega_{33}^\varepsilon \end{bmatrix}.
$$

The initially isotropic ceramic becomes transversally isotropic during the poling process with the plane of isotropy perpendicular to the poling axis. This symmetry state plays a significant role in investigations of poled piezoelectric materials. The material matrices have the following structure:

$$
\mathbf{C}_E = \begin{bmatrix} C_{11}^E & C_{12}^E & C_{12}^E & 0 & 0 & 0 \\ C_{12}^E & C_{22}^E & C_{23}^E & 0 & 0 & 0 \\ C_{12}^E & C_{23}^E & C_{22}^E & 0 & 0 & 0 \\ 0 & 0 & 0 & \frac{C_{22}^E - C_{23}^E}{2} & 0 & 0 \\ 0 & 0 & 0 & 0 & C_{44}^E & 0 \\ 0 & 0 & 0 & 0 & 0 & C_{44}^E \end{bmatrix},
\tag{4.95}
$$

$$
\mathbf{e} = \begin{bmatrix} e_{11} & e_{12} & e_{12} & 0 & 0 & 0 \\ 0 & 0 & 0 & 0 & 0 & e_{26} \\ 0 & 0 & 0 & 0 & e_{26} & 0 \end{bmatrix}, \quad \boldsymbol{\omega}_\varepsilon = \begin{bmatrix} \omega_{11}^\varepsilon & 0 & 0 \\ 0 & \omega_{22}^\varepsilon & 0 \\ 0 & 0 & \omega_{22}^\varepsilon \end{bmatrix}.
$$

From the above depicted structures we can see that the directional properties depend on the poling axis. Since we want to unify the procedure with the pure anisotropic relations, we coincide the poling axis with the longitudinal direction of the laminate model. We can observe the equality of the stiffness matrices (4.12) and (4.95). Structure of the piezoelectric matrix depends on the poling direction, which can attain two limit configurations: coincidence with x_1-axis or with x_2-axis. Between this states the structure corresponds to monoclinic (see (4.93)).

It is illustrated in the following scheme:

$$
\| x_1 \begin{bmatrix} e_{11} & e_{12} & e_{12} & 0 & 0 & 0 \\ 0 & 0 & 0 & 0 & 0 & e_{26} \\ 0 & 0 & 0 & 0 & e_{26} & 0 \end{bmatrix}
$$

$$\Downarrow$$

$$
\text{in between} \begin{bmatrix} e_{11} & e_{12} & e_{13} & 0 & 0 & e_{16} \\ e_{21} & e_{22} & e_{23} & 0 & 0 & e_{26} \\ 0 & 0 & 0 & e_{34} & e_{35} & 0 \end{bmatrix} \tag{4.96}
$$

$$\Downarrow$$

$$
\| x_2 \begin{bmatrix} 0 & 0 & 0 & 0 & 0 & e_{16} \\ e_{21} & e_{22} & e_{21} & 0 & 0 & 0 \\ 0 & 0 & 0 & e_{16} & 0 & 0 \end{bmatrix}
$$

Let us consider a rotation of the material coordinate system about x_3 axis by an angle of $90°$ and $-90°$, i.e. the poling direction coincides with x_2 axis. Considering a transversally isotropic material in pure anisotropic elasticity, the resulting stiffness matrices will be equal, so will be for a piezoelectric material. The difference is only in the piezoelectric matrix, where the absolute values of the matrix element will be same, but their signs will be opposite. Structure of the permittivity matrices will be also equal. It follows from the above that the poling has an unique orientation and contrary to the adopted laminate theory there are no symmetries in rotations of the longitudinal directions. More about the matrix structure of individual crystal classes can be found in [76, p. 123].

4.2.6 Transformation of the coordinate system

Similarly to pure anisotropic elasticity, we define transformation relations to investigate material configurations with a poling axis arbitrary oriented in the plane $x_3 = 0$. As was stated in the previous section, we coincide the longitudinal direction L with the poling axis and the plane of isotropy is defined by transversal directions TT'. Let us designate the principal material coordinate system LTT' as x_i^*. We assemble the stiffness, piezoelectric and permittivity matrices in these coordinates and perform the inverse by using (4.92) to obtain the compliance matrix $\mathbf{S}_D^*$, piezoelectric matrix $\mathbf{g}^*$ and non-permittivities[2] $\boldsymbol{\beta}_\sigma^*$. Then the relation (4.26) can be used to transform the compliance matrix of a piezoelectric material, i.e.

$$
\mathbf{S}_D = \left(\mathbf{K}^{-1}\right)^{\mathsf{T}} \mathbf{S}_D^* \mathbf{K}^{-1}, \tag{4.97}
$$

where the transformation matrix $\mathbf{K}$ is defined in (4.21).

To derive the transformation of the piezoelectric and dielectric constants, we proceed from the constitutive equation $(4.89)_4$. Transformation of the electric intensity and electric displacement is realized by using

$$
\mathbf{D} = \boldsymbol{\Omega} \mathbf{D}^*,
$$
$$
\mathbf{E} = \boldsymbol{\Omega} \mathbf{E}^*, \tag{4.98}
$$

where the transformation matrix $\boldsymbol{\Omega}$ is defined in (4.18). The angle θ defines a rotation about x_3 axis in the counter-clockwise direction and physically refers to the poling direction, see Fig. 4.1.

---

[2]Dielectric permittivity has not an inverse quantity. It is stated in some papers that the inverse is electric susceptibility χ_e, but these parameters are not inverse, but it holds that $\chi_e = \omega_\varepsilon - 1$. Owing to this fact, we adopted the Hwu's non-permittivity [20].

Considering a homogeneous non-dispersive linear anisotropic material, the relation between the electric displacement and electric intensity in the coordinate system x_i^* is

$$\mathbf{E}^* = \boldsymbol{\beta}_\sigma^* \mathbf{D}^*. \tag{4.99}$$

Inserting (4.98) into Eq. (4.99) we get

$$\boldsymbol{\Omega}^{-1}\mathbf{E} = \boldsymbol{\beta}_\sigma^* \boldsymbol{\Omega}^{-1}\mathbf{D}. \tag{4.100}$$

After multiplication by $\boldsymbol{\Omega}$ from the left we obtain the relation in the new coordinate system:

$$\mathbf{E} = \boldsymbol{\Omega}\boldsymbol{\beta}_\sigma^* \boldsymbol{\Omega}^{-1}\mathbf{D} = \boldsymbol{\beta}_\sigma \mathbf{D}, \tag{4.101}$$

where

$$\boldsymbol{\beta}_\sigma = \boldsymbol{\Omega}\boldsymbol{\beta}_\sigma^* \boldsymbol{\Omega}^{-1} \tag{4.102}$$

is the transformation of the non-permittivity matrix from the coordinate system x_i^* to x_i.

Analogically, a transformation relation for piezoelectric matrix can be defined. The coupling relation between piezoelectricity and elasticity (see $(4.89)_4$) in the coordinate system x_i^* is

$$-\mathbf{E}^* = \mathbf{g}^* \boldsymbol{\sigma}^*. \tag{4.103}$$

Substituting (4.98) and (4.20) into (4.103) one obtains

$$-\boldsymbol{\Omega}^{-1}\mathbf{E} = \mathbf{g}^* \mathbf{K}^{-1}\boldsymbol{\sigma}. \tag{4.104}$$

After multiplication by $\boldsymbol{\Omega}$ from the left we get

$$\mathbf{E} = \boldsymbol{\Omega}\mathbf{g}^* \mathbf{K}^{-1}\boldsymbol{\sigma} = \mathbf{g}\boldsymbol{\sigma}, \tag{4.105}$$

from which we get the transformation relation for the piezoelectric constants:

$$\mathbf{g} = \boldsymbol{\Omega}\mathbf{g}^* \mathbf{K}^{-1}. \tag{4.106}$$

4.2.7 Constitutive laws for piezoelectric materials in two-dimensional state

Analytical solutions to fully-coupled piezoelectric problems in three-dimensional systems exist under very restrictive geometry assumptions. On the other hand, the numerical solutions are in generally computationally expensive. To avoid these limitations, it is convenient to simplify the 3D problem into a mathematically two-dimensional formulation, which is much easier from both analytical and numerical point of view. The problem dealing with piezoelectric materials can be simplified to a plane problem when in-plane and anti-plane relations are decoupled. Section 4.2.5 shows that when a monoclinic piezoelectric material with symmetry axis parallel to $x_3 = 0$ is considered, all assumptions are fulfilled to extend the LES formalism to piezoelectric materials. Despite the fact that ideal piezoelectric materials are homogeneous ceramics, its poling direction can be apprehended as the longitudinal directions in the sense of dominant material properties. This fact enables extension of pure anisotropic elasticity to piezoelectric materials. The conception of the principal material directions as an analogy with fibre orientations provides a great utility to model the problem.

In two-dimensional anisotropic plane problems, generalized plane strain ($\varepsilon_3 = 0$) or generalized plane stress ($\sigma_3 = 0$) can be introduced. As for elastic fields described in section 4.1.5, two states for electric fields can also be considered: open circuit condition ($D_3 = 0$) when the

faces of the piezoelectric body are in contact with a non-conducting media and the top an bottom surfaces are free of charge, and short circuit condition ($E_3 = 0$) when the top and bottom surfaces are held at the same electric potential [20]. By combining the previous conditions, a two-dimensional state of the piezoelectric material can be divided into four different situations, i.e.:

1. Generalized plane strain and short circuit: $\varepsilon_3 = 0$ and $E_3 = 0$.

2. Generalized plane strain and open circuit: $\varepsilon_3 = 0$ and $D_3 = 0$.

3. Generalized plane stress and short circuit: $\sigma_3 = 0$ and $E_3 = 0$.

4. Generalized plane stress and open circuit: $\sigma_3 = 0$ and $D_3 = 0$.

The constitutive laws (4.89) under the above plane conditions can be reduced by eliminating the terms associated with the zero values of ε_3, (or σ_3) and E_3 (or D_3) and replacing σ_3, (or ε_3) and D_3 (or E_3) according to the generalized relation for the reduced elastic compliances [9, 17]. The matrix form of the constitutive laws for a piezoelectric material in two dimensional state are [20]:

State 1: $\varepsilon_3 = 0$ and $E_3 = 0$

$$
\begin{Bmatrix} \boldsymbol{\sigma}^0 \\ \mathbf{D}^0 \end{Bmatrix} = \begin{bmatrix} \mathbf{C}_E^0 & \mathbf{e}^{0\mathsf{T}} \\ \mathbf{e}^0 & -\boldsymbol{\omega}_\varepsilon^0 \end{bmatrix} \begin{Bmatrix} \boldsymbol{\varepsilon}^0 \\ -\mathbf{E}^0 \end{Bmatrix}, \quad \begin{Bmatrix} \boldsymbol{\varepsilon}^0 \\ \mathbf{D}^0 \end{Bmatrix} = \begin{bmatrix} \hat{\mathbf{S}}_E & -\hat{\mathbf{d}}^{\mathsf{T}} \\ \hat{\mathbf{d}} & -\hat{\omega}_\sigma \end{bmatrix} \begin{Bmatrix} \boldsymbol{\sigma}^0 \\ -\mathbf{E}^0 \end{Bmatrix},
$$
$$
\begin{Bmatrix} \boldsymbol{\sigma}^0 \\ -\mathbf{E}^0 \end{Bmatrix} = \begin{bmatrix} \mathbf{C}_D' & -\mathbf{h}'^{\mathsf{T}} \\ \mathbf{h}' & -\beta_\varepsilon' \end{bmatrix} \begin{Bmatrix} \boldsymbol{\varepsilon}^0 \\ \mathbf{D}^0 \end{Bmatrix}, \quad \begin{Bmatrix} \boldsymbol{\varepsilon}^0 \\ -\mathbf{E}^0 \end{Bmatrix} = \begin{bmatrix} \hat{\mathbf{S}}_D' & \hat{\mathbf{g}}'^{\mathsf{T}} \\ \hat{\mathbf{g}}' & -\hat{\beta}_\sigma' \end{bmatrix} \begin{Bmatrix} \boldsymbol{\sigma}^0 \\ \mathbf{D}^0 \end{Bmatrix},
$$

(4.107a)

where

$$
\boldsymbol{\sigma}^0 = \begin{Bmatrix} \sigma_1 \\ \sigma_2 \\ \sigma_4 \\ \sigma_5 \\ \sigma_6 \end{Bmatrix} \quad \boldsymbol{\varepsilon}^0 = \begin{Bmatrix} \varepsilon_1 \\ \varepsilon_2 \\ \varepsilon_4 \\ \varepsilon_5 \\ \varepsilon_6 \end{Bmatrix} \quad \mathbf{C}_E^0 = \begin{bmatrix} C_{11}^E & C_{12}^E & C_{14}^E & C_{15}^E & C_{16}^E \\ C_{12}^E & C_{22}^E & C_{24}^E & C_{25}^E & C_{26}^E \\ C_{14}^E & C_{24}^E & C_{44}^E & C_{45}^E & C_{46}^E \\ C_{15}^E & C_{25}^E & C_{45}^E & C_{55}^E & C_{56}^E \\ C_{16}^E & C_{26}^E & C_{46}^E & C_{56}^E & C_{66}^E \end{bmatrix},
$$
$$
\mathbf{E}^0 = \begin{Bmatrix} E_1 \\ E_2 \end{Bmatrix}, \quad \mathbf{D}^0 = \begin{Bmatrix} D_1 \\ D_2 \end{Bmatrix}, \quad \mathbf{e}^0 = \begin{bmatrix} e_{11} & e_{12} & e_{14} & e_{15} & e_{16} \\ e_{21} & e_{22} & e_{24} & e_{25} & e_{26} \end{bmatrix},
$$
$$
\boldsymbol{\omega}_\varepsilon^0 = \begin{bmatrix} \omega_{11}^\varepsilon & \omega_{12}^\varepsilon \\ \omega_{12}^\varepsilon & \omega_{22}^\varepsilon \end{bmatrix},
$$

(4.107b)

$$
\hat{\mathbf{S}}_D' = \begin{bmatrix} \hat{S}_{11}'^D & \hat{S}_{12}'^D & \hat{S}_{14}'^D & \hat{S}_{15}'^D & \hat{S}_{16}'^D \\ \hat{S}_{12}'^D & \hat{S}_{22}'^D & \hat{S}_{24}'^D & \hat{S}_{25}'^D & \hat{S}_{26}'^D \\ \hat{S}_{14}'^D & \hat{S}_{24}'^D & \hat{S}_{44}'^D & \hat{S}_{45}'^D & \hat{S}_{46}'^D \\ \hat{S}_{15}'^D & \hat{S}_{25}'^D & \hat{S}_{45}'^D & \hat{S}_{55}'^D & \hat{S}_{56}'^D \\ \hat{S}_{16}'^D & \hat{S}_{26}'^D & \hat{S}_{46}'^D & \hat{S}_{56}'^D & \hat{S}_{66}'^D \end{bmatrix}, \quad \hat{\mathbf{g}}' = \begin{bmatrix} \hat{g}_{11}' & \hat{g}_{12}' & \hat{g}_{14}' & \hat{g}_{15}' & \hat{g}_{16}' \\ \hat{g}_{21}' & \hat{g}_{22}' & \hat{g}_{24}' & \hat{g}_{25}' & \hat{g}_{26}' \end{bmatrix},
$$
$$
\hat{\beta}_\sigma' = \begin{bmatrix} \hat{\beta}_{11}'^\sigma & \hat{\beta}_{12}'^\sigma \\ \hat{\beta}_{12}'^\sigma & \hat{\beta}_{22}'^\sigma \end{bmatrix}.
$$

(4.107c)

The matrix elements are recomputed by

$$
\hat{S}_{ij}'^D = \hat{S}_{ij}^D + \frac{\hat{g}_{3i}\hat{g}_{3j}}{\hat{\beta}_{33}^\sigma} = \hat{S}_{ji}'^D, \quad \hat{g}_{ij}' = \hat{g}_{ij} - \frac{\hat{\beta}_{3i}^\sigma \hat{g}_{3j}}{\hat{\beta}_{33}^\sigma}, \quad \hat{\beta}_{ij}'^\sigma = \hat{\beta}_{ij}^\sigma - \frac{\hat{\beta}_{3i}^\sigma \hat{\beta}_{3j}^\sigma}{\hat{\beta}_{33}^\sigma} = \hat{\beta}_{ji}'^\sigma,
$$

(4.107d)

in which

$$\hat{S}_{ij}^D = S_{ij}^D - \frac{S_{3i}^D S_{3j}^D}{S_{33}^D} = \hat{S}_{ji}^D, \quad \hat{g}_{ij} = g_{ij} - \frac{g_{i3}S_{3j}^D}{S_{33}^D}, \quad \hat{\beta}_{ij}^\sigma = \beta_{ij}^\sigma + \frac{g_{i3}g_{j3}}{S_{33}^D} = \hat{\beta}_{ji}^\sigma. \tag{4.107e}$$

The expressions for $\hat{\mathbf{S}}_E$, $\hat{\mathbf{d}}$, $\hat{\boldsymbol{\omega}}_\sigma$, $\hat{\mathbf{C}}_D'$, $\hat{\boldsymbol{\beta}}_\varepsilon'$ are obtained analogically. The individual equations in (4.107a) are called after the letter of the matrix of piezoelectric coefficients, i.e. e-type, d-type, h-type and g-type [66]. Mostly, only the e-type and g-type constitutive laws (4.107a) are used, therefore in the other three states only this two equation systems are stated.

State 2: $\varepsilon_3 = 0$ and $D_3 = 0$

$$\left\{\begin{matrix} \boldsymbol{\sigma}^0 \\ \mathbf{D}^0 \end{matrix}\right\} = \begin{bmatrix} \mathbf{C}_E' & \mathbf{e}'^\mathsf{T} \\ \mathbf{e}' & -\boldsymbol{\omega}_\varepsilon' \end{bmatrix} \left\{\begin{matrix} \boldsymbol{\varepsilon}^0 \\ -\mathbf{E}^0 \end{matrix}\right\}, \quad \left\{\begin{matrix} \boldsymbol{\varepsilon}^0 \\ -\mathbf{E}^0 \end{matrix}\right\} = \begin{bmatrix} \hat{\mathbf{S}}_D & \hat{\mathbf{g}}^\mathsf{T} \\ \hat{\mathbf{g}} & -\hat{\boldsymbol{\beta}}_\sigma \end{bmatrix} \left\{\begin{matrix} \boldsymbol{\sigma}^0 \\ \mathbf{D}^0 \end{matrix}\right\}, \tag{4.108}$$

State 3: $\sigma_3 = 0$ and $E_3 = 0$

$$\left\{\begin{matrix} \boldsymbol{\sigma}^0 \\ \mathbf{D}^0 \end{matrix}\right\} = \begin{bmatrix} \hat{\mathbf{C}}_E & \hat{\mathbf{e}}^\mathsf{T} \\ \hat{\mathbf{e}} & -\hat{\boldsymbol{\omega}}_\varepsilon \end{bmatrix} \left\{\begin{matrix} \boldsymbol{\varepsilon}^0 \\ -\mathbf{E}^0 \end{matrix}\right\}, \quad \left\{\begin{matrix} \boldsymbol{\varepsilon}^0 \\ -\mathbf{E}^0 \end{matrix}\right\} = \begin{bmatrix} \mathbf{S}_D' & \mathbf{g}'^\mathsf{T} \\ \mathbf{g}' & -\beta_\sigma' \end{bmatrix} \left\{\begin{matrix} \boldsymbol{\sigma}^0 \\ \mathbf{D}^0 \end{matrix}\right\}, \tag{4.109}$$

State 4: $\sigma_3 = 0$ and $D_3 = 0$

$$\left\{\begin{matrix} \boldsymbol{\sigma}^0 \\ \mathbf{D}^0 \end{matrix}\right\} = \begin{bmatrix} \hat{\mathbf{C}}_E' & \hat{\mathbf{e}}'^\mathsf{T} \\ \hat{\mathbf{e}}' & -\hat{\boldsymbol{\omega}}_\varepsilon' \end{bmatrix} \left\{\begin{matrix} \boldsymbol{\varepsilon}^0 \\ -\mathbf{E}^0 \end{matrix}\right\}, \quad \left\{\begin{matrix} \boldsymbol{\varepsilon}^0 \\ -\mathbf{E}^0 \end{matrix}\right\} = \begin{bmatrix} \mathbf{S}_D^0 & \mathbf{g}^{0\mathsf{T}} \\ \mathbf{g}^0 & -\beta_\sigma^0 \end{bmatrix} \left\{\begin{matrix} \boldsymbol{\sigma}^0 \\ \mathbf{D}^0 \end{matrix}\right\}, \tag{4.110}$$

The remaining material characteristics are considered as follows:

$$C_{ij}'^E = C_{ij}^E + \frac{e_{3i}e_{3j}}{\omega_{33}^\varepsilon} = C_{ji}'^E, \quad e_{ij}' = e_{ij} - \frac{\omega_{3i}^\varepsilon e_{3j}}{\omega_{33}^\varepsilon}, \quad \omega_{ij}'^\varepsilon = \omega_{ij}^\varepsilon - \frac{\omega_{3i}^\varepsilon \omega_{3j}^\varepsilon}{\omega_{33}^S} = \omega_{ji}'^\varepsilon,$$

$$\hat{C}_{ij}^E = C_{ij}^E - \frac{C_{3i}^E C_{3j}^E}{C_{33}^E} = \hat{C}_{ji}^E, \quad \hat{e}_{ij} = e_{ij} - \frac{e_{i3}C_{3j}^E}{C_{33}^E}, \quad \hat{\omega}_{ij}^\varepsilon = \omega_{ij}^\varepsilon + \frac{e_{i3}e_{j3}}{C_{33}^E},$$

$$\hat{C}_{ij}'^E = \hat{C}_{ij}^E + \frac{\hat{e}_{3i}\hat{e}_{3j}}{\hat{\omega}_{33}^\varepsilon} = \hat{C}_{ji}'^E, \quad \hat{e}_{ij}' = \hat{e}_{ij} - \frac{\hat{\omega}_{3i}^\varepsilon \hat{e}_{3j}}{\hat{\omega}_{33}^\varepsilon}, \quad \hat{\omega}_{ij}'^\varepsilon = \hat{\omega}_{ij}^\varepsilon - \frac{\hat{\omega}_{3i}^\varepsilon \hat{\omega}_{3j}^\varepsilon}{\hat{\omega}_{33}^S} = \hat{\omega}_{ji}'^\varepsilon,$$

$$S_{ij}'^D = S_{ij}^D + \frac{g_{3i}g_{3j}}{\beta_{33}^\sigma} = S_{ji}'^D, \quad g_{ij}' = g_{ij} - \frac{\beta_{3i}^\sigma g_{3j}}{\beta_{33}^\sigma}, \quad \beta_{ij}'^\sigma = \beta_{ij}^\sigma - \frac{\beta_{3i}^\sigma \beta_{3j}^\sigma}{\beta_{33}^\sigma} = \beta_{ji}'^\sigma.$$

$$\tag{4.111}$$

The parameters $\hat{S}_{ij}^D$, $\hat{g}_{ij}$, $\hat{\beta}_{ij}^\sigma$, $\hat{S}_{ij}'^D$, $\hat{g}_{ij}'$, $\hat{\beta}_{ij}'^\sigma$ are defined in (4.107d) and (4.107e).

As in the three-dimensional state, it is sometimes more convenient to use inversion of the e-type and g-type compound matrices. Transformation between this two types can be done simply by inverting the compound matrix by the same way as in the three-dimensional state (4.92), such as for state 1:

$$\begin{bmatrix} \mathbf{C}_E^0 & \mathbf{e}^{0\mathsf{T}} \\ \mathbf{e}^0 & -\boldsymbol{\omega}_\varepsilon^0 \end{bmatrix} \begin{bmatrix} \hat{\mathbf{S}}_D' & \hat{\mathbf{g}}'^\mathsf{T} \\ \hat{\mathbf{g}}' & -\hat{\boldsymbol{\beta}}_\sigma' \end{bmatrix} = \mathbf{I}, \quad \begin{bmatrix} \mathbf{C}_D'^0 & -\mathbf{h}'^\mathsf{T} \\ \mathbf{h}' & -\boldsymbol{\beta}_\varepsilon' \end{bmatrix} \begin{bmatrix} \hat{\mathbf{S}}_E & -\hat{\mathbf{d}}^\mathsf{T} \\ \hat{\mathbf{d}} & -\hat{\boldsymbol{\omega}}_\sigma \end{bmatrix} = \mathbf{I} \tag{4.112}$$

and for state 2, 3 and 4:

$$\begin{bmatrix} \mathbf{C}_E' & \mathbf{e}'^\mathsf{T} \\ \mathbf{e}' & -\boldsymbol{\omega}_\varepsilon' \end{bmatrix} \begin{bmatrix} \hat{\mathbf{S}}_D & \hat{\mathbf{g}}^\mathsf{T} \\ \hat{\mathbf{g}} & -\hat{\boldsymbol{\beta}}_\sigma \end{bmatrix} = \mathbf{I}, \quad \begin{bmatrix} \hat{\mathbf{C}}_E & \hat{\mathbf{e}}^\mathsf{T} \\ \hat{\mathbf{e}} & -\hat{\boldsymbol{\omega}}_\varepsilon \end{bmatrix} = \begin{bmatrix} \mathbf{S}_D' & \mathbf{g}'^\mathsf{T} \\ \mathbf{g}' & -\beta_\sigma' \end{bmatrix} = \mathbf{I},$$

$$\begin{bmatrix} \hat{\mathbf{C}}_E' & \hat{\mathbf{e}}'^\mathsf{T} \\ \hat{\mathbf{e}}' & -\hat{\boldsymbol{\omega}}_\varepsilon' \end{bmatrix} \begin{bmatrix} \mathbf{S}_D^0 & \mathbf{g}^{0\mathsf{T}} \\ \mathbf{g}^0 & -\beta_\sigma^0 \end{bmatrix} = \mathbf{I}. \tag{4.113}$$

Note that the order of the coordinate transformation and conversion to generalized plane state are commutative operations. In the present algorithm, material characteristic are firstly transformed and then converted to generalized plane state.

4.2.8 Expanded Lekhnitskii-Eshelby-Stroh formalism for piezoelectric media

Solutions presented in [5, 10, 77, 78, 79, 80] show that equations for piezoelectric anisotropic problems have the same structure as those for corresponding anisotropic pure elastic materials. A closed form solution of a central crack based on the expanded Stroh formalism was derived in [5], while a solution for an elliptic inclusion and hole was presented in [11, 80, 81]. A first attempt to express material the matrices explicitly was performed in [82]. The most significant work was done by Hwu in [20, 21, 22, 83] and also in his monograph [17], where he summed up the previous research and expanded the Stroh formalism, the Key matrix, and the unified definition [84] to piezoelectric media. Hirai et al. [23] and Abe et al. [24] applied the theory to certain bi-material notch configurations including determination of stress intensity factors by using the Ψ-integral method.

Similar progress was carried out in extending the Lekhnitskii formalism in [45, 46]. A general solution for piezoelectric anisotropic materials was derived in [47, 48, 49, 50, 51, 52]. Xu and Rajapakse [85], Chue and Chen [53] or Chen [86] investigated composite piezoelectric wedges and junctions, i.e. bi-materials composed from both piezoelectric and anisotropic materials. Singularity exponents and stress intensity factors of an interface crack in isotropic metal/piezoelectric or insulator/piezoelectric bi-materials were computed in [26, 87, 88]. Banks-Sills et al. [12] computed stress intensity factors by using the M-integral method.

Kah Soh et al. [89] or Liou and Sung [90] used the modified Lekhnitskii and Stroh approach to find explicit expressions for the Barnett-Lothe tensors. Crack singularity solved by boundary integral equations was reported in [91]. Two-dimensional analysis of a semi-infinite crack by employing the Green's function was investigated in [50]. An interesting introduction to non-linear piezoelectric fracture mechanics was presented by Kuna [92]. Authors in [93] developed a new hybrid finite element method for a plane piezoelectric problem. One of the most significant method for investigating piezoelectric materials is the boundary element method [94], employed for example by Li et al. [95].

Suo [44] developed the LES formalism for evaluating the stress singularity of anisotropic bi-material notches. However, its limit case – an interface crack – is primarily treated as the Hilbert problem, as can be seen in [25, 80, 96, 97, 98, 99, 100]. The present work employs the expanded[3] LES formalism for a piezoelectric continuum based on the studies [9, 17, 19] and applies it to the problem of a piezoelectric bi-material notch and interface crack.

Governing differential equations

Deriving of the expanded LES formalism for piezoelectric materials is based on the fourth set of the g-type constitutive equations $(4.107a)_4$. It corresponds to the generalized plane state described in section 4.1.5 and short circuit, i.e. $\varepsilon_3 = 0$ and $E_3 = 0$. In the following chapters, only this plane state is assumed, all other combinations would be derived analogically.

In the absence of body forces and free charges, the equilibrium equations are

$$\frac{\partial \sigma_{ij}}{\partial x_j} = 0, \quad \frac{\partial D_i}{\partial x_i} = 0, \tag{4.114}$$

where the repeated indices imply summation. In contrast to the Lekhnitskii's nomenclature used in section 4.1.7, it is more convenient to use the Hwu's variable indexing as in (4.90) for

---

[3]According to Hwu [17], the "expanded" formalism is used for expansion to piezoelectric materials, while the "extended" Stroh formalism is used for problems involving temperature. However, the classification is not commonly accepted in the research community. For example Fang [66] uses "extended" for both Stroh and Lekhnitskii formalism. We suggest to follow the Hwu's classification.

piezoelectric materials and rewrite coordinates as $x \to x_1$, $y \to x_2$, $z \to x_3$. The stresses and electric displacements can be denoted by two Airy stress functions φ and ψ from (4.41) and an electric displacement function χ by

$$\sigma_1 = \frac{\partial^2 \varphi}{\partial x_2^2}, \quad \sigma_2 = \frac{\partial^2 \varphi}{\partial x_1^2}, \quad \sigma_6 = -\frac{\partial^2 \varphi}{\partial x_1 \partial x_2}, \quad \sigma_5 = \frac{\partial \psi}{\partial x_2}, \quad \sigma_4 = -\frac{\partial \psi}{\partial x_1},$$
$$D_1 = \frac{\partial \chi}{\partial x_2}, \quad D_2 = -\frac{\partial \chi}{\partial x_1}, \tag{4.115}$$

which satisfy the equilibrium equation (4.114) automatically. Substituting (4.115) in the constitutive equations $(4.107a)_4$ and then making use of the compatibility equations for piezoelectric materials

$$\frac{\partial^2 \varepsilon_1}{\partial x_2^2} + \frac{\partial^2 \varepsilon_2}{\partial x_1^2} - \frac{\partial^2 \varepsilon_6}{\partial x_1 \partial x_2} = 0, \quad \frac{\partial \varepsilon_5}{\partial x_2} - \frac{\partial \varepsilon_4}{\partial x_1} = 0, \quad \frac{\partial E_1}{\partial x_2} - \frac{\partial E_2}{\partial x_1} = 0, \tag{4.116}$$

we obtain a system of second order partial differential equations for the unknown stress and electric displacement functions φ, ψ and χ:

$$\begin{aligned} L_4 \varphi + M_3 \chi + L_3 \psi &= 0, \\ M_3 \varphi + P_2 \chi + M_2 \psi &= 0, \\ L_3 \varphi + M_2 \chi + L_2 \psi &= 0, \end{aligned} \tag{4.117a}$$

where the differential operators L_2, L_3, L_4, M_2, M_3, P_2 are defined by [52, 66]

$$L_2 = \hat{S}'^D_{44} \frac{\partial^2}{\partial x_1^2} - 2\hat{S}'^D_{45} \frac{\partial^2}{\partial x_1 \partial x_2} + \hat{S}'^D_{55} \frac{\partial^2}{\partial x_2^2},$$

$$L_3 = -\hat{S}'^D_{24} \frac{\partial^3}{\partial x_1^3} + (\hat{S}'^D_{25} + \hat{S}'^D_{46}) \frac{\partial^3}{\partial x_1^2 \partial x_2} - (\hat{S}'^D_{14} + \hat{S}'^D_{56}) \frac{\partial^3}{\partial x_1 \partial x_2^2} + \hat{S}'^D_{15} \frac{\partial^3}{\partial x_3^3},$$

$$L_4 = \hat{S}'^D_{22} \frac{\partial^4}{\partial x_1^4} - 2\hat{S}'^D_{26} \frac{\partial^4}{\partial x_1^3 \partial x_2} + (2\hat{S}'^D_{12} + \hat{S}'^D_{66}) \frac{\partial^4}{\partial x_1^2 \partial x_2^2} - 2\hat{S}'^D_{16} \frac{\partial^4}{\partial x_1 \partial x_2^3} + \hat{S}'^D_{11} \frac{\partial^4}{\partial x_2^4},$$

$$M_2 = \hat{g}'_{24} \frac{\partial^2}{\partial x_1^2} - (\hat{g}'_{14} + \hat{g}'_{25}) \frac{\partial^2}{\partial x_1 \partial x_2} + \hat{g}'_{15} \frac{\partial^2}{\partial x_2^2}, \tag{4.117b}$$

$$M_3 = -\hat{g}'_{22} \frac{\partial^3}{\partial x_1^3} + (\hat{g}'_{12} + \hat{g}'_{26}) \frac{\partial^3}{\partial x_1^2 \partial x_2} - (\hat{g}'_{21} + \hat{g}'_{16}) \frac{\partial^3}{\partial x_1 \partial x_2^2} + \hat{g}'_{11} \frac{\partial^3}{\partial x_2^3},$$

$$P_2 = -\hat{\beta}'^\sigma_{22} \frac{\partial^2}{\partial x_1^2} + 2\hat{\beta}'^\sigma_{12} \frac{\partial^2}{\partial x_1 \partial x_2} - \hat{\beta}'^\sigma_{11} \frac{\partial^2}{\partial x_2^2}.$$

General solution

We assume herein that the partial solutions of the stress functions are zero due to the absence of body forces and free charges (see Eqs. (4.44)). Then, by eliminating ψ and χ from the equation (4.117a) one gets

$$\left(L_4 L_2 P_2 + 2 L_3 M_2 M_3 - P_2 L_3^2 - L_4 M_2^2 - L_2 M_3^2 \right) \varphi = 0. \tag{4.118}$$

Let us suppose that φ is a function of a complex variable, i.e.

$$\varphi = \varphi(z), \quad z = x_1 + \mu x_2. \tag{4.119}$$

Substituting it into (4.118) and considering a nonzero solution of φ, we get a characteristic equation [20]

$$l_4(\mu) l_2(\mu) \rho_2(\mu) + 2 l_3(\mu) m_2(\mu) m_3(\mu) - \rho_2(\mu) l_3^2(\mu) - l_4(\mu) m_2^2(\mu) - l_2(\mu) m_3^2(\mu) = 0, \tag{4.120a}$$

where

$$
\begin{aligned}
l_2(\mu) &= \hat{S}'^D_{55}\mu^2 - 2\hat{S}'^D_{45}\mu + \hat{S}'^D_{44}, \\
l_3(\mu) &= \hat{S}'^D_{15}\mu^3 - (\hat{S}'^D_{14} + \hat{S}'^D_{56})\mu^2 + (\hat{S}'^D_{25} + \hat{S}'^D_{46})\mu - \hat{S}'^D_{24}, \\
l_4(\mu) &= \hat{S}'^D_{11}\mu^4 - 2\hat{S}'^D_{16}\mu^3 + (2\hat{S}'^D_{12} + \hat{S}'^D_{66})\mu^2 - 2\hat{S}'^D_{26}\mu + \hat{S}'^D_{22}, \\
m_2(\mu) &= \hat{g}'_{15}\mu^2 - (\hat{g}'_{14} + \hat{g}'_{25})\mu + \hat{g}'_{24}, \\
m_3(\mu) &= \hat{g}'_{11}\mu^3 - (\hat{g}'_{21} + \hat{g}'_{16})\mu^2 + (\hat{g}'_{12} + \hat{g}'_{26})\mu - \hat{g}'_{22}, \\
\rho_2(\mu) &= -\hat{\beta}'^\sigma_{11}\mu^2 + 2\hat{\beta}'^\sigma_{12}\mu - \hat{\beta}'^\sigma_{22}.
\end{aligned}
\tag{4.120b}
$$

Since the strain energy is positive, the material eigenvalues μ_k obtained from the eighth-degree eigenrelation (4.120a) occur in four pairs of complex conjugates (in contrast to pure anisotropic elasticity described in section 4.1.7, where three pairs of complex conjugates appeared). The arrangement condition (4.50) can be extended to

$$
\mu_{k+4} = \overline{\mu}_k, \qquad \Im\mu_k > 0, \quad k = 1,2,3,4.
\tag{4.121}
$$

The general solutions φ, ψ and χ of (4.117a) have the form [53]

$$
\varphi = 2\Re\sum_{k=1}^4 \varphi_k(z_k), \quad \psi = 2\Re\sum_{k=1}^4 \psi_k(z_k), \quad \chi = 2\Re\sum_{k=1}^4 \chi_k(z_k), \quad z_k = x_1 + \mu_k x_2.
\tag{4.122}
$$

The similar material assumptions, as for the pure elastic anisotropic materials, can be introduced in order to illustrate the expansion to piezoelectric materials. When considering a monoclinic material with symmetry plane at $z = 0$ (the matrix structure in (4.93)), the elastic compliances in $l_3(\mu)$ and piezoelectric coefficients in $m_2(\mu)$ all vanish. The octic equation (4.120a) is then reduced to

$$
l_2(\mu)\left(l_4(\mu)\rho_2(\mu) - m_3^2(\mu)\right) = 0,
\tag{4.123}
$$

where the product of $l_2(\mu)$ and the bracket assures that the in-plane and anti-plane fields can be decoupled[4]. Then $l_4\rho_2 - m_3^2 = 0$ yields to three material eigenvalues μ_1, μ_2, μ_4 for the in-plane field and anti-plane relation $l_2 = 0$ gives one eigenvalue μ_3.

Eliminating χ from Eq. (4.117a) with a substitution of (4.119) and consecutive integration gives the relation between stress functions:

$$
\begin{aligned}
\psi_k(z_k) &= \lambda_k\varphi'_k(z_k), \quad \text{for} \quad k = 1,2,4, \\
\psi_k(z_k) &= \frac{1}{\lambda_k}\varphi'_k(z_k), \quad \text{for} \quad k = 3,
\end{aligned}
\tag{4.124}
$$

where [52, 53]

$$
\begin{aligned}
\lambda_k &= -\frac{l_3(\mu_k)\rho_2(\mu_k) - m_3(\mu_k)m_2(\mu_k)}{\rho_2(\mu_k)l_2(\mu_k) - m_2^2(\mu_k)}, \quad \text{for} \quad k = 1,2, \\
\lambda_k &= -\frac{l_3(\mu_k)\rho_2(\mu_k) - m_3(\mu_k)m_2(\mu_k)}{\rho_2(\mu_k)l_4(\mu_k) - m_3^2(\mu_k)}, \quad \text{for} \quad k = 3, \\
\lambda_k &= -\frac{l_4(\mu_k)m_2(\mu_k) - l_3(\mu_k)m_3(\mu_k)}{m_2(\mu_k)l_3(\mu_k) - m_3(\mu_k)l_2(\mu_k)}, \quad \text{for} \quad k = 4.
\end{aligned}
\tag{4.125}
$$

---

[4]This is not the only case of decoupled in-plane and anti-plane fields. Other cases, such as degenerate case or materials with hexagonal symmetry can be found in [53]

Similarly, eliminating ψ from equations (4.117a) with substitution of (4.119) and consecutive integration gives the relation [70]:

$$\begin{aligned}
\chi_k(z_k) &= \xi_k \varphi_k'(z_k), \quad \text{for} \quad k = 1,2,3, \\
\chi_k(z_k) &= \frac{1}{\xi_k} \varphi_k'(z_k), \quad \text{for} \quad k = 4,
\end{aligned} \tag{4.126}$$

where [12, 46, 49, 52, 53]

$$\begin{aligned}
\xi_k &= -\frac{l_2(\mu_k)m_3(\mu_k) - l_3(\mu_k)m_2(\mu_k)}{\rho_2(\mu_k)l_2(\mu_k) - m_2^2(\mu_k)}, \quad \text{for} \quad k = 1,2, \\
\xi_k &= -\frac{l_4(\mu_k)m_2(\mu_k) - l_3(\mu_k)m_3(\mu_k)}{m_3(\mu_k)m_2(\mu_k) - l_3(\mu_k)\rho_2(\mu_k)}, \quad \text{for} \quad k = 3, \\
\xi_k &= -\frac{l_2(\mu_k)m_3(\mu_k) - l_3(\mu_k)m_2(\mu_k)}{l_2(\mu_k)l_4(\mu_k) - l_3^2(\mu_k)}, \quad \text{for} \quad k = 4.
\end{aligned} \tag{4.127}$$

The stress functions (4.122) can be then rewritten as

$$\begin{aligned}
\varphi &= 2\Re\left\{\varphi_1(z_1) + \varphi_2(z_2) + \varphi_3(z_3) + \varphi_4(z_4)\right\}, \\
\psi &= 2\Re\left\{\lambda_1\varphi_1'(z_1) + \lambda_2\varphi_2'(z_2) + \frac{1}{\lambda_3}\varphi_3'(z_3) + \lambda_4\varphi_4'(z_4)\right\}, \\
\chi &= 2\Re\left\{\xi_1\varphi_1'(z_1) + \xi_2\varphi_2'(z_2) + \xi_3\varphi_3'(z_3) + \frac{1}{\xi_4}\varphi_4'(z_4)\right\}.
\end{aligned} \tag{4.128}$$

Since the terms λ_1, λ_2, λ_3, λ_4 and ξ_3, become zero for a monoclinic material and φ_3 is the arbitrary function, we introduce a new stress function $f_k(z_k)$ that absorbs the coefficients as follows:

$$f_1(z_1) = \varphi_1'(z_1), \quad f_2(z_2) = \varphi_2'(z_2), \quad f_3(z_3) = \frac{1}{\lambda_3}\varphi_3'(z_3), \quad f_4(z_4) = \frac{1}{\xi_4}\varphi_4'(z_4). \tag{4.129}$$

Substituting (4.128) into (4.115) by involving the new functions (4.129) and considering a monoclinic material, we obtain the following expressions of the stresses and electric displacements:

$$\begin{aligned}
\sigma_1 &= 2\Re\left\{\mu_1^2 f_1'(z_1) + \mu_2^2 f_2'(z_2) + \mu_4^2 \xi_4 f_4'(z_4)\right\}, \\
\sigma_2 &= 2\Re\left\{f_1'(z_1) + f_2'(z_2) + \xi_4 f_4'(z_4)\right\}, \\
\sigma_6 &= -2\Re\left\{\mu_1 f_1'(z_1) + \mu_2 f_2'(z_2) + \mu_4 \xi_4 f_4'(z_4)\right\}, \\
\sigma_5 &= 2\Re\left\{\mu_3 f_3'(z_3)\right\}, \\
\sigma_4 &= -2\Re\left\{f_3'(z_3)\right\}, \\
D_1 &= 2\Re\left\{\mu_1 \xi_1 f_1'(z_1) + \mu_2 \xi_2 f_2'(z_2) + \mu_4 f_4'(z_4)\right\}, \\
D_2 &= -2\Re\left\{\xi_1 f_1'(z_1) + \xi_2 f_2'(z_2) + f_4'(z_4)\right\},
\end{aligned} \tag{4.130}$$

where the prime denotes a first derivative with respect to z_k. Note that $\sigma_6 = \tau_{xy}$, $\sigma_5 = \tau_{xz}$ and $\sigma_4 = \tau_{yz}$.

The displacements and electric potentials are determined by inserting (4.130) into (4.107a)$_4$, which leads to

$$\frac{\partial u_1}{\partial x_1} = \hat{S}'^D_{11}\sigma_1 + \hat{S}'^D_{12}\sigma_2 + \hat{S}'^D_{14}\sigma_4 + \hat{S}'^D_{15}\sigma_5 + \hat{S}'^D_{16}\sigma_6 + \hat{g}'_{11}D_1 + \hat{g}'_{21}D_2,$$

$$\frac{\partial u_2}{\partial x_2} = \hat{S}'^D_{12}\sigma_1 + \hat{S}'^D_{22}\sigma_2 + \hat{S}'^D_{24}\sigma_4 + \hat{S}'^D_{25}\sigma_5 + \hat{S}'^D_{26}\sigma_6 + \hat{g}'_{12}D_1 + \hat{g}'_{22}D_2,$$

$$\frac{\partial u_3}{\partial x_2} = \hat{S}'^D_{14}\sigma_1 + \hat{S}'^D_{24}\sigma_2 + \hat{S}'^D_{44}\sigma_4 + \hat{S}'^D_{45}\sigma_5 + \hat{S}'^D_{46}\sigma_6 + \hat{g}'_{14}D_1 + \hat{g}'_{24}D_2,$$

$$\frac{\partial u_3}{\partial x_1} = \hat{S}'^D_{15}\sigma_1 + \hat{S}'^D_{25}\sigma_2 + \hat{S}'^D_{45}\sigma_4 + \hat{S}'^D_{55}\sigma_5 + \hat{S}'^D_{56}\sigma_6 + \hat{g}'_{15}D_1 + \hat{g}'_{25}D_2, \qquad (4.131)$$

$$\frac{\partial u_1}{\partial x_2} + \frac{\partial u_2}{\partial x_1} = \hat{S}'^D_{16}\sigma_1 + \hat{S}'^D_{26}\sigma_2 + \hat{S}'^D_{46}\sigma_4 + \hat{S}'^D_{56}\sigma_5 + \hat{S}'^D_{66}\sigma_6 + \hat{g}'_{16}D_1 + \hat{g}'_{26}D_2,$$

$$\frac{\partial \phi}{\partial x_1} = \hat{g}'_{11}\sigma_1 + \hat{g}'_{12}\sigma_2 + \hat{g}'_{14}\sigma_4 + \hat{g}'_{15}\sigma_5 + \hat{g}'_{16}\sigma_6 - \hat{\beta}'^\sigma_{11}D_1 - \hat{\beta}'^\sigma_{12}D_2,$$

$$\frac{\partial \phi}{\partial x_2} = \hat{g}'_{21}\sigma_1 + \hat{g}'_{22}\sigma_2 + \hat{g}'_{24}\sigma_4 + \hat{g}'_{25}\sigma_5 + \hat{g}'_{26}\sigma_6 - \hat{\beta}'^\sigma_{12}D_1 - \hat{\beta}'^\sigma_{22}D_2,$$

where u_1, u_2, u_3 are the displacements in x_1, x_2, x_3 directions and ϕ is the electric potential. For a monoclinic material, the following constants are zero: $\hat{S}'^D_{14} = \hat{S}'^D_{15} = \hat{S}'^D_{24} = \hat{S}'^D_{25} = \hat{S}'^D_{46} = \hat{S}'^D_{56} = 0$ and $\hat{g}'_{14} = \hat{g}'_{15} = \hat{g}'_{24} = \hat{g}'_{25} = 0$. Integrating the equations (4.131) we obtain

$$u_1 = 2\Re\left\{\sum_{k=1}^{4} a_{1k}f_k(z_k)\right\},$$

$$u_2 = 2\Re\left\{\sum_{k=1}^{4} a_{2k}f_k(z_k)\right\},$$

$$\qquad (4.132a)$$

$$u_3 = 2\Re\left\{\sum_{k=1}^{4} a_{3k}f_k(z_k)\right\},$$

$$\phi = 2\Re\left\{\sum_{k=1}^{4} a_{4k}f_k(z_k)\right\},$$

where

$$a_{1k} = \mu_k^2\hat{S}'^D_{11} + \hat{S}'^D_{12} - \mu_k\hat{S}'^D_{16} + \xi_k\left(\mu_k\hat{g}'_{11} - \hat{g}'_{21}\right), \quad k = 1,2$$

$$a_{2k} = \left[\mu_k^2\hat{S}'^D_{12} + \hat{S}'^D_{22} - \mu_k\hat{S}'^D_{26} + \xi_k\left(\mu_k\hat{g}'_{12} - \hat{g}'_{22}\right)\right]/\mu_k, \quad k = 1,2$$

$$a_{4k} = \left[\mu_k^2\hat{g}'_{21} + \hat{g}'_{22} - \mu_k\hat{g}'_{26} + \xi_k\left(-\mu_k\hat{\beta}'^\sigma_{12} + \hat{\beta}'^\sigma_{22}\right)\right]/\mu_k, \quad k = 1,2$$

$$a_{14} = \left(\mu_4^2\hat{S}'^D_{11} + \hat{S}'^D_{12} - \mu_4\hat{S}'^D_{16}\right)\xi_4 + \mu_4\hat{g}'_{11} - \hat{g}'_{21},$$

$$a_{24} = \left[\left(\mu_4^2\hat{S}'^D_{12} + \hat{S}'^D_{22} - \mu_4\hat{S}'^D_{26}\right)\xi_4 + \mu_4\hat{g}'_{12} - \hat{g}'_{22}\right]/\mu_4,$$

$$\qquad (4.132b)$$

$$a_{44} = \left[\left(\mu_4^2\hat{g}'_{21} + \hat{g}'_{22} - \mu_4\hat{g}'_{26}\right)\xi_4 - \mu_4\hat{\beta}'^\sigma_{12} + \hat{\beta}'^\sigma_{22}\right]/\mu_4,$$

$$a_{3k} = 0, \quad k = 1,2,4$$

$$a_{13} = 0,$$

$$a_{23} = 0,$$

$$a_{43} = 0,$$

$$a_{33} = \left(\mu_3\hat{S}_{45} - \hat{S}_{44}\right)/\mu_3.$$

Leugering [101] published a work that deals with expansion the Eshelby's theorem [63] to piezo-electricity. By using the notation (4.61), but with $k = 1,2,\ldots,4$, the Stroh matrix notation is adopted once more. Let us write the complex potentials into a vector as

$$\mathbf{f}(z) = \begin{Bmatrix} f_1(z_1) \\ f_2(z_2) \\ f_3(z_3) \\ f_3(z_4) \end{Bmatrix}, \quad z_k = x + \mu_k y, \quad k = 1,2,3,4. \tag{4.133}$$

Then the displacements and tractions can be written in the matrix form as follows:

$$\mathbf{u}(z) = 2\Re\left\{\mathbf{A}\mathbf{f}(z)\right\}, \tag{4.134a}$$

$$\mathbf{T}(z) = 2\Re\left\{\mathbf{L}\mathbf{f}(z)\right\}. \tag{4.134b}$$

The displacements and stress function vectors have the following form:

$$\mathbf{u}(z) = \begin{Bmatrix} u_1 \\ u_2 \\ u_3 \\ \phi \end{Bmatrix}, \quad \mathbf{T}(z) = \begin{Bmatrix} T_1 \\ T_2 \\ T_3 \\ T_D \end{Bmatrix}. \tag{4.135}$$

T_1, T_2, T_3 and T_D are the components of the stress function vector and electric charge q along the semi-infinite line passing through the origin of the coordinate system $x_1 x_2$ and ϕ is the electric potential. The structure of the matrices $\mathbf{A}$ and $\mathbf{L}$ is:

$$\mathbf{A} = \begin{bmatrix} a_{11} & a_{12} & a_{13} & a_{14} \\ a_{21} & a_{22} & a_{23} & a_{24} \\ a_{31} & a_{32} & a_{33} & a_{34} \\ a_{41} & a_{42} & a_{43} & a_{44} \end{bmatrix}, \quad \mathbf{L} = \begin{bmatrix} -\mu_1 & -\mu_2 & 0 & -\mu_4\xi_4 \\ 1 & 1 & 0 & \xi_4 \\ 0 & 0 & -1 & 0 \\ -\xi_1 & -\xi_2 & 0 & -1 \end{bmatrix}, \tag{4.136}$$

while the matrix elements a_{ik} are defined by (4.132b). Assuming generalized plane strain, each of the characteristic roots μ_k and each corresponding column of $\mathbf{A}$ are extracted from the eigenvalue problem of the Stroh formalism [7], [44]

$$\left[\mathbf{Q} + \mu_k\left(\mathbf{R} + \mathbf{R}^\mathsf{T}\right) + \mu_k^2\mathbf{T}\right]\mathbf{a} = 0, \tag{4.137}$$

where the matrices $\mathbf{Q}$, $\mathbf{R}$, $\mathbf{T}$ have now the dimension 4 and their elements are defined by

$$\begin{aligned} Q_{ik} &= C_{i1k1}^E, & Q_{i4} = Q_{4i} = e_{11i}, & i = 1,2,3, & Q_{44} = -\omega_{11}^\varepsilon \\ R_{ik} &= C_{i1k2}^E, & R_{i4} = R_{4i} = e_{12i}, & i = 1,2,3, & R_{44} = -\omega_{12}^\varepsilon \\ T_{ik} &= C_{i2k2}^E, & T_{i4} = T_{4i} = e_{22i}, & i = 1,2,3, & T_{44} = -\omega_{22}^\varepsilon. \end{aligned} \tag{4.138}$$

The matrix $\mathbf{A}$ is multiplied by an arbitrary normalization coefficient, i.e.

$$\mathbf{A} = \begin{bmatrix} c_1 a_{11} & c_2 a_{12} & c_3 a_{13} & c_4 a_{14} \\ c_1 a_{21} & c_2 a_{22} & c_3 a_{23} & c_4 a_{24} \\ c_1 a_{31} & c_2 a_{32} & c_3 a_{33} & c_4 a_{34} \\ c_1 a_{41} & c_2 a_{42} & c_3 a_{43} & c_4 a_{44} \end{bmatrix}, \quad \mathbf{L} = \begin{bmatrix} -c_1\mu_1 & -c_2\mu_2 & 0 & -c_4\mu_4\xi_4 \\ c_1 & c_2 & 0 & c_4\xi_4 \\ 0 & 0 & -c_3 & 0 \\ -c_1\xi_1 & -c_2\xi_2 & 0 & -c_4 \end{bmatrix}. \tag{4.139}$$

Each column is normalized arbitrary by coefficients c_i. The material eigenvalues μ_k are the roots of the characteristic sixth-order polynomial

$$\left|\mathbf{Q} + \mu_k\left(\mathbf{R} + \mathbf{R}^\mathsf{T}\right) + \mu_k^2\mathbf{T}\right| = 0. \tag{4.140}$$

The matrices $\mathbf{L}$ and $\mathbf{A}$ are associated with

$$L_{ij} = \sum_{k=1}^{4} \left[R_{ik} + \mu_j T_{ik} \right] a_{kj} = 0. \tag{4.141}$$

As for pure anisotropic elasticity, comparing the uniquely normalized Lekhnitskii matrices (4.136) with those in (4.139) derived by Hwu [20], the normalization coefficients will be eliminated by using the relations (4.141).

Boundary conditions

The generalized stress functions T_i are related to the stresses and electric displacements by

$$\sigma_{i1} = -T_{i,2}, \quad \sigma_{i2} = T_{i,1}, \quad i = 1,2,3, \quad D_1 = -T_{4,2}, \quad D_2 = T_{4,1}. \tag{4.142}$$

The operation $()_{,i}$ denotes derivation with respect to x_i. $f_k(z_k)$ are four holomorphic functions of the complex variables z_k, which will be determined through the satisfaction of the boundary conditions on the lateral surface. The first fundamental problem lies in prescribing the tractions $\hat{t}_x$, $\hat{t}_y$ and $\hat{t}_z = 0$ along the boundary by

$$\sigma_1 n_1 + \sigma_{12} n_2 = \hat{t}_1, \quad \sigma_{12} n_1 + \sigma_2 n_2 = \hat{t}_2, \quad \sigma_{13} n_1 + \tau_{23} n_2 = 0,$$
$$D_1 n_1 + D_2 n_2 = \hat{t}_4, \tag{4.143}$$

where $\hat{t}_1$, $\hat{t}_2$, $\hat{t}_3$ are the prescribed surface tractions and $\hat{t}_4$ is the prescribed electric displacement on the normal direction of the surface. The normal vector $\mathbf{n}$ is defined by (4.72). The tangential direction s is chosen so that when we face the direction of increasing s, the material lies on the right side (see Fig. 4.2). By integration of the prescribed surface tractions from zero to infinity along a straight line, we can specify the following boundary conditions for a piezoelectric notch:

$$2\Re \left\{ \mu_1 f_1(z_1) + \mu_2 f_2(z_2) + \mu_4 f_4(z_4) \right\} = \hat{T}_1 + c_1,$$
$$2\Re \left\{ f_1(z_1) + f_2(z_2) + f_4(z_4) \right\} = \hat{T}_2 + c_2,$$
$$2\Re \left\{ f_3(z_3) \right\} = c_3, \tag{4.144}$$
$$2\Re \left\{ \xi_1 f_1(z_1) + \xi_2 f_2(z_2) + \xi_4 f_4(z_4) \right\} = \hat{T}_4 + c_4.$$

The second fundamental problem is represented by displacements prescribed along the boundary. By using (4.132a) we get

$$2\Re \left\{ \sum_{k=1}^{4} a_{1k} f_k(z_k) \right\} = \hat{u}_1,$$

$$2\Re \left\{ \sum_{k=1}^{4} a_{2k} f_k(z_k) \right\} = \hat{u}_2,$$

$$2\Re \left\{ \sum_{k=1}^{4} a_{3k} f_k(z_k) \right\} = \hat{u}_3, \tag{4.145}$$

$$2\Re \left\{ \sum_{k=1}^{4} a_{4k} f_k(z_k) \right\} = \hat{\phi},$$

where $\hat{u}_1$, $\hat{u}_2$, $\hat{u}_3$ are the prescribed displacements and $\hat{\phi}$ is the prescribed electric potential.

5 Methods and results

5.1 Stress singularity of an anisotropic bi-material notch and interface crack

In the present work, two types of common general stress concentrators are considered – an interface crack and a bi-material notch. When a monoclinic material is considered, the in-plane and anti-plane relations are decoupled. When a sample is loaded in the $x_1 x_2$ plane, we can focus only on the in-plane problem. There are two well known plane elasticity methods for stress singularity description – the Lekhnitskii and the Stroh formalism. They are based on the theory of complex variable functions. It simplifies the solution so that the elastic variable description is shrunk only to three material eigenvalues. The Lekhnitskii formalism [6] was derived for a cylindrical body bounded by a cylindrical surface and all relation are in terms of the elastic compliances. In addition, the stresses and displacements depend only on x_1, x_2, which is satisfied only by the assumption of the in-plane loading. The Stroh formalism [7, 8, 9, 63] starts with the two-dimensional displacements and its relations depend on the elastic stiffnesses.

As it was mentioned earlier in section 4.1.7, where a transversally isotropic, or more generally a monoclinic material is considered, both Stroh and Lekhnitskii formalisms are formally indistinguishable, i.e. the material eigenvalues, stress and displacement relations and singularity exponents have the same form. Suo [44] introduced the Lekhnitskii-Eshelby-Stroh formalism, which linked both techniques together. Its structure is described in section 4.1.7. That approach enables simplification in the eigenvalue extraction or eliminating the scaling factors needed in the Stroh formalism. The LES formalism is dominantly used for investigating stress singularities of V-notches and transversally isotropic bi-material wedges, of which stress term exponents are real values, as was reported for example in [19, 39, 102, 103, 104, 105, 106].

All previously mentioned authors assumed that the singularity exponents δ are only real values. Then, the relations (4.63) for the stresses and displacements can be expressed as

$$\mathbf{u}(z) = 2\Re\left\{\mathbf{A}\mathbf{f}(z)\right\} = 2\Re\left\{\mathbf{A}\mathbf{Z}^\delta \mathbf{v}\right\}, \tag{5.1a}$$

$$\mathbf{T}(z) = 2\Re\left\{\mathbf{L}\mathbf{f}(z)\right\} = 2\Re\left\{\mathbf{L}\mathbf{Z}^\delta \mathbf{v}\right\}, \tag{5.1b}$$

where

$$\mathbf{v} = \begin{Bmatrix} v_1 \\ v_2 \end{Bmatrix} \tag{5.2}$$

is the eigenvector corresponding to the singular order δ. Moreover, due to the assumption of a monoclinic material, the structure of the material matrices $\mathbf{A}$ and $\mathbf{L}$ defined in Eqs. (4.65) and (4.60b) enables that the in-plane and anti-plane components of the displacements and stresses can be decoupled. Then, the following analysis is considered as a two-dimensional in-plane problem and the dimension of the material matrices is 2×2, i.e.

$$\mathbf{A} = \begin{bmatrix} a_{11} & a_{12} \\ a_{21} & a_{22} \end{bmatrix}, \quad \mathbf{L} = \begin{bmatrix} -\mu_1 & -\mu_2 \\ 1 & 1 \end{bmatrix}, \quad \mathbf{u} = \begin{Bmatrix} u_1 \\ u_2 \end{Bmatrix}, \quad \mathbf{T} = \begin{Bmatrix} T_1 \\ T_2 \end{Bmatrix}. \tag{5.3}$$

The elements a_{ij}, $i,j = 1,2$, are defined in Eq. (4.60b). When the notch angle ω_i exceeds a certain angle, the eigenvalue δ turns into a complex value and the form in (5.1) is not valid, or more precisely, the neglected imaginary components corresponding to the individual singularity exponents δ are not equal and do not mutually subtract.

Setting the notch angles ω_i to their limit values 2π, an interface crack can be modelled. This special case has been mostly treated as the Hilbert problem [42, 44, 57, 107, 108]. In such case, the singular solution has an oscillatory character and the singularity exponent equals to

$$\delta = \frac{1}{2} \pm i\varepsilon, \tag{5.4}$$

where ε is so called oscillatory index. Suo [44] proposed the generalized Dundurs parameters [109], by which the oscillatory index is expressed as

$$\varepsilon = \frac{1}{2\pi} \ln \left(\frac{1-\beta}{1+\beta} \right). \tag{5.5}$$

The parameter β is derived in [44, 110] only for a material with principal axes coincident with the reference coordinate system. Considering a monoclinic material defined in Eq. (4.10), the relation (5.5) has to be modified.

It follows from the survey that in the literature, there has been a gap in investigation of the very closed notches whose stress term order become complex-valued. This state can occur when the delaminated interface has face angles very close to the interface crack. In the following paragraphs it will be presented that the LES formalism described in the previously stated papers can be extended through notches with the complex-valued oscillatory index to interface cracks. The definitions for the stresses and displacements have a slightly different form. The next goal is the expansion of the LES formalism for piezoelectric materials. However, the theory for pure elastic anisotropic bi-materials has to be firstly investigated in order to get limits of its application.

5.1.1 Formulation of the fundamental equations describing the stress singularity of a transversally isotropic bi-material notch

Profant et al. [19] proposed the formulation of the orthotropic bi-material notch based on the LES formalism and following the Hwu's concept [17] which generalizes Eq. (5.1) to the case of the complex singularity exponent δ. Assuming stress singularity at the wedge apex, the complex potentials are expressed as

$$\mathbf{f}(z) = \mathbf{Z}^\delta \mathbf{v}. \tag{5.6}$$

If the singularity exponent δ is generally a complex number, the stress function vectors and displacements are considered in the following form:

$$\mathbf{u}(z) = \mathbf{A}\mathbf{Z}^\delta \mathbf{v} + \overline{\mathbf{A}\mathbf{Z}}^\delta \mathbf{w}, \tag{5.7a}$$

$$\mathbf{T}(z) = \mathbf{L}\mathbf{Z}^\delta \mathbf{v} + \overline{\mathbf{L}\mathbf{Z}}^\delta \mathbf{w}, \tag{5.7b}$$

where $\mathbf{A}$ and $\mathbf{L}$ have the structure (5.3) and their elements are defined in (4.65) and (4.60b). $\mathbf{v} = \{v_1, v_2\}^\mathsf{T}$, $\mathbf{w} = \{w_1, w_2\}^\mathsf{T}$ are the eigenvectors associated with the eigenvalue δ, which is determined through the satisfaction of the boundary conditions at the notch tip. If δ is a real value, the eigenvectors $\mathbf{v}$ and $\mathbf{w}$ will be complex conjugate and the displacements and stress function vectors are obtained in the form of (5.1).
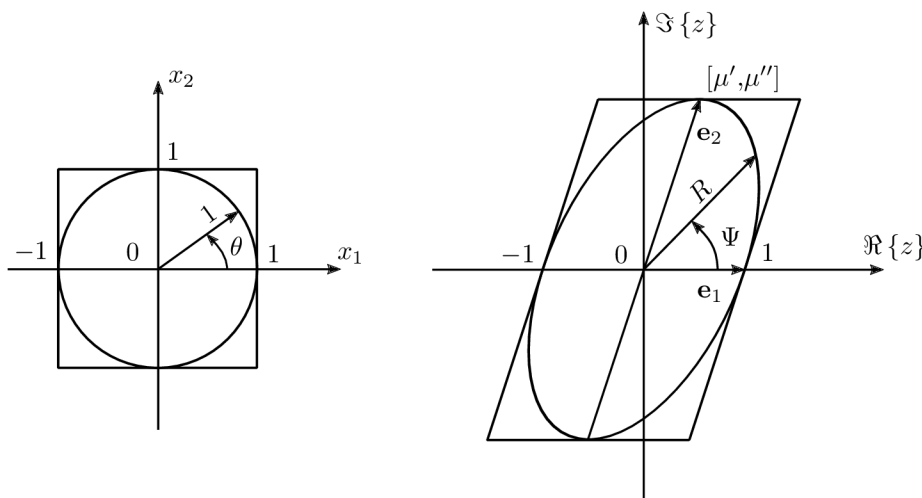
Fig. 5.1: Cartesian coordinates mapping to a complex plane. An unit circle is mapped to the ellipse defined by vectors $\mathbf{e}_1$, $\mathbf{e}_2$.

5.1.2 Transversally isotropic materials

The LES formalism is defined under the assumption of transversally isotropic, or generally monoclinic materials if principal material directions L and T are arbitrary oriented in x_1x_2 plane. The complex functions $\mathbf{Z}^\delta$ are of the form

$$\mathbf{Z}^\delta = \mathrm{diag}\left[z_1^\delta, z_2^\delta\right],\tag{5.8}$$

where

$$z_i = x_1 + \mu_i x_2, \quad i = 1,2.\tag{5.9}$$

The material eigenvalues μ_i, $i = 1,2$ are extracted from Eq. (4.49a) for each material. Note that if anti-plane relations are taken into account, one more material eigenvalue μ_3 is obtained.

It is more convenient to express the independent variables x_1, x_2 appearing in 5.9 in terms of the polar coordinates r, θ, while the stresses and displacements are considered in the Cartesian coordinates x_i. We say that the formalism is defined in dual coordinate systems [9, 17]. With the origin located at the wedge apex, the transformation relations between the Cartesian and polar coordinates are

$$x_1 = r\cos\theta, \qquad x_2 = r\sin\theta.\tag{5.10}$$

By substitution (5.10) into (5.9), the definition (5.8) holds

$$\mathbf{Z}^\delta = \mathrm{diag}\left[r^\delta\left(\cos\theta + \mu_1\sin\theta\right)^\delta, r^\delta\left(\cos\theta + \mu_2\sin\theta\right)^\delta\right].\tag{5.11}$$

To make later differentiation of $\mathbf{Z}$ easier, a mathematical simplification introduced by Ting [9] is implemented. Let us define the material eigenvalue as a summation of its real and imaginary part, i.e. $\mu_i = \mu_i' + i\mu_i''$. Then, the complex variable

$$z_i = \left(x_1 + \mu_i' x_2\right) + i\mu_i'' x_2\tag{5.12}$$

is a mapping from the x_1x_2-plane to the complex plane (see Fig. 5.1) [111]. It represents a mathematical trick, where the whole space, over which the solution is searched, is deformed
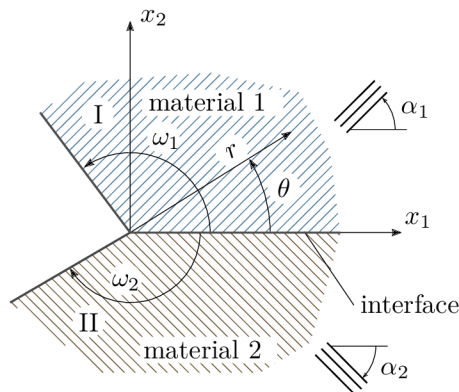
Fig. 5.2: Geometry of a bi-material notch characterized by two regions I and II. The notch faces are defined by angles ω_1 and ω_2. The material interface is always considered at $\theta = 0$. The angles α_1 and α_2 denote the fibre orientation, i.e. the longitudinal material direction.

in order to avoid the complicated description of an anisotropic continuum properties in a non-deformed space. The space distortion supplies the material anisotropy and it is proportional to $[\mu',\mu'']$ [9]. Eq. (5.11) is then defined as follows:

$$\mathbf{Z}^\delta = \text{diag} \left[r^\delta R_1^\delta \, \text{e}^{i\delta\Psi_1}, r^\delta R_2^\delta \, \text{e}^{i\delta\Psi_2} \right], \tag{5.13}$$

where

$$R_i^2 = \left(\cos\theta + \mu_i' \sin\theta \right)^2 + \left(\mu_i'' \sin\theta \right)^2, \quad i = 1,2 \tag{5.14}$$

and

$$\Psi_i = \begin{cases} \arctan \left(\frac{\mu_i'' \sin\theta}{\cos\theta + \mu_i' \sin\theta} \right) & \text{for} \quad \theta > -\pi \\ -\pi & \text{for} \quad \theta = -\pi \end{cases}, \quad i = 1,2. \tag{5.15}$$

Note that in comparison to [19], the relation (5.15) is reduced from four to only two cases. This could be done due to using Python's `np.arctan2`[1] function, which fixes a discontinuity of the arctangent and simulates the complex function $\text{Arg}(z)$. The complex conjugation of (5.13) is performed simply as

$$\overline{\mathbf{Z}}^\delta = \text{diag} \left[r^\delta R_1^\delta \, \text{e}^{-i\delta\Psi_1}, r^\delta R_2^\delta \, \text{e}^{-i\delta\Psi_2} \right]. \tag{5.16}$$

5.1.3 Formulation of the eigenvalue problem

In the previous sections, the fundamental matrices of the LES formalism were defined as functions of the singularity exponent δ, which is a root of the characteristic equation for the notch geometry and prescribed notch tip boundary conditions. Let us consider a bi-material notch illustrated in Fig. 5.2, where each wedge occupies the region $0 < \theta < \omega_1$ or $\omega_2 < \theta < 0$. The notch faces are stress free which imposes the following boundary conditions:

$$\begin{aligned} \mathbf{T}^{\text{I}}(\omega_1) &= 0, \\ \mathbf{T}^{\text{II}}(\omega_2) &= 0. \end{aligned} \tag{5.17}$$

It is assumed that the bi-material interface coincides with x_1 axis. The displacement and traction continuity conditions are prescribed along the interface $\theta = 0$ as

$$\mathbf{u}^{\text{I}}(0) = \mathbf{u}^{\text{II}}(0), \tag{5.18a}$$

---

[1]The functions is contained in numpy library, of which procedures are based on FORTRAN LAPACK functions.

$$\mathbf{T}^{\mathrm{I}}(0) = \mathbf{T}^{\mathrm{II}}(0). \tag{5.18b}$$

A bi-material notch composed of two monoclinic materials with the principal material symmetry arbitrary oriented in the plane $x_3 = 0$ is considered. By substituting (5.7) into (5.17) and (5.18), one gets eight homogeneous algebraic equations for the exponent δ, which can be written in the matrix form as

$$\begin{bmatrix} \mathbf{L}^{\mathrm{I}}\mathbf{Z}_1^{\mathrm{I}\delta}(\mathbf{L}^{\mathrm{I}})^{-1} & \overline{\mathbf{L}}^{\mathrm{I}}\overline{\mathbf{Z}}_1^{\mathrm{I}\delta}(\overline{\mathbf{L}}^{\mathrm{I}})^{-1} & \mathbf{0} & \mathbf{0} \\ \mathbf{0} & \mathbf{0} & \mathbf{L}^{\mathrm{II}}\mathbf{Z}_2^{\mathrm{II}\delta}(\mathbf{L}^{\mathrm{II}})^{-1} & \overline{\mathbf{L}}^{\mathrm{II}}\overline{\mathbf{Z}}_2^{\mathrm{II}\delta}(\overline{\mathbf{L}}^{\mathrm{II}})^{-1} \\ \mathbf{A}^{\mathrm{I}}\mathbf{Z}_0^{\mathrm{I}\delta}(\mathbf{L}^{\mathrm{I}})^{-1} & \overline{\mathbf{A}}^{\mathrm{I}}\overline{\mathbf{Z}}_0^{\mathrm{I}\delta}(\overline{\mathbf{L}}^{\mathrm{I}})^{-1} & -\mathbf{A}^{\mathrm{II}}\mathbf{Z}_0^{\mathrm{II}\delta}(\mathbf{L}^{\mathrm{II}})^{-1} & -\overline{\mathbf{A}}^{\mathrm{II}}\overline{\mathbf{Z}}_0^{\mathrm{II}\delta}(\overline{\mathbf{L}}^{\mathrm{II}})^{-1} \\ \mathbf{L}^{\mathrm{I}}\mathbf{Z}_0^{\mathrm{I}\delta}(\mathbf{L}^{\mathrm{I}})^{-1} & \overline{\mathbf{L}}^{\mathrm{I}}\overline{\mathbf{Z}}_0^{\mathrm{I}\delta}(\overline{\mathbf{L}}^{\mathrm{I}})^{-1} & -\mathbf{L}^{\mathrm{II}}\mathbf{Z}_0^{\mathrm{II}\delta}(\mathbf{L}^{\mathrm{II}})^{-1} & -\overline{\mathbf{L}}^{\mathrm{II}}\overline{\mathbf{Z}}_0^{\mathrm{II}\delta}(\overline{\mathbf{L}}^{\mathrm{II}})^{-1} \end{bmatrix} \begin{Bmatrix} \mathbf{L}^{\mathrm{I}}\mathbf{v}^{\mathrm{I}} \\ \overline{\mathbf{L}}^{\mathrm{I}}\mathbf{w}^{\mathrm{I}} \\ \mathbf{L}^{\mathrm{II}}\mathbf{v}^{\mathrm{II}} \\ \overline{\mathbf{L}}^{\mathrm{II}}\mathbf{w}^{\mathrm{II}} \end{Bmatrix} = \mathbf{0}. \tag{5.19}$$

The matrix $\mathbf{0}$ denotes a 2×2 zero matrix on the left-hand side and a 8×1 zero vector on the right-hand side of the equation (5.19). The subscript denotes the index of the angle ω_i, while the superscript stands for association with the material region. With the reference to the assumption that the interface always coincides with x_1 axis, i.e. $\omega_0 = 0°$, it follows that

$$\mathbf{Z}_0^{k\delta} = \mathbf{I}, \quad \overline{\mathbf{Z}}_0^{k\delta} = \mathbf{I}, \quad k = \mathrm{I}, \mathrm{II}, \tag{5.20}$$

where $\mathbf{I}$ is a 2×2 identity matrix. Introducing

$$\mathbf{X}_j^k = \mathbf{L}^k\mathbf{Z}_j^{k\delta}\left(\omega_j\right)(\mathbf{L}^k)^{-1}, \quad \overline{\mathbf{X}}_j^k = \overline{\mathbf{L}}^k\overline{\mathbf{Z}}_j^{k\delta}\left(\omega_j\right)(\overline{\mathbf{L}}^k)^{-1}, \tag{5.21a}$$

$$\mathbf{Y}_j^k = (\overline{\mathbf{X}}_j^k)^{-1}\mathbf{X}_j^k, \quad j = 1, 2, \tag{5.21b}$$
$$j = 1 \implies k = \mathrm{I}, \quad j = 2 \implies k = \mathrm{II},$$

$$\mathbf{B}_0^k = i\mathbf{A}^k(\mathbf{L}^k)^{-1}, \quad \overline{\mathbf{B}}_0^k = -i\overline{\mathbf{A}}^k(\overline{\mathbf{L}}^k)^{-1}, \tag{5.21c}$$

the system (5.19) can be rewritten as

$$\begin{bmatrix} \mathbf{X}_1^{\mathrm{I}} & \overline{\mathbf{X}}_1^{\mathrm{I}} & \mathbf{0} & \mathbf{0} \\ \mathbf{0} & \mathbf{0} & \mathbf{X}_2^{\mathrm{II}} & \overline{\mathbf{X}}_2^{\mathrm{II}} \\ \mathbf{B}_0^{\mathrm{I}} & -\overline{\mathbf{B}}_0^{\mathrm{I}} & -\mathbf{B}_0^{\mathrm{II}} & \overline{\mathbf{B}}_0^{\mathrm{II}} \\ \mathbf{I} & \mathbf{I} & -\mathbf{I} & -\mathbf{I} \end{bmatrix} \begin{Bmatrix} \mathbf{L}^{\mathrm{I}}\mathbf{v}^{\mathrm{I}} \\ \overline{\mathbf{L}}^{\mathrm{I}}\mathbf{w}^{\mathrm{I}} \\ \mathbf{L}^{\mathrm{II}}\mathbf{v}^{\mathrm{II}} \\ \overline{\mathbf{L}}^{\mathrm{II}}\mathbf{w}^{\mathrm{II}} \end{Bmatrix} = \mathbf{0}. \tag{5.22}$$

The equations in (5.22) can be reduced to the algebraic system of two equations

$$\mathbf{K}\left(\delta\right)\mathbf{L}^{\mathrm{I}}\mathbf{v}^{\mathrm{I}} = \mathbf{0}, \tag{5.23}$$

where $\mathbf{0}$ is now a 2×1 zero vector and the matrix $\mathbf{K}$ is expressed by

$$\mathbf{K} = \mathbf{B}_0^{\mathrm{I}} + \overline{\mathbf{B}}_0^{\mathrm{I}}\mathbf{Y}_1^{\mathrm{I}} - \left(\mathbf{B}_0^{\mathrm{II}} + \overline{\mathbf{B}}_0^{\mathrm{II}}\mathbf{Y}_2^{\mathrm{II}}\right)\left(\mathbf{I} - \mathbf{Y}_2^{\mathrm{II}}\right)^{-1}\left(\mathbf{I} - \mathbf{Y}_1^{\mathrm{I}}\right). \tag{5.24}$$

The reduction is described in detail in Appendix B. The eigenvectors $\mathbf{v}^{\mathrm{I}}$ are extracted by the backward substitution of δ to $\mathbf{K}\left(\delta\right)$. To avoid computational complications, the eigenproblem (5.24) was modified by Desmorat and Leckie [110], presented also in [112], but only for cases when δ is real. The real part of the eigenvector $\mathbf{L}^{\mathrm{I}}\mathbf{v}^{\mathrm{I}}$ is defined as

$$\Re\left\{\mathbf{L}^{\mathrm{I}}\mathbf{v}^{\mathrm{I}}\right\} = \frac{1}{2}\left(\mathbf{L}^{\mathrm{I}}\mathbf{v}^{\mathrm{I}} + \overline{\mathbf{L}}^{\mathrm{I}}\overline{\mathbf{v}}^{\mathrm{I}}\right). \tag{5.25}$$

After applying this procedure, it can be proved that if the eigenvalue δ is real, the eigenvectors $\mathbf{v}$ and $\mathbf{w}$ are complex conjugate. The relation (B.2a) can be rewritten as

$$\overline{\mathbf{L}}^{\mathrm{I}}\overline{\mathbf{v}}^{\mathrm{I}} = -\mathbf{Y}_1^{\mathrm{I}}\mathbf{L}^{\mathrm{I}}\mathbf{v}^{\mathrm{I}}. \tag{5.26}$$

By combination of two previous equations (5.25) and (5.26), the real part (5.25) can be expressed as

$$\Re\left\{\mathbf{L}^{\mathrm{I}}\mathbf{v}^{\mathrm{I}}\right\} = \frac{1}{2}\left(\mathbf{L}^{\mathrm{I}}\mathbf{v}^{\mathrm{I}} - \mathbf{Y}_1^{\mathrm{I}}\mathbf{L}^{\mathrm{I}}\mathbf{v}^{\mathrm{I}}\right) = \frac{1}{2}\left(\mathbf{I} - \mathbf{Y}_1^{\mathrm{I}}\right)\mathbf{L}^{\mathrm{I}}\mathbf{v}^{\mathrm{I}}. \tag{5.27}$$

Substituting $\mathbf{L}^{\mathrm{I}}\mathbf{v}^{\mathrm{I}}$ from Eq. (5.27) into (5.23) we get the modified eigenproblem

$$\mathbf{K}\left(\mathbf{I} - \mathbf{Y}_1^{\mathrm{I}}\right)^{-1}2\Re\left\{\mathbf{L}^{\mathrm{I}}\mathbf{v}^{\mathrm{I}}\right\} = \mathbf{0}, \tag{5.28}$$

which leads to the equality between the eigenvectors $\mathbf{v}$ and $\mathbf{w}$ if δ is real:

$$\mathbf{w} = \overline{\mathbf{v}}. \tag{5.29}$$

The generally complex eigenvector $\mathbf{v}^{\mathrm{I}}$ is evaluated from (5.27) as

$$\mathbf{v}^{\mathrm{I}} = \left(\mathbf{L}^{\mathrm{I}}\right)^{-1}\left(\mathbf{I} - \mathbf{Y}_1^{\mathrm{I}}\right)^{-1}2\Re\left\{\mathbf{L}^{\mathrm{I}}\mathbf{v}^{\mathrm{I}}\right\}. \tag{5.30}$$

The eigenvector $\mathbf{v}^{\mathrm{II}}$ for the second material is computed from (B.5) as

$$\mathbf{v}^{\mathrm{II}} = \left(\mathbf{L}^{\mathrm{II}}\right)^{-1}\left(\mathbf{I} - \mathbf{Y}_2^{\mathrm{II}}\right)^{-1}\left(\mathbf{I} - \mathbf{Y}_1^{\mathrm{I}}\right)\mathbf{L}^{\mathrm{I}}\mathbf{v}^{\mathrm{I}}. \tag{5.31}$$

Note that to get an unique value of the stress intensity factor H, we have to normalize the vector $\mathbf{L}^{\mathrm{I}}\mathbf{v}^{\mathrm{I}}$ in (5.30). The remaining eigenvectors, i.e. $\mathbf{L}^{\mathrm{II}}\mathbf{v}^{\mathrm{II}}$ and $\overline{\mathbf{L}}^{\mathrm{I}}\mathbf{w}^{\mathrm{I}}$, $\overline{\mathbf{L}}^{\mathrm{II}}\mathbf{w}^{\mathrm{II}}$ satisfy the normality automatically.

In the case of complex δ, the previous formalism can be also used. However, some relations have to be modified. Let us start from the right-hand side of Eq. (5.27). Employing the general form (B.2a) we get

$$\frac{1}{2}\left(\mathbf{I} - \mathbf{Y}_1^{\mathrm{I}}\right)\mathbf{L}^{\mathrm{I}}\mathbf{v}^{\mathrm{I}} = \frac{1}{2}\left(\mathbf{L}^{\mathrm{I}}\mathbf{v}^{\mathrm{I}} + \overline{\mathbf{L}}^{\mathrm{I}}\mathbf{w}^{\mathrm{I}}\right) = \mathbf{L}_a^{\mathrm{I}}\mathbf{v}_a^{\mathrm{I}}, \tag{5.32}$$

where the index a stands for an average value of both eigenvectors with no physical meaning. By solving the modified eigenproblem (5.28) for a complex δ, the resulting eigenvector would not be purely real. Therefore, Eq. (5.28) can be expanded as

$$\mathbf{K}\left(\mathbf{I} - \mathbf{Y}_1^{\mathrm{I}}\right)^{-1}2\mathbf{L}_a^{\mathrm{I}}\mathbf{v}_a^{\mathrm{I}} = \mathbf{0}. \tag{5.33}$$

The eigenvector $\mathbf{v}^{\mathrm{I}}$ is calculated from the accordingly modified relations (5.30), i.e.

$$\mathbf{v}^{\mathrm{I}} = \left(\mathbf{L}^{\mathrm{I}}\right)^{-1}\left(\mathbf{I} - \mathbf{Y}_1^{\mathrm{I}}\right)^{-1}2\mathbf{L}_a^{\mathrm{I}}\mathbf{v}_a^{\mathrm{I}}. \tag{5.34}$$

The eigenvector $\mathbf{v}^{\mathrm{II}}$ of the second material is obtained from Eq. (5.31). The values of $\mathbf{w}^{\mathrm{I}}$ and $\mathbf{w}^{\mathrm{II}}$ are determined from (B.2a) and (B.2b):

$$\mathbf{w}^{\mathrm{I}} = -\left(\overline{\mathbf{L}}^{\mathrm{I}}\right)^{-1}\mathbf{Y}_1^{\mathrm{I}}\mathbf{L}^{\mathrm{I}}\mathbf{v}^{\mathrm{I}}, \tag{5.35a}$$

$$\mathbf{w}^{\mathrm{II}} = -\left(\overline{\mathbf{L}}^{\mathrm{II}}\right)^{-1}\mathbf{Y}_2^{\mathrm{II}}\mathbf{L}^{\mathrm{II}}\mathbf{v}^{\mathrm{II}}. \tag{5.35b}$$

	Young's modulus [GPa]		Poisson's ratio [-]		shear modulus [GPa]	fibre orientation [°]
	E_L	E_T	ν_{LT}	$\nu_{TT'}$	G_{LT}	α
material 1	100	50	0.3	0.3	30	0
material 2	400	50	0.3	0.3	30	90

Tab. 5.1: Material properties of transversally isotropic materials. It follows from (4.12) and (4.16) that $E_T = E_{T'}$.

To get a non-trivial solution of (5.28), the following relation must be held:

$$\det\left[\mathbf{K}\left(\mathbf{I} - \mathbf{Y}_1^{\mathrm{I}}\right)^{-1}\right] = 0, \tag{5.36}$$

which leads to a nonlinear characteristic equation, which has an unlimited number of solutions δ_i. In the literature, δ is sometimes called eigenvalue. This is not mathematically exact, but it fulfils the physical meaning. Since the strain energy cannot be unbounded from the physical point of view, eigenvalues from the interval $0 < \Re\{\delta\} < 1$ have to be considered.

The previous procedure has determined the parameters for defining the so-called regular solution. It can be proved that $\hat{\delta}_i = -\delta_i$ also satisfies the characteristic equation (5.33), see [113]. This so-called auxiliary solution is a mathematical tool allowing the evaluation the GSIFs via the Betti's theorem-based path-independent integral introduced hereafter. It represents a stress field at the notch tip with singularity stronger than the regular one and hence it exhibits unbounded energy. By reinserting $\hat{\delta}_i$ into (5.33) and by employing (5.34), the corresponding auxiliary eigenvector $\hat{\mathbf{v}}^{\mathrm{I}}$ can be evaluated as well as the remaining auxiliary eigenvectors $\hat{\mathbf{v}}^{\mathrm{II}}$, $\hat{\mathbf{w}}^{\mathrm{I}}$ and $\hat{\mathbf{w}}^{\mathrm{II}}$, by application of (5.31), (5.35a) and (5.35b).

Example 1: Material eigenvalues of a transversally isotropic material A transversally isotropic material with fibres oriented in the x_1x_2-plane by the angle α_i (see Fig. 5.2) is considered. The material properties are stated in Tab. 5.1. In the first step, the determination of the material eigenvalues μ_1 and μ_2 for in-plane field was carried out. Under the assumption of the monoclinic material and in-plane problem only, the equation (4.49a) is reduced to

$$l_4(\mu) = 0, \tag{5.37}$$

where l_4 is defined in (4.49b). As the equation is written in the form of a polynomial of the unknown variable μ, the Python function `polynomial.polyroots` from the `numpy` package is suitable to be used instead of a general root-finding algorithm. Nevertheless, the procedure requires an attention in its output values. They have to be reordered so that the requirement (4.50) is satisfied. If the principal material directions coincide with global Cartesian axes x_1 and x_2, i.e. the longitudinal axis is either parallel or perpendicular to x_1-axis, the material constants $\hat{S}_{16}$ and $\hat{S}_{26}$ vanish. For such case, Suo [44] developed an explicit solution for determination of the material eigenvalues. The characteristic equation (5.37) can be then expressed in the form

$$\lambda\mu^4 + 2\rho\lambda^{\frac{1}{2}}\mu^2 + 1 = 0, \tag{5.38a}$$

where

$$\lambda = \frac{\hat{S}_{11}}{\hat{S}_{22}}, \quad \rho = \frac{2\hat{S}_{12} + \hat{S}_{66}}{2\sqrt{\hat{S}_{11}\hat{S}_{22}}}. \tag{5.38b}$$

	μ_1	μ_2
material 1, $\alpha_1 = 0°$	$-0.1478 + 1.1656i$	$0.1478 + 1.1656i$
material 2, $\alpha_2 = 0°$	$0.7805i$	$3.4766i$
material 1 $\alpha_1 = 40°$	$-0.1635 + 0.8948i$	$-0.1598 + 1.1522i$

Tab. 5.2: Material eigenvalues for certain material configurations.

Fig. 5.3: The HSV phase portrait of the characteristic function $f(\delta) = \det[\mathbf{K}(\mathbf{I} - \mathbf{Y}_1^{\mathrm{I}})^{-1}]$ defined in (5.36) and the contour plot for $f(\delta) = 0$ for a bi-material notch with geometry $\omega_1 = 125°$, $\omega_2 = -180°$ and materials defined in Tab. 5.1. The intersections of the curves of different colour give the searched roots.

The roots of the characteristic equation (5.38a) are determined by

$$\mu_1 = i\lambda^{-\frac{1}{4}}(n+m), \quad \mu_2 = i\lambda^{-\frac{1}{4}}(n-m), \quad \text{for} \quad 1 < \rho < \infty,$$
$$\mu_1 = \lambda^{-\frac{1}{4}}(in+m), \quad \mu_2 = \lambda^{-\frac{1}{4}}(in-m), \quad \text{for} \quad -1 < \rho < 1, \qquad (5.39)$$
$$\mu_1 = \mu_2 = i\lambda^{-\frac{1}{4}}, \quad \text{for} \quad \rho = 1,$$

where

$$n = \sqrt{\frac{1+\rho}{2}}, \quad m = \sqrt{\left|\frac{1-\rho}{2}\right|}. \qquad (5.40)$$

The case $\rho = 1$ corresponds to a material with the cubic symmetry and the case $\lambda = \rho = 1$ to the isotropic material, which are together the so-called degenerated states of anisotropy.

The material eigenvalues have the form of $\mu_{1,2} = \mp a + bi$ or they are purely imaginary for two fibre configurations described in the previous paragraph. If an arbitrary fibre orientation is included, the real and imaginary parts of μ_1 and μ_2 become distinct. The compliance matrix has to be recomputed by using the transformation relation (4.26). Values for three material configurations are stated in Tab. 5.2.
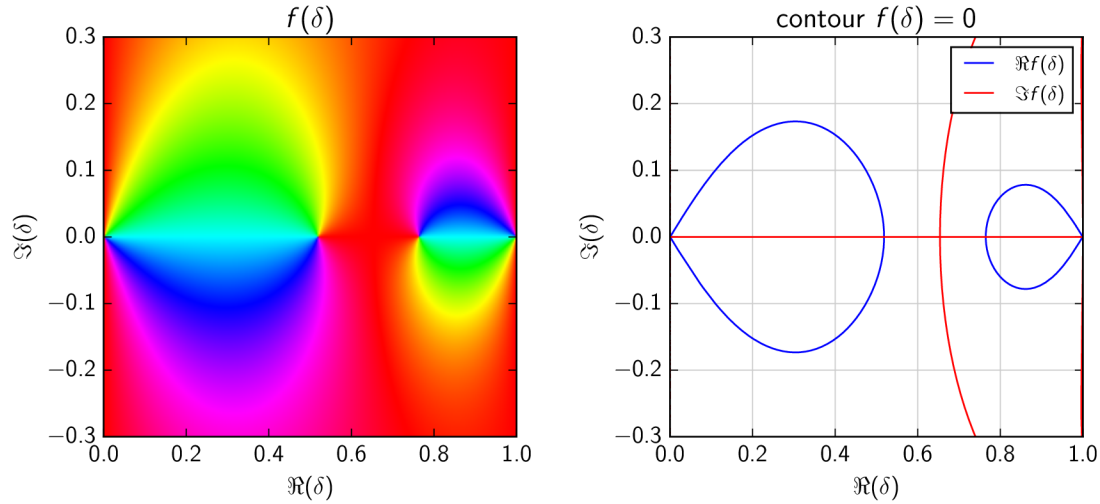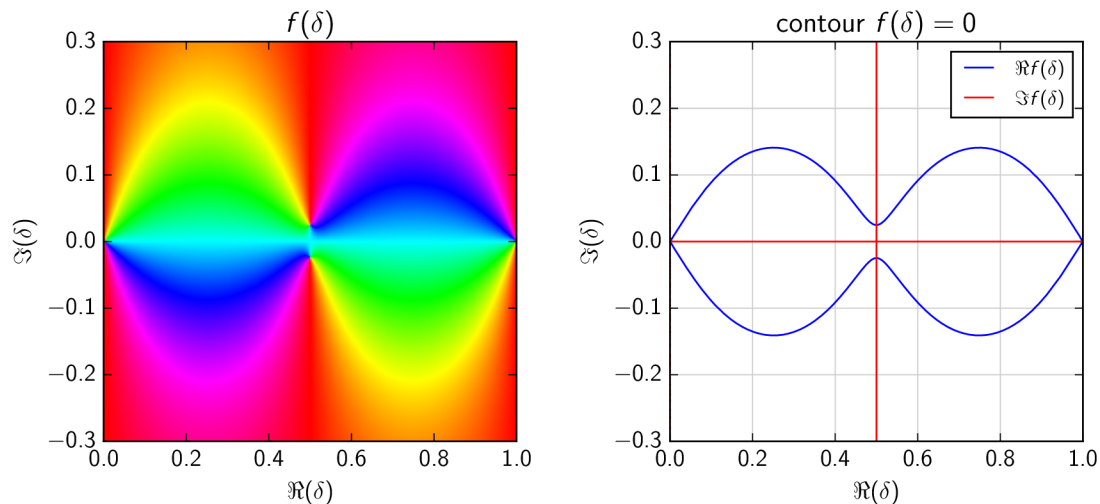
Fig. 5.4: The HSV phase portrait of the characteristic function $f(\delta) = \det[\mathbf{K}(\mathbf{I} - \mathbf{Y}_1^{\mathrm{I}})^{-1}]$ defined in (5.36) and the contour plot for $f(\delta) = 0$ for an interface crack with geometry $\omega_1 = 180°$, $\omega_2 = -180°$ and materials defined in Tab. 5.1. The intersections of the curves of different colour give the searched roots.

Example 2: Singularity exponents and eigenvectors of a transversally isotropic bi-material notch The characteristic function (5.36) is a complex function, which has generally complex roots. A convenient tool to investigate the complex function development is the phase portrait described in Appendix A, which is based on the recomputing of a complex number in terms of hue, saturation and value. Let us consider a bi-material notch defined by angles $\omega_1 = 125°$, $\omega_2 = -180°$ and material characteristics defined in Tab. 5.1. The complex function $f(\delta) = \det[\mathbf{K}(\mathbf{I} - \mathbf{Y}_1^{\mathrm{I}})^{-1}]$ defined in Eq. (5.36) is depicted in Fig. 5.3. It can be seen that on the interval $0 < \Re\{\delta\} < 1$ the characteristic function has two real roots, i.e. $\delta_1 = 0.5186$ and $\delta_2 = 0.7647$. In the interval limits $[0,0]$ and $[1,0]$, which delimit the singular exponents, the transcendental characteristic function has two poles. The same root identification can be done for a wedge with complex roots. The characteristic function for an interface crack, i.e. $\omega_1 = 180°$, $\omega_2 = -180°$ is depicted in Fig. 5.4. It is obvious that there are two complex conjugate roots $\delta_1 = 0.5 + 0.02474i$, $\delta_2 = 0.5 - 0.02474i$ and two poles in the points $\delta = 0$ and $\delta = 1$. Note that the determinant of the matrix on the left-hand side of (5.19) has roots at points $\delta = 0$ and $\delta = 1$.

The root identification algorithm was developed in Python programming language, based on the **findroot** from the **mpmath** library [114]. The default secant method was used and the tolerance error has been set to 1×10^{-15}. It is advised to prove whether the calculated solution represents the root. By re-inserting the root into the characteristic equation (5.36) a numerical zero has to be obtained. The second possibility is to set **verify=True** into key arguments of the root-finding method. The next verification that could be done is to check continuity of displacements and tractions (along the material interface). This will be discussed in the next numerical example.

Fig. 5.5 shows a dependence of the singularity exponents δ on the notch angle ω_1 while the angle $\omega_2 = -180$ remains fixed. For an unreal limit case $\omega_1 = 0$, δ_1 is approaching 1, while δ_2 goes to 2. The second term δ_2 is singular for $\omega_1 < 77°$ only and the eigenvalues δ_1 and δ_2
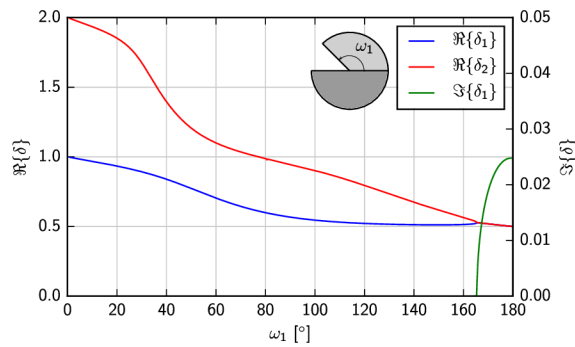
Fig. 5.5: The exponent δ_i dependence on the notch geometry ω_1, materials are defined in Tab. 5.1.

become complex conjugate when $\omega_1 > 165°$. The notch angle $\omega_1 = 180°$ represents an interface crack with $\Re\{\delta_1\} = \Re\{\delta_2\} = 0.5$. The received results can be compared with Chen [115], in which the same values of δ_i for the varying notch geometry are obtained.

The right eigenvectors are evaluated by the backward substitution of δ to (5.28) or (5.33) and by using `linalg.eig` of `scipy`[2] library. The required eigenvector corresponds to the zero eigenvalue of the matrices on the left-hand side of (5.28) or (5.33), respectively. One eigenvector for each singularity exponent δ_i is obtained. In order to get unique stress intensity factors H, the eigenvectors have to be normalized properly. Employing (5.28), the eigenvector $\mathbf{L}^{\mathrm{I}}\mathbf{v}^{\mathrm{I}}$ is normalized by

$$\mathbf{L}^{\mathrm{I}}\mathbf{v}^{\mathrm{I}} = \frac{\left(\mathbf{I} - \mathbf{Y}_1^{\mathrm{I}}\right)^{-1} 2\Re\left\{\mathbf{L}^{\mathrm{I}}\mathbf{v}^{\mathrm{I}}\right\}}{\left\|\left(\mathbf{I} - \mathbf{Y}_1^{\mathrm{I}}\right)^{-1} 2\Re\left\{\mathbf{L}^{\mathrm{I}}\mathbf{v}^{\mathrm{I}}\right\}\right\|}, \tag{5.41a}$$

or analogically for a complex δ

$$\mathbf{L}^{\mathrm{I}}\mathbf{v}^{\mathrm{I}} = \frac{\left(\mathbf{I} - \mathbf{Y}_1^{\mathrm{I}}\right)^{-1} 2\mathbf{L}_a^{\mathrm{I}}\mathbf{v}_a^{\mathrm{I}}}{\left\|\left(\mathbf{I} - \mathbf{Y}_1^{\mathrm{I}}\right)^{-1} 2\mathbf{L}_a^{\mathrm{I}}\mathbf{v}_a^{\mathrm{I}}\right\|}. \tag{5.41b}$$

Subsequently, the eigenvectors $\mathbf{v}^{\mathrm{I}}$, $\mathbf{v}^{\mathrm{II}}$, $\mathbf{w}^{\mathrm{I}}$ and $\mathbf{w}^{\mathrm{II}}$ are determined by using the definitions (5.30) (or (5.34) for a complex eigenvalue), (5.31), (5.35a) and (5.35b). Note that in the numerical algorithm, the relations (5.30) and (5.34) are not distinguished and the procedure output is either real for real eigenvalues δ or complex for complex δ and in the text there are written separately in order to observe the formality. Tab. 5.3 shows eigenvectors for a bi-material notch with real singularity exponents. We can see that the vectors $\mathbf{v}$ and $\mathbf{w}$ for the individual material regions I or II are complex conjugate. Then, the imaginary parts of both addends in (5.7) are equal, but with an opposite sign, and the simplified relation (5.1a) can be used.

The eigenvectors for an interface crack as a special case of the bi-material notch are given in Tab. 5.4. The vectors $\mathbf{v}$ and $\mathbf{w}$ are now distinct, but after substitution to (5.7) we get real-valued expressions for displacements $\mathbf{u}$ and resultant tractions $\mathbf{T}$. It will be discussed in the next example in detail. It can be easily proved that the structure of the eigenvectors is not changed when the arbitrary fibre orientations α_1 and α_2 are considered.

Since the LES formalism derived in section 4.1.7 considers also an arbitrary fibre orientation (in the plane $x_1 x_2$), an effect of fibre orientation was also studied (see Fig. 5.6(a)). The angle of fibre orientation attain the values $\alpha_1 \in (0°, 180°)$. The state for $\alpha_1 = 0°$ and $\alpha_1 = 180°$

---

[2]Both `scipy` and `numpy` libraries are based on LAPACK libraries programmed in FORTRAN language.

δ	$\mathbf{v}^{\mathrm{I}}$	$\mathbf{w}^{\mathrm{I}}$	$\mathbf{v}^{\mathrm{II}}$	$\mathbf{w}^{\mathrm{II}}$
δ_1	$\left\{\begin{array}{l}0.52054 + 3.40988i\\0.46619 - 3.32334i\end{array}\right\}$	$\left\{\begin{array}{l}0.52054 - 3.40988i\\0.46619 + 3.32334i\end{array}\right\}$	$\left\{\begin{array}{l}1.27408 + 0.04509i\\-0.28735 + 0.01257i\end{array}\right\}$	$\left\{\begin{array}{l}1.27408 - 0.04509i\\-0.28735 - 0.01257i\end{array}\right\}$
δ_2	$\left\{\begin{array}{l}4.88166 - 0.76065i\\-5.34670 + 0.20628i\end{array}\right\}$	$\left\{\begin{array}{l}4.88166 + 0.76065i\\-5.34670 - 0.20628i\end{array}\right\}$	$\left\{\begin{array}{l}-0.34464 - 0.89033i\\-0.12041 + 0.38015i\end{array}\right\}$	$\left\{\begin{array}{l}-0.34464 + 0.89033i\\-0.12041 - 0.38015i\end{array}\right\}$

Tab. 5.3: Eigenvectors corresponding to the singularity exponents $\delta_1 = 0.5186$ and $\delta_2 = 0.7647$ of a bi-material notch with material characteristics defined in 5.1 and $\omega_1 = 125°$, $\omega_2 = -180°$.

δ	$\mathbf{v}^{\mathrm{I}}$	$\mathbf{w}^{\mathrm{I}}$	$\mathbf{v}^{\mathrm{II}}$	$\mathbf{w}^{\mathrm{II}}$
δ_1	$\left\{\begin{array}{l}0.83013 + 0.33470i\\-0.83013 + 0.33470i\end{array}\right\}$	$\left\{\begin{array}{l}5.23087 + 0.28652i\\-5.23087 + 0.28652i\end{array}\right\}$	$\left\{\begin{array}{l}0.50303i\\0.07000i\end{array}\right\}$	$\left\{\begin{array}{l}1.13871i\\-0.46932i\end{array}\right\}$
δ_2	$\left\{\begin{array}{l}6.11052 - 0.33470i\\-6.11052 - 0.33470i\end{array}\right\}$	$\left\{\begin{array}{l}0.96972 - 0.39098i\\-0.96972 - 0.39098i\end{array}\right\}$	$\left\{\begin{array}{l}-1.33020i\\0.54824i\end{array}\right\}$	$\left\{\begin{array}{l}-0.58763i\\-0.08177i\end{array}\right\}$

Tab. 5.4: Eigenvectors corresponding to the singularity exponents $\delta_1 = 0.5 + 0.02474i$ and $\delta_2 = 0.5 - 0.02474i$ of an interface crack with material characteristics defined in 5.1 and $\omega_1 = 180°$, $\omega_2 = -180°$.
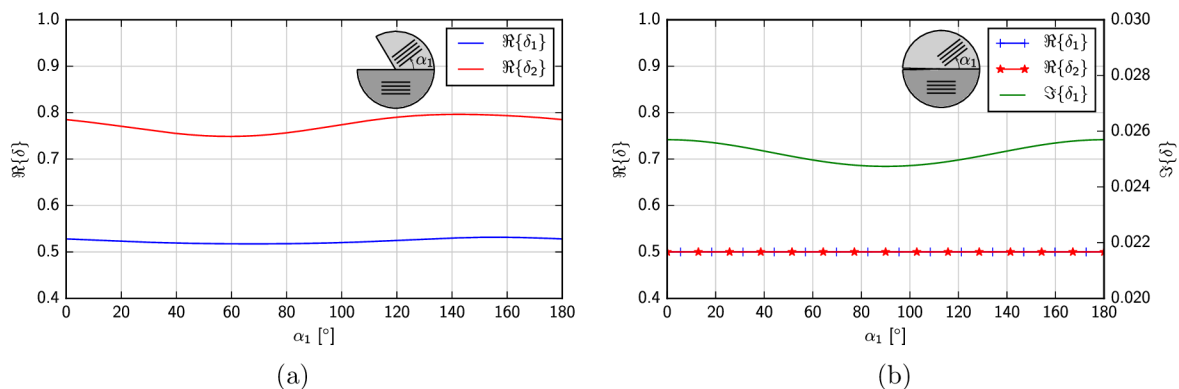
Fig. 5.6: The exponent δ_i dependence on the notch geometry on the angle of fibre orientation α_1 of a bi-material notch defined by (a) $\omega_1 = 125°$ and (b) $\omega_1 = 180°$, $\omega_2 = -180°$ and materials defined in Tab. 5.1.

corresponds to the same configuration and the graphs of both stress singularity exponents have the same character. These results can be compared with the study done by Chen [115] or by Hwu et al. [58] with application of the Stroh formalism. However, there is not clearly distinguished which singular exponent belongs to anti-plane field. The same study was done for an interface crack (Fig. 5.6(b)). Both eigenvalues have the real part $\Re\{\delta_1\} = \Re\{\delta_2\} = 0.5$ and their imaginary parts are complex conjugate with the minimal value of the oscillatory index for $\alpha_1 = 90°$.

5.1.4 Problem redefinition by introducing the shape functions

As the in-plane problem of transversally isotropic material leads to two generally complex singularity exponents δ_1 and δ_2, the resulting displacements and stress functions are obtained by superposition of the individual solutions (5.7) for each δ_i, where the generally complex valued weights represent the GSIFs (see Eq (2.5)).

Displacements and stress functions are expressed as

$$\mathbf{u}(z) = H_1 \left(\mathbf{A}\mathbf{Z}^{\delta_1}\mathbf{v}_1 + \overline{\mathbf{A}\mathbf{Z}}^{\delta_1}\mathbf{w}_1 \right) + H_2 \left(\mathbf{A}\mathbf{Z}^{\delta_2}\mathbf{v}_2 + \overline{\mathbf{A}\mathbf{Z}}^{\delta_2}\mathbf{w}_2 \right), \tag{5.42a}$$

$$\mathbf{T}(z) = H_1 \left(\mathbf{L}\mathbf{Z}^{\delta_1}\mathbf{v}_1 + \overline{\mathbf{L}\mathbf{Z}}^{\delta_1}\mathbf{w}_1 \right) + H_2 \left(\mathbf{L}\mathbf{Z}^{\delta_2}\mathbf{v}_2 + \overline{\mathbf{L}\mathbf{Z}}^{\delta_2}\mathbf{w}_2 \right), \tag{5.42b}$$

where the indices 1,2 denote association to the eigenvalue δ_1 or δ_2, respectively. In order to simplify the numerical algorithm and relations for the Ψ-integral, it is convenient to introduce the angular functions $\boldsymbol{\eta}_i$ and $\boldsymbol{\lambda}_i$, $i = 1,2$ defined as follows:

$$\boldsymbol{\eta}_i(\theta) = \mathbf{A}\mathbf{Z}^{\delta_i}(\theta)\mathbf{v}_i + \overline{\mathbf{A}\mathbf{Z}}^{\delta_i}(\theta)\mathbf{w}_i, \tag{5.43a}$$

$$\boldsymbol{\lambda}_i(\theta) = \mathbf{L}\mathbf{Z}^{\delta_i}(\theta)\mathbf{v}_i + \overline{\mathbf{L}\mathbf{Z}}^{\delta_i}(\theta)\mathbf{w}_i, \tag{5.43b}$$

where the angular variable θ in the bracket of $\mathbf{Z}^\delta(\theta)$ emphasizes that the radial variable r^δ was excluded. The complex functions (5.13) and (5.16) can be then rewritten as [19]

$$\begin{aligned} \mathbf{Z}^\delta &= r^\delta \mathbf{Z}^\delta(\theta) = r^\delta \operatorname{diag}\left[R_1^\delta \, \mathrm{e}^{i\delta\Psi_1}, R_2^\delta \, \mathrm{e}^{i\delta\Psi_2} \right], \\ \overline{\mathbf{Z}}^\delta &= r^\delta \overline{\mathbf{Z}}^\delta(\theta) = r^\delta \operatorname{diag}\left[R_1^\delta \, \mathrm{e}^{-i\delta\Psi_1}, R_2^\delta \, \mathrm{e}^{-i\delta\Psi_2} \right]. \end{aligned} \tag{5.44}$$

Displacements and stress functions can be expressed by using the shape functions (5.43) as

$$\mathbf{u}(r,\theta) = H_1 r^{\delta_1}\boldsymbol{\eta}_1(\theta) + H_2 r^{\delta_2}\boldsymbol{\eta}_2(\theta), \tag{5.45a}$$

$$\mathbf{T}(r,\theta) = H_1 r^{\delta_1}\boldsymbol{\lambda}_1(\theta) + H_2 r^{\delta_2}\boldsymbol{\lambda}_2(\theta), \tag{5.45b}$$

in which

$$\boldsymbol{\eta}_i(\theta) = \begin{Bmatrix} \eta_1^i \\ \eta_2^i \end{Bmatrix}, \quad \boldsymbol{\lambda}_i(\theta) = \begin{Bmatrix} \lambda_1^i \\ \lambda_2^i \end{Bmatrix}, \quad i = 1,2. \tag{5.46}$$

Example 3: Shape functions of a transversally isotropic bi-material notch   The shape functions $\boldsymbol{\eta}_1$, $\boldsymbol{\eta}_2$ and $\boldsymbol{\lambda}_1$, $\boldsymbol{\lambda}_2$ for a bi-material notch $\omega_1 = 125°$, $\omega_2 = -180°$ (with real singularity exponents) are shown in Fig. 5.7. We can see that all imaginary parts (dashed lines) are zero, which match up with the statement that imaginary parts of both addends of (5.43a) or (5.43b) subtract from each other. A different situation occurs when δ_i are complex conjugate. The shape functions are then generally complex (see Fig. 5.8), because the eigenvectors $\mathbf{v}$ and $\mathbf{w}$ are not complex conjugate. It implies that the generalized stress intensity factors will be also complex, but not complex conjugate.

(a)

(b)
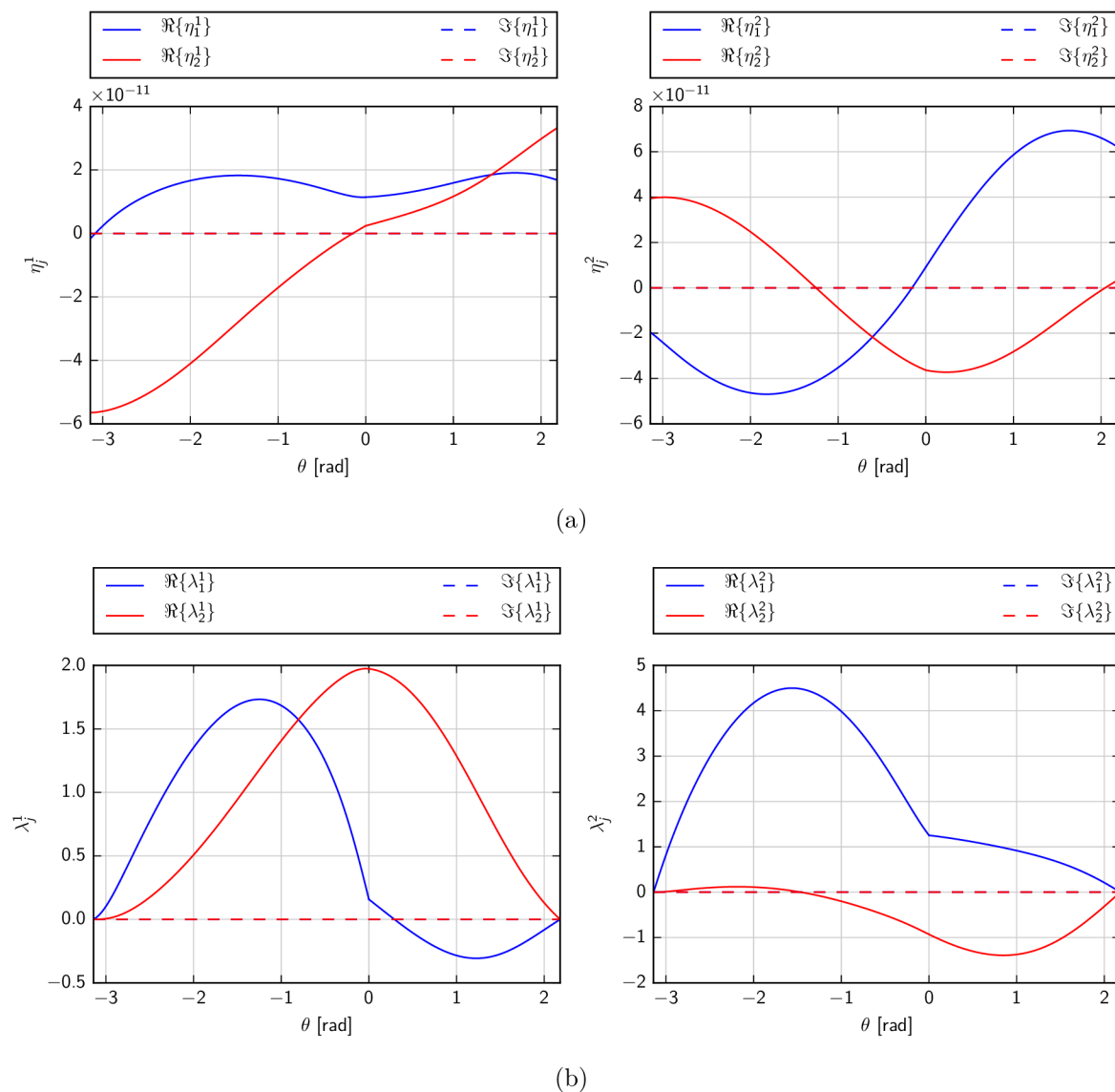
Fig. 5.7: Components of the shape function vectors (a) $\boldsymbol{\eta}_1$, $\boldsymbol{\eta}_2$ and (b) $\boldsymbol{\lambda}_1$, $\boldsymbol{\lambda}_2$ for a bi-material notch $\omega_1 = 125°$, $\omega_2 = -180°$ (materials defined in Tab. 5.1).

5.1.5 Determination of the generalized stress intensity factors

Generalized stress intensity factors determine an amplitude of the displacements and stresses characterized by the normalized shape functions (5.43). In the present work, GSIFs are determined by using the Ψ-integral method outlined in section 2.5. This method was firstly introduced by Sinclair et al. [116] or Vu-Quoc and Tran [117], and deeply investigated by Hwu [17]. It is based on the theorem of Betti and Rayleigh [118]. Contrary to the J-integral introduced by Rice [119], the path-interdependence of the Ψ-integral is also preserved for multi-material stress concentrators.

The Betti's reciprocal theorem claims that if an elastic body is subjected to two systems of body and surface forces, the work that would be done by the first system in acting through the displacements due to the second system of forces is equal to the work that would be done by the

(a)

(b)
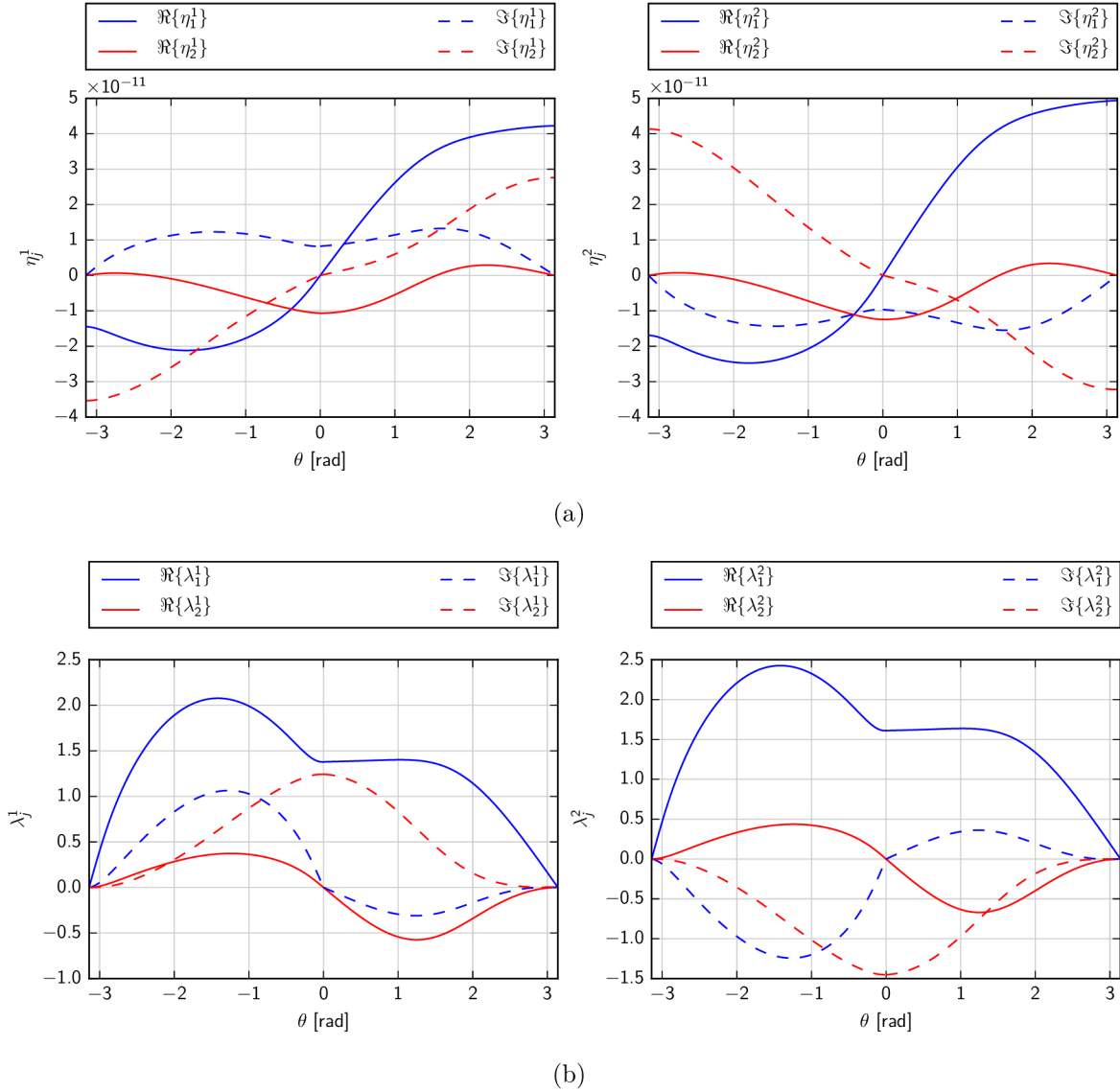
Fig. 5.8: Components of the shape function vectors (a) $\boldsymbol{\eta}_1$, $\boldsymbol{\eta}_2$ and (b) $\boldsymbol{\lambda}_1$, $\boldsymbol{\lambda}_2$ for an interface crack $\omega_1 = 180°$, $\omega_2 = -180°$ (materials defined in Tab. 5.1).

second system in acting through the displacements due to the first system of forces [17]. Let us then choose the first system to be regular (actual singular fields) and the second system to be the auxiliary (also called complementary). Neglecting the body forces (assumed by Lekhnitskii formalism), the Ψ-integral is characterized as

$$\oint_\Gamma \left(\mathbf{u}^\mathsf{T}\hat{\mathbf{t}} - \hat{\mathbf{u}}^\mathsf{T}\mathbf{t} \right) \mathrm{d}s = 0. \tag{5.47}$$

The vectors $\hat{\mathbf{u}}$, $\hat{\mathbf{t}}$ are the auxiliary solutions to the displacements and tractions corresponding to the exponent $\hat{\delta}_i = -\delta_i$. It can be proved that each regular solution of the eigenvalue problem (5.36), generating the basis functions in (5.45a), i.e. $r^{\delta_i}\boldsymbol{\eta}_i(\theta)$, is associated with the dual solution $r^{\hat{\delta}_i}\hat{\boldsymbol{\eta}}_i(\theta)$ of the same eigenvalue problem, where $\hat{\delta}_i = -\delta_i$ [113]. The auxiliary solutions are defined

Fig. 5.9: Scheme of a closed Ψ-integral contour around the bi-material notch tip. The closed path is $\Gamma = \Gamma_1 + \Sigma_1 + \Gamma_2 + \Sigma_2$.
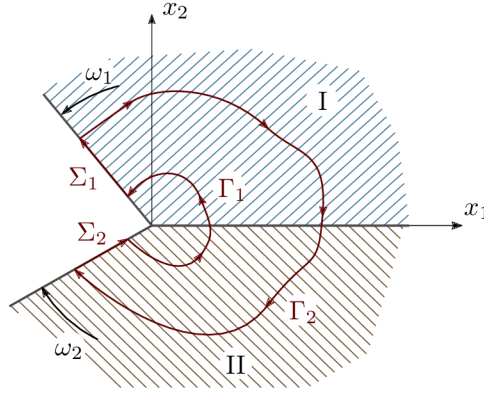
as

$$\hat{\mathbf{u}}_i(r,\theta) = \hat{H}_i r^{-\delta_i} \hat{\boldsymbol{\eta}}_i(\theta), \tag{5.48a}$$

$$\hat{\mathbf{T}}_i(r,\theta) = \hat{H}_i r^{-\delta_i} \hat{\boldsymbol{\lambda}}_i(\theta), \quad i = 1,2, \tag{5.48b}$$

where $\hat{H}_i = 1$. The auxiliary eigenfunctions have the following structure:

$$\hat{\boldsymbol{\eta}}_i(\theta) = \mathbf{A}\mathbf{Z}^{-\delta_i}(\theta)\hat{\mathbf{v}}_i + \overline{\mathbf{A}\mathbf{Z}}^{-\delta_i}(\theta)\hat{\mathbf{w}}_i \tag{5.49a}$$

$$\hat{\boldsymbol{\lambda}}_i(\theta) = \mathbf{L}\mathbf{Z}^{-\delta_i}(\theta)\hat{\mathbf{v}}_i + \overline{\mathbf{L}\mathbf{Z}}^{-\delta_i}(\theta)\hat{\mathbf{w}}_i. \tag{5.49b}$$

The eigenvectors $\hat{\mathbf{v}}$, $\hat{\mathbf{w}}$ are computed by the same procedure described in Example 2 just by substituting $\hat{\delta}_i = -\delta_i$ into the algorithm. The auxiliary functions for the same above studied geometric configurations are depicted in Figs. C.1 and C.2 in Appendix C.1.

The vectors $\mathbf{u}$ and $\mathbf{t}$ represent either the regular asymptotic or the full-field solution obtained numerically. In the first case, the vector $\mathbf{u}$ is given by (5.45a) and the vector $\mathbf{t}$ is given by the derivative of (5.45b) with respect to θ,

$$\mathbf{t} = \frac{\partial \mathbf{T}}{\partial s} = -\frac{\partial \mathbf{T}}{r\partial \theta} = -\frac{\mathbf{T}_{,\theta}}{r}. \tag{5.50}$$

The tangential direction s is chosen so that when one faces the direction of increasing s, the material lies on the right-hand side. Substituting (5.45b) into (5.50) we get expressions for the traction vector in terms of the shape functions:

$$-\mathbf{t}(r,\theta) = H_1 r^{\delta_1 - 1}\boldsymbol{\lambda}_1'(\theta) + H_2 r^{\delta_2 - 1}\boldsymbol{\lambda}_2'(\theta), \tag{5.51}$$

where $()'$ denotes differentiation with respect to θ. A derivative of $\boldsymbol{\lambda}(\theta)$ defined in (5.43b) is

$$\boldsymbol{\lambda}_i'(\theta) = \mathbf{L}\left(\mathbf{Z}^{\delta_i}(\theta)\right)'\mathbf{v}_i + \overline{\mathbf{L}}\left(\overline{\mathbf{Z}}^{\delta_i}(\theta)\right)'\mathbf{w}_i. \tag{5.52}$$

where

$$\left(\mathbf{Z}^{\delta}(\theta)\right)' = \mathrm{diag}\left[\delta R_1^{\delta-1}\,\mathrm{e}^{i(\delta-1)\Psi_1}\left[-\sin(\theta) + \mu_1\cos(\theta)\right],\right.$$
$$\left.\delta R_2^{\delta-1}\,\mathrm{e}^{i(\delta-1)\Psi_2}\left[-\sin(\theta) + \mu_2\cos(\theta)\right]\right] \tag{5.53}$$
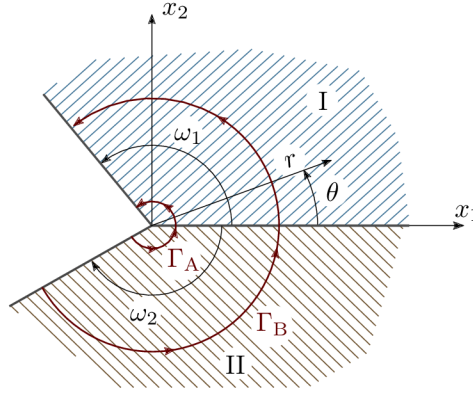
Fig. 5.10: Scheme of two circular Ψ-integral contours Γ_A and Γ_B.

and

$$
\left(\overline{\mathbf{Z}}^\delta(\theta)\right)' = \mathrm{diag}\Big[\delta R_1^{\delta-1}\,\mathrm{e}^{-i(\delta-1)\Psi_1}\left[-\sin(\theta)+\overline{\mu}_1\cos(\theta)\right],
$$
$$
\delta R_2^{\delta-1}\,\mathrm{e}^{-i(\delta-1)\Psi_2}\left[-\sin(\theta)+\overline{\mu}_2\cos(\theta)\right]\Big].\quad(5.54)
$$

The auxiliary tractions are obtained analogically by employing (5.50):

$$
-\hat{\mathbf{t}}_i(r,\theta) = H_i r^{-\delta_i-1}\hat{\boldsymbol{\lambda}}_i'(\theta),\quad(5.55)
$$

and

$$
\hat{\boldsymbol{\lambda}}_i'(\theta) = \mathbf{L}\left(\mathbf{Z}^{-\delta_i}(\theta)\right)'\hat{\mathbf{v}}_i + \overline{\mathbf{L}}\left(\overline{\mathbf{Z}}^{-\delta_i}(\theta)\right)'\hat{\mathbf{w}}_i.\quad(5.56)
$$

Γ is a closed contour in a simply connected region. Let us consider a contour $\Gamma = \Gamma_1 + \Sigma_1 + \Gamma_2 + \Sigma_2$ as shown in Fig. 5.9. The integral (5.47) can be rewritten as follows:

$$
\int_{\Gamma_1}\left(\mathbf{u}^\mathsf{T}\hat{\mathbf{t}}-\hat{\mathbf{u}}^\mathsf{T}\mathbf{t}\right)\mathrm{d}s + \int_{\Sigma_1}\left(\mathbf{u}^\mathsf{T}\hat{\mathbf{t}}-\hat{\mathbf{u}}^\mathsf{T}\mathbf{t}\right)\mathrm{d}s + \int_{\Gamma_2}\left(\mathbf{u}^\mathsf{T}\hat{\mathbf{t}}-\hat{\mathbf{u}}^\mathsf{T}\mathbf{t}\right)\mathrm{d}s + \int_{\Sigma_1}\left(\mathbf{u}^\mathsf{T}\hat{\mathbf{t}}-\hat{\mathbf{u}}^\mathsf{T}\mathbf{t}\right)\mathrm{d}s = 0.
$$
$$
(5.57)
$$

Since the notch faces are assumed to be traction free (boundary conditions (5.17)), the terms corresponding to the contours Σ_1 and Σ_2 equal to zero and Eq. (5.57) reduces to

$$
\int_{\Gamma_1}\left(\mathbf{u}^\mathsf{T}\hat{\mathbf{t}}-\hat{\mathbf{u}}^\mathsf{T}\mathbf{t}\right)\mathrm{d}s + \int_{\Gamma_2}\left(\mathbf{u}^\mathsf{T}\hat{\mathbf{t}}-\hat{\mathbf{u}}^\mathsf{T}\mathbf{t}\right)\mathrm{d}s = 0.\quad(5.58)
$$

Let us denote $\Gamma_A = \Gamma_1$ and $\Gamma_B = -\Gamma_2$, i.e. we changed the orientation of the second contour so that both are oriented in the counter-clockwise direction (the paths emanate from ω_2 to ω_1). We get

$$
\int_{\Gamma_A}\left(\mathbf{u}^\mathsf{T}\hat{\mathbf{t}}-\hat{\mathbf{u}}^\mathsf{T}\mathbf{t}\right)\mathrm{d}s = \int_{\Gamma_B}\left(\mathbf{u}^\mathsf{T}\hat{\mathbf{t}}-\hat{\mathbf{u}}^\mathsf{T}\mathbf{t}\right)\mathrm{d}s,\quad(5.59)
$$

which proved that the Ψ-integral is path-independent for free-free multi-material wedges [59]. For simplicity, a circular counter-clockwise paths Γ_A and Γ_B through the region dominated by the singular field are chosen, see Fig. 5.10. The Ψ-integral for a bi-material notch characterised by angles ω_1 and ω_2 becomes

$$
\Psi = \int_{\omega_2}^{\omega_1}\left(\mathbf{u}^\mathsf{T}\hat{\mathbf{t}}-\hat{\mathbf{u}}^\mathsf{T}\mathbf{t}\right)r\,\mathrm{d}\theta.\quad(5.60)
$$

Obviously, if the integration contour shrinks to the notch tip, the full-field solution reduces to the asymptotic solution (5.45a) and (5.51). Inserting the regular solutions (5.45a), (5.51) and auxiliary solutions (5.48a), (5.55) into (5.60), we obtain

$$\Psi\left(\mathbf{u}, r^{-\delta_i}\hat{\boldsymbol{\eta}}_i(\theta)\right) = \sum_{j=1}^{2} H_j \Psi\left(r^{\delta_j}\boldsymbol{\eta}_j(\theta), r^{-\delta_i}\hat{\boldsymbol{\eta}}_i(\theta)\right), \quad i = 1,2. \tag{5.61}$$

Since the regular and corresponding auxiliary solutions are orthogonal with respect to the integral (2.14), it follows for the individual integrals that [17, 117]

$$\Psi\left(r^{\delta_j}\boldsymbol{\eta}_j(\theta), r^{-\delta_i}\hat{\boldsymbol{\eta}}_i(\theta)\right) = \begin{cases} \text{const} \neq 0 & \text{for} \quad i = j, \\ 0 & \text{for} \quad i \neq j. \end{cases} \tag{5.62}$$

Applying (5.62), the Ψ-integral (5.61) computed along a path very close to the crack tip gives an important result for the GSIFs evaluation

$$\begin{aligned} \Psi\left(\mathbf{u}, r^{-\delta_i}\hat{\boldsymbol{\eta}}_i(\theta)\right) &= \Psi\left(r^{\delta_i}\boldsymbol{\eta}_i(\theta), r^{-\delta_i}\hat{\boldsymbol{\eta}}_i(\theta)\right) = \\ &= \int_{\omega_2}^{\omega_1} \left(H_i r^{\delta}\boldsymbol{\eta}_i^{\mathsf{T}}(\theta) r^{-\delta_i-1}\hat{\boldsymbol{\lambda}}_i'(\theta) - r^{-\delta_i}\hat{\boldsymbol{\eta}}_i^{\mathsf{T}}(\theta) H_i r^{\delta_i-1}\boldsymbol{\lambda}_i'(\theta)\right) r\,\mathrm{d}\theta = \\ &= H_i \int_{\omega_2}^{\omega_1} \left(r^{\delta_i-\delta_i-1+1}\boldsymbol{\eta}_i^{\mathsf{T}}(\theta)\hat{\boldsymbol{\lambda}}_i'(\theta) - r^{-\delta_i+\delta_i-1+1}\hat{\boldsymbol{\eta}}_i^{\mathsf{T}}(\theta)\boldsymbol{\lambda}_i'(\theta)\right) \mathrm{d}\theta = \\ &= H_i \int_{\omega_2}^{\omega_1} \left(\boldsymbol{\eta}_i^{\mathsf{T}}(\theta)\hat{\boldsymbol{\lambda}}_i'(\theta) - \hat{\boldsymbol{\eta}}_i^{\mathsf{T}}(\theta)\boldsymbol{\lambda}_i'(\theta)\right) \mathrm{d}\theta, \end{aligned} \tag{5.63}$$

which is independent on the radial coordinate r. The Ψ-integral with a contribution of the regular and auxiliary fields is zero when the contour is not in the singular dominance region. Note that the integration path and the boundary defined in 4.2 are oppositely oriented. Reorienting the boundary leads to changing the sings of $\mathbf{t}$ and $\hat{\mathbf{t}}$ defined in (5.51) and (5.55).

Making use of the Ψ-integral path-independence, the GSIFs can be evaluated when the right-hand side of Eq. (5.63) is put equal to the Ψ-integral computed along the remote contour which contains a full-field solution to the vectors $\mathbf{u}$ and $\mathbf{t}$. In the present work the full-field solution is approximated using FEM implemented in ANSYS software [120]. The integration contour is chosen far away from the bi-material notch tip. Let us introduce the integral

$$\Psi\left(\mathbf{u}^{\mathrm{FEM}}, r_c^{-\delta_i}\hat{\boldsymbol{\eta}}_i(\theta)\right) = \int_{\omega_2}^{\omega_1} \left(\left(\mathbf{u}^{\mathrm{FEM}}\right)^{\mathsf{T}} r_c^{-\delta_i-1}\hat{\boldsymbol{\lambda}}_i'(\theta) + r_c^{-\delta_i}\hat{\boldsymbol{\eta}}_i^{\mathsf{T}}(\theta)\mathbf{t}^{\mathrm{FEM}}\right) r_c\,\mathrm{d}\theta, \tag{5.64}$$

where r_c is the radius of the circular path far away from the notch singularity. Note that the signs follow from the orientation of the outward normal and the integration contour. Elements of the vector $\mathbf{u}^{\mathrm{FEM}} = [u_1^{\mathrm{FEM}}, u_2^{\mathrm{FEM}}]^{\mathsf{T}}$ are the direct output from the finite element analysis, but elements of the vector $\mathbf{t}^{\mathrm{FEM}}$ on the surface of the contour have to be computed from the stresses by using the Cauchy's formula $t_i = \sigma_{ij}n_j$, in the matrix form written as

$$\mathbf{t}^{\mathrm{FEM}} = \boldsymbol{\sigma}^{\mathrm{FEM}}\mathbf{n}, \tag{5.65}$$

where $\boldsymbol{\sigma}^{\mathrm{FEM}}$ is the two-dimensional stress tensor and $\mathbf{n}$ is the outer normal to the domain enclosed by a circular integrating path of the radius r_c defined as

$$\boldsymbol{\sigma}^{\mathrm{FEM}} = \begin{bmatrix} \sigma_{11}^{\mathrm{FEM}} & \sigma_{12}^{\mathrm{FEM}} \\ \sigma_{21}^{\mathrm{FEM}} & \sigma_{22}^{\mathrm{FEM}} \end{bmatrix}, \quad \mathbf{n} = \begin{Bmatrix} \cos(\theta) \\ \sin(\theta) \end{Bmatrix}. \tag{5.66}$$
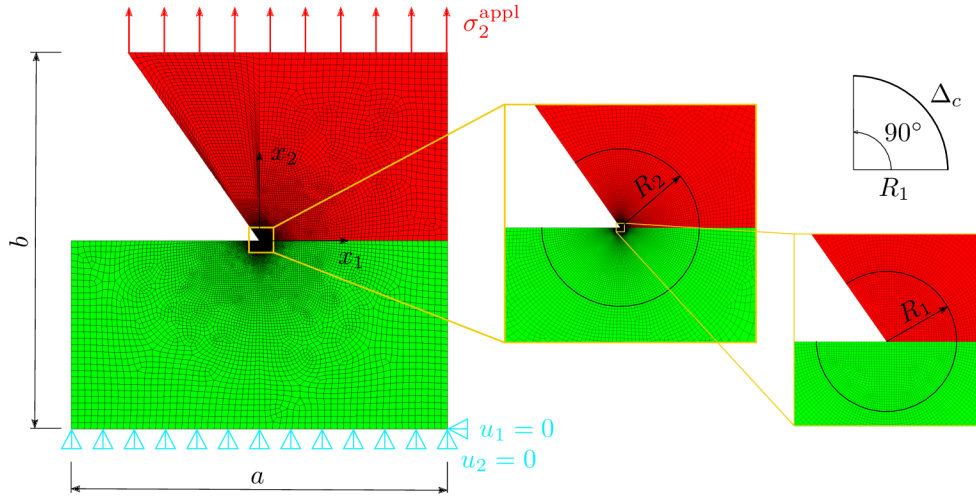
Fig. 5.11: Finite element mesh of the bi-material notch model with scaled regions with a refined and mapped mesh. The loading and constrains are depicted on the left.

Note that the normal vector introduced in (5.66) has now a different orientation than in (4.72), because it is normal to the domain enclosed by the circular contour. Applying the analogy with the standard dot product, the Ψ-integrals (5.63) and (5.64) project analytical and numerical solution of the same problem into the basis function of a dual function space generated by the auxiliary solutions (5.49). Hence, both Ψ-integrals (5.63) and (5.64) are equal and the following relations hold

$$
\begin{aligned}
\Psi\left(\mathbf{u}^{\mathrm{FEM}}, r_c^{-\delta_i}\hat{\boldsymbol{\eta}}_i(\theta)\right) &= \Psi\left(H_1 r_c^{\delta_1}\boldsymbol{\eta}_1(\theta) + H_2 r_c^{\delta_2}\boldsymbol{\eta}_2(\theta), r_c^{-\delta_i}\hat{\boldsymbol{\eta}}_i(\theta)\right) = \\
&= H_1\Psi\left(r_c^{\delta_1}\boldsymbol{\eta}_1(\theta), r_c^{-\delta_i}\hat{\boldsymbol{\eta}}_i(\theta)\right) + H_2\Psi\left(r_c^{\delta_2}\boldsymbol{\eta}_2(\theta), r_c^{-\delta_i}\hat{\boldsymbol{\eta}}_i(\theta)\right), \quad i=1,2.
\end{aligned} \quad (5.67)
$$

Applying (5.62), two separate definitions for each index $i=1,2$ are obtained:

$$
\begin{aligned}
\Psi\left(\mathbf{u}^{\mathrm{FEM}}, r_c^{-\delta_1}\hat{\boldsymbol{\eta}}_1(\theta)\right) &= H_1\Psi\left(r_c^{\delta_1}\boldsymbol{\eta}_1(\theta), r_c^{-\delta_1}\hat{\boldsymbol{\eta}}_1(\theta)\right), \\
\Psi\left(\mathbf{u}^{\mathrm{FEM}}, r_c^{-\delta_2}\hat{\boldsymbol{\eta}}_2(\theta)\right) &= H_2\Psi\left(r_c^{\delta_2}\boldsymbol{\eta}_2(\theta), r_c^{-\delta_2}\hat{\boldsymbol{\eta}}_2(\theta)\right),
\end{aligned} \quad (5.68)
$$

from which the generalized stress intensity factors can be extracted as

$$
\begin{aligned}
H_1 &= \frac{\Psi\left(\mathbf{u}^{\mathrm{FEM}}, r_c^{-\delta_1}\hat{\boldsymbol{\eta}}_1(\theta)\right)}{\Psi\left(r_c^{\delta_1}\boldsymbol{\eta}_1(\theta), r_c^{-\delta_1}\hat{\boldsymbol{\eta}}_1(\theta)\right)}, \\
H_2 &= \frac{\Psi\left(\mathbf{u}^{\mathrm{FEM}}, r_c^{-\delta_2}\hat{\boldsymbol{\eta}}_2(\theta)\right)}{\Psi\left(r_c^{\delta_2}\boldsymbol{\eta}_2(\theta), r_c^{-\delta_2}\hat{\boldsymbol{\eta}}_2(\theta)\right)}.
\end{aligned} \quad (5.69)
$$

5.1.6 Finite element model of a bi-material notch

The knowledge of the character of the stress singularity represented by the exponents δ_i is necessary for the GSIFs evaluation. The FEM analysis is an important component of the procedure that allows one to get a complete description of the singular stress field at the bi-material notch tip. A script code in the APDL programming language in ANSYS software was created in order to gain the output data on the desired circular contour. The geometry of the FEM model is

depicted in Fig. 5.11. The finite element mesh in the vicinity of the notch tip consists of two regions. The small circle delimited by the radius $R_1 = 0.001\,\text{mm}$ has a free mesh, because using of special singular elements would cause a mesh distortion for a finer element length. The region between R_1 and $R_2 = 7\,\text{mm}$ is the area of the interest, from which the stresses and displacements are extracted and the mesh here is fine and mapped so that each element has a square-like shape. All desired nodal results are saved to a text file and consequently imported by using a Python script, where the displacement and stress fields are reconstructed by using `scipy.interpolate` package, namely `griddata` function. This procedure requires a homogeneous and well-structured finite element mesh. The data on the circular path are interpolated by using `scint.splrep` and `scint.splev` libraries. The advantage of this method is that only one computation with a fine mesh in ANSYS is necessary in order to reconstruct a circular path with an arbitrary radius. The second advantage is that employing of adaptive integration methods for evaluating the Ψ-integral is available.

The 8-node quadratic plane element `PLANE183` was used with plane strain enabled. As was stated in the previous paragraphs, only plane strain state is considered in the studies, because from the computational point of view, the constitutive equations for plane stress can be analogically modified (see section 4.1.5). A variable notch geometry is enabled, the face angles ω_1, ω_2 could attain values between $0°$ and $180°$, while the bi-material interface remains fixed at $\omega_0 = 0°$. The fibre orientation is realized by orienting the element coordinate system by angles α_1 and α_2, respectively. Dimensions of the two-dimensional model are $a = 180\,\text{mm}$ and $b = 180\,\text{mm}$.

When investigating a stress concentrator in a technical component by using FEM, the sub-modelling technique is widely used. This method consists in performing two computations. The whole model with a coarse mesh is analysed. Output of this analysis represents boundary conditions to a second model, which analyses the singular region more closely, meshed very fine. Boundary conditions of the sub-model can be both displacements and forces. In the present work, the finite element model is constrained according to Fig. 5.11. Nodes at the bottom edge are fixed in the x_2 direction and, on top of that, the right lateral node is fixed in the x_1 direction in order to avoid a rigid body motion. The upper side is loaded with the applied stress $\sigma_2^{\text{appl}} = 100\,\text{MPa}$. Displacements u_2 on the upper boundary are coupled in order to minimize the non-uniform loading. After deformation, the origin of the coordinate system of the finite element mesh does not coincide with the origin of the coordinate system of the analytical solution $(5.45)_1$. Hence, the notch tip displacements have to be subtracted from all body displacements. It has to be reminded that the notch faces have to remain mechanically unloaded (zero tractions $\mathbf{t}$).

Example 4: Study of the Ψ-integral path-independence for a transversally isotropic bi-material notch   Before we proceed to investigate the path-independence of the Ψ-integral, the finite element model with respect to element size is checked. Let us set the integration radius to $r_c = 2\,\text{mm}$. The only parameter that controls the mesh density is the line division parameter Δ_c of the R_1 and R_2 perimeters related to the arc of $90°$. The another divisions, edge lengths and spacing ratios are computed based on this value in order to achieve the best mesh topology and element shape. It implies from the results in Fig. 5.12 that the most appropriate angular division is $\Delta_c = 60$. This value gives us a sufficient angular division, by which reliable results are obtained and minimal computational time is achieved.

All integrals were evaluated by using the Romberg's method implemented in the library `scipy.integrate.romberg`. An advantage of this method, compared to the trapezoidal rule, for example, consists in possibility of usage of the adaptive integration step, owing to that a better accuracy is achieved. Therefore, an interpolation function for the nodal results is de-
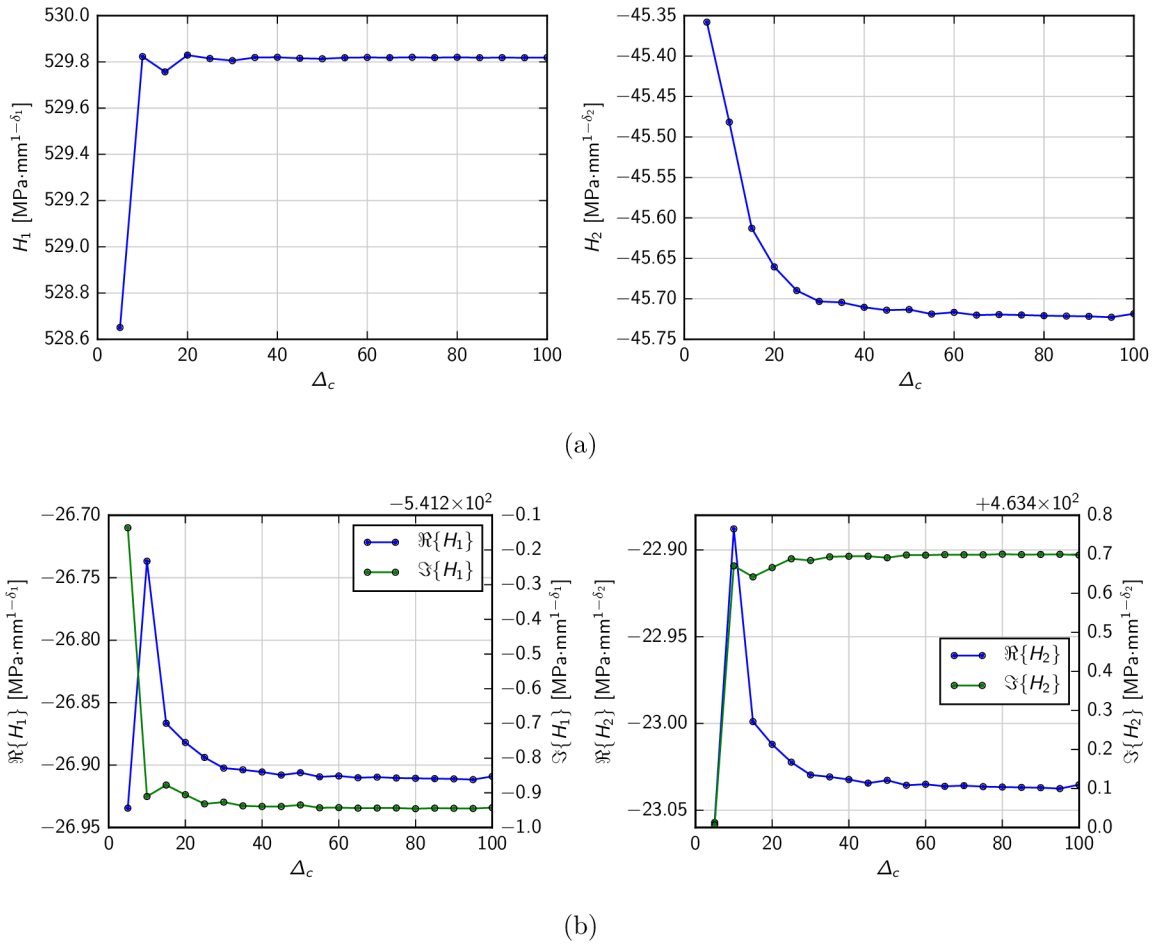
(a)

(b)

Fig. 5.12: Study of the minimal mesh density. The governing parameter was the generalized stress intensity factor H_i. The studied cases were (a) a bi-material notch given by $\omega_1 = 125°$ and (b) an interface crack ($\omega_1 = 180°$). The second notch face was $\omega_2 = -180°$. The materials are defined in Tab. 5.1, the singularity exponents are (a) $\delta_1 = 0.5186$, $\delta_2 = 0.7647$ and (b) $\delta_1 = 0.5 + 0.02474i$, $\delta_2 = 0.5 - 0.02474i$.

fined in order to get an approximative value in each point of the contour. For that purpose, a linear interpolation function was used, because the cubic spline caused numerical instabilities near boundaries and in the vicinity of the interface. Since the mesh density is very fine, we can assume that the error will be minimal. From the computational point of view, the integrals are evaluated for each material region separately, because the discontinuity of σ_{11} causes a numerical error if integration of the whole path from ω_2 to ω_1 is performed. The resulting integrals for the whole path are the sum of the particular integrals for the individual material regions.

The study of Ψ-integral path-independence was carried out for forty integration radii r_c between 0.0005 mm and 4 mm. As in the previous studies, two representative cases were investigated – a bi-material notch with real singularity exponents ($\omega_1 = 125°$, $\omega_2 = -180°$) and an interface crack with complex conjugate singularity exponents ($\omega_1 = 180°$, $\omega_2 = -180°$). To prove the path-independence, the GSIF as the governing parameter was chosen. Since the denominator in the definitions (5.69) for GSIFs does not depend on r_c, the independence of the integrals in the numerator is tested. The results in Fig. 5.13 show that all integrals for
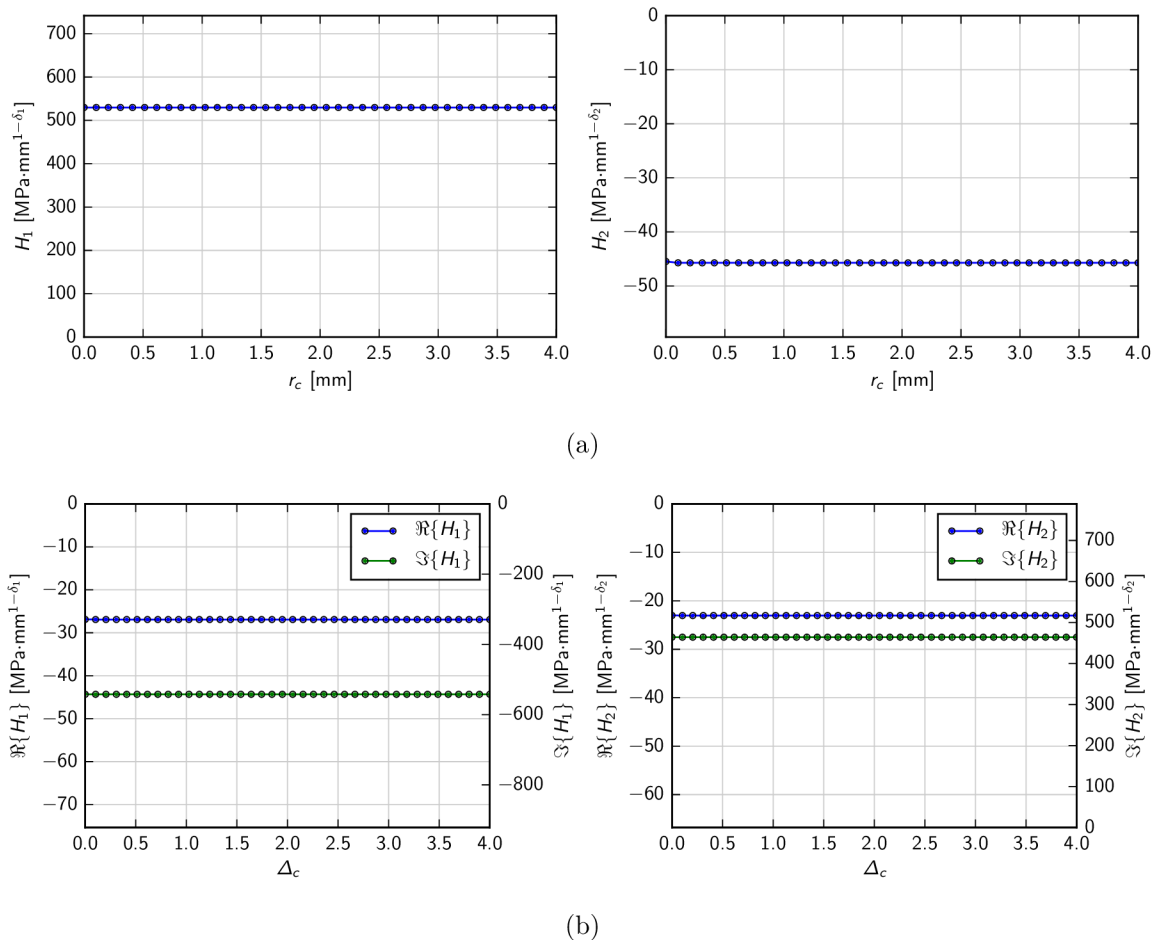
(a)

(b)

Fig. 5.13: Test of path-independence of the GSIFs on the integration contour radius enclosing (a) a transversally orthotropic bi-material notch characterized by $\omega_1 = 125°$, $\delta_1 = 0.5186$, $\delta_2 = 0.7647$ and (b) an interface crack with $\delta_1 = 0.5 + 0.02474i$, $\delta_2 = 0.5 - 0.02474i$. Materials are defined in Tab. 5.1.

both notch configurations are path-independent, which is in accordance with [59]. The small discrepancy near zero is caused by the finite element mesh, because the first integration radius $r_c = 0.0005\,\mathrm{mm}$ lies in the first circle characterized by $R_1 = 0.001\,\mathrm{mm}$, where the mesh is unstructured and also quite rough comparing to the magnitude of r_c. The complex GSIFs in Fig. 5.13(b) were decomposed to real and imaginary parts, which were investigated separately. For the next studies, $r_c = 2\,\mathrm{mm}$ is chosen.

Here, a sign of the GSIF is discussed. As an experienced reader knows from the Irwin's theory, the stress intensity factors for a crack under mode I loading are always positive. The sign of the GSIF for a bi-material notch depends on the orientation of their corresponding eigenvectors $\mathbf{v}$ and $\mathbf{w}$. In the case of real singularity exponents δ, the sign of the GSIF can be changed just by multiplying the corresponding eigenvector by -1. A different situation occurs when the stress term orders δ are complex conjugate. The problem leads to two complex and distinct stress intensity factors, which cannot be distinguished by virtue of a negative or positive sign. Same problem arise when we want to recompute the unit from $\mathrm{Pa}\cdot\mathrm{m}^{1-\delta}$ to $\mathrm{MPa}\cdot\mathrm{mm}^{1-\delta}$. The value in SI units is multiplied by the constant $10^{-6}\cdot 10^{3(1-\delta)}$, which is for the first case a real

number, but a complex number for the second case. This can cause a sign change by the real and imaginary parts of the GSIF. This effect can be eliminated by employing the unified definition introduced by Hwu [59].

There is a question how to compare the individual fracture parameters among themselves. If we change one or both notch face angles ω_1 and ω_2 or a material parameter, we get different stress term orders δ_i, which leads to different units of the generalized stress intensity factors. From the engineering point of view, configurations which differ only from the external loading can be compared. Other possibility is a comparison of the resulting stress development or a change in the potential energy of the body, when it is disturbed by the crack of small finite length [19, 121].

5.1.7 Stress and displacement fields of a transversally isotropic bi-material notch

The displacement field is expressed directly by the Williams' asymptotic expansion (5.45a) with the knowledge of the analytical form of the angular function (5.43a). The stresses in the coordinate system arbitrary rotated with respect to x_3 axis are expressed from the stress functions as

$$\begin{aligned}
\sigma_{ss} &= -\mathbf{s}^\mathsf{T}\mathbf{T}_{,n} \\
\sigma_{sn} &= -\mathbf{n}^\mathsf{T}\mathbf{T}_{,n} = \mathbf{s}^\mathsf{T}\mathbf{T}_{,s} \\
\sigma_{nn} &= \mathbf{n}^\mathsf{T}\mathbf{T}_{,s},
\end{aligned}\tag{5.70}$$

where normals $\mathbf{n}$ and $\mathbf{s}$ are defined by

$$\mathbf{s} = \begin{Bmatrix}\cos\theta \\ \sin\theta\end{Bmatrix}, \quad \mathbf{n} = \begin{Bmatrix}-\sin\theta \\ \cos\theta\end{Bmatrix}.\tag{5.71}$$

Note that the normal $\mathbf{n}$ has been introduced in (4.72). The stresses in the Cartesian coordinate system given by axes x_1, x_2 are obtained by setting $\theta = 0$ in the definitions (5.71). According to Fig. 4.2 it holds that $s \to x_1$ and $n \to x_2$. Substituting (5.7b) into (5.70) leads to

$$\begin{aligned}
\boldsymbol{\sigma}^1 &= -H\left\{\mathbf{L}\frac{\mathrm{d}\mathbf{Z}^\delta}{\mathrm{d}x_2}\mathbf{v} + \overline{\mathbf{L}}\frac{\mathrm{d}\overline{\mathbf{Z}}^\delta}{\mathrm{d}x_2}\mathbf{w}\right\}, \\
\boldsymbol{\sigma}^2 &= H\left\{\mathbf{L}\frac{\mathrm{d}\mathbf{Z}^\delta}{\mathrm{d}x_1}\mathbf{v} + \overline{\mathbf{L}}\frac{\mathrm{d}\overline{\mathbf{Z}}^\delta}{\mathrm{d}x_1}\mathbf{w}\right\},
\end{aligned}\tag{5.72}$$

where the stresses are ordered in the vectors as

$$\boldsymbol{\sigma}^1 = \begin{Bmatrix}\sigma_{11} \\ \sigma_{12}\end{Bmatrix}, \quad \boldsymbol{\sigma}^2 = \begin{Bmatrix}\sigma_{21} \\ \sigma_{22}\end{Bmatrix}.\tag{5.73}$$

Since $\mathbf{Z}^\delta$ is expressed in polar coordinates (see (5.8)), we can make these mathematical operation:

$$\begin{aligned}
\frac{\mathrm{d}Z_i^\delta}{\mathrm{d}x_2} &= \frac{\mathrm{d}Z_i^\delta}{\mathrm{d}z_i}\frac{\mathrm{d}z_i}{\mathrm{d}x_2} = \frac{\mathrm{d}Z_i^\delta}{\mathrm{d}z_i}\frac{\mathrm{d}z_i}{\mathrm{d}x_2} = \delta Z_i^{\delta-1}\mu_i, \\
\frac{\mathrm{d}Z_i^\delta}{\mathrm{d}x_1} &= \frac{\mathrm{d}Z_i^\delta}{\mathrm{d}x_1}\frac{\mathrm{d}z_i}{\mathrm{d}z_i} = \frac{\mathrm{d}Z_i^\delta}{\mathrm{d}z_i}\frac{\mathrm{d}z_i}{\mathrm{d}x_1} = \delta Z_i^{\delta-1}, \\
z_i &= x_1 + \mu_i x_2, \quad i = 1,2.
\end{aligned}\tag{5.74}$$

Eq. (5.72) can be then rewritten as

$$\boldsymbol{\sigma}^1 = -H\left\{\mathbf{L}\delta\mathbf{Z}^{\delta-1}\boldsymbol{\mu}\mathbf{v} + \overline{\mathbf{L}\mathbf{Z}}^{\delta-1}\overline{\boldsymbol{\mu}}\mathbf{w}\right\},$$

$$\boldsymbol{\sigma}^2 = H\left\{\mathbf{L}\delta\mathbf{Z}^{\delta-1}\mathbf{v} + \overline{\mathbf{L}\mathbf{Z}}^{\delta-1}\mathbf{w}\right\},$$

$$\boldsymbol{\mu} = \begin{bmatrix} \mu_1 & 0 \\ 0 & \mu_2 \end{bmatrix}, \quad \overline{\boldsymbol{\mu}} = \begin{bmatrix} \overline{\mu}_1 & 0 \\ 0 & \overline{\mu}_2 \end{bmatrix}. \tag{5.75}$$

For programming purposes, the equations (5.75) can be modified by means of the shape function $\boldsymbol{\lambda}$ introduced in (5.43b). Decomposing the complex function $\mathbf{Z}^{\delta-1}$ in the same way as in (5.44) leads to

$$\mathbf{Z}^{\delta-1} = r^{\delta-1}\mathbf{Z}^{\delta-1}(\theta) = r^{\delta-1}\,\mathrm{diag}\left[R_1^{\delta-1}\,\mathrm{e}^{i(\delta-1)\Psi_1}, R_2^{\delta-1}\,\mathrm{e}^{i(\delta-1)\Psi_2}\right],$$

$$\overline{\mathbf{Z}}^{\delta-1} = r^{\delta-1}\overline{\mathbf{Z}}^{\delta-1}(\theta) = r^{\delta-1}\,\mathrm{diag}\left[R_1^{\delta-1}\,\mathrm{e}^{-i(\delta-1)\Psi_1}, R_2^{\delta-1}\,\mathrm{e}^{-i(\delta-1)\Psi_2}\right]. \tag{5.76}$$

Let us introduce the following functions:

$$\tilde{\boldsymbol{\lambda}}_{i,x_2}(\theta) = \mathbf{L}\delta_i\mathbf{Z}^{\delta_i-1}(\theta)\boldsymbol{\mu}\mathbf{v}_i + \overline{\mathbf{L}}\delta_i\overline{\mathbf{Z}}^{\delta_i-1}(\theta)\overline{\boldsymbol{\mu}}\mathbf{w}_i, \quad i = 1,2,3, \tag{5.77a}$$

$$\tilde{\boldsymbol{\lambda}}_{i,x_1}(\theta) = \mathbf{L}\delta_i\mathbf{Z}^{\delta_i-1}(\theta)\mathbf{v}_i + \overline{\mathbf{L}}\delta_i\overline{\mathbf{Z}}^{\delta_i-1}(\theta)\mathbf{w}_i, \quad i = 1,2,3, \tag{5.77b}$$

where the subscripts $,x_1$ and $,x_2$ denote differentiation with respect to the Cartesian coordinates x_1, x_2, i.e.

$$\tilde{\boldsymbol{\lambda}}_{,x_i}(x_1,x_2) = \frac{\mathrm{d}\tilde{\boldsymbol{\lambda}}(x_1,x_2)}{\mathrm{d}x_i}, \quad i = 1,2. \tag{5.78}$$

Considering both singularity exponents δ_i, the equations (5.75) can be expressed by employing (5.77a) and (5.77b) as

$$\boldsymbol{\sigma}^1 = -H_1 r^{\delta_1-1}\tilde{\boldsymbol{\lambda}}_{1,x_2}(\theta) - H_2 r^{\delta_2-1}\tilde{\boldsymbol{\lambda}}_{2,x_2}(\theta),$$

$$\boldsymbol{\sigma}^2 = H_1 r^{\delta_1-1}\tilde{\boldsymbol{\lambda}}_{1,x_1}(\theta) + H_2 r^{\delta_2-1}\tilde{\boldsymbol{\lambda}}_{2,x_1}(\theta). \tag{5.79}$$

Example 5: Displacement and stress reconstruction in the vicinity of the transversally isotropic bi-material notch tip The input parameters, boundary conditions and external loading remain identical as in the previous examples the including materials defined in Tab. 5.1. Fig. 5.14 illustrates the dominance of the stronger stress singularity $1 - \delta_1$, contributions of H_2 to the stress amplitude is not very significant. It is obvious from Fig. 5.5 that δ_1 has always stronger singularity, but the difference fades away with closing the notch angle to its limit state, i.e. $\omega_1 \rightarrow 180°$.

The stresses and displacements in Fig. 5.14 were evaluated along the circular path enclosing the notch tip on the radius $r = 0.001$ mm, which shows a very good correspondence between the analytical and FEM solution. The superscripts H_i, $i = 1,2$ of plotted quantities listed in the legend indicate particular asymptotic terms in Eqs. (5.45) and (5.79). The stresses and displacements depicted on the radius $r = 2$ mm farer from the tip (see Fig. 5.15) illustrate that the analytical solutions differ from FEM more significantly. The most noticeable mismatch can be observed by σ_{11}, where the difference is higher for radii far from the tip. This phenomenon is causes by the effect of T-stress [122].

The same study was performed for an interface crack from the previous examples. Fig. 5.16 and 5.17 illustrate the displacement and stress distribution on the circular paths $r = 0.001$ mm
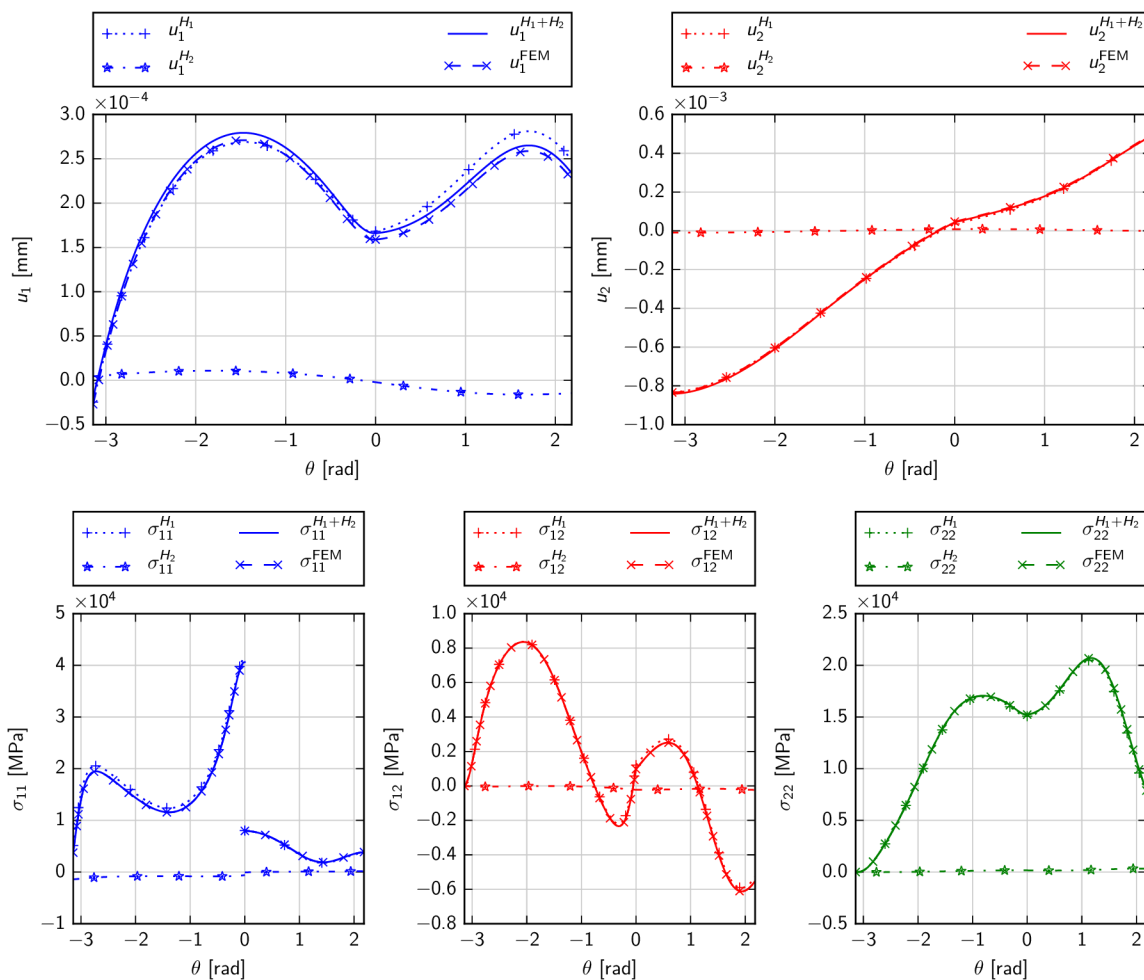
Fig. 5.14: The displacement and stress components on the circular path $r = 0.001\,\mathrm{mm}$ of a bi-material notch $\omega_1 = 125°$, $\omega_2 = -180°$. Materials are defined in Tab. 5.1, singularity exponents are $\delta_1 = 0.5186$, $\delta_2 = 0.7647$.

and $r = 2\,\mathrm{mm}$. Here, the singularity rate is equal for both stress term orders δ_i. However, one can see that the shape functions for a complex δ_i are complex-valued (see 5.8). Then, also the components of displacements $H_i r^{\delta_i} \boldsymbol{\eta}_i(\theta)$ or stress function vectors $H_i r^{\delta_i} \boldsymbol{\lambda}_i(\theta)$, $i = 1,2$ are complex. In Fig. C.3 we can see that their imaginary parts have the same magnitude but an opposite sign and the total displacements or stress functions will be real. In the graphs in Fig 5.16 and 5.17 and in all following graphs the imaginary parts of the individual singularity exponents δ_i are omitted and only real part is depicted.

The GSIFs of above studied bi-material combinations are stated in Tab.5.5. The real singularity exponent δ implies that the corresponding GSIF is real-valued. For complex conjugate singularity exponents δ_i we get two distinct complex-valued GSIFs. In contrast to that, studies investigating interface cracks by the Hilbert problem [44, 57, 108] provide two complex conjugate stress intensity factors, but this difference is based on the formulation of the eigenvalue problem.

The LES formalism presented within the dissertation is able to cover arbitrary fibre orientations in the $x_1 x_2$ plane. In the most research studies, fibres either parallel or perpendicular to the global Cartesian coordinate system were considered, i.e. the principal material direction
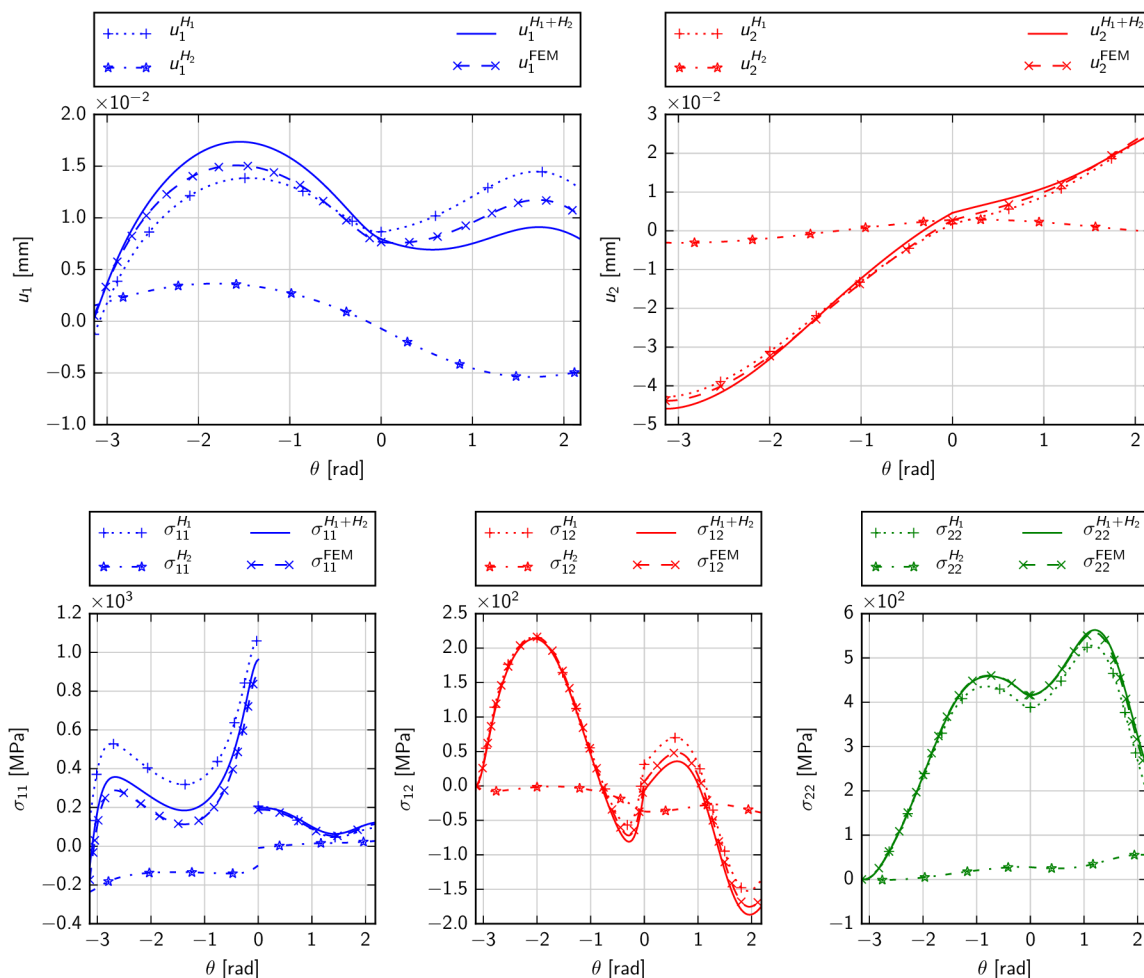
Fig. 5.15: The displacement and stress components on the circular path $r = 2\,\mathrm{mm}$ of a bi-material notch $\omega_1 = 125°$, $\omega_2 = -180°$. Materials are defined in Tab. 5.1, singularity exponents are $\delta_1 = 0.5186$, $\delta_2 = 0.7647$.

L coincides with either x_1 or x_2 axis. The stresses and displacements for the interface crack from the previous case, but with fibres of the material 1 rotated about $\alpha_1 = 50°$, are stated in Appendix C.3 in Fig. C.4. A study of the singularity exponent on the fibre orientation was reported in [115].
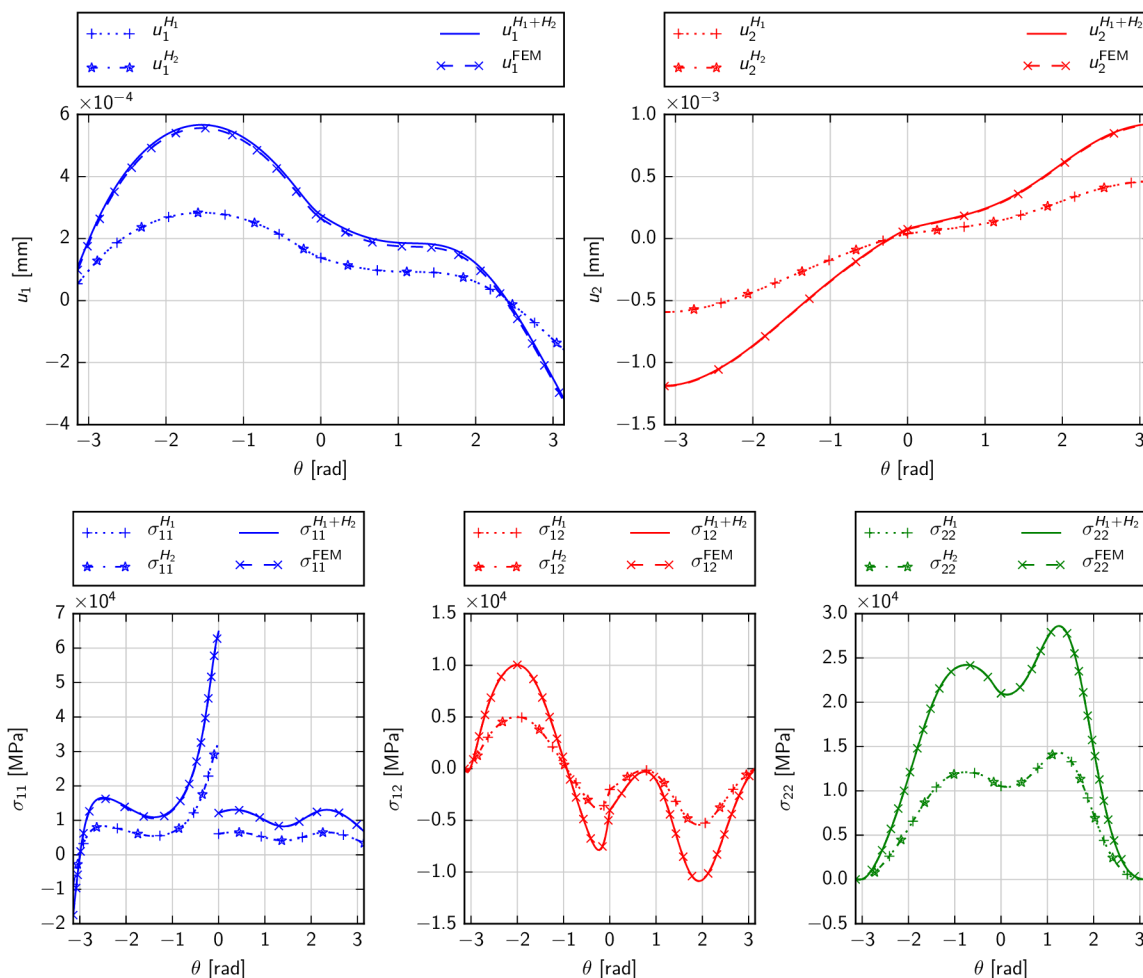
Fig. 5.16: The displacement and stress components on the circular path $r = 0.001\,\text{mm}$ of an interface crack $\omega_1 = 180°$, $\omega_2 = -180°$. Materials are defined in Tab. 5.1, singularity exponents are $\delta_1 = 0.5 + 0.02474i$, $\delta_2 = 0.5 - 0.02474i$.

5.1.8 Problem redefinition for modelling an isotropic/transversally isotropic bi-material notch

The LES formalism is primarily derived for anisotropic materials. If the the Young's and shear moduli, Poisson's ratios are equal in the longitudinal and transversal direction, respectively, the stiffness matrix attains the form of the isotropic material. Nevertheless, using of the relations defined in (4.60b) causes that the matrices $\mathbf{A}$ and $\mathbf{L}$ are degenerate or non-semisimple and cannot be no longer inverted. There are double material eigenvalue $\mu_{1,2} = i$. Let us consider a bi-material notch composed of one isotropic and one transversally isotropic material. To describe the elastic field of the isotropic material, the Muskhelishvili complex potential method [42] was implemented in the framework of previously described LES formalism. Though authors in [57, 60, 110, 123, 124] dealt with bi-material orthotropic/isotropic notches, nobody published detailed results for notches with complex values of δ.

Let us distinguish the parameters describing the isotropic material with asterisk. The com-
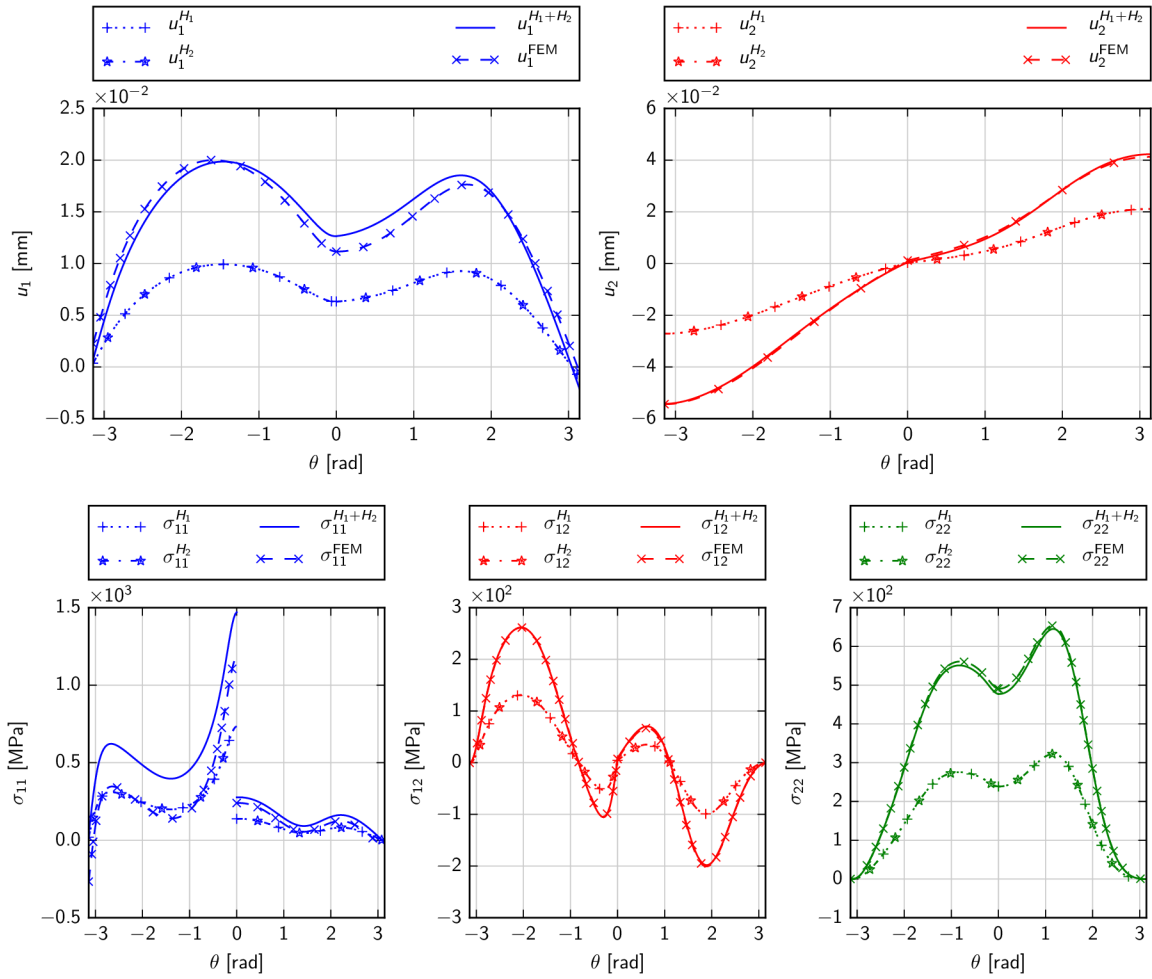
Fig. 5.17: The displacement and stress components on the circular path $r = 2\,\mathrm{mm}$ of an interface crack $\omega_1 = 180°$, $\omega_2 = -180°$. Materials are defined in Tab. 5.1, singularity exponents are $\delta_1 = 0.5 + 0.02474i$, $\delta_2 = 0.5 - 0.02474i$.

plex potentials $\mathbf{f}^*(z)$ are assumed as [125]

$$\mathbf{f}^*(z) = \mathbf{f}(z) + (\overline{z} - z)\,\mathbf{Q}\,\frac{\mathrm{d}\mathbf{f}(z)}{\mathrm{d}z}, \tag{5.80}$$

where

$$\mathbf{Q} = \begin{bmatrix} 0 & 0 \\ 1 & 0 \end{bmatrix}.$$

The components of complex potentials are sought in the form of

$$\mathbf{f}(z) = \begin{Bmatrix} \varphi(z) \\ \psi(z) \end{Bmatrix}. \tag{5.81}$$

The Muskhelishvili complex potentials $\varphi(z)$, $\psi(z)$ are assumed in the same form as in (5.8), i.e.

$$\varphi(z) = z^\delta v_1, \quad \psi(z) = z^\delta v_2, \tag{5.82}$$

ω_1 [°]	δ_1 δ_2	H_1 [MPa $\cdot$ mm$^{1-\delta_1}$] H_2 [MPa $\cdot$ mm$^{1-\delta_2}$]
90	0.5672 0.9456	186.8 131.9
125	0.5186 0.7647	529.8 −45.72
170	0.5187 + 0.01890i 0.5187 − 0.01890i	−33.89 − 692.5i −30.63 + 625.8i
180	0.5 + 0.02474i 0.5 − 0.02474i	−26.91 − 542.1i −23.04 + 464.1i

Tab. 5.5: GSIFs for four transversally orthotropic bi-material notches defined by ω_1 and $\omega_2 = -180°$ and material characteristics in 5.1.

where the complex variable z now becomes

$$z = r\left(\cos\theta + i\sin\theta\right). \tag{5.83}$$

Note that if the eigenvalues $\mu_{1,2} = i$ of the degenerate material are substituted into the simplified notation (5.13), the same relation as (5.81) are obtained. However, this representation provides only one linearly independent complex potential. The second potential is created by differentiation of the first one, because a function and its derivatives are linearly independent. The displacements and stress functions are expressed as

$$\mathbf{u}^*(z) = \mathbf{A}^* \mathbf{Z}^{*\delta} \mathbf{v} + \overline{\mathbf{A}^* \mathbf{Z}^{*\delta}} \mathbf{w}, \tag{5.84a}$$

$$\mathbf{T}^*(z) = \mathbf{L}^* \mathbf{Z}^{*\delta} \mathbf{v} + \overline{\mathbf{L}^* \mathbf{Z}^{*\delta}} \mathbf{w}, \tag{5.84b}$$

with matrices $\mathbf{A}^*$ and $\mathbf{L}^*$ defined as follows:

$$\mathbf{A}^* = \frac{1}{4Gi}\begin{bmatrix} \kappa i & -i \\ \kappa & 1 \end{bmatrix}, \quad \mathbf{L}^* = \frac{1}{2}\begin{bmatrix} i & -i \\ 1 & 1 \end{bmatrix}. \tag{5.85}$$

$\kappa = 3 - 4\nu$ for plane strain and $\kappa = (3-\nu)/(1+\nu)$ for plane stress, where ν is the Poisson's ratio of the isotropic material, and G is the shear modulus defined by

$$G = \frac{E}{2(1-\nu)}. \tag{5.86}$$

Applying (5.80), the function (5.13) attains the form

$$\mathbf{Z}^{*\delta} = \begin{bmatrix} z^\delta & 0 \\ (\overline{z}-z)\,\delta z^{\delta-1} & z^\delta \end{bmatrix} = \begin{bmatrix} r^\delta\,\mathrm{e}^{i\delta\theta} & 0 \\ -2i r^\delta \delta\,\mathrm{e}^{i(\delta-1)\theta}\sin\theta & r^\delta\,\mathrm{e}^{i\delta\theta} \end{bmatrix}. \tag{5.87}$$

The complex conjugation of (5.87) leads to:

$$\overline{\mathbf{Z}}^{*\delta} = \begin{bmatrix} r^\delta\,\mathrm{e}^{-i\delta\theta} & 0 \\ 2i r^\delta \delta\,\mathrm{e}^{-i(\delta-1)\theta}\sin\theta & r^\delta\,\mathrm{e}^{-i\delta\theta} \end{bmatrix}. \tag{5.88}$$

In the following paragraphs, the eigenvalue problem for an isotropic/transversally isotropic

bi-material notch is modified. When the relations for displacements and stress functions are known for both material states, the eigenvalue problem can be redefined in terms of the equations (5.84) and (5.7). Let us consider the bi-material notch geometry in Fig. 5.2, where the material 1 is isotropic, characterized by the material parameters E and μ. Let us redefine the matrices (5.85), (5.84) and (5.87) for the region I as:

$$
\begin{aligned}
\mathbf{A}^{\mathrm{I}} &= \mathbf{A}^{*}, \quad \mathbf{L}^{\mathrm{I}} = \mathbf{L}^{*} \\
\mathbf{u}^{\mathrm{I}} &= \mathbf{u}^{*}, \quad \mathbf{T}^{\mathrm{I}} = \mathbf{T}^{*} \\
\mathbf{Z}_1^{\mathrm{I}\delta} &= \mathbf{Z}_1^{*\delta}, \quad \mathbf{Z}_0^{\mathrm{I}\delta} = \mathbf{Z}_0^{*\delta},
\end{aligned}
\tag{5.89}
$$

while the corresponding relations for region II remain unchanged. The eigenvalue problem is introduced by substituting these relations into the boundary conditions (5.17) and (5.18). The system of eight homogeneous algebraic equations has the same form as (5.19). Note that the identity (5.20) is valid also for the isotropic material, i.e.

$$
\mathbf{Z}_0^{*\delta} = \mathbf{I}, \quad \overline{\mathbf{Z}}_0^{*\delta} = \mathbf{I}.
\tag{5.90}
$$

Then, the eigenvalue problem can be modified and reduced by (5.21)–(5.36). All other procedures remain identical, with complex potentials and material matrices corresponding to the considered region, i.e. the normalization (5.41a) or (5.41b), shape functions (5.43) and the Ψ-integral (5.47)–(5.69). The finite element model has the same properties and geometry, except for the material 1, for which isotropic properties are considered.

The relations for the asymptotic stress extraction (5.79) have to be also modified. The stresses have the following form:

$$
\begin{aligned}
\boldsymbol{\sigma}^{*1} &= H_1 r^{\delta_1-1}\tilde{\boldsymbol{\lambda}}_{1,x_2}^{*}(\theta) + H_2 r^{\delta_2-1}\tilde{\boldsymbol{\lambda}}_{2,x_2}^{*}(\theta), \\
\boldsymbol{\sigma}^{*2} &= H_1 r^{\delta_1-1}\tilde{\boldsymbol{\lambda}}_{1,x_1}^{*}(\theta) + H_2 r^{\delta_2-1}\tilde{\boldsymbol{\lambda}}_{2,x_1}^{*}(\theta),
\end{aligned}
\tag{5.91}
$$

where the derivatives of the shape functions are given by

$$
\tilde{\boldsymbol{\lambda}}_{i,x_2}^{*}(\theta) = \mathbf{B}^{*}\delta_i \mathbf{Z}^{*\delta_i-1}(\theta)\mathbf{v}_i + \overline{\mathbf{B}}^{*}\delta_i \overline{\mathbf{Z}}^{*\delta_i-1}(\theta)\mathbf{w}_i, \quad i=1,2,
\tag{5.92a}
$$

$$
\tilde{\boldsymbol{\lambda}}_{i,x_i}^{*}(\theta) = \mathbf{L}^{*}\delta_i \mathbf{Z}^{*\delta_i-1}(\theta)\mathbf{v}_i + \overline{\mathbf{L}}^{*}\delta_i \overline{\mathbf{Z}}^{*\delta_i-1}(\theta)\mathbf{w}_i, \quad i=1,2,
\tag{5.92b}
$$

where

$$
\mathbf{B}^{*} = \frac{1}{2}\begin{bmatrix} 3 & -1 \\ i & -i \end{bmatrix}
\tag{5.93}
$$

and

$$
\begin{aligned}
\mathbf{Z}^{*\delta-1} &= r^{\delta-1}\mathbf{Z}^{*\delta-1}(\theta) = r^{\delta-1}\begin{bmatrix} \delta\,\mathrm{e}^{i(\delta-1)\theta} & 0 \\ -2i\delta(\delta-1)\,\mathrm{e}^{i(\delta-2)\theta}\sin\theta & \delta\,\mathrm{e}^{i(\delta-1)\theta} \end{bmatrix}, \\
\overline{\mathbf{Z}}^{*\delta-1} &= r^{\delta-1}\overline{\mathbf{Z}}^{*\delta-1}(\theta) = r^{\delta-1}\begin{bmatrix} \delta\,\mathrm{e}^{-i(\delta-1)\theta} & 0 \\ 2i\delta(\delta-1)\,\mathrm{e}^{-i(\delta-2)\theta}\sin\theta & \delta\,\mathrm{e}^{-i(\delta-1)\theta} \end{bmatrix}.
\end{aligned}
\tag{5.94}
$$

Subscripts $_{,x_1}$ and $_{,x_2}$ denote differentiation with respect to x_1, x_2.
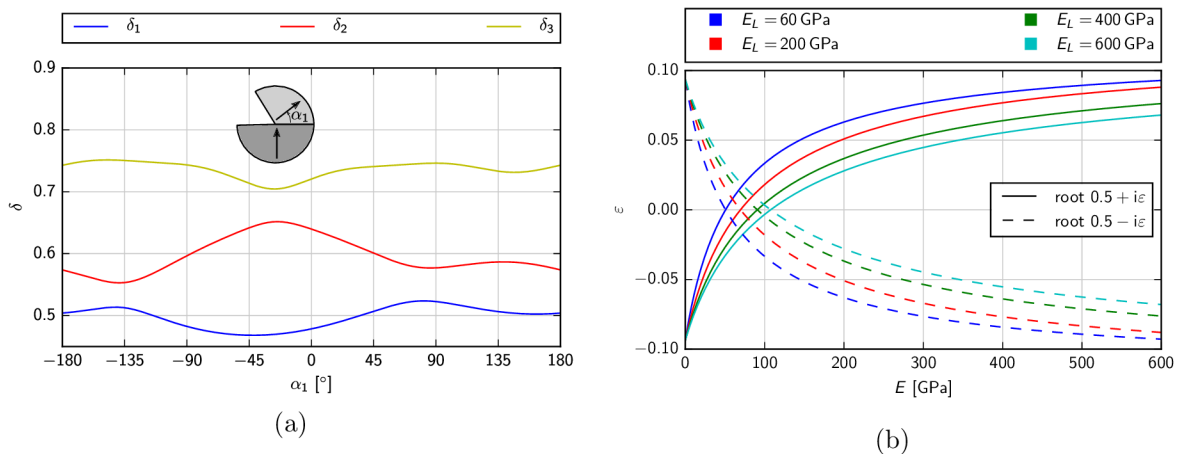
Fig. 5.18: (a) Dependence of the singularity exponents δ_i on the notch angle ω_1, material 1 is defined by $E = 200\,\mathrm{MPa}$, $\nu = 0.3$, material 2 is stated in Tab. 5.1, (b) the oscillatory index ε dependence on the Young's modulus E of the material 1 and four cases of material 2.

Example 6: Singularity exponents and displacement and stress reconstruction in the vicinity of the isotropic/transversally isotropic bi-material notch tip For the sake of brevity, we do not repeat all studies of the previous notch material configuration and we focus on the most interest ones, in which the different behaviour of the actual notch material configuration is expected. Let us consider a bi-material notch, where the material 1 is isotropic with following material properties: $E = 200\,\mathrm{MPa}$, $\nu = 0.3$. The material 2 is transversally isotropic with material properties stated in Tab. 5.1. Firstly, a study of the singularity exponent δ dependence on the notch angle ω_1 is performed, while $\omega_2 = -180°$ remains fixed. The result is illustrated in Fig. 5.18(a). It can be seen that the graph is similar to Fig. 5.5 for transversally isotropic bi-material notch.

A subsequent study was realized in order to investigate a variation of the oscillatory indices. Fig. 5.18(b) shows the dependency of the oscillatory indices on the Young's modulus E of the material 1 for four cases of longitudinal moduli E_L of the material 2. We see that the oscillatory indices are always symmetric with respect to zero, because the eigenvalues δ are complex conjugate. Then, the zero value of the oscillatory indices, contrary to its non-zero value implicitly assumed in the literature, is expected for the particular values of E. The zero values of ε_i are successively for $E = 50.73\,\mathrm{GPa}$, $E = 69.51\,\mathrm{GPa}$, $E = 90.71\,\mathrm{GPa}$, $E = 107.5\,\mathrm{GPa}$. A correlation of these moduli with another material parameters is not obvious.

The effect of the fibre orientation α_2 on the oscillatory indices for three Young's moduli of the material 1 is illustrated in Fig. 5.19. The oscillatory indices for an isotropic/transversally isotropic bi-material notch do not depend on the fibre orientation of the material 2.

The integration radius of the Ψ-integral procedure is chosen in accordance with the previous bi-material notch configurations. Let us consider a bi-material notch defined by $\omega_1 = 170°$, $\omega_2 = -180°$. The material parameters of the material 1 are $E = 200\,\mathrm{MPa}$ and $\nu = 0.3$ and properties of the material 2 are adopted from Tab. 5.1, but with fibre orientation $\alpha_2 = 50°$. The FEM model is loaded according to Fig. 5.11 with $\sigma_2^{\mathrm{appl}} = 100\,\mathrm{MPa}$. Two complex conjugate singularity exponents $\delta_{1,2} = 0.5092 \pm 0.0354i$ are obtained. The GSIFs are $H_1 = 532.1 + 228.8i$ MPa·mm$^{1-\delta_1}$ and $H_2 = 424.9 - 182.7i$ MPa·mm$^{1-\delta_2}$. The stresses and displacements on the radii $r = 0.001\,\mathrm{mm}$ and $r = 2\,\mathrm{mm}$ are shown in Fig. 5.20 and Fig. 5.21, respectively. A very good correspondence between the analytical and FEM solution is observed.
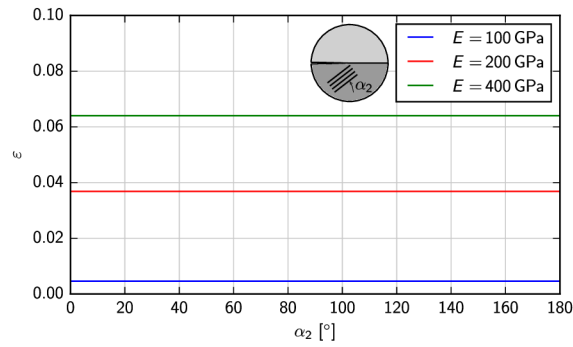
Fig. 5.19: Dependence study of the oscillatory index ε on the fibre orientation α_2 of the material 2 and four cases of material 1.
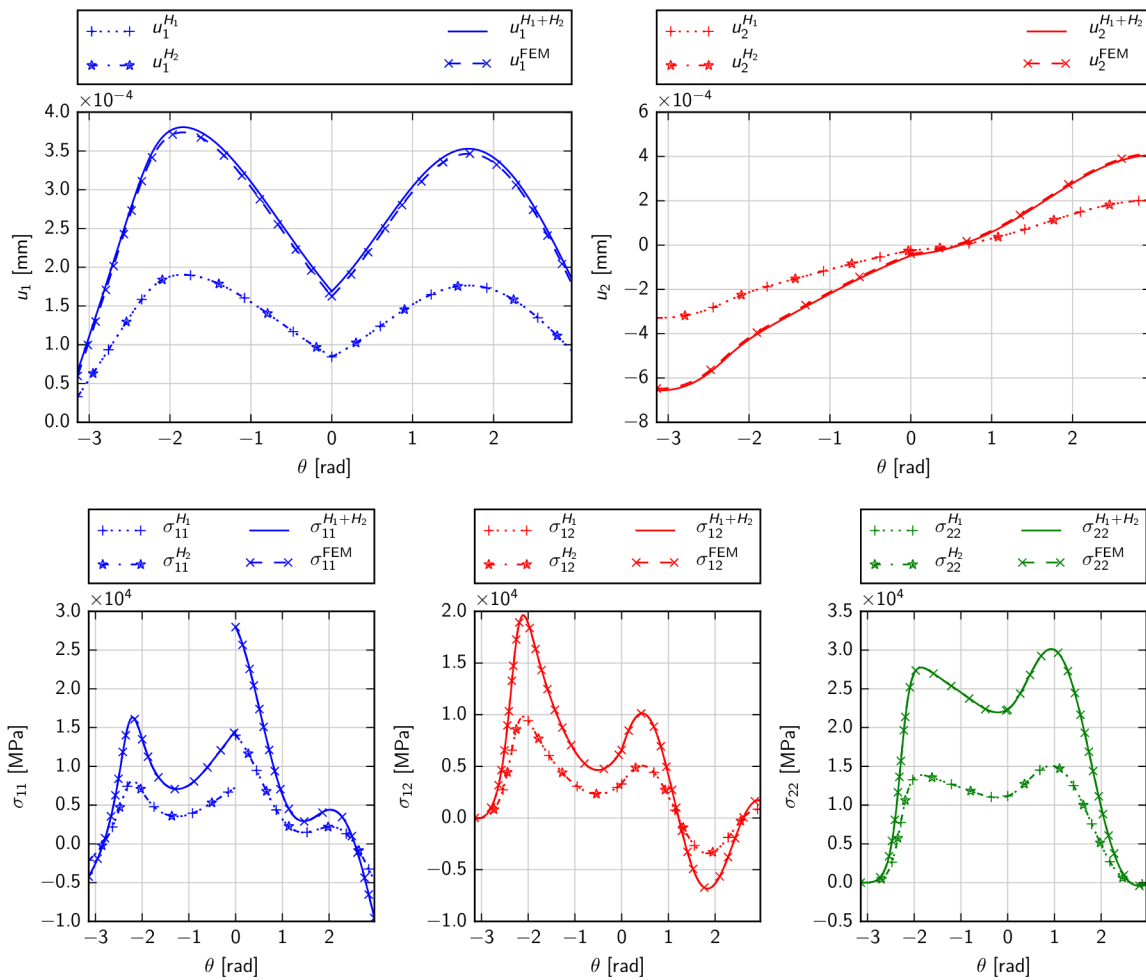
Fig. 5.20: The displacement and stress components on the circular path $r = 0.001\,\text{mm}$ of an isotropic/transversally isotropic bi-material notch $\omega_1 = 170°$, $\omega_2 = -180°$. Material 1 is isotropic ($E = 200\,\text{MPa}$ and $\nu = 0.3$), material 2 is defined in Tab. 5.1 with fibre orientation $\alpha_2 = 50°$, singularity exponents are $\delta_1 = 0.5092 + 0.03536i$, $\delta_2 = 0.5092 - 0.03536i$.
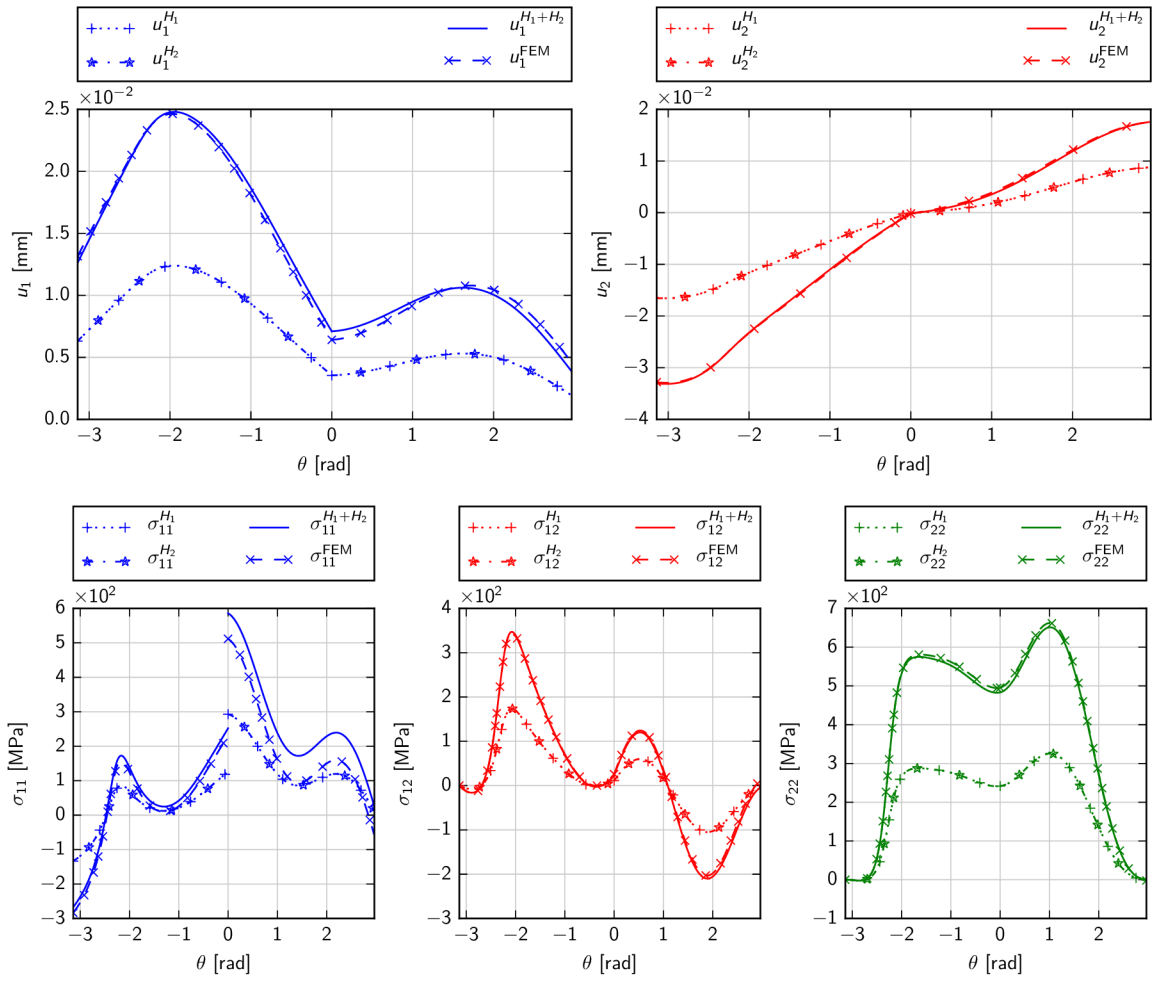
Fig. 5.21: The displacement and stress components on the circular path $r = 2\,\text{mm}$ of an isotropic/transversally isotropic bi-material notch $\omega_1 = 170°$, $\omega_2 = -180°$. Material 1 is isotropic ($E = 200\,\text{MPa}$ and $\nu = 0.3$), material 2 is defined in Tab. 5.1 with fibre orientation $\alpha_2 = 50°$, singularity exponents are $\delta_1 = 0.5092 + 0.03536i$, $\delta_2 = 0.5092 - 0.03536i$.

5.2 Stress singularity of a piezoelectric bi-material notch and interface crack

The analogy between theories describing pure anisotropic elasticity and piezoelectric electro-mechanical behaviour was outlined in section 4.2.7. With respect to the material symmetry, monoclinic materials with the symmetry axis parallel to $x_3 = 0$ have to be considered. This is the most general configuration when the expanded LES formalism can be employed. Then, stress and displacement relations in the x_3 direction are functions of the x_1 and x_2 coordinates only. The in-plane and anti-plane fields are decoupled, which enables the problem simplification. Under the assumption of external loads parallel to the plane defined by $x_3 = 0$, we can focus only on the in-plane field. Note that the anti-plane stresses or strains are not zero, but their effects are induced by in-plane loads. More detailed studies of anti-plane fields were reported in [53, 126, 127, 128, 129, 130, 131].

The present research of singular stress concentrators in the piezoelectric materials as well as in the anisotropic ones is mostly limited to the cases when the principal material directions are in coincidence with the global Cartesian axes. This brings about simplifications of the governing equations in the same manner as for pure anisotropic elastic bodies described by the equations (5.38)–(5.40). Additionally, there has also been a gap in linking between bi-material piezoelectric notches and interface cracks, which are investigated dominantly as the Hilbert problem (see [25, 26, 96, 98, 132]).

5.2.1 Formulation of the fundamental equations describing stress singularity of a piezoelectric bi-material notch

In the following paragraphs the expanded LES formalism for piezoelectric media introduced in section 4.2.8 is investigated. The in-plane complex representation of displacements and stresses for a piezoelectric bi-material wedge with the generally complex singularity exponents δ_i has the same form as (5.1), i.e.

$$\mathbf{u}(z) = \mathbf{A}\mathbf{Z}^{\delta}\mathbf{v} + \overline{\mathbf{A}\mathbf{Z}}^{\delta}\mathbf{w}, \tag{5.95a}$$

$$\mathbf{T}(z) = \mathbf{L}\mathbf{Z}^{\delta}\mathbf{v} + \overline{\mathbf{L}\mathbf{Z}}^{\delta}\mathbf{w}, \tag{5.95b}$$

where

$$\mathbf{u}(z) = \begin{Bmatrix} u_1 \\ u_2 \\ \phi \end{Bmatrix}, \quad \mathbf{T}(z) = \begin{Bmatrix} T_1 \\ T_2 \\ T_D \end{Bmatrix}, \tag{5.96a}$$

$$\mathbf{A} = \begin{bmatrix} a_{11} & a_{12} & a_{14} \\ a_{21} & a_{22} & a_{24} \\ a_{41} & a_{42} & a_{44} \end{bmatrix}, \quad \mathbf{L} = \begin{bmatrix} -\mu_1 & -\mu_2 & -\mu_4\xi_4 \\ 1 & 1 & \xi_4 \\ -\xi_1 & -\xi_2 & -1 \end{bmatrix}, \quad \mathbf{v} = \begin{Bmatrix} v_1 \\ v_2 \\ v_3 \end{Bmatrix}, \quad \mathbf{w} = \begin{Bmatrix} w_1 \\ w_2 \\ w_3 \end{Bmatrix}. \tag{5.96b}$$

Elements of the matrices $\mathbf{A}$ and $\mathbf{L}$ are introduced in (4.132b) and (4.127). To avoid a confusion, we kept the index 3 for the anti-plane parameters (consistent with pure anisotropic elasticity). But this was not applied to the eigenvectors, their indices do not have a directional correspondence. The singularity exponents δ_i and their corresponding eigenvectors are determined through the satisfaction of the boundary conditions at the tip of the bi-material notch.

5.2.2 Transversally isotropic materials

A poled piezoelectric ceramic has different material characteristics in the direction of poling than in the plane perpendicular to poling, in which the material behaviour is isotropic. Similarly to pure anisotropic elasticity, the matrices $\mathbf{A}$, $\mathbf{L}$ are non-degenerate if the poling direction is perpendicular with the x_3 axis. In the case of semi-degenerate or degenerate materials, i.e. when the poling direction coincide with x_3 axis, the general solution (5.95) requires a special treatment, see [17, p. 385].

Poled piezoelectric ceramics have transversally isotropic properties in the sense of both elastic and electric characteristics. We focus only on these technical types of non-degenerate ferroelectric materials with hexagonal crystals. The typical representatives are lead zirconate titanate, such as PZT-4, PZT-5H, PZT-6B, PZT-7, PZT-7A, barium titanate $BaTiO_3$, or zinc oxide ZnO. These functional ceramics possess very good actuating strain (maximal to 0.2%), high stiffness and a fast response.

The complex function $\mathbf{Z}^\delta$ has the form

$$\mathbf{Z}^\delta = \mathrm{diag} \left[z_1^\delta, z_2^\delta \, z_3^\delta \right], \tag{5.97}$$

where

$$z_i = x_1 + \mu_i x_2, \quad i = 1,2,3. \tag{5.98}$$

The material eigenvalues are evaluated from (4.123) reduced to the in-plane problem. Three material eigenvalues μ_1, μ_2, μ_3[3] are obtained for each material. The complex function $\mathbf{Z}^\delta$ can be also expressed in the polar coordinates in order easily specify the boundary conditions. Using (5.10), (5.12), (5.14) and (5.15), in which the indices are extended to $i = 1,2,3$, we can write

$$\mathbf{Z}^\delta = \mathrm{diag} \left[r^\delta R_1^\delta \, \mathrm{e}^{i\delta\Psi_1}, r^\delta R_2^\delta \, \mathrm{e}^{i\delta\Psi_2}, r^\delta R_3^\delta \, \mathrm{e}^{i\delta\Psi_3} \right] \tag{5.99}$$

and for the complex conjugate function

$$\overline{\mathbf{Z}}^\delta = \mathrm{diag} \left[r^\delta R_1^\delta \, \mathrm{e}^{-i\delta\Psi_1}, r^\delta R_2^\delta \, \mathrm{e}^{-i\delta\Psi_2}, r^\delta R_3^\delta \, \mathrm{e}^{-i\delta\Psi_3} \right]. \tag{5.100}$$

5.2.3 Formulation of the eigenvalue problem

With the previous assumptions, the eigenvalue problem presented in section 5.1.3 can be expanded to the piezoelectric materials. The boundary conditions (5.17) express that the notch faces are traction free and electrically insulated (impermeable, i.e. charge-free and the normal component of electric displacement D vanishes). The boundary conditions (5.17) imply that normal electrical displacement is zero on the notch faces, i.e. $D_n^{\mathrm{I}} = D_n^{\mathrm{II}} = 0$. This electric boundary condition is still debated, but it requires much simpler mathematical treatment and the zero surface charge condition is not violated, if one material has significantly higher permittivity than the second one, e.g. a piezoelectric ceramic in a contact with air [70]. The conditions (5.18) assure stress and electric displacement continuity in the direction normal to the interface, and displacement and electric potential continuity. The eigenvalue problem (5.19) has the same structure and the identical algebraic modifications (5.20)–(5.35) expanded to the dimensions of the piezoelectric problem can be employed. Here, the matrix $\mathbf{0}$ is 3×3 on the left-hand side, 12×1 on the right-hand side and $\mathbf{I}$ is a 3×3 identity matrix. The unknown exponents δ_i can be determined from the nonlinear characteristic equation (5.36). Within the dissertation, values bounded only on the interval $0 < \Re\{\delta\} < 1$ are considered.

---

[3]The eigenvalue μ_4 will be solution of the anti-plane characteristic equation $l_2(\mu) = 0$.
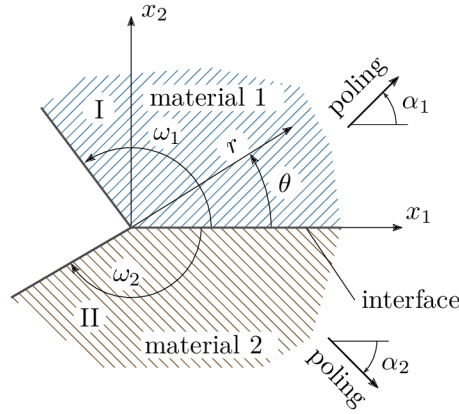
Fig. 5.22: Geometry of a bi-material notch characterized by two regions I and II. The notch faces are defined by angles ω_1 and ω_2. The bi-material interface is always considered at $\theta = 0$. The angles α_1 and α_2 denote poling directions of the materials I and II, respectively.

The auxiliary solutions needed for the determination of GSIFs by using the Ψ-integral is constructed in the same manner as for the pure anisotropic elasticity, i.e. considering $\hat{\delta} = -\delta$ as the exponent of the auxiliary solution. The eigenvectors $\hat{\mathbf{v}}^{\mathrm{I}}$ are evaluated by reinserting of the exponents $\hat{\delta}_i$ into (5.33) by employing (5.34). The remaining eigenvectors $\hat{\mathbf{v}}^{\mathrm{II}}$, $\hat{\mathbf{w}}^{\mathrm{I}}$ and $\hat{\mathbf{w}}^{\mathrm{II}}$ can be determined from (5.31), (5.35a) and (5.35b).

Example 7: Material eigenvalues of a piezoelectric material Let us consider a piezo-electric material with poling direction parallel with the x_1x_2-plane. The poling direction is characterizes by the angle α_i (see Fig. 5.22). Note that poling has a directional character, which corresponds to the polarization. It means, contrary to the fibre orientation of pure anisotropic elastic materials, that the poling direction rotated about for example $90°$ and $-90°$ does not give the identical material behaviour. The stiffness and permittivity matrices $\mathbf{S}_D$ and $\boldsymbol{\beta}_\sigma$, respectively, have the same structure for both poling orientations, but the only difference is in the structure of the piezoelectric matrix $\mathbf{g}$, of which elements have opposite signs for the above mentioned poling configurations. We will apply the formalism on common transversally isotropic piezoelectric materials, whose elastic, piezoelectric and electric characteristics are stated in Tab. 5.6. In many studies, the material properties are defined for poling in x_3-axis. To keep the formalism consistent with the LES for pure anisotropic elasticity, the poling direction is considered parallel with x_1-axis. The elastic, piezoelectric constants and permittivities can be reordered by the following procedure: $C_{11}^{E,x_1} = C_{33}^{E,x_3}$, $C_{12}^{E,x_1} = C_{13}^{E,x_3}$, $C_{23}^{E,x_1} = C_{12}^{E,x_3}$, $C_{22}^{E,x_1} = C_{11}^{E,x_3}$, $C_{44}^{E,x_1} = C_{44}^{E,x_3}$, $e_{11}^{x_1} = e_{33}^{x_3}$, $e_{12}^{x_1} = e_{13}^{x_3}$, $e_{26}^{x_1} = e_{15}^{x_3}$, $\omega_{11}^{\varepsilon,x_1} = \omega_{33}^{\varepsilon,x_3}$, $\omega_{22}^{\varepsilon,x_1} = \omega_{11}^{\varepsilon,x_3}$, where the superscripts $,x_1$ or $,x_3$ stand for poling in the x_1- or x_3-axis, respectively.

Since the in-plane problem only is considered, the material eigenvalues are evaluated from the second bracket in Eq. (4.123):

$$l_4(\mu)\rho_2(\mu) - m_3^2(\mu) = 0, \tag{5.101}$$

where $l_4(\mu)$, $\rho_2(\mu)$, $m_3(\mu)$ are defined in (4.120b). The using of the same numerical procedure as in the case of pure anisotropic elasticity is conditioned by the formulation of the equation (5.101) in the form of a polynomial, i.e

$$a_0 + a_1\mu + a_2\mu^2 + a_3\mu^3 + a_4\mu^4 + a_5\mu^5 + a_6\mu^6 = 0, \tag{5.102a}$$

material constants		PZT-4	PZT-5H	PZT-6B	PZT-7A	BaTiO$_3$
C_{11}^E	$\times 10^{10}$ [Pa]	11.3	11.7	16.3	13.1	14.6
C_{12}^E	$\times 10^{10}$ [Pa]	7.43	5.30	6.00	7.42	6.60
C_{23}^E	$\times 10^{10}$ [Pa]	7.78	5.50	6.00	7.62	6.60
C_{22}^E	$\times 10^{10}$ [Pa]	13.9	12.6	16.8	14.8	15.0
C_{44}^E	$\times 10^{10}$ [Pa]	2.56	3.53	2.71	2.54	4.40
e_{11}	[Cm^{-2}]	13.8	23.3	7.10	9.50	17.5
e_{12}	[Cm^{-2}]	-6.98	-6.50	-0.90	-2.10	-4.35
e_{26}	[Cm^{-2}]	13.4	17.0	4.60	9.70	11.4
ω_{11}^ε	$\times 10^{-9}$ [C(Vm)$^{-1}$]	5.47	13.0	3.40	7.35	11.2
ω_{22}^ε	$\times 10^{-9}$ [C(Vm)$^{-1}$]	6.00	15.1	3.60	8.11	9.87

Tab. 5.6: Material properties of some transversally isotropic piezoelectric ceramics poled in x_1-direction [23, 24, 25].

poling direction	μ_1	μ_2	μ_3
$\alpha = 0°$	$-0.2183 + 0.86483i$	$0.8396i$	$0.2183 + 0.86483i$
$\alpha = 50°$	$0.0944 + 1.3004i$	$0.1266 + 0.7898i$	$0.1757 + 1.0154i$
$\alpha = 90°$	$-0.2744 + 1.0871i$	$1.1910i$	$0.2744 + 1.0871i$
$\alpha = 180°$	$-0.2183 + 0.86483i$	$0.8396i$	$0.2183 + 0.86483i$

Tab. 5.7: Material eigenvalues for certain poling directions α of PZT-4.

where

$$a_0 = -\hat{S}_{22}^{\prime D} \hat{\beta}_{22}^{\prime \sigma} - \hat{g}_{22}^{\prime 2},$$

$$a_1 = 2 \left(\hat{S}_{26}^{\prime D} \hat{\beta}_{22}^{\prime \sigma} + \hat{S}_{22}^{\prime D} \hat{\beta}_{12}^{\prime \sigma} + \hat{g}_{22}'(\hat{g}_{12}' + \hat{g}_{26}') \right),$$

$$a_2 = -(2\hat{S}_{12}^{\prime D} + \hat{S}_{66}^{\prime D})\hat{\beta}_{22}^{\prime \sigma} - 4\hat{S}_{26}^{\prime D}\hat{\beta}_{12}^{\prime \sigma} - \hat{S}_{22}^{\prime D}\hat{\beta}_{11}^{\prime \sigma} - 2\hat{g}_{22}'(\hat{g}_{21}' + \hat{g}_{16}') - (\hat{g}_{12}' + \hat{g}_{26}')^2,$$

$$a_3 = 2 \left(\hat{S}_{16}^{\prime D} \hat{\beta}_{22}^{\prime \sigma} + (2\hat{S}_{12}^{\prime D} + \hat{S}_{66}^{\prime D})\hat{\beta}_{12}^{\prime \sigma} + \hat{S}_{26}^{\prime D}\hat{\beta}_{11}^{\prime \sigma} + \hat{g}_{11}'\hat{g}_{22}' + (\hat{g}_{12}' + \hat{g}_{26}')(\hat{g}_{21}' + \hat{g}_{16}') \right), \qquad (5.102b)$$

$$a_4 = -(2\hat{S}_{12}^{\prime D} + \hat{S}_{66}^{\prime D})\hat{\beta}_{11}^{\prime \sigma} - 4\hat{S}_{16}^{\prime D}\hat{\beta}_{12}^{\prime \sigma} - \hat{S}_{11}^{\prime D}\hat{\beta}_{22}^{\prime \sigma} - 2\hat{g}_{11}'(\hat{g}_{12}' + \hat{g}_{26}') - (\hat{g}_{21}' + \hat{g}_{16}')^2,$$

$$a_5 = 2 \left(\hat{S}_{16}^{\prime D} \hat{\beta}_{11}^{\prime \sigma} + \hat{S}_{11}^{\prime D}\hat{\beta}_{12}^{\prime \sigma} + \hat{g}_{11}'(\hat{g}_{21}' + \hat{g}_{16}') \right),$$

$$a_6 = -\hat{S}_{11}^{\prime D}\hat{\beta}_{11}^{\prime \sigma} - \hat{g}_{11}^{\prime 2}.$$

Then, the numerical procedure `polynomial.polyroots` from `numpy` library can be employed. In the case of an in-plane piezoelectric problem, three pairs of complex conjugate material eigenvalues are obtained. They are reordered according to (4.121).

In many studies, the poling direction is considered parallel with either x_1- or x_2-axis. Then, the material eigenvalues have the form $\mu_{1,3} = \mp a + bi$, $\mu_2 = ci$. When an arbitrary fibre orientation is considered, the real and imaginary parts of μ_1 and μ_3 are distinct. This is illustrated in Tab. 5.7 for PZT-4. The values for poling direction $\alpha = 90°$ agree with those in [52]. Note that for the cases $\alpha = 0°$ and $\alpha = 180°$ we get equal material eigenvalues, but as was mentioned in the previous paragraph, the material behaviour is different due to the opposite signs in the piezoelectric matrix $\hat{\mathbf{g}}'$.
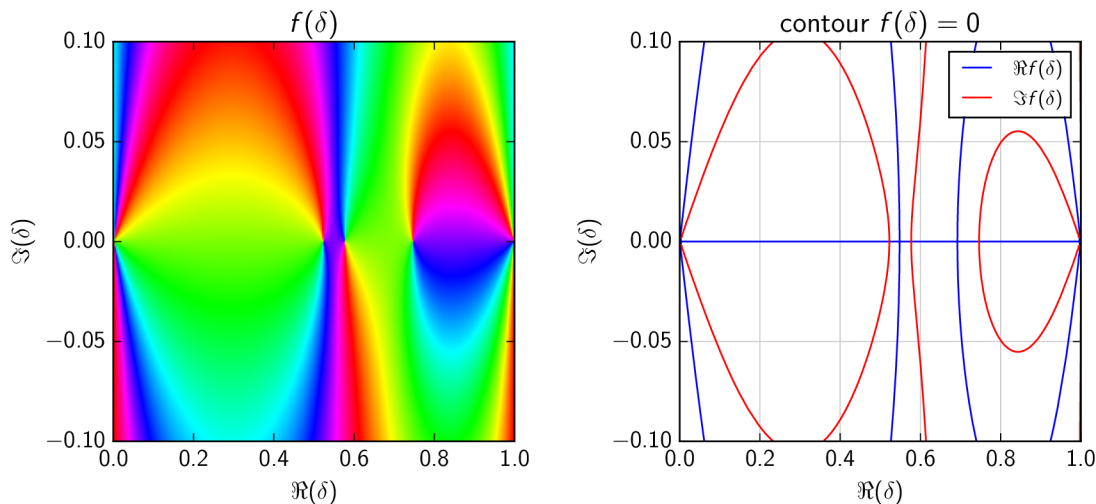
Fig. 5.23: The HSV phase portrait of the characteristic function $f(\delta) = \det[\mathbf{K}(\mathbf{I} - \mathbf{Y}_1^I)^{-1}]$ defined in (5.36) and the contour plot for $f(\delta) = 0$ for a PZT-5H/BaTiO$_3$ bi-material notch with geometry $\omega_1 = 120°$, $\omega_2 = -180°$. The intersections of the curves of different colour give the searched roots.

Example 8: Singularity exponents and eigenvectors of a piezoelectric bi-material notch The exponents δ_i can be also real or complex, but there are certain dissimilarities in comparison to pure anisotropic elasticity. In the root-finding procedure `findroot`, the Muller's method was chosen instead of the default secant method, which provided incorrect roots for some notch and material configurations or converged very slowly. The tolerance error remained 1×10^{-15}.

Let us consider PZT-5H/BaTiO$_3$ bi-material combination (the order will always be material 1/material 2) and a bi-material notch described by $\omega_1 = 120°$ and $\omega_2 = -180°$. In all following examples, the poling direction is parallel with x_2-axis ($\alpha_1 = \alpha_2 = 90°$) if it is not specified otherwise. The phase portrait of the transcendental function (5.36) is depicted in Fig. 5.23. We have obtained three real roots $\delta_1 = 0.5226$, $\delta_2 = 0.5770$ and $\delta_3 = 0.7462$ of the characteristic function (5.36) on the interval $0 < \Re\{\delta\} < 1$. In the case of an interface crack ($\omega_1 = 180°$), there are two complex conjugate roots $\delta_1 = 0.5 + 0.01293i$, $\delta_2 = 0.5 - 0.01293i$ and the third root is real, $\delta_3 = 0.5$, see Fig. 5.24. The real parts of the exponents are equal to 0.5. The imaginary part of the complex conjugate roots $\delta_{1,2}$ is the oscillatory index. The characteristic function (5.36) has two poles in the points $\delta = 0$ and $\delta = 1$ in the case of the notch as well as the interface crack.

Different results are obtained when we consider an interface crack between PZT-5H and PZT-4 materials. Note that the crack faces are considered to be impermeable, i.e. free of electric charge. One can see in Fig. 5.25 that there are three real roots $\delta_1 = 0.4558$, $\delta_2 = 0.5$ and $\delta_3 = 0.5442$ contrary to complex ones in the previous material combination. Why is the oscillatory index missing? Actually, it is not missing. The answer will be more clear by comparing the results with Ou and Wu [25], who investigated the interface crack in terms of the Hilbert problem, e.g. [44]. They found out that there are two types of singularities in the case of an interface crack between two piezoelectric materials – the oscillatory singularity when exponents have the oscillatory index ε or non-oscillatory singularity with the parameter $i\kappa$. In

Fig. 5.24: The HSV phase portrait of the characteristic function $f(\delta) = \det[\mathbf{K}(\mathbf{I} - \mathbf{Y}_1^{\mathrm{I}})^{-1}]$ defined in (5.36) and the contour plot for $f(\delta) = 0$ for a PZT-5H/BaTiO$_3$ interface crack with geometry $\omega_1 = 180°$, $\omega_2 = -180°$. The intersections of the curves of different colour give the searched roots.

the first case, the eigenvalues have the form

$$\delta_{1,2} = 0.5 \pm i\varepsilon, \tag{5.103}$$

while in the latter case

$$\delta_{1,3} = 0.5 \pm i(i\kappa) = 0.5 \mp \kappa, \tag{5.104}$$

which are real numbers. The bi-materials with an interface crack are then divided into two classes: ε-class and κ-class. Contrary to the Hilbert problem formulation used in [25], the employed procedure for solution of the eigenvalue problem (5.22) and (5.21) does not provide for κ-class bi-materials the parameter $i\kappa$ and the value 0.5 separately, but they are merged in the resulting roots δ of the characteristic function (5.36). When taking a look at the exponents for the PZT-5H/PZT-4 bi-material more closely, it can be seen that δ_1 and δ_3 are symmetric with respect to the $\delta_2 = 0.5$. Then the parameter κ can be extracted by subtracting the value 0.5 from δ_1 or δ_3, respectively. The obtained results of δ_1 and δ_2 for ε-class or δ_1 and δ_3 for κ-class bi-materials compared with the values reported in the literature are summarized in Tab. 5.8 and Tab. 5.9. The remaining exponents are always $\delta_3 = 0.5$ or $\delta_2 = 0.5$, respectively. Tab. 5.9 gives the parameter κ extracted from the obtained exponent using Eq. (5.104). One can see that the all received values of δ_1 and δ_2 or δ_3 coincide with the values reported in [25, 133].

A study of the dependence of the exponents δ_i on the notch angle ω_1 shows us more about the differences between particular bi-material classes. Let the angle $\omega_2 = -180°$ be fixed and the angle ω_1 changes on the interval $0 < \omega_1 < 180°$. The dependence of the exponents δ_i on the angle ω_1 for PZT-5H/BaTiO$_3$ bi-material is shown in Fig. 5.26(a). Similar behaviour can be obtained for all ε-class bi-materials. The eigenvalues δ_1 and δ_2 are real-valued almost in the whole interval $0 < \omega_1 < 180°$ except for the values $\omega_1 > 168°$, where they become complex conjugate. Note that the imaginary part of δ_2 is not plotted because it has the same values as $\Im\{\delta_1\}$ but with an opposite sign. The third exponent δ_3 corresponds to the non-singular
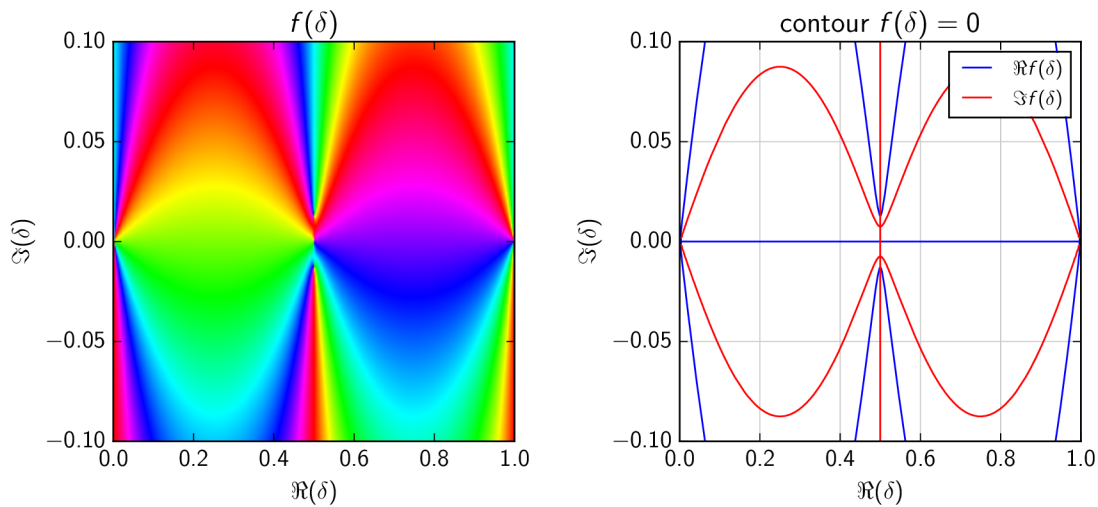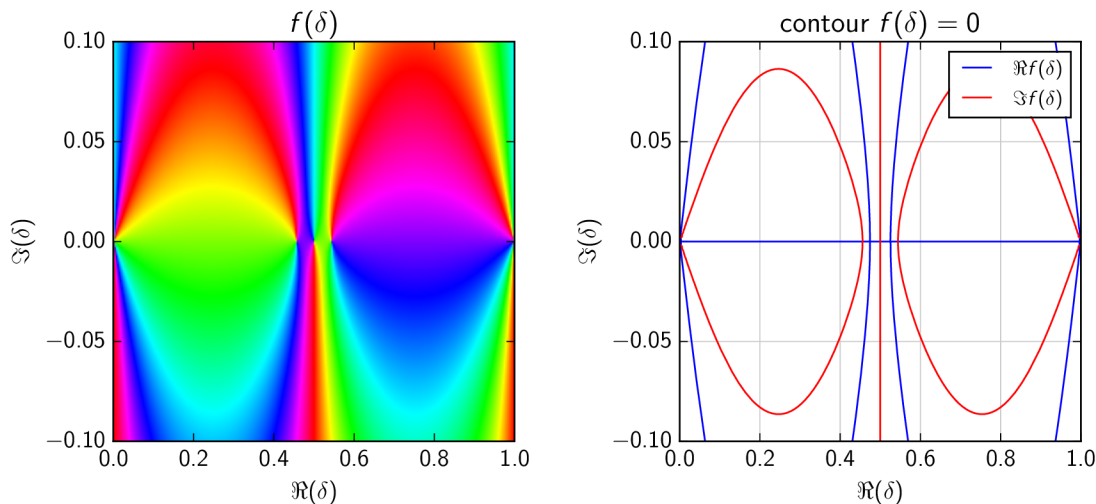
Fig. 5.25: The HSV phase portrait of the characteristic function $f(\delta) = \det[\mathbf{K}(\mathbf{I} - \mathbf{Y}_1^{\mathrm{I}})^{-1}]$ defined in (5.36) and the contour plot for $f(\delta) = 0$ for a PZT-5H/PZT-4 interface crack with geometry $\omega_1 = 180°$, $\omega_2 = -180°$. The intersections of the curves of different colour give the searched roots.

bi-materials	δ_1	δ_2	oscillatory index ε	comparison with Ou and Wu [25]
PZT-5H/BaTiO$_3$	$0.5 + 0.01293i$	$0.5 - 0.01293i$	0.01293	0.0130
PZT-5H/PZT-6B	$0.5 + 0.02189i$	$0.5 - 0.02189i$	0.02189	0.0219
PZT-5H/PZT-7A†	$0.5 + 0.00697i$	$0.5 - 0.00697i$	0.00697	0.0069
PZT-6B/PZT-7A	$0.5 + 0.00547i$	$0.5 - 0.00547i$	0.00547	0.0055

† $\delta_{1,2} = 0.5 \pm 0.00697i$ computed by Hwu and Kuo [21] by using the expanded Stroh formalism

Tab. 5.8: Oscillatory indices of ε-class bi-materials and their comparison with results in [25].

character of the stress and electric displacement field at the notch tip because $\delta_3 > 1$ up to $\omega_1 = 78°$ and it is always real. The real parts of complex conjugate eigenvalues δ_1 and δ_2 as well as the third exponent δ_3 converge to the value 0.5 for $\omega_1 \rightarrow 180°$. It has to be pointed out that δ_3 is not equal to the real parts of neither δ_1 nor δ_2 for very closed notch configurations. The dependency for other material combination, PZT-7A/BaTiO$_3$, is stated in Appendix D in Fig. D.1. It is obvious that the oscillatory index ε emerges in considerably smaller region of the angle ω_1 than in the previous case.

The same study was carried out for PZT-5H/PZT4 bi-material, one of representatives of the κ-class bi-materials. One can see in Fig. 5.26(b) the different dependency of the exponents δ_i on the ω_1 in contrast to the previous study. The third eigenvalue δ_3 provides the stress and electric displacement field at the notch tip, which is singular when $\delta_3 < 1$ for $\omega_1 > 75°$. Moreover, it is real-valued in the whole interval $0 < \omega_1 < 180°$. The exponents δ_1 and δ_2 are complex conjugate for $139° < \omega_1 < 166°$. For the interface crack as the limit case of the notch, the exponent δ_2 converges to 0.5, while the exponents δ_1 and δ_3 become symmetric with respect to the exponent δ_2. The same bi-material was investigated by Hirai et al. [23]. Unfortunately their results do not agree with our ones.

bi-materials	δ_1	δ_3	non-oscillatory index κ	comparison with Ou and Wu [25]
PZT-4/BaTiO$_3$	0.44914	0.55086	0.05086	0.0508
PZT-4/PZT-5H	0.45585	0.54415	0.04415	0.0442
PZT-4/PZT-6B	0.48316	0.51684	0.01684	0.0168
PZT-4/PZT-7A	0.47525	0.52475	0.02475	0.0247
PZT-6B/BaTiO$_3$	0.49039	0.50961	0.00961	0.0095
PZT-7A/BaTiO$_3$	0.47936	0.52064	0.02064	0.0206

Tab. 5.9: Non-oscillatory indices of κ-class bi-materials and their comparison with [25].

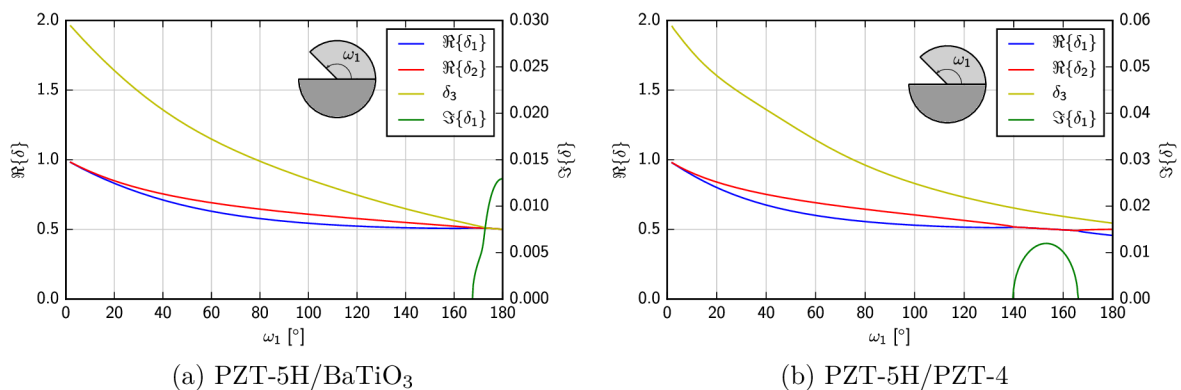(a) PZT-5H/BaTiO$_3$ (b) PZT-5H/PZT-4

Fig. 5.26: The exponent δ_i dependence on the notch geometry ω_1. Poling directions are $\alpha_1 = 90°$, $\alpha_2 = 90°$.

Comparing the graphs in Fig. 5.26(a) one can conclude that the bi-material classification introduced by Ou and Wu [25] for interface cracks cannot be applied to bi-material notches with a geometry characterized by an arbitrary angle ω_1. Depending on the angle ω_1 both bi-materials PZT-5H/BaTiO$_3$ and PZT-5H/PZT-4 exhibit both the ε-class type and κ-class type behaviour. In the case of PZT-5H/PZT-4 bi-material there exists even a value range of $139 < \omega_1 < 166°$ where simultaneously ε and κ differ from zero.

Ou and Wu bi-material classification also fails for interface cracks if one of the poling angles α_1 and/or α_2 differs from 90° as can be seen from the dependency of the exponents δ_i on the poling angle α_1 while the angle $\alpha_2 = 90°$ remains fixed. The PZT-5H/BaTiO$_3$ bi-material combination in Fig. 5.27(a) leads to two complex conjugate exponents δ_1 and δ_2 in a small interval $70° < \alpha_1 < 90°$ while their real parts are equal to 0.5. The third exponent is constant $\delta_3 = 0.5$. The exponents δ_1 and δ_3 become abruptly real-valued and symmetric with respect to δ_2 for the remaining values of α_1. Observe that with increasing miss-orientation of the poling orientations the exponent δ_1 starts to decrease and reaches a lowest value for anti-parallel poling orientation, i.e. for $\alpha_1 = -90°$. It is worth of noting that the stress and electric displacement field at the tip of the interface crack exhibits then a strong singularity, i.e. $\delta_1 < 0.5$.

The PZT-5H/PZT-4 bi-material notch has the real exponents δ_i in the agreement with Ou and Wu bi-material classification. In this case, the maximum of the singularity exponent δ_1 is again reached for parallel poling orientation and the minimum for anti-parallel poling orientation. The same parallelism effect of poling directions of the both materials in the cracked bi-material is shown in Figs. D.2(a) and D.2(b), but for the case of $\alpha_1 = \alpha_2 = 0$. The result that the always parallel poling directions maximize the singularity exponent of the stress and electric
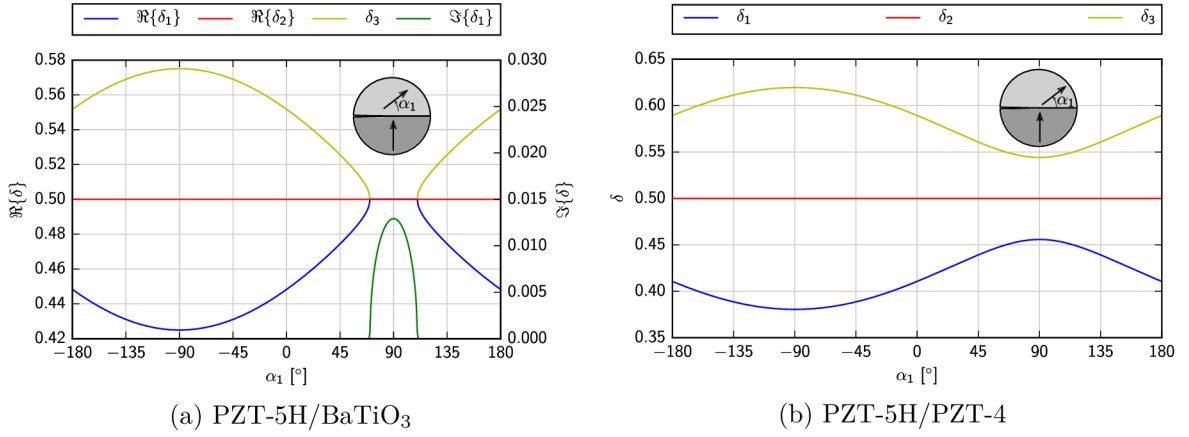
(a) PZT-5H/BaTiO$_3$ (b) PZT-5H/PZT-4

Fig. 5.27: The dependence of the interface crack exponents δ_i on the poling direction α_1. The poling direction $\alpha_2 = 90°$.

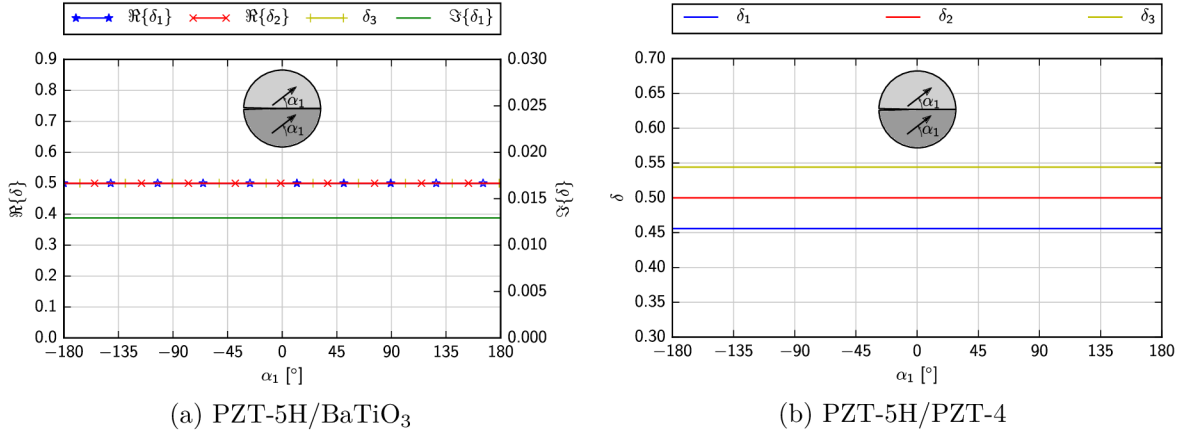(a) PZT-5H/BaTiO$_3$ (b) PZT-5H/PZT-4

Fig. 5.28: The dependence of the interface crack exponents δ_i on the poling direction α_1. The poling direction $\alpha_2 = \alpha_1$.

displacement field independently on the orientation of the poling directions with respect to the crack plane, is illustrated in Fig. 5.28.

The similar study was performed for non-symmetric bi-material notches. Two characteristic notch configurations have been investigated to get an idea about the exponents δ_i behaviour. Consider the PZT-5H/BaTiO$_3$ bi-material notch defined by $\omega_1 = 120°$ and $\omega_2 = 180°$. It is shown in Fig. 5.26(a) that there are three real exponents δ_i. Fig. 5.29(a) shows that variation of the poling direction α_1 does not affect the exponents δ_i, which remain real-valued. In contrast to that result, the PZT-5H/BaTiO$_3$ bi-material notch has two complex conjugate exponents δ_1, δ_2 and the real one δ_3 for $80° < \alpha_1 < 130°$. Three real exponents δ_i occur for the remaining values $0 < \alpha_1 < 80°$ and $130° < \alpha_1 < 180°$. Similar behaviour can be seen in Chen [86] for a right angle wedge in PZT-5H/PZT-4 bi-material. Thus, it can be concluded that the ε and κ classification of a bi-material is applicable only for an interface crack with poling directions $\alpha_1 = \alpha_2 = 90°$. It follows from the above investigation that a bi-material notch problem solved by (5.22) and (5.21) can have either three real exponents δ_i or two complex conjugates exponents δ_1, δ_2 with an oscillatory index ε and one real exponent δ_3. Closing a notch by $\omega_1 \to 180°$, two unique exponent developments – type A (Fig. 5.26(a)) or type B (Fig. 5.26(b)) are observed for
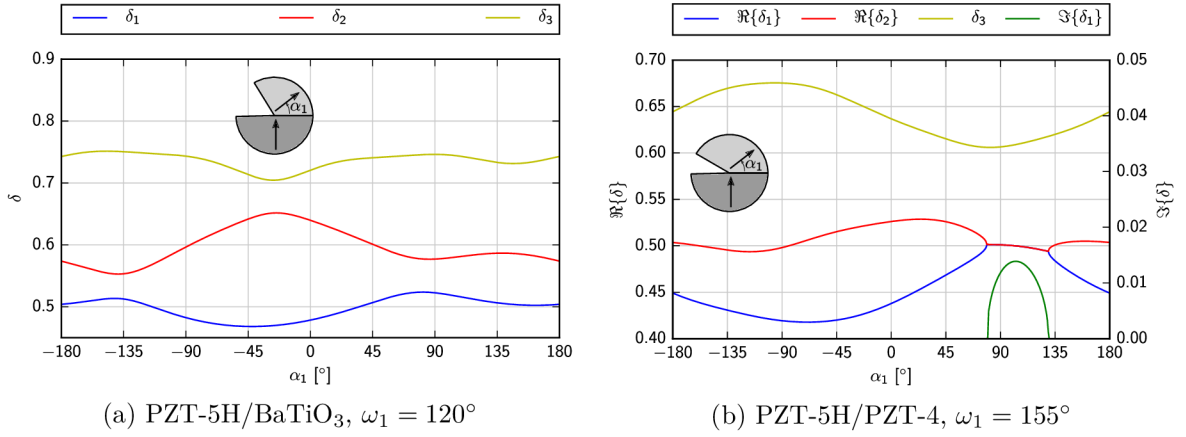
(a) PZT-5H/BaTiO$_3$, $\omega_1 = 120°$ (b) PZT-5H/PZT-4, $\omega_1 = 155°$

Fig. 5.29: Dependence study of the singularity exponents δ on the poling direction α_1 for two geometries of a bi-material notch. Poling direction $\alpha_2 = 90°$.

the poling directions $\alpha_1 = \alpha_2 = 90°$. Their limit configuration, an interface crack for $\omega_1 = 180°$, has either three real exponents (two δ_1 and δ_3 symmetric with respect to third one $\delta_2 = 0.5$) or two complex conjugate exponents δ_1, δ_2 with real parts 0.5 and one real exponent $\delta_3 = 0.5$. However, by changing the poling direction α_1, bi-materials can switch from one to another set of exponents δ_i. Furthermore, the interface crack is the only one concentrator where the symmetry of two exponents, e.g. δ_1 and δ_3, with respect to the third one δ_2 occurs. That is the reason why the classification introduced in Ou and Wu [25] cannot be used in the present study for general singular stress concentrators.

As a piezoelectric bi-material notch has two characteristic sets of exponents, eigenvectors have also two typical forms. A disproportion of elastic, piezoelectric and permittivity constants causes that the matrices appearing in the constitutive laws are ill-conditioned and hence the procedure `scipy.linalg.eig` gives erroneous results. For this reason, it is suitable to use an alternative method of the evaluation of the eigenvectors $\mathbf{v}_i^{\mathrm{I}}$, $\mathbf{v}_i^{\mathrm{II}}$, $\mathbf{w}_i^{\mathrm{I}}$, $\mathbf{w}_i^{\mathrm{II}}$ and their auxiliary complements $\hat{\mathbf{v}}_i^{\mathrm{I}}$, $\hat{\mathbf{v}}_i^{\mathrm{II}}$, $\hat{\mathbf{w}}_i^{\mathrm{I}}$, $\hat{\mathbf{w}}_i^{\mathrm{II}}$. By substituting δ_i into (5.28) (or (5.33) if δ_i is complex) we get

$$\mathbf{K}^*(\delta_i)\mathbf{v}_i^* = \mathbf{0}, \tag{5.105a}$$

where

$$\mathbf{K}^* = \mathbf{K}\left(\mathbf{I} - \mathbf{Y}_1^{\mathrm{I}}\right)^{-1}, \quad \mathbf{v}^* = 2\Re\left\{\mathbf{L}^{\mathrm{I}}\mathbf{v}^{\mathrm{I}}\right\} = \mathbf{0}, \quad \text{or} \quad \mathbf{v}^* = 2\mathbf{L}_a^{\mathrm{I}}\mathbf{v}_a^{\mathrm{I}}. \tag{5.105b}$$

Eq. (5.105a) can be expressed in the matrix form as

$$\begin{bmatrix} K_{11}^{i*} & K_{12}^{i*} & K_{13}^{i*} \\ K_{21}^{i*} & K_{22}^{i*} & K_{23}^{i*} \\ K_{31}^{i*} & K_{32}^{i*} & K_{33}^{i*} \end{bmatrix} \begin{Bmatrix} v_1^{i*} \\ v_2^{i*} \\ v_3^{i*} \end{Bmatrix} = \begin{Bmatrix} 0 \\ 0 \\ 0 \end{Bmatrix}. \tag{5.106}$$

Because of the singularity of the matrix $\mathbf{K}^*(\delta_i)$, one vector component is chosen, i.e. $v_3^{i*} = 1$, to eliminate one row of $\mathbf{K}^*(\delta_i)$. The system (5.106) is then reordered as follows:

$$\begin{bmatrix} K_{11}^{i*} & K_{12}^{i*} \\ K_{21}^{i*} & K_{22}^{i*} \end{bmatrix} \begin{Bmatrix} v_1^{i*} \\ v_2^{i*} \end{Bmatrix} = \begin{Bmatrix} -K_{13}^{i*} \\ -K_{23}^{i*} \end{Bmatrix}. \tag{5.107}$$

δ	$\mathbf{v}$	$\mathbf{w}$
δ_1	$\mathbf{v}^{\mathrm{I}} = \left\{ \begin{array}{c} 1.01825 + 2.47345i \\ -0.19379 - 0.01713i \\ -1.43309\mathrm{e}{-}10 + (6.58147\mathrm{e}{-}10)i \end{array} \right\}$	$\mathbf{w}^{\mathrm{I}} = \left\{ \begin{array}{c} 1.01825 - 2.47345i \\ -0.19379 + 0.01713i \\ -1.43309\mathrm{e}{-}10 - (6.58147\mathrm{e}{-}10)i \end{array} \right\}$
	$\mathbf{v}^{\mathrm{II}} = \left\{ \begin{array}{c} 1.23043 + 1.74304i \\ -0.76890 + 0.11476i \\ -3.18326\mathrm{e}{-}10 + (4.16499\mathrm{e}{-}10)i \end{array} \right\}$	$\mathbf{w}^{\mathrm{II}} = \left\{ \begin{array}{c} 1.23043 - 1.74304i \\ -0.76890 - 0.11476i \\ -3.18326\mathrm{e}{-}10 - (4.16499\mathrm{e}{-}10)i \end{array} \right\}$
δ_2	$\mathbf{v}^{\mathrm{I}} = \left\{ \begin{array}{c} -0.20437 + 1.71736i \\ 0.09387 + 0.04536i \\ -3.58696\mathrm{e}{-}10 + (3.89404\mathrm{e}{-}10)i \end{array} \right\}$	$\mathbf{w}^{\mathrm{I}} = \left\{ \begin{array}{c} -0.20437 - 1.71736i \\ 0.09387 - 0.04536i \\ -3.58696\mathrm{e}{-}10 - (3.89404\mathrm{e}{-}10)i \end{array} \right\}$
	$\mathbf{v}^{\mathrm{II}} = \left\{ \begin{array}{c} 0.09557 + 1.91080i \\ -0.07205 - 0.02546i \\ -4.09823\mathrm{e}{-}10 + (3.45040\mathrm{e}{-}10)i \end{array} \right\}$	$\mathbf{w}^{\mathrm{II}} = \left\{ \begin{array}{c} 0.09557 - 1.91080i \\ -0.07205 + 0.02546i \\ -4.09823\mathrm{e}{-}10 - (3.45040\mathrm{e}{-}10)i \end{array} \right\}$
δ_3	$\mathbf{v}^{\mathrm{I}} = \left\{ \begin{array}{c} -0.29351 + 0.63030i \\ -0.06068 - 0.13216i \\ -8.14879\mathrm{e}{-}10 - (1.34862\mathrm{e}{-}10)i \end{array} \right\}$	$\mathbf{w}^{\mathrm{I}} = \left\{ \begin{array}{c} -0.29351 - 0.63030i \\ -0.06068 + 0.13216i \\ -8.14879\mathrm{e}{-}10 + (1.34862\mathrm{e}{-}10)i \end{array} \right\}$
	$\mathbf{v}^{\mathrm{II}} = \left\{ \begin{array}{c} -1.31872 + 0.87143i \\ -0.20858 - 0.66727i \\ -5.08349\mathrm{e}{-}10 - (2.90745\mathrm{e}{-}10)i \end{array} \right\}$	$\mathbf{w}^{\mathrm{II}} = \left\{ \begin{array}{c} -1.31872 - 0.87143i \\ -0.20858 + 0.66727i \\ -5.08349\mathrm{e}{-}10 + (2.90745\mathrm{e}{-}10)i \end{array} \right\}$

Tab. 5.10: Eigenvectors corresponding to exponents $\delta_1 = 0.5154$, $\delta_2 = 0.5642$ and $\delta_3 = 0.7299$ of a PZT-5H/PZT-4 piezoelectric bi-material notch for $\omega_1 = 120°$, $\omega_2 = -180°$, $\alpha_1 = 90°$ and $\alpha_2 = 90°$.

The remaining vector components can be now solved as an ordinary system of two linear equations. In connection with the LES formalism we can define

$$\Re\left\{\mathbf{L}^{\mathrm{I}}\mathbf{v}_i^{\mathrm{I}}\right\} = \left\{ \begin{array}{c} v_1^{i*} \\ v_2^{i*} \\ 1 \end{array} \right\}. \tag{5.108}$$

The eigenvectors $\mathbf{L}^{\mathrm{I}}\mathbf{v}_i^{\mathrm{I}}$ can be firstly normalized by using (5.41a) or (5.41b) and subsequently evaluated by applying (5.30) or (5.34), (5.31) and (5.35). It has to be pointed out that the expressions (5.30) and (5.34) are not distinguished in the numerical algorithm.

Eigenvectors for the PZT-5H/PZT-4 bi-material notch defined by $\omega_1 = 120°$, $\omega_2 = -180°$ and poled in x_2-axis are stated in Tab. 5.10, while for an interface crack of PZT-5H/BaTiO$_3$ bi-material poled in x_2-axis are in Tab. 5.11. It can be seen that the eigenvector structure is same as by pure anisotropic elasticity, i.e. the eigenvectors $\mathbf{v}$ and $\mathbf{w}$ are complex conjugate for a real singular exponent δ and generally not complex conjugate for a complex-valued δ.

5.2.4 Expanded shape functions

Displacements and stress functions were redefined in terms of shape functions in section 5.1.4. Same treatment can be done for piezoelectric materials just by extending the addend with the third term, i.e.

$$\mathbf{u}(r,\theta) = H_1 r^{\delta_1}\boldsymbol{\eta}_1(\theta) + H_2 r^{\delta_2}\boldsymbol{\eta}_2(\theta) + H_3 r^{\delta_3}\boldsymbol{\eta}_3(\theta), \tag{5.109a}$$

$$\mathbf{T}(r,\theta) = H_1 r^{\delta_1}\boldsymbol{\lambda}_1(\theta) + H_2 r^{\delta_2}\boldsymbol{\lambda}_2(\theta) + H_3 r^{\delta_3}\boldsymbol{\lambda}_3(\theta), \tag{5.109b}$$

δ	$\mathbf{v}$	$\mathbf{w}$
δ_1	$\mathbf{v}^{\mathrm{I}} = \left\{ \begin{array}{c} 0.33567 + 0.21016i \\ 0.06121 \\ -1.03589\mathrm{e}{-}10 + (0.44011\mathrm{e}{-}10)i \end{array} \right\}$	$\mathbf{w}^{\mathrm{I}} = \left\{ \begin{array}{c} 0.39072 - 3.42865i \\ -0.10605 \\ -2.62627\mathrm{e}{-}10 - (9.44911\mathrm{e}{-}10)i \end{array} \right\}$
	$\mathbf{v}^{\mathrm{II}} = \left\{ \begin{array}{c} 0.32512 + 0.10606i \\ 0.02515 \\ -0.55929\mathrm{e}{-}10 + (0.16120\mathrm{e}{-}10)i \end{array} \right\}$	$\mathbf{w}^{\mathrm{II}} = \left\{ \begin{array}{c} 0.35495 - 3.08419i \\ 0.02265 \\ -0.78607\mathrm{e}{-}10 - (5.22511\mathrm{e}{-}10)i \end{array} \right\}$
δ_2	$\mathbf{v}^{\mathrm{I}} = \left\{ \begin{array}{c} 0.42379 + 3.71880i \\ -0.11503 \\ -2.84852\mathrm{e}{-}10 + (10.2488\mathrm{e}{-}10)i \end{array} \right\}$	$\mathbf{w}^{\mathrm{I}} = \left\{ \begin{array}{c} 0.36407 - 0.22794i \\ 0.06639 \\ -1.12356\mathrm{e}{-}10 - (0.47735\mathrm{e}{-}10)i \end{array} \right\}$
	$\mathbf{v}^{\mathrm{II}} = \left\{ \begin{array}{c} 0.38498 + 3.34518i \\ 0.02457 \\ -0.85260\mathrm{e}{-}10 + (5.66729\mathrm{e}{-}10)i \end{array} \right\}$	$\mathbf{w}^{\mathrm{II}} = \left\{ \begin{array}{c} 0.35263 - 0.11504i \\ 0.02727 \\ -0.60662\mathrm{e}{-}10 - (0.17484\mathrm{e}{-}10)i \end{array} \right\}$
δ_3	$\mathbf{v}^{\mathrm{I}} = \left\{ \begin{array}{c} 0.24554 + 2.72943i \\ 0.50892 \\ -1.90684\mathrm{e}{-}10 + (7.55132\mathrm{e}{-}10)i \end{array} \right\}$	$\mathbf{w}^{\mathrm{I}} = \left\{ \begin{array}{c} 0.24554 - 2.72943i \\ 0.50892 \\ -1.90684\mathrm{e}{-}10 - (7.55132\mathrm{e}{-}10)i \end{array} \right\}$
	$\mathbf{v}^{\mathrm{II}} = \left\{ \begin{array}{c} 0.41885 + 2.16557i \\ 0.16229 \\ -0.84048\mathrm{e}{-}10 + (3.65881\mathrm{e}{-}10)i \end{array} \right\}$	$\mathbf{w}^{\mathrm{II}} = \left\{ \begin{array}{c} 0.41885 - 2.16558i \\ 0.16229 \\ -0.84048\mathrm{e}{-}10 - (3.65881\mathrm{e}{-}10)i \end{array} \right\}$

Tab. 5.11: Eigenvectors corresponding to exponents $\delta_1 = 0.5 + 0.01293i$, $\delta_2 = 0.5 + 0.01293i$ and $\delta_3 = 0.5$ of a PZT-5H/BaTiO$_3$ piezoelectric interface crack for $\omega_1 = 180°$, $\omega_2 = -180°$, $\alpha_1 = 90°$ and $\alpha_2 = 90°$.

where $\boldsymbol{\eta}_i$ and $\boldsymbol{\lambda}_i$ are defined in (5.43). The matrices $\mathbf{A}$, $\mathbf{L}$ and eigenvectors $\mathbf{v}_i^{\mathrm{I}}$, $\mathbf{v}_i^{\mathrm{II}}$, $\mathbf{w}_i^{\mathrm{I}}$, $\mathbf{w}_i^{\mathrm{II}}$ are expressed in Eq. (5.96b). Components of the shape functions are

$$\boldsymbol{\eta}_i(\theta) = \left\{ \begin{array}{c} \eta_1^i \\ \eta_2^i \\ \eta_3^i \end{array} \right\}, \quad \boldsymbol{\lambda}_i(\theta) = \left\{ \begin{array}{c} \lambda_1^i \\ \lambda_2^i \\ \lambda_3^i \end{array} \right\}, \quad i = 1,2,3. \tag{5.110}$$

The complex potentials are simply expanded as

$$\begin{aligned} \mathbf{Z}^\delta &= r^\delta \mathbf{Z}^\delta(\theta) = r^\delta \, \mathrm{diag} \left[R_1^\delta \, \mathrm{e}^{i\delta\Psi_1}, R_2^\delta \, \mathrm{e}^{i\delta\Psi_2}, R_3^\delta \, \mathrm{e}^{i\delta\Psi_3} \right], \\ \overline{\mathbf{Z}}^\delta &= r^\delta \overline{\mathbf{Z}}^\delta(\theta) = r^\delta \, \mathrm{diag} \left[R_1^\delta \, \mathrm{e}^{-i\delta\Psi_1}, R_2^\delta \, \mathrm{e}^{-i\delta\Psi_2}, R_3^\delta \, \mathrm{e}^{-i\delta\Psi_3} \right], \end{aligned} \tag{5.111}$$

where R_i and Ψ_i are given by (5.14) and (5.15).

Example 9: Shape functions of a piezoelectric bi-material notch   The shape functions of a PZT-5H/PZT-4 bi-material notch with face angles $\omega_1 = 120°$, $\omega_2 = -180°$ and an interface crack for PZT-5H/BaTiO$_3$ bi-material are shown in Fig. 5.30 and Fig. 5.31. The structure of the functions is identical with the shape functions of pure anisotropic elasticity, i.e. when the eigenvalue is complex, so is the shape function. The third components of $\boldsymbol{\eta}$ and $\boldsymbol{\lambda}$ were depicted in a separate graph due to its scale and units. It is worth noticing that η_1 and η_2 correspond to the displacements $\mathbf{u}$, while η_3 is related to the electric potential ϕ. The shape functions λ_1 and λ_2 are related to the stress function $\mathbf{T}$, λ_3 describes the electric displacement D.

(a)

(b)
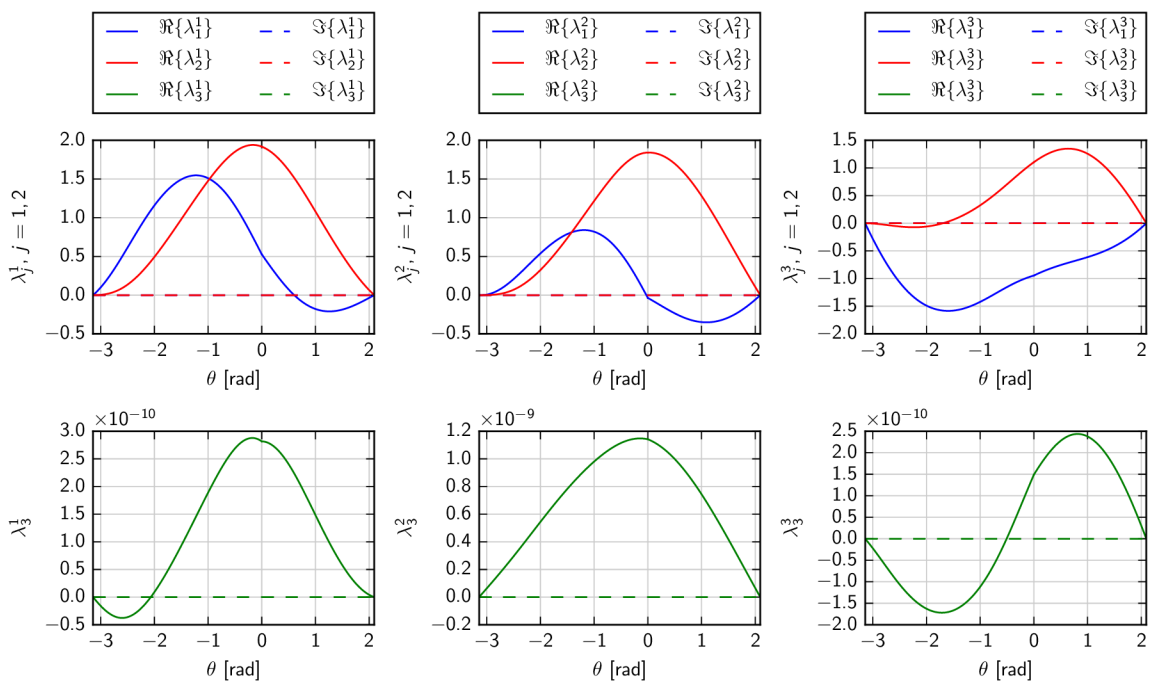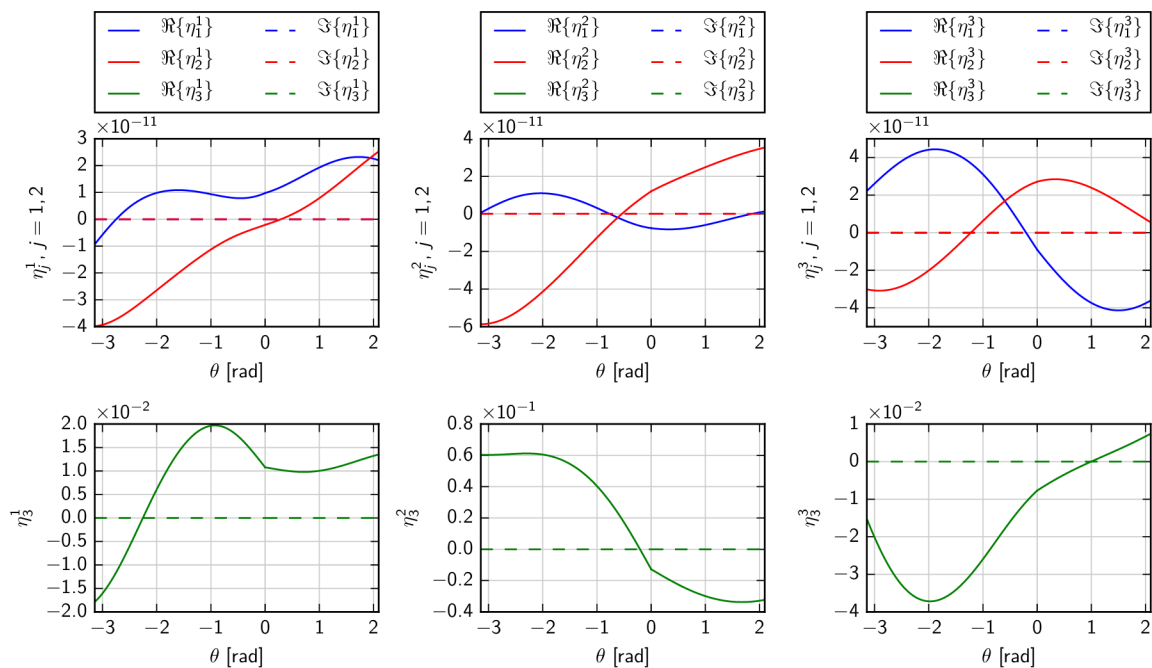
Fig. 5.30: Components of the shape function vectors (a) $\boldsymbol{\eta}_1$, $\boldsymbol{\eta}_2$, $\boldsymbol{\eta}_3$ and (b) $\boldsymbol{\lambda}_1$, $\boldsymbol{\lambda}_2$, $\boldsymbol{\lambda}_3$ for a PZT-5H/PZT-4 bi-material notch defined by $\omega_1 = 120°$, $\omega_2 = -180°$.
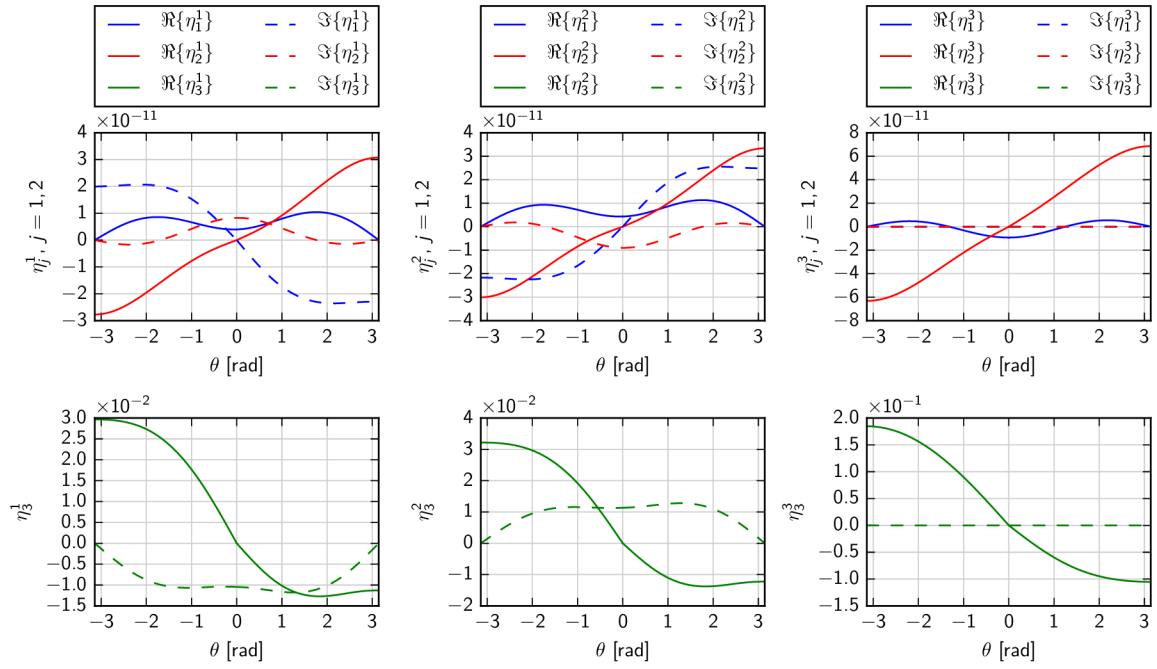
(a)
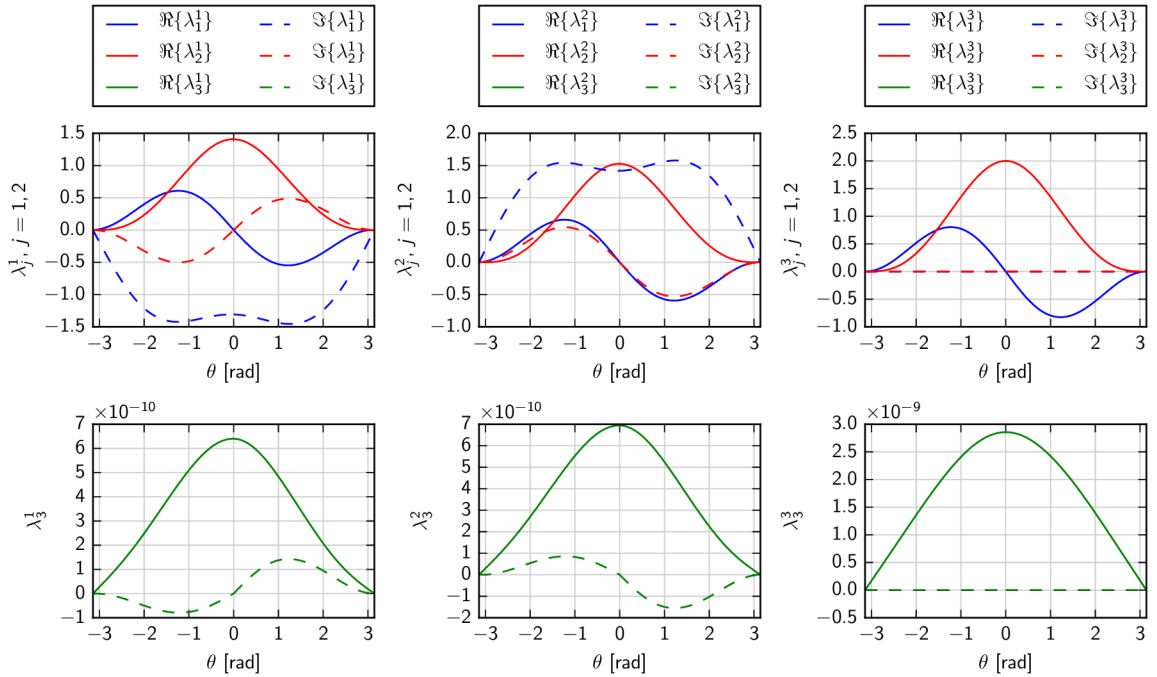
(b)

Fig. 5.31: Components of the shape function vectors (a) $\boldsymbol{\eta}_1$, $\boldsymbol{\eta}_2$, $\boldsymbol{\eta}_3$ and (b) $\boldsymbol{\lambda}_1$, $\boldsymbol{\lambda}_2$, $\boldsymbol{\lambda}_3$ for an interface crack of PZT-5H/BaTiO$_3$ bi-material.

5.2.5 Determination of the generalized stress intensity factors

This paragraph directly follows section 5.1.5, which introduced the Ψ-integral applied to pure anisotropic bi-material notches. The definitions (5.47)–(5.60) assume traction free notch faces. Considering of piezoelectric material implies that the notch faces are also electrically impermeable, i.e. $D_n = 0$ along the notch faces, as follows from the boundary conditions (5.17). It makes sense from the physical point of view. When the face is not mechanically loaded, it means that it is in a contact with air, which has permittivity very close to vacuum and the circuit is open. This is the most common case that can be investigated in engineering applications. If the notch faces will be in a contact with a body of higher permittivity, the boundary conditions (5.17) will be different and the whole formalism including the Ψ-integral (5.58) has to be modified. Within the following section, traction free and electrically open (impermeable) notch faces are assumed.

The relations for the auxiliary solutions (5.48) and corresponding auxiliary shape functions (5.49) were expanded according to the dimensions of the piezoelectric problem, i.e. $i = 1,2,3$. The eigenvectors $\hat{\mathbf{v}}$, $\hat{\mathbf{w}}$ are computed by using the same algorithm described in Example 8 just by substituting $\hat{\delta}_i = -\delta_i$. The development of the auxiliary solutions corresponding to the regular solutions depicted in Fig. 5.30 and 5.31 is shown in Appendix D.1 (Fig. D.3 and D.4).

Substituting (5.109b) into (5.50) we get the traction vector

$$-\mathbf{t}(r,\theta) = H_1 r^{\delta_1-1} \boldsymbol{\lambda}_1'(\theta) + H_2 r^{\delta_2-1} \boldsymbol{\lambda}_2'(\theta) + H_3 r^{\delta_3-1} \boldsymbol{\lambda}_3'(\theta), \tag{5.112}$$

where $()'$ denotes differentiation with respect to θ and $\boldsymbol{\lambda}'(\theta)$ is defined in (5.52). The auxiliary solutions corresponding to Eq. (5.112) are expressed in (5.55) and (5.56). The first derivative of the complex potentials $\mathbf{Z}^\delta(\theta)$ and $\overline{\mathbf{Z}}^\delta(\theta)$ can be written as:

$$\left(\mathbf{Z}^\delta(\theta)\right)' = \operatorname{diag}\left[\delta R_1^{\delta-1} e^{i(\delta-1)\Psi_1} \left[-\sin(\theta) + \mu_1 \cos(\theta)\right],\right.$$
$$\delta R_2^{\delta-1} e^{i(\delta-1)\Psi_2} \left[-\sin(\theta) + \mu_2 \cos(\theta)\right],$$
$$\left.\delta R_3^{\delta-1} e^{i(\delta-1)\Psi_3} \left[-\sin(\theta) + \mu_3 \cos(\theta)\right]\right] \tag{5.113}$$

and

$$\left(\overline{\mathbf{Z}}^\delta(\theta)\right)' = \operatorname{diag}\left[\delta R_1^{\delta-1} e^{-i(\delta-1)\Psi_1} \left[-\sin(\theta) + \overline{\mu}_1 \cos(\theta)\right],\right.$$
$$\delta R_2^{\delta-1} e^{-i(\delta-1)\Psi_2} \left[-\sin(\theta) + \overline{\mu}_2 \cos(\theta)\right]$$
$$\left.\delta R_3^{\delta-1} e^{-i(\delta-1)\Psi_3} \left[-\sin(\theta) + \overline{\mu}_3 \cos(\theta)\right]\right]. \tag{5.114}$$

The substitution of these regular and auxiliary solutions for the piezoelectric problem into (5.60) maintains all the orthogonality and path-independence properties of the Ψ-integral and does not modify the relations (5.61)–(5.63).

The second integral (5.64) is constructed in the same manner as for pure anisotropic bi-materials, i.e. by using the auxiliary displacements and tractions as the virtual state and the FEM solution as the full-field one. The tractions are computed by using the Cauchy's formula $t_i = \sigma_{ij} n_j$ expanded to piezoelectric problems, i.e.

$$\mathbf{t}^{\mathrm{FEM}} = \boldsymbol{\sigma}^{\mathrm{FEM}} \mathbf{n}, \tag{5.115}$$

where $\boldsymbol{\sigma}^{\mathrm{FEM}}$ is the expanded two-dimensional stress-electric displacement tensor

$$\boldsymbol{\sigma}^{\mathrm{FEM}} = \begin{bmatrix} \sigma_{11}^{\mathrm{FEM}} & \sigma_{12}^{\mathrm{FEM}} \\ \sigma_{21}^{\mathrm{FEM}} & \sigma_{22}^{\mathrm{FEM}} \\ D_1^{\mathrm{FEM}} & D_2^{\mathrm{FEM}} \end{bmatrix} \tag{5.116}$$

and $\mathbf{n}$ has the same form as in (5.66). The displacement vector is expanded with the electric potential ϕ as the third component, i.e. $\mathbf{u}^{\mathrm{FEM}} = [u_1^{\mathrm{FEM}}, u_2^{\mathrm{FEM}}, \phi^{\mathrm{FEM}}]^{\mathsf{T}}$. The integral $\Psi\left(\mathbf{u}^{\mathrm{FEM}}, r_c^{-\delta_i}\hat{\boldsymbol{\eta}}_i(\theta)\right)$ has the form

$$\Psi\left(\mathbf{u}^{\mathrm{FEM}}, r_c^{-\delta_i}\hat{\boldsymbol{\eta}}_i(\theta)\right) = \Psi\left(H_1 r_c^{\delta_1}\boldsymbol{\eta}_1(\theta) + H_2 r_c^{\delta_2}\boldsymbol{\eta}_2(\theta) + H_3 r_c^{\delta_3}\boldsymbol{\eta}_3(\theta), r_c^{-\delta_i}\hat{\boldsymbol{\eta}}_i(\theta)\right) =$$
$$= H_1\Psi\left(r^{\delta_1}\boldsymbol{\eta}_1(\theta), r_c^{-\delta_i}\hat{\boldsymbol{\eta}}_i(\theta)\right) + H_2\Psi\left(r^{\delta_2}\boldsymbol{\eta}_2(\theta), r_c^{-\delta_i}\hat{\boldsymbol{\eta}}_i(\theta)\right) +$$
$$+ H_3\Psi\left(r^{\delta_3}\boldsymbol{\eta}_3(\theta), r_c^{-\delta_i}\hat{\boldsymbol{\eta}}_i(\theta)\right), \quad i = 1,2,3. \quad (5.117)$$

Applying the orthogonality (5.62), three separate relations are obtained:

$$\begin{aligned}
\Psi\left(\mathbf{u}^{\mathrm{FEM}}, r_c^{-\delta_1}\hat{\boldsymbol{\eta}}_1(\theta)\right) &= H_1\Psi\left(r_c^{\delta_1}\boldsymbol{\eta}_1(\theta), r_c^{-\delta_1}\hat{\boldsymbol{\eta}}_1(\theta)\right), \\
\Psi\left(\mathbf{u}^{\mathrm{FEM}}, r_c^{-\delta_2}\hat{\boldsymbol{\eta}}_2(\theta)\right) &= H_2\Psi\left(r_c^{\delta_2}\boldsymbol{\eta}_2(\theta), r_c^{-\delta_2}\hat{\boldsymbol{\eta}}_2(\theta)\right), \\
\Psi\left(\mathbf{u}^{\mathrm{FEM}}, r_c^{-\delta_3}\hat{\boldsymbol{\eta}}_3(\theta)\right) &= H_3\Psi\left(r_c^{\delta_3}\boldsymbol{\eta}_3(\theta), r_c^{-\delta_3}\hat{\boldsymbol{\eta}}_3(\theta)\right),
\end{aligned} \quad (5.118)$$

from which three generalized stress intensity factors for a piezoelectric problem can be expressed:

$$\begin{aligned}
H_1 &= \frac{\Psi\left(\mathbf{u}^{\mathrm{FEM}}, r_c^{-\delta_1}\hat{\boldsymbol{\eta}}_1(\theta)\right)}{\Psi\left(r_c^{\delta_1}\boldsymbol{\eta}_1(\theta), r_c^{-\delta_1}\hat{\boldsymbol{\eta}}_1(\theta)\right)}, \\[2mm]
H_2 &= \frac{\Psi\left(\mathbf{u}^{\mathrm{FEM}}, r_c^{-\delta_2}\hat{\boldsymbol{\eta}}_2(\theta)\right)}{\Psi\left(r_c^{\delta_2}\boldsymbol{\eta}_2(\theta), r_c^{-\delta_2}\hat{\boldsymbol{\eta}}_2(\theta)\right)}, \\[2mm]
H_3 &= \frac{\Psi\left(\mathbf{u}^{\mathrm{FEM}}, r_c^{-\delta_3}\hat{\boldsymbol{\eta}}_3(\theta)\right)}{\Psi\left(r_c^{\delta_3}\boldsymbol{\eta}_3(\theta), r_c^{-\delta_3}\hat{\boldsymbol{\eta}}_3(\theta)\right)}.
\end{aligned} \quad (5.119)$$

5.2.6 Finite element model of a piezoelectric bi-material notch

The finite element model for a piezoelectric bi-material notch was based on the model for the anisotropic bi-material notch described in section 5.1.6. The notch geometry, mesh structure and topology remain unchanged (see Fig. 5.11). The difference resides in the element type. ANSYS has `PLANE223` at coupled field analyses' disposal. Plane piezoelectric problems are treated by using 8-node quadratic element `PLANE223`. By setting `KEYOPT,e_type,1,1001` an electrostatic-structural coupled field analysis with piezoelectric effect is enabled. We have to pay heed to some issues.

At first, there are only two plane deformation states to be set – plane strain and plane stress. Plane strain is derived from the first equation of (4.89), while plane stress from the fourth equation of (4.89), which is practically an inverse of the first one. Then, the first option corresponds to the state 1 (generalized plane strain and short circuit: $\varepsilon_3 = 0$ and $E_3 = 0$), while the latter one is the state 4 (generalized plane stress and open circuit: $\sigma_3 = 0$ and $D_3 = 0$), see 4.2.7. The electro-mechanical parameters were compared with a FEM model created in FEniCS Project[4], but the comparison is not quoted here. Within the following text, plane strain and short circuit is considered for the FEM model.

Material properties are inputted to the ANSYS in the form of e-type matrices – the stiffness

---

[4]`https://fenicsproject.org/`

mechanical quantity		unit	electrical quantity		unit
force	F	N	charge	Q	C
stress	σ	$\mathrm{Pa} = \frac{\mathrm{N}}{\mathrm{m}^2}$	electric displacement	D	$\frac{\mathrm{C}}{\mathrm{m}^2}$
displacement	u	m	voltage	ϕ	V
strain	ε	$1 = \frac{\mathrm{m}}{\mathrm{m}}$	electric intensity	E	$\frac{\mathrm{V}}{\mathrm{m}}$
elastic constants	C	$\mathrm{Pa} = \frac{\mathrm{N}}{\mathrm{m}^2}$	dielectric permittivity	ε	$\frac{\mathrm{C}}{\mathrm{Vm}} = \frac{\mathrm{F}}{\mathrm{m}} = \frac{\mathrm{N}}{\mathrm{V}^2}$

Tab. 5.12: The electromechanical analogy.

matrix $\mathbf{C}_E$, piezoelectric matrix $\mathbf{e}$ and dielectric constants represented by the relative anisotropic permittivity at constant strain. The relative permittivity is obtained by

$$\omega_{ij}^r = \frac{\omega_{ij}^\varepsilon}{\omega_0}, \quad i,j = 1,2,3 \tag{5.120}$$

where $\omega_0 = 8.854 \times 10^{-12}\,\mathrm{F\,m^{-1}}$ is the vacuum permittivity. It si convenient to set the material data in the form corresponding to the poling in x_1-axis. A different poling direction is realized by rotating element coordinate systems by angles α_1 and α_2.

Boundary conditions are represented by prescribed stresses,displacements, electric displacements and electric potentials. To understand the connection between mechanical and electric fields, it is suitable to introduce the electromechanical analogy of the physical quantities. Neglecting the piezoelectric contributions in the first set of (4.86), we see that the elastic and electric constitutive equations have the same form, i.e.

$$\sigma_{ij} = C_{ijkl}^E \varepsilon_{kl},$$
$$D_j = \omega_{jk}^\varepsilon E_k. \tag{5.121}$$

The elastic constants C_{ijkl}^E and dielectric permittivities ω_{jk}^ε characterise the mechanical and electrical properties of the material, respectively. Another analogous quantities and their units are summarized in Tab. 5.12. The boundary conditions prescribed along the boundaries of the FE model are illustrated in Fig. 5.32. Zero displacements and zero electric potential are prescribed on the lower side of the model. The displacement at the right lateral node is fixed in the x_1 direction in order to avoid a rigid body motion. The upper side is loaded with the applied stress $\sigma_2^{\mathrm{appl}} = 10\,\mathrm{kPa}$ and electric displacement $D_2^{\mathrm{appl}} = 0.01\,\mathrm{Cm^{-2}}$. The displacements on the upper side were coupled in the x_2 direction in order to minimize the non-uniform loading. With respect to the electromechanical analogy, the electric potentials were also coupled. The coordinate systems of the deformed FEM solution and the analytical solution are not coincident, both notch tip displacements and electric potentials have to be subtracted from all body displacements and potentials, respectively. It has to be reminded that notch faces have to remain mechanically and electrically unloaded (zero tractions and electric displacements).

The Python function `scipy.interpolate.griddata` is used for reconstruction of both mechanical and electrical fields. The procedures `scint.splrep` and `scint.splev` are employed for data interpolation on the circular path enclosing the notch tip. From the programming point of view, all numerical procedures for the pure anisotropic bi-material notch were simply expanded.
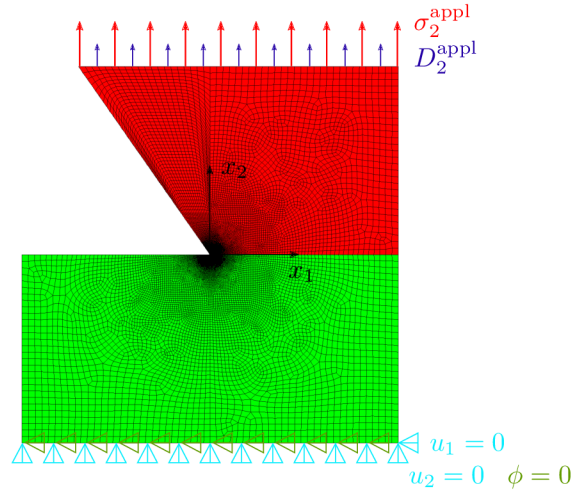
Fig. 5.32: Finite element mesh of a piezoelectric bi-material notch with mechanical and electrical boundary conditions.

Example 10: Study of the Ψ-integral path-independence for a piezoelectric bi-material notch   Algorithms controlling the mesh structure are the same as for the anisotropic bi-material notch. The only parameter that controls the mesh size of the model is Δ_c, which sets the number of elements on the perimeter R_1 and R_2, related to the arc of 90° (see Fig. 5.11). The other line division parameters are functions of this parameter and notch dimensions. This algorithm ensures that the mesh is well-structured. An advantage of such structure is obvious form mesh density studies in Fig. 5.33. The governing parameters were the generalized stress intensity factors H_1, H_2, H_3. It is obvious that changes of the stress intensity factor are small in comparison to their magnitudes. The relative error was between 0.2% and 0.4%. Although these errors are negligible, every small error negatively affects the solution of the mechanical and electrical quantities due to the ill-conditioned matrices of the LES-formalism. The mesh has to be fine also due to the linear interpolation of the circular contour, on which the electro-mechanical parameters are depicted. Then, the mesh size $\Delta_c = 60$ will be considered in the following studies.   Integration was performed by the Romberg's integration method by employing Python's function `scipy.integrate.romberg`. The computation was realized in the same manner as in Example 4, i.e. all integrals were evaluated for each material separately. Forty radii between 0.0005 mm and 4 mm were investigated for two representative cases: a PZT-5H/PZT-4 bi-material notch with the face angles $\omega_1 = 120°$, $\omega_2 = -180°$, which has real singularity exponents and an interface crack for PZT-5H/BaTiO$_3$ with two complex conjugate singularity exponents and one real. The results in Fig. 5.34 show that all Ψ-integrals are path independent on the integration path. Note that the complex intensity factors were decomposed to real and imaginary parts.

It has to be pointed out that the default settings of the integration algorithm in Python are inappropriate to get the results in Fig. 5.34. The third components of the eigenvectors $\mathbf{v}$ and $\mathbf{w}$ from (5.34) are much smaller in comparison to the remaining ones (see Tab. 5.10 and 5.11). That brings about problems with the relative tolerance in the Romberg's integration procedure, which default value is 1.48×10^{-8}. It is higher than the order of the Ψ-integral appearing in the denominator of (5.69), i.e. in the Ψ-integral involving the auxiliary and regular solutions (5.43)$_1$, (5.49) and (5.52). It was found out that the relative error has to be set to 1.48×10^{-25} to get sufficiently precise results for all bi-material configurations. Hereinafter, the value $r_c = 2$ mm is chosen as the radius of the integration path of the Ψ-integrals in (5.69).
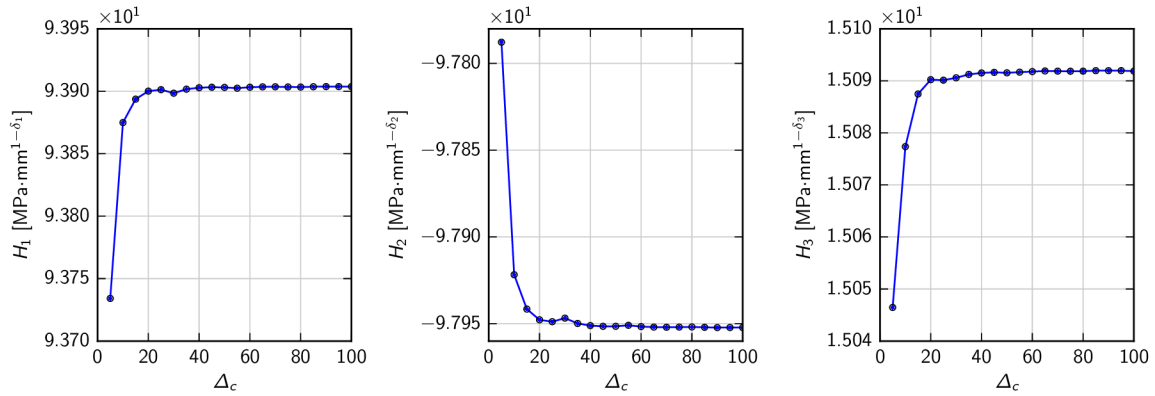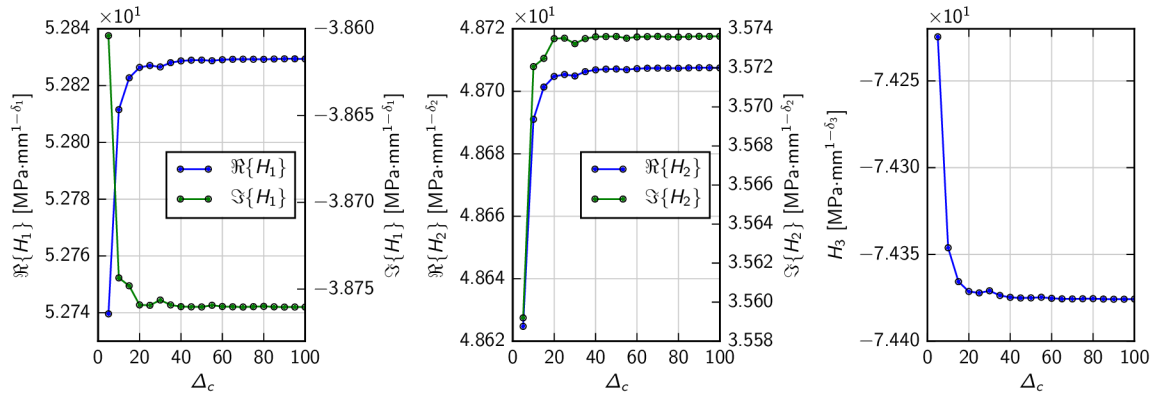
(a) PZT-5H/PZT-4, $\omega_1 = 120°$

(b) PZT-5H/BaTiO$_3$, $\omega_1 = 180°$

Fig. 5.33: Study of the minimal mesh density of (a) a piezoelectric bi-material notch given by $\omega_1 = 120°$ and $\omega_2 = -180°$ and (b) a piezoelectric interface crack. The material is defined in Tab. 5.6. The singularity exponents are (a) $\delta_1 = 0.5154$, $\delta_2 = 0.5642$, $\delta_3 = 0.7299$ and (b) $\delta_1 = 0.5+0.01293i$, $\delta_2 = 0.5 - 0.01293i$, $\delta_3 = 0.5$.

5.2.7 Electro-elastic fields of a piezoelectric bi-material notch

The displacements, stresses, electric displacements and electric potentials are expressed by the Williams' asymptotic expansions (5.109a) and (5.109b), where the analytical forms of the angular functions (5.43a) and (5.43b) are known. The stresses in the coordinate system arbitrary rotated with respect to x_3 axis are defined as

$$
\begin{aligned}
\sigma_{ss} &= -\mathbf{s}^{\mathsf{T}}\mathbf{T}_{,n} \\
\sigma_{sn} &= -\mathbf{n}^{\mathsf{T}}\mathbf{T}_{,n} = \mathbf{s}^{\mathsf{T}}\mathbf{T}_{,s} \\
\sigma_{nn} &= \mathbf{n}^{\mathsf{T}}\mathbf{T}_{,s}, \\
D_s &= -\mathbf{i}_3^{\mathsf{T}}\mathbf{T}_{,n}, \\
D_n &= \mathbf{i}_3^{\mathsf{T}}\mathbf{T}_{,s},
\end{aligned}
\tag{5.122}
$$

(a) PZT-5H/PZT-4, $\omega_1 = 120°$
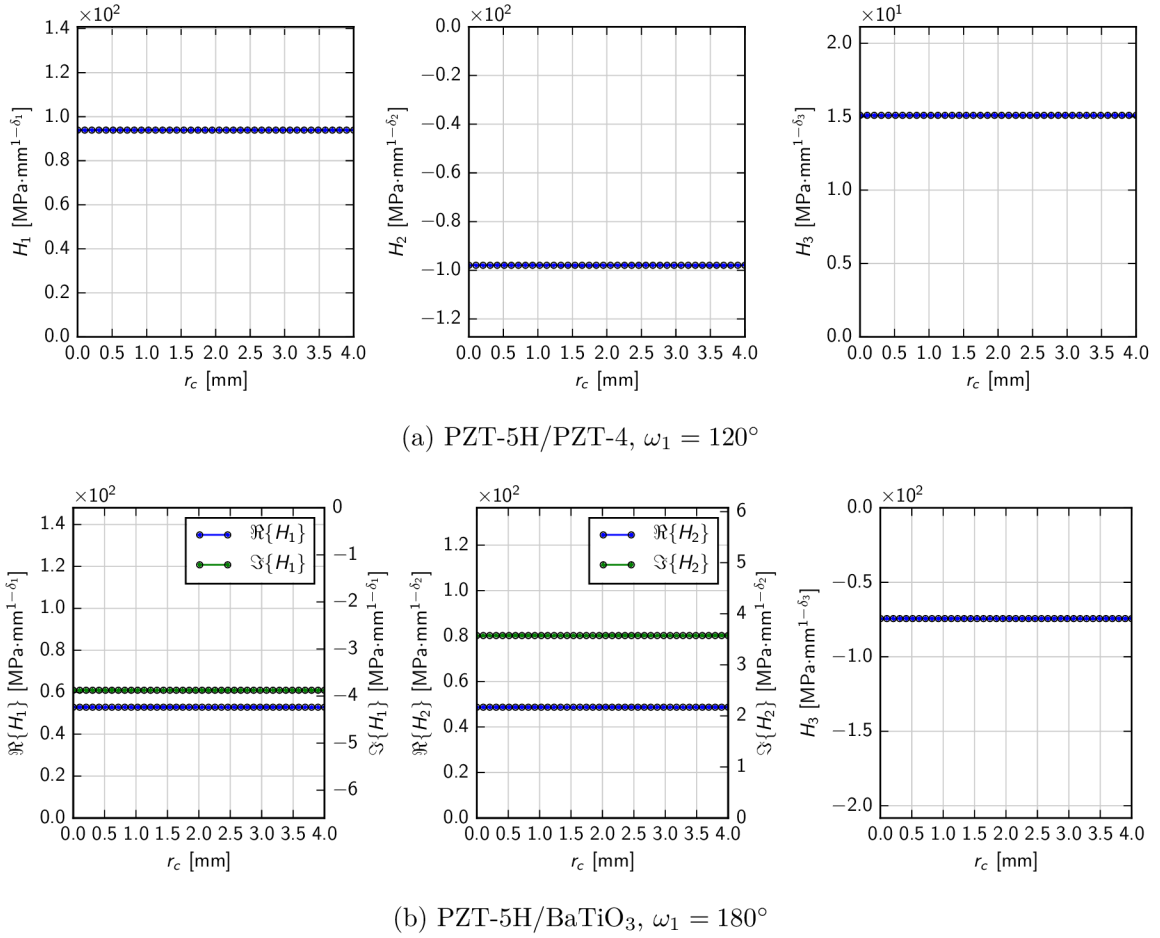

(b) PZT-5H/BaTiO$_3$, $\omega_1 = 180°$

Fig. 5.34: Test of path-independence of the GSIFs on the integration contour radius enclosing (a) the piezoelectric bi-material notch characterized by $\omega_1 = 120°$, $\omega_2 = -180°$, $\delta_1 = 0.5154$, $\delta_2 = 0.5642$, $\delta_3 = 0.7299$ and (b) the piezoelectric interface crack with $\delta_1 = 0.5 + 0.01293i$, $\delta_2 = 0.5 - 0.01293i$, $\delta_3 = 0.5$.

where the normals $\mathbf{n}$, $\mathbf{s}$ and $\mathbf{i}_3$ are defined in [17]

$$\mathbf{s} = \begin{Bmatrix} \cos\theta \\ \sin\theta \\ 0 \end{Bmatrix}, \quad \mathbf{n} = \begin{Bmatrix} -\sin\theta \\ \cos\theta \\ 0 \end{Bmatrix}, \quad \mathbf{i}_3 = \begin{Bmatrix} 0 \\ 0 \\ 1 \end{Bmatrix}. \tag{5.123}$$

By setting $\theta = 0$ in (5.122), stresses in the Cartesian coordinate system given by axes x_1, x_2 are obtained. Substituting (5.95) into (5.122) we get

$$\boldsymbol{\sigma}^1 = -H \left\{ \mathbf{L} \frac{\mathrm{d}\mathbf{Z}^\delta}{\mathrm{d}x_2} \mathbf{v} + \overline{\mathbf{L}} \frac{\mathrm{d}\overline{\mathbf{Z}}^\delta}{\mathrm{d}x_2} \mathbf{w} \right\},$$

$$\boldsymbol{\sigma}^2 = H \left\{ \mathbf{L} \frac{\mathrm{d}\mathbf{Z}^\delta}{\mathrm{d}x_1} \mathbf{v} + \overline{\mathbf{L}} \frac{\mathrm{d}\overline{\mathbf{Z}}^\delta}{\mathrm{d}x_1} \mathbf{w} \right\}, \tag{5.124}$$

where the matrices $\mathbf{A}$, $\mathbf{L}$ and the eigenvectors $\mathbf{v}$, $\mathbf{w}$ are defined in (5.96b). The extended vectors $\boldsymbol{\sigma}^1$, $\boldsymbol{\sigma}^2$ have the form

$$\boldsymbol{\sigma}^1 = \begin{Bmatrix} \sigma_{11} \\ \sigma_{12} \\ D_1 \end{Bmatrix}, \quad \boldsymbol{\sigma}^2 = \begin{Bmatrix} \sigma_{21} \\ \sigma_{22} \\ D_2 \end{Bmatrix}. \tag{5.125}$$

Considering (5.74) for $i = 1,2,3$, Eq. (5.124) can be rewritten as

$$\boldsymbol{\sigma}^1 = -H \left\{ \mathbf{L}\delta\mathbf{Z}^{\delta-1}\boldsymbol{\mu}\mathbf{v} + \overline{\mathbf{L}\mathbf{Z}}^{\delta-1}\overline{\boldsymbol{\mu}}\mathbf{w} \right\},$$

$$\boldsymbol{\sigma}^2 = H \left\{ \mathbf{L}\delta\mathbf{Z}^{\delta-1}\mathbf{v} + \overline{\mathbf{L}\mathbf{Z}}^{\delta-1}\mathbf{w} \right\},$$

$$\boldsymbol{\mu} = \begin{bmatrix} \mu_1 & 0 & 0 \\ 0 & \mu_2 & 0 \\ 0 & 0 & \mu_3 \end{bmatrix}, \quad \overline{\boldsymbol{\mu}} = \begin{bmatrix} \overline{\mu}_1 & 0 & 0 \\ 0 & \overline{\mu}_2 & 0 \\ 0 & 0 & \overline{\mu}_3 \end{bmatrix}. \tag{5.126}$$

Generalizing the functions (5.76) to

$$\mathbf{Z}^{\delta-1} = r^{\delta-1}\mathbf{Z}^{\delta-1}(\theta) = r^{\delta-1} \operatorname{diag}\left[R_1^{\delta-1}\,\mathrm{e}^{i(\delta-1)\Psi_1}, R_2^{\delta-1}\,\mathrm{e}^{i(\delta-1)\Psi_2}, R_3^{\delta-1}\,\mathrm{e}^{i(\delta-1)\Psi_3} \right],$$

$$\overline{\mathbf{Z}}^{\delta-1} = r^{\delta-1}\overline{\mathbf{Z}}^{\delta-1}(\theta) = r^{\delta-1} \operatorname{diag}\left[R_1^{\delta-1}\,\mathrm{e}^{-i(\delta-1)\Psi_1}, R_2^{\delta-1}\,\mathrm{e}^{-i(\delta-1)\Psi_2}, R_3^{\delta-1}\,\mathrm{e}^{-i(\delta-1)\Psi_3} \right] \tag{5.127}$$

and employing (5.77a) and (5.77b), the expressions for generalized stresses are obtained, i.e.

$$\boldsymbol{\sigma}^1 = -H_1 r^{\delta_1-1}\tilde{\boldsymbol{\lambda}}_{1,x_2}(\theta) - H_2 r^{\delta_2-1}\tilde{\boldsymbol{\lambda}}_{2,x_2}(\theta) - H_3 r^{\delta_3-1}\tilde{\boldsymbol{\lambda}}_{3,x_2}(\theta),$$

$$\boldsymbol{\sigma}^2 = H_1 r^{\delta_1-1}\tilde{\boldsymbol{\lambda}}_{1,x_1}(\theta) + H_2 r^{\delta_2-1}\tilde{\boldsymbol{\lambda}}_{2,x_1}(\theta) + H_3 r^{\delta_3-1}\tilde{\boldsymbol{\lambda}}_{3,x_1}(\theta). \tag{5.128}$$

Subscripts $_{,x_1}$ and $_{,x_2}$ denote differentiation with respect to the Cartesian coordinates x_1, x_2 introduced in (5.78).

Example 11: Displacement, stress, electric displacement and potential reconstruction in the vicinity of the piezoelectric bi-material notch tip   We focus on the two above investigated bi-material configuration, i.e. PZT-5H/PZT-4 and PZT-5H/BaTiO$_3$. In following studies, the poling directions $\alpha_1 = 90°$, $\alpha_2 = 90°$ are considered, if it is not specified otherwise. The asymptotic stresses, electric displacements, displacements and electric potentials calculated along the circular path with radius $r = 0.001\,\mathrm{mm}$ encircling the notch tip in the bi-material PZT-5H/PZT-4 together with results obtained by FEM are shown in Fig. 5.35. The superscripts H_i, $i = 1,2,3$ of plotted quantities listed in the legend indicate particular asymptotic terms in Eqs. (5.109a) and (5.128). The plots show a very good agreement of the asymptotic solution with the complete FEM solution obtained using a very fine mesh, which also demonstrates the accuracy of GSIFs calculations. Results of the same calculations, but performed along the circular path with radius $r = 2\,\mathrm{mm}$ are shown in Fig. 5.36. We can see that the correspondence is still very good, more significant changes occur in the electric displacements.

The same study was carried out for an interface crack for PZT-5H/BaTiO$_3$ bi-material. Figs. 5.37 and 5.38 show the electro-elastic parameters on circular paths around the notch tip. The contribution of the components corresponding to the complex conjugate exponents δ_1 and δ_2 to the total mechanical stresses and displacements as well as the electric displacements and potential are equivalent. The correspondence between the asymptotic and FEM solution is very good for both radii $r = 0.001\,\mathrm{mm}$ and $r = 2\,\mathrm{mm}$, respectively.

According to our best knowledge, only poling directions coinciding with one of the Cartesian coordinate axis, mostly x_2 or x_3, have been considered in currently published studies. Such

Fig. 5.35: The displacements, stress components, electric displacement components and electric potential of a PZT-5H/PZT-4 bi-material notch on the circular path $r = 0.001\,\text{mm}$, $\omega_1 = 120°$, $\omega_2 = -180°$, the singularity exponents are $\delta_1 = 0.5154$, $\delta_2 = 0.5642$, $\delta_3 = 0.7299$.
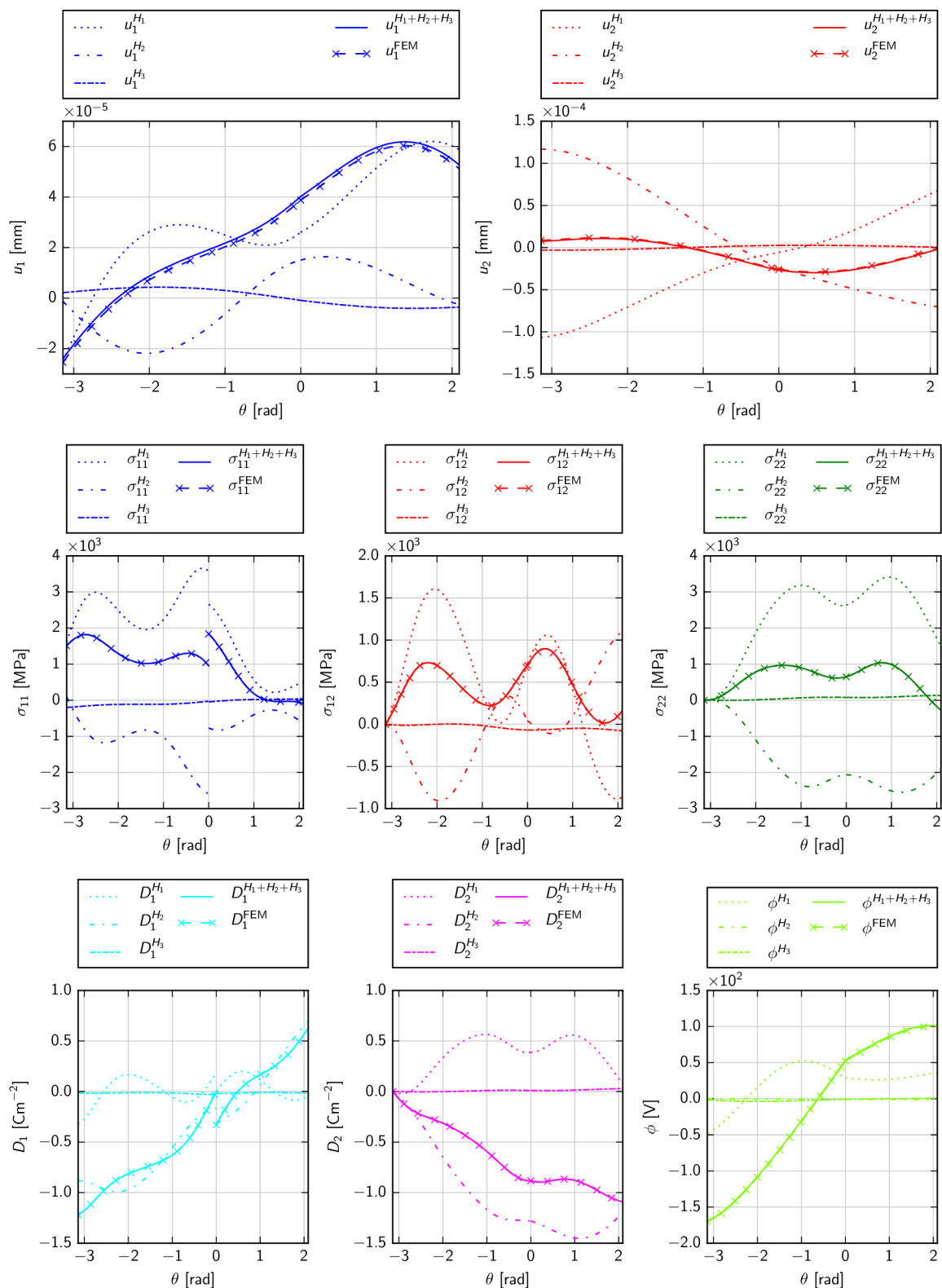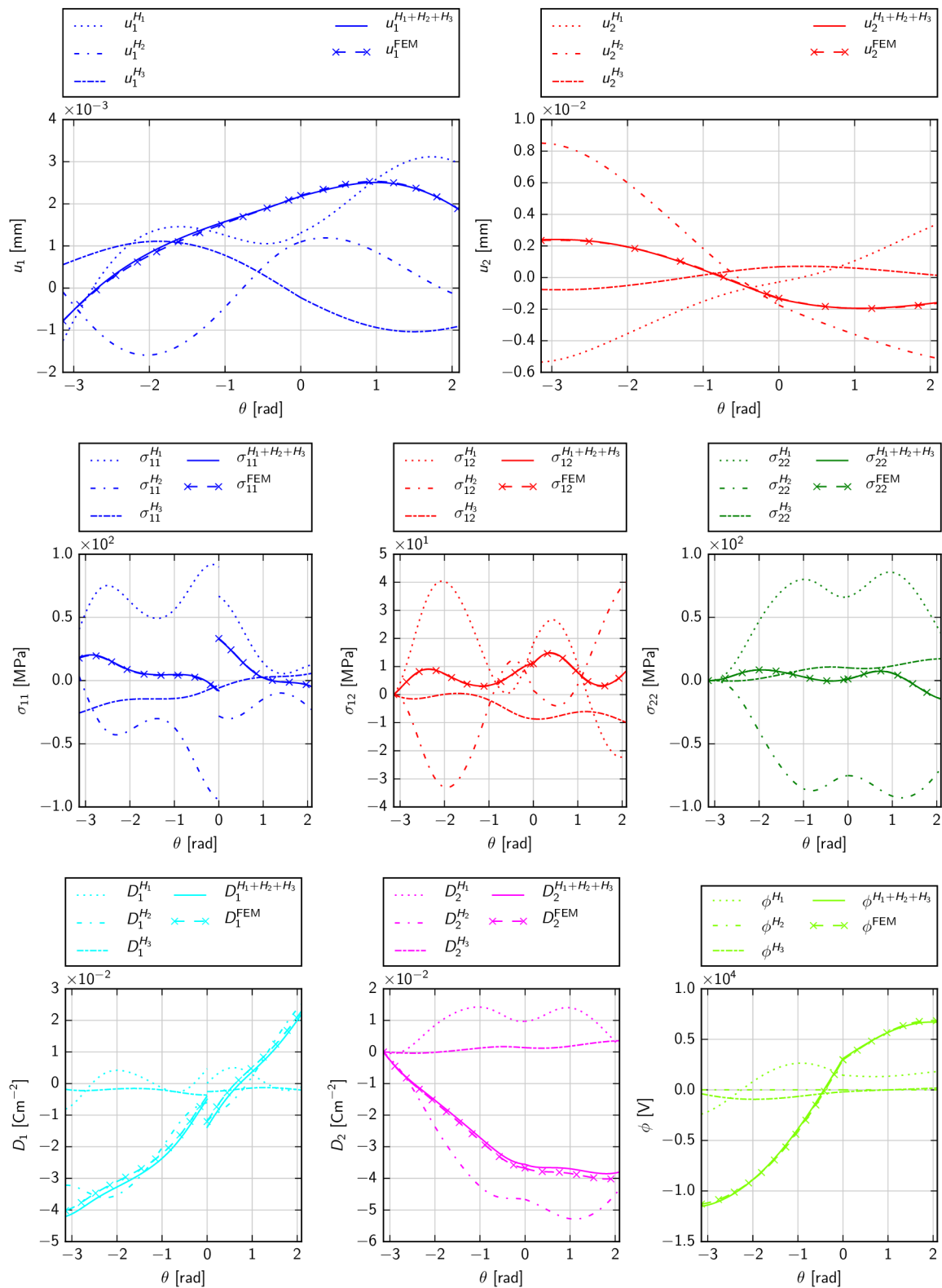
Fig. 5.36: The displacements, stress components, electric displacement components and electric potential of a PZT-5H/PZT-4 bi-material notch on the circular path $r = 2\,\mathrm{mm}$, $\omega_1 = 120°$, $\omega_2 = -180°$, the singularity exponents are $\delta_1 = 0.5154$, $\delta_2 = 0.5642$, $\delta_3 = 0.7299$.

an orientation is related to the manufacturing technology, operational purpose and relations for material eigenvalues. But there are some situations that can cause an abrupt change of poling direction. When a body is subjected to a high compressive load in the direction of the spontaneous polarization or to the high tensile load perpendicular to the direction of the spontaneous polarization, the electric domain can be switch by 90°. The polarization can be also switched by application of an electric field with a different direction, which can force the crystal to transform to one of the another five possible configurations. The expanded LES formalism can provide a solution with the arbitrary poling direction in the plane $x_1 x_2$. The graphs in Figs. D.5 and D.6 show the stresses, displacements, as well as electric displacements and electric potential for a PZT-5H/PZT-4 bi-material notch defined by angles $\omega_1 = 155°$, $\omega_2 = -180°$, where the poling of the PZT-5H is $\alpha_1 = 40°$. One can observe an excellent agreement between the full-field FEM solution and the asymptotic solution in Eqs. (5.45) and (5.128) calculated along the circular paths with radii $r = 0.001$ mm and 2 mm, respectively.

The asymptotic and finite element solutions along the bi-material interface are shown in Fig. 5.39. A very good agreement of both solutions for stresses can be observed up to the distance of 10 mm from the crack tip, while the dominance region of the first singular term for electric displacement is smaller.

The GSIFs for some notch configurations for above stated material combinations are stated in Tab. 5.13 and 5.14. If the exponent δ_i is real-valued, so is the corresponding GSIF. Two distinct complex GSIFs are obtained for complex conjugate exponents δ_i. The third exponent is always real, just as its stress intensity factor.

ω_1 [°]	δ_1 δ_2 δ_3	$H_1 \, [\text{MPa} \cdot \text{mm}^{1-\delta_1}]$ $H_2 \, [\text{MPa} \cdot \text{mm}^{1-\delta_2}]$ $H_3 \, [\text{MPa} \cdot \text{mm}^{1-\delta_3}]$
90	0.5407 0.6232 0.8898	41.09 -34.42 3.456
120	0.5154 0.5642 0.7299	93.93 -97.95 15.10
150	$0.5062 + 0.01161i$ $0.5062 - 0.01161i$ 0.6210	$-114.4 + 107.2i$ $-113.0 - 105.8i$ -40.47
170	0.4764 0.4969 0.5674	-146.4 -112.1 -55.83
180	0.4559 0.5 0.5441	-108.5 -62.15 -65.85

Tab. 5.13: Generalized stress intensity factors for a PZT-5H/PZT-4 piezoelectric bi-material notches defined by ω_1 and $\omega_2 = -180°$.

The application of the fracture mechanics concept requires the knowledge of the conventional stress intensity factors K_I, K_{II}, K_{IV}. The proper definition for stress intensity factors for the piezoelectric bi-material notches is the unified definition proposed by Hwu and Ikeda [22]. Stress
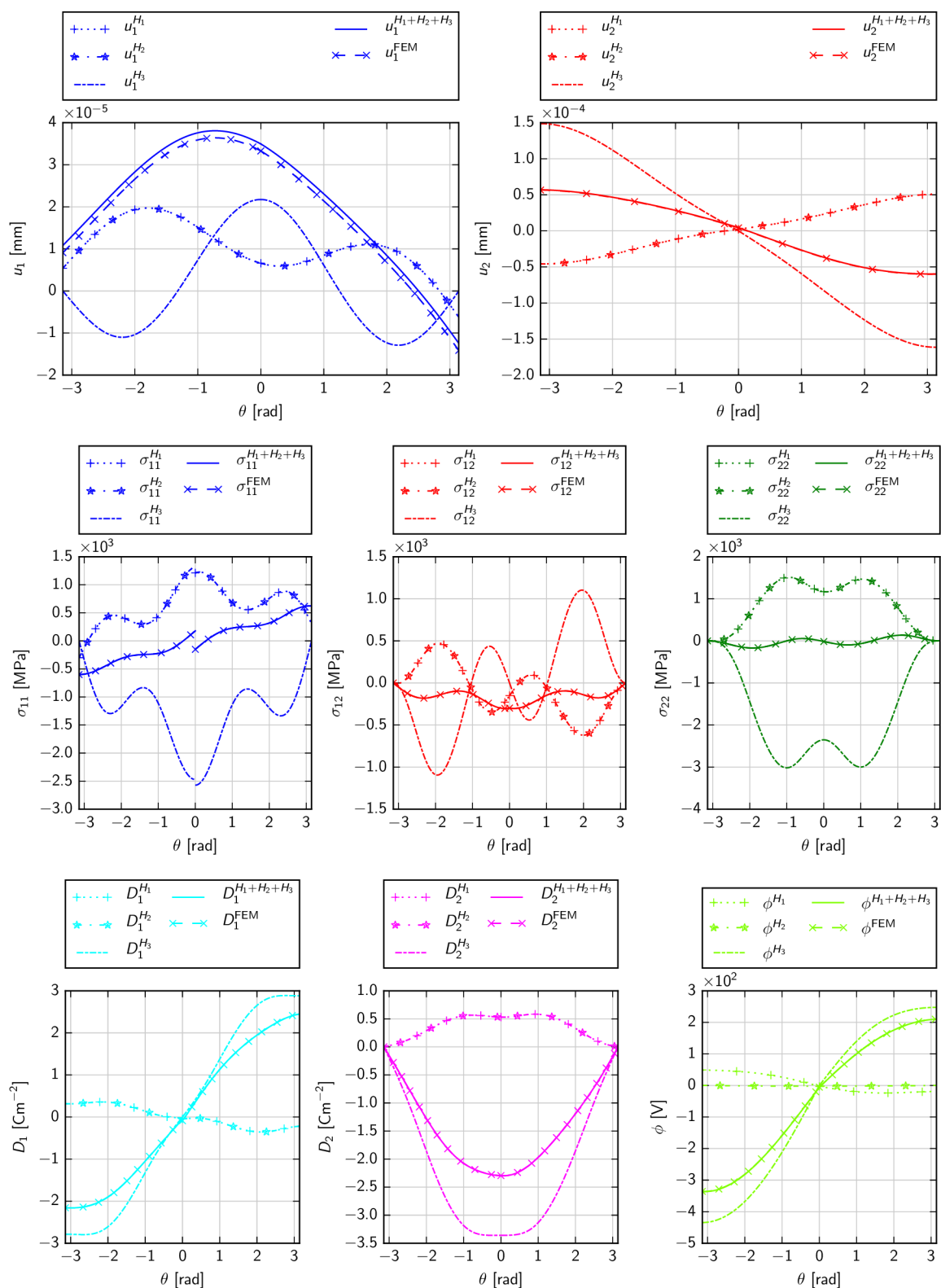
Fig. 5.37: The displacements, stress components, electric displacement components and electric potential of a PZT-5H/BaTiO$_3$ interface crack on the circular path $r = 0.001\,\text{mm}$, $\omega_1 = 180°$, $\omega_2 = -180°$, the singularity exponents are $\delta_1 = 0.5 + 0.01293i$, $\delta_2 = 0.5 - 0.01293i$, $\delta_3 = 0.5$.
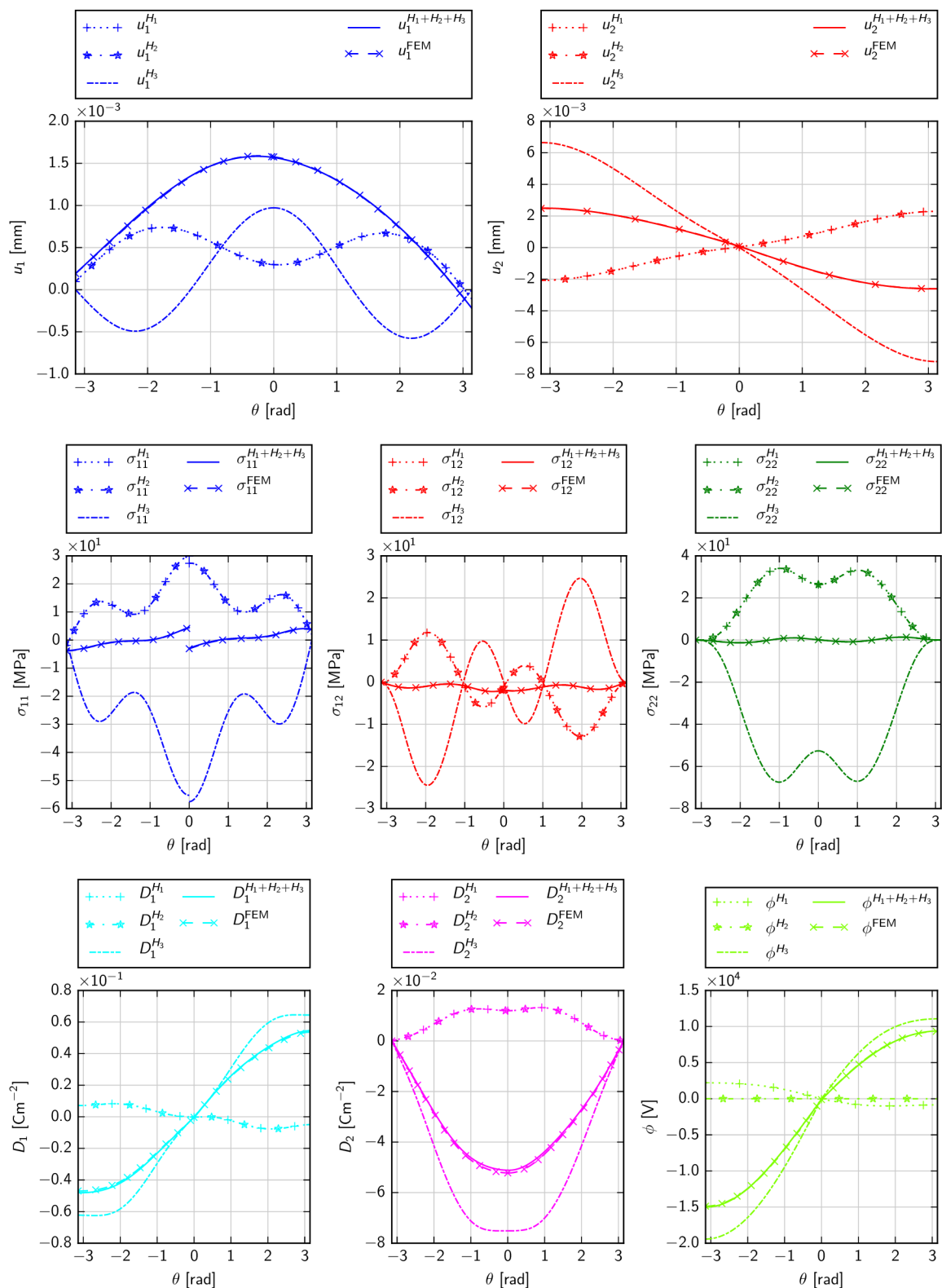
Fig. 5.38: The displacements, stress components, electric displacement components and electric potential of a PZT-5H/BaTiO$_3$ interface crack on the circular path $r = 2\,\text{mm}$, $\omega_1 = 180°$, $\omega_2 = -180°$, the singularity exponents are $\delta_1 = 0.5 + 0.01293i$, $\delta_2 = 0.5 - 0.01293i$, $\delta_3 = 0.5$.
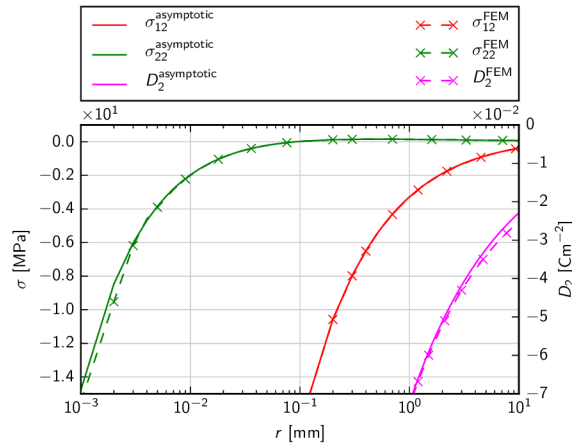
Fig. 5.39: Stress and electric displacement distribution along the bi-material interface for a PZT-5H/BaTiO$_3$ interface crack.

$\omega_1 \; [\degree]$	δ_1 δ_2 δ_3	$H_1 \, [\text{MPa} \cdot \text{mm}^{1-\delta_1}]$ $H_2 \, [\text{MPa} \cdot \text{mm}^{1-\delta_2}]$ $H_3 \, [\text{MPa} \cdot \text{mm}^{1-\delta_3}]$
90	0.5582 0.6256 0.9212	1.430 -3.775 -0.2342
120	0.5226 0.5770 0.7462	3.287 -6.313 -1.738
150	0.5079 $0.5359i$ 0.6036	1.608 -14.74 -9.917
170	$0.5099 + 0.004000i$ $0.5099 - 0.004000i$ 0.5244	$-53.19 - 107.4i$ $-52.24 + 105.5i$ -100.4
180	$0.5 + 0.01293i$ $0.5 - 0.01293i$ 0.5	$53.82 - 3.876i$ $48.71 + 3.574i$ -74.38

Tab. 5.14: Generalized stress intensity factors for a PZT-5H/BaTiO$_3$ piezoelectric bi-material notches defined by ω_1 and $\omega_2 = -180\degree$.

intensity factors of the in-plane problem are given as

$$\begin{Bmatrix} K_{\text{II}} \\ K_{\text{I}} \\ K_{\text{IV}} \end{Bmatrix} = \lim_{r \to 0} \sqrt{2\pi} r^{1-\Re\{\delta_c\}} \mathbf{\Lambda} \langle (r/\ell)^{-i\varepsilon_i} \rangle \mathbf{\Lambda}^{-1} \begin{Bmatrix} \sigma_{12} \\ \sigma_{22} \\ D_2 \end{Bmatrix}, \quad i = 1,2,3, \tag{5.129}$$

where

$$\mathbf{\Lambda} = \mathbf{\Lambda}(\theta = 0) = [\boldsymbol{\lambda}_1(\theta = 0), \boldsymbol{\lambda}_2(\theta = 0), \boldsymbol{\lambda}_3(\theta = 0)]. \tag{5.130}$$

The brackets $\langle \rangle$ stand for the 3×3 diagonal matrix, δ_c is the most critical singularity exponent and ℓ is the length parameter which may be chosen arbitrarily. Substituting (5.128) into (5.130),
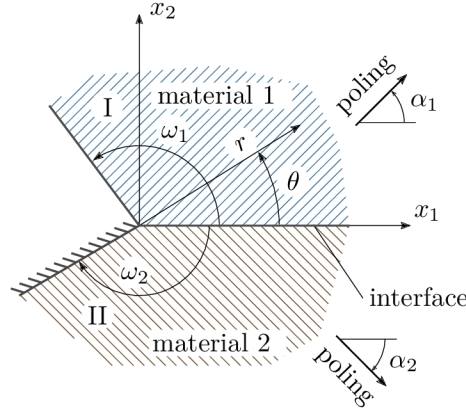
Fig. 5.40: Geometry of a bi-material notch characterized by two regions I and II. The notch faces are defined by angles ω_1 and ω_2, where the face corresponding to the latter angle is mechanically clamped and electrically closed. The material interface is always considered at $\theta = 0$. The angles α_1 and α_2 denote poling direction of the materials I and II, respectively.

the relation between stress intensity factors K and GSIFs H is obtained:

$$\begin{Bmatrix} K_{\text{II}} \\ K_{\text{I}} \\ K_{\text{IV}} \end{Bmatrix} = \sqrt{2\pi}\mathbf{\Lambda}\langle(\Re\{\delta_c\} + i\varepsilon_i)/\ell^{i\varepsilon_i}\rangle \begin{Bmatrix} H_1 \\ H_2 \\ H_3 \end{Bmatrix}, \quad i = 1,2,3. \tag{5.131}$$

Using the relation (5.131), the near tip solution (5.45) can be rewritten in terms of K_{II}, K_{I}, K_{IV} as

$$\mathbf{u}(r,\theta) = \frac{1}{\sqrt{2\pi}}r^{\Re\{\delta_c\}}\mathbf{E}(\theta)\langle(\Re\{\delta_c\} + i\varepsilon_i)^{-1}(r/\ell)^{i\varepsilon_i}\rangle\mathbf{\Lambda}^{-1}\begin{Bmatrix} K_{\text{II}} \\ K_{\text{I}} \\ K_{\text{IV}} \end{Bmatrix}, \tag{5.132a}$$

$$\mathbf{T}(r,\theta) = \frac{1}{\sqrt{2\pi}}r^{\Re\{\delta_c\}}\mathbf{\Lambda}(\theta)\langle(\Re\{\delta_c\} + i\varepsilon_i)^{-1}(r/\ell)^{i\varepsilon_i}\rangle\mathbf{\Lambda}^{-1}\begin{Bmatrix} K_{\text{II}} \\ K_{\text{I}} \\ K_{\text{IV}} \end{Bmatrix}, \tag{5.132b}$$

where

$$\mathbf{E}(\theta) = [\boldsymbol{\eta}_1(\theta),\boldsymbol{\eta}_2(\theta),\boldsymbol{\eta}_3(\theta)]. \tag{5.133}$$

5.2.8 Problem redefinition for modelling a piezoelectric bi-material notch with a clamped notch face

The presented eigenvalue problem was derived under the assumption of traction free and electrically open notch faces, see boundary conditions (5.17). Within the following paragraph, a modified algorithm for modelling a piezoelectric bi-material notch with one clamped face is proposed. Another cases of boundary conditions can be modelled analogically, but they are not presented here due to their similar form. Some studies, in which a single or permeable interface crack was considered, were reported in [100, 130, 134, 135].

Let us consider a piezoelectric bi-material notch with a geometry and boundary conditions depicted in Fig. 5.40. The notch face corresponding to the notch angle ω_2 is clamped. The

boundary conditions (5.17) have the form

$$\mathbf{T}^{\mathrm{I}}(\omega_1) = 0,$$
$$\mathbf{u}^{\mathrm{II}}(\omega_2) = 0.$$
(5.134)

From the structure of the generalized displacement vector (5.96a) can be seen that the second face is mechanically clamped and electrically closed. Another combinations of the boundary conditions of the notch face, such as clamped and electrically open, cannot be covered by the above presented eigenvalue problem (5.19). The asymptotic solution of that kind of problems was reported for example in [85, 128, 136, 137]. Substituting (5.95) into (5.134) and interface continuity conditions (5.18) we obtain a system of twelve algebraic equation for the exponent δ, written in the matrix form as

$$
\begin{bmatrix}
\mathbf{L}^{\mathrm{I}}\mathbf{Z}_1^{\mathrm{I}\delta}(\mathbf{L}^{\mathrm{I}})^{-1} & \overline{\mathbf{L}}^{\mathrm{I}}\overline{\mathbf{Z}}_1^{\mathrm{I}\delta}(\overline{\mathbf{L}}^{\mathrm{I}})^{-1} & \mathbf{0} & \mathbf{0} \\
\mathbf{0} & \mathbf{0} & \mathbf{A}^{\mathrm{II}}\mathbf{Z}_2^{\mathrm{II}\delta}(\mathbf{L}^{\mathrm{II}})^{-1} & \overline{\mathbf{A}}^{\mathrm{II}}\overline{\mathbf{Z}}_2^{\mathrm{II}\delta}(\overline{\mathbf{L}}^{\mathrm{II}})^{-1} \\
\mathbf{A}^{\mathrm{I}}\mathbf{Z}_0^{\mathrm{I}\delta}(\mathbf{L}^{\mathrm{I}})^{-1} & \overline{\mathbf{A}}^{\mathrm{I}}\overline{\mathbf{Z}}_0^{\mathrm{I}\delta}(\overline{\mathbf{L}}^{\mathrm{I}})^{-1} & -\mathbf{A}^{\mathrm{II}}\mathbf{Z}_0^{\mathrm{II}\delta}(\mathbf{L}^{\mathrm{II}})^{-1} & -\overline{\mathbf{A}}^{\mathrm{II}}\overline{\mathbf{Z}}_0^{\mathrm{II}\delta}(\overline{\mathbf{L}}^{\mathrm{II}})^{-1} \\
\mathbf{L}^{\mathrm{I}}\mathbf{Z}_0^{\mathrm{I}\delta}(\mathbf{L}^{\mathrm{I}})^{-1} & \overline{\mathbf{L}}^{\mathrm{I}}\overline{\mathbf{Z}}_0^{\mathrm{I}\delta}(\overline{\mathbf{L}}^{\mathrm{I}})^{-1} & -\mathbf{L}^{\mathrm{II}}\mathbf{Z}_0^{\mathrm{II}\delta}(\mathbf{L}^{\mathrm{II}})^{-1} & -\overline{\mathbf{L}}^{\mathrm{II}}\overline{\mathbf{Z}}_0^{\mathrm{II}\delta}(\overline{\mathbf{L}}^{\mathrm{II}})^{-1}
\end{bmatrix}
\begin{Bmatrix}
\mathbf{L}^{\mathrm{I}}\mathbf{v}^{\mathrm{I}} \\
\overline{\mathbf{L}}^{\mathrm{I}}\mathbf{w}^{\mathrm{I}} \\
\mathbf{L}^{\mathrm{II}}\mathbf{v}^{\mathrm{II}} \\
\overline{\mathbf{L}}^{\mathrm{II}}\mathbf{w}^{\mathrm{II}}
\end{Bmatrix} = \mathbf{0},
\quad (5.135)
$$

where $\mathbf{0}$ denotes a 3×3 zero matrix on the left-hand side and a 12×1 zero vector on the right-hand side of the equation (5.135). The subscript denotes the index of the angle ω_i and the superscript stands for association with the material region. With (5.20), the system can be rewritten as

$$
\begin{bmatrix}
\mathbf{X}_1^{\mathrm{I}} & \overline{\mathbf{X}}_1^{\mathrm{I}} & \mathbf{0} & \mathbf{0} \\
\mathbf{0} & \mathbf{0} & \mathbf{B}_2^{\mathrm{II}} & \overline{\mathbf{B}}_2^{\mathrm{II}} \\
\mathbf{B}_0^{\mathrm{I}} & -\overline{\mathbf{B}}_0^{\mathrm{I}} & -\mathbf{B}_0^{\mathrm{II}} & \overline{\mathbf{B}}_0^{\mathrm{II}} \\
\mathbf{I} & \mathbf{I} & -\mathbf{I} & -\mathbf{I}
\end{bmatrix}
\begin{Bmatrix}
\mathbf{L}^{\mathrm{I}}\mathbf{v}^{\mathrm{I}} \\
\overline{\mathbf{L}}^{\mathrm{I}}\mathbf{w}^{\mathrm{I}} \\
\mathbf{L}^{\mathrm{II}}\mathbf{v}^{\mathrm{II}} \\
\overline{\mathbf{L}}^{\mathrm{II}}\mathbf{w}^{\mathrm{II}}
\end{Bmatrix} = \mathbf{0},
\quad (5.136)
$$

where the matrix elements introduced in (5.21) are redefined as

$$\mathbf{X}_1^{\mathrm{I}} = \mathbf{L}^{\mathrm{I}}\mathbf{Z}_1^{\mathrm{I}\delta}(\omega_1)(\mathbf{L}^{\mathrm{I}})^{-1}, \quad \overline{\mathbf{X}}_1^{\mathrm{I}} = \overline{\mathbf{L}}^{\mathrm{I}}\overline{\mathbf{Z}}_1^{\mathrm{I}\delta}(\omega_1)(\overline{\mathbf{L}}^{\mathrm{I}})^{-1},$$
(5.137a)

$$\mathbf{B}_2^{\mathrm{II}} = \mathbf{A}^{\mathrm{II}}\mathbf{Z}_2^{\mathrm{II}\delta}(\omega_2)(\mathbf{L}^{\mathrm{II}})^{-1}, \quad \overline{\mathbf{B}}_2^{\mathrm{II}} = \overline{\mathbf{A}}^{\mathrm{II}}\overline{\mathbf{Z}}_2^{\mathrm{II}\delta}(\omega_2)(\overline{\mathbf{L}}^{\mathrm{II}})^{-1}.$$
(5.137b)

This system can be reduced to the algebraic system of two equations given by (5.23) and (5.24), where

$$\mathbf{Y}_1^{\mathrm{I}} = (\overline{\mathbf{X}}_1^{\mathrm{I}})^{-1}\mathbf{X}_1^{\mathrm{I}}, \quad \mathbf{Y}_2^{\mathrm{II}} = (\overline{\mathbf{B}}_2^{\mathrm{II}})^{-1}\mathbf{B}_2^{\mathrm{II}}.$$
(5.138)

Then, the procedure represented in Eqs. (5.25)–(5.35) for the piezoelectric problem and reduction of the algebraic system introduced in Appendix B can be used. The unknown exponents δ_i are determined from the nonlinear characteristic equation (5.36). The auxiliary solutions, eigenvector evaluation, expanded shape functions, Ψ-integral and electro-elastic field reconstruction are computed by using the procedures introduced in sections 5.2.3–5.2.7. Note that the contour Σ_2 in (5.57) (see Fig. 5.9) is also zero due to the zero displacements and electric potential. The FEM model is constrained according to the boundary conditions (5.134), i.e. displacements and electric potential are set to zero along the second notch face. The applied stress and electric displacement is identical to the previous piezoelectric bi-material problem. Settings for all numerical procedures remain the same as in the previous examples. For the sake of brevity, the Ψ-integral path independence and the mesh density studies are not performed.
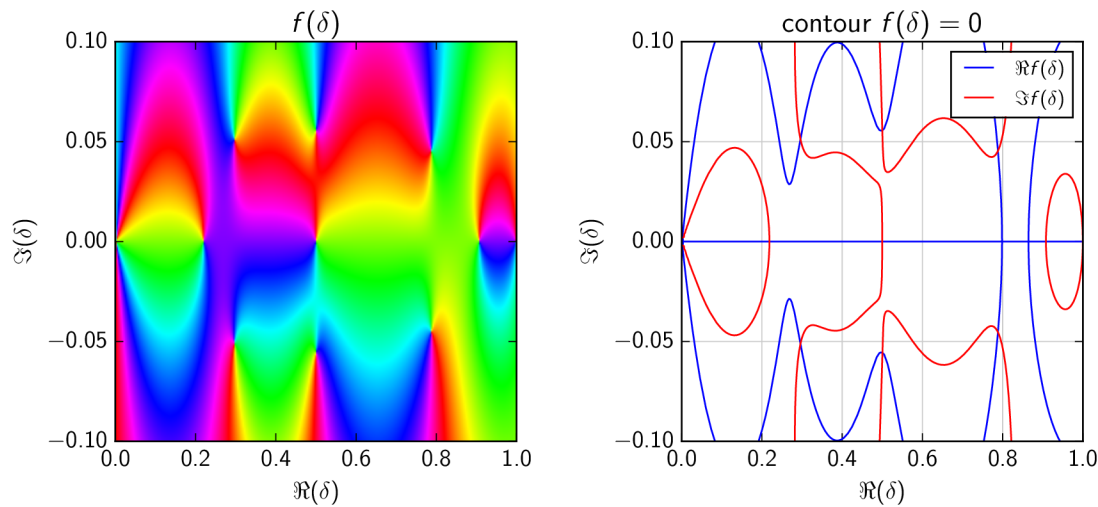
Fig. 5.41: The HSV phase portrait of the characteristic function $f(\delta) = \det[\mathbf{K}(\mathbf{I}-\mathbf{Y}_1^{\mathrm{I}})^{-1}]$ defined in (5.36) and the contour plot for $f(\delta) = 0$ for a PZT-5H/BaTiO$_3$ bi-material notch with geometry $\omega_1 = 120°$, $\omega_2 = -180°$. The latter notch face is mechanically clamped and electrically closed. The intersections of the curves of different colour give the searched roots.

Example 12: Singularity exponents and electro-elastic field reconstruction of a piezoelectric bi-material notch with a clamped face Consider a PZT-5H/BaTiO$_3$ bi-material notch with the local geometry and free/clamped boundary conditions of the notch faces illustrated in Fig. 5.40. The notch geometry is defined by the angles $\omega_1 = 150$ and $\omega_2 = -180$. The poling direction is parallel with x_2-axis, i.e. $\alpha_1 = \alpha_2 = 90°$. The phase portrait of the transcendental function (5.36) is depicted in Fig. 5.41. It can be observed that on the interval $0 < \Re\{\delta\} < 1$ there are two real and two pairs of complex conjugate roots: $\delta_1 = 0.2187$, $\delta_{2,3} = 0.2961 \pm 0.05114i$, $\delta_{4,5} = 0.7883 \pm 0.04532i$, $\delta_6 = 0.9079$. The character of the singularity exponents is considerably different in comparison to singularity exponents of the notch with traction-free faces. A dependence study of the exponents δ_i on the notch angle ω_1 sheds some light on this problem. Fig. 5.42(a) shows the singularity exponents δ_i for a PZT-5H/BaTiO$_3$ bi-material combination. In the case of an interface crack, there are six rots of the characteristic function (5.36): two real δ_1, δ_6 and two complex conjugate pairs $\delta_{2,3}$, $\delta_{4,5}$. When taking a look at the exponents more closely, it can be seen that δ_1, δ_2, δ_3 and δ_4, δ_5, δ_6 are symmetric with respect to 0.5. Note that the imaginary parts of the complex roots $\delta_{2,3}$ and $\delta_{4,5}$ have the same magnitude. However, in contrast to the free/free piezoelectric bi-material notch, the value 0.5 is not the root of the eigenvalue problem (5.136) (see Fig. 5.26). The exponent δ_1 remain real and $\delta_{2,3}$ are complex for all notch angles ω_1. All six exponents are singular up to $\omega_1 = 130°$.

The same study was carried out for a PZT-5H/PZT-4 bi-material (see Fig. 5.42(a)). The roots in the case of the interface crack have the same structure, i.e. δ_1, δ_2, δ_3 and δ_4, δ_5, δ_6 are symmetric with respect to 0.5 and the imaginary parts of the complex roots $\delta_{2,3}$ and $\delta_{4,5}$ have the same magnitude. The exponent δ_1 remain real for all notch angles ω_1, while $\delta_{2,3}$ turns real-valued for $38° < \omega_1 < 145°$ and $\omega_1 < 15°$. All six exponents are singular up to $\omega_1 = 130°$. The abrupt changes in the development of the δ_6 (angles $\omega_1 = 100°$ and $\omega_1 = 45°$) indicate that the sixth root become complex conjugate with the next non-singular term between these angles. The main conclusion is that the character of the roots δ_i as a function of the notch geometry
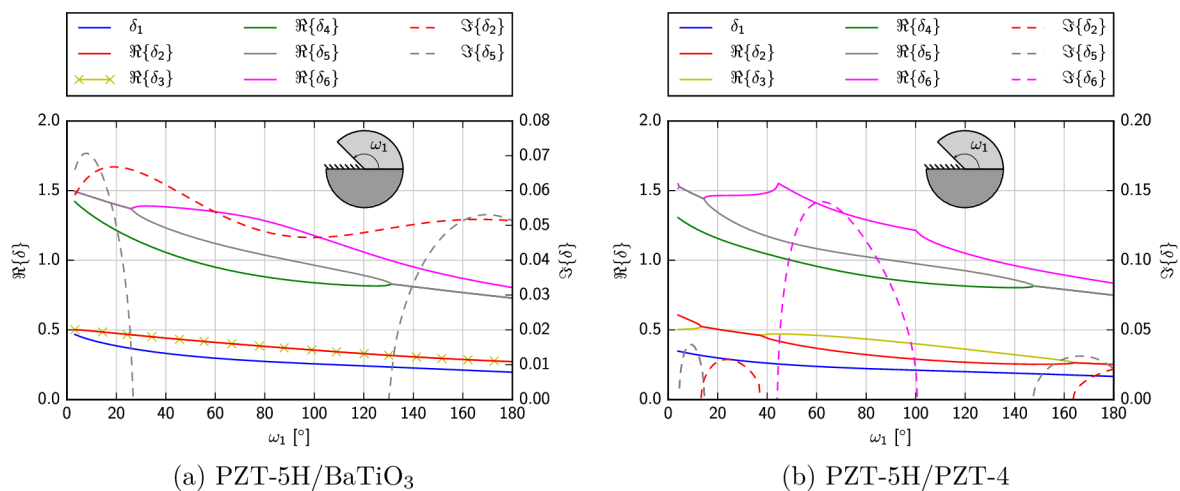
Fig. 5.42: The exponent δ_i dependence on the notch geometry ω_1 for free/clamped piezoelectric bi-material notch. Poling directions are $\alpha_1 = 90°$, $\alpha_2 = 90°$.

is more complicated than for free/free bi-material notches. The HSV phase plot represents a convenient tool to visualize the roots for subsequent setting the initial guess for the root finding algorithm.

As there are more singularity exponents than in the case of a free/free piezoelectric bi-material notch, procedures for eigenvector extraction, shape function determination and GSIF calculation can be just expanded for the higher number of the exponents. The generalized displacements (5.109a) and the generalized stresses (5.128) attain then the form

$$\mathbf{u}(r,\theta) = \sum_{i=1}^{6} H_i r^{\delta_i} \boldsymbol{\eta}_i(\theta) \tag{5.139}$$

and

$$\boldsymbol{\sigma}^1 = -\sum_{i=1}^{6} H_i r^{\delta_i - 1} \tilde{\boldsymbol{\lambda}}_{i,x_2}(\theta),$$

$$\boldsymbol{\sigma}^2 = \sum_{i=1}^{6} H_i r^{\delta_i - 1} \tilde{\boldsymbol{\lambda}}_{i,x_1}(\theta). \tag{5.140}$$

The asymptotic stresses, electric displacements, displacements and electric potentials calculated along the circular path with radius $r = 2\,\mathrm{mm}$ encircling the notch tip in the bi-material PZT-5H/BaTiO$_3$ together with results obtained by FEM are shown in Fig. 5.43. The superscripts H_i, $i = 1,2,\ldots,6$ of plotted quantities listed in the legend indicate particular asymptotic terms in Eqs. (5.139) and (5.140). The plots show a very good agreement of the asymptotic solution with the complete FEM solution obtained using a very fine mesh.
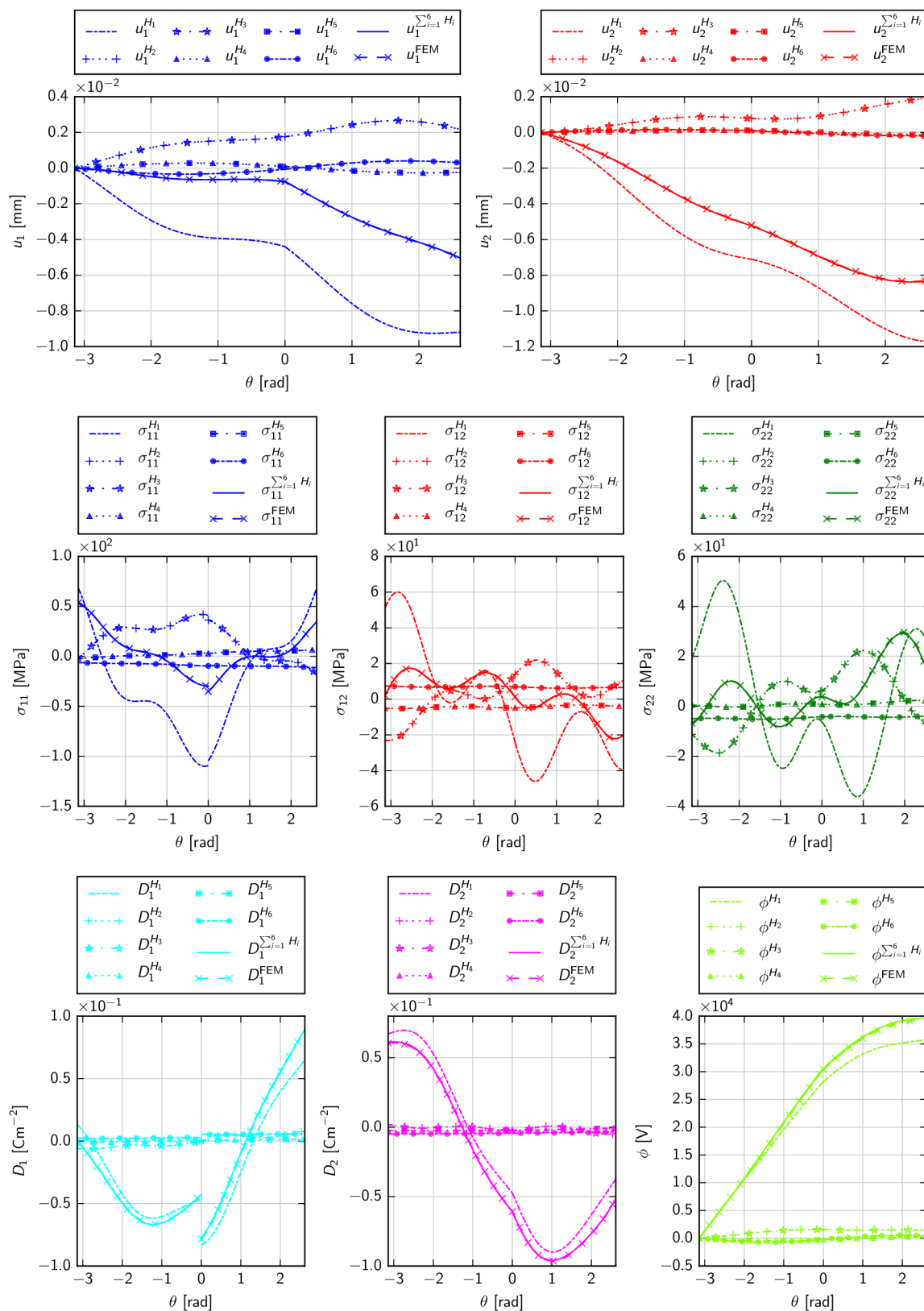
Fig. 5.43: The displacements, stress components, electric displacement components and electric potential of a free/clamped PZT-5H/BaTiO$_3$ bi-material notch on the circular path $r = 2\,\text{mm}$, $\omega_1 = 150°$, $\omega_2 = -180°$, the singularity exponents are $\delta_1 = 0.2187$, $\delta_{2,3} = 0.2961 \pm 0.05114i$, $\delta_{4,5} = 0.7883 \pm 0.04532i$, $\delta_6 = 0.9079$.

5.2.9 Problem redefinition for modelling a non-piezoelectric/piezoelectric bi-material notch

Previous bi-material configurations described bi-material notches composed of two ferroelectric piezoelectric materials, a specific configuration used for example in piezoelectric actuators. In constructions which employ piezoelectric elements, piezoelectric materials are coupled to electrodes, which conduct the electric charge, or to insulators, e.g. an underlay or insulating pads between piezoelectric and electrodes, or simply to the body of a construction. Solving problems of bi-materials consisting of combinations of piezoelectric and non-piezoelectric solids requires specific changes in the standard formalism used in the previous examples.

The first step in the modification of the expanded LES formalism for piezoelectric materials to pure elastic non-piezoelectric materials is to set the piezoelectric constants to zero, i.e. $e_{ijk} = 0$ for any i,j,k. The elastic and electric fields are then decoupled and both direct and converse piezoelectric effects vanish. The latter phenomenon is sometimes confused with electrostriction, which is a property of all materials [65, 138], since atoms, molecules, ions or polarizable domains can be distorted under an application of electric excitation. Let us consider solid dielectrics only. If a crystal does not become charged under any uniform mechanical load, i.e. it is non-piezoelectric, the applied voltage will nevertheless induce a mechanical strain. Furthermore, the strain remains unchanged when the electrical field is reversed [68]. Such behaviour has a quadratic character and the strain tensor is expressed as

$$\varepsilon_{ij} = Q_{ijkl} D_k D_l, \tag{5.141}$$

where Q_{ijkl} are the electrostrictive coefficients [139]. However, for materials with piezoelectric properties, the electrostriction is superposed with the converse piezoelectric effect (compare with Eq. $(4.86)_4$), which has a linear behaviour, i.e.

$$\varepsilon_{ij} = g_{kij} D_k + Q_{ijkl} D_k D_l. \tag{5.142}$$

During a pure electrical loading, strains corresponding to the stress components that induce electric charge have linear behaviour, whereas the other ones behave quadratic. Under standard operating conditions ($E^{\mathrm{appl}} = 0.1\text{--}5\,\mathrm{MVm}^{-1}$), the quadratic component is sufficiently small when a material is piezoelectric [140]. But for non-piezoelectric dielectrics, the linear component is zero and the electrostrictive strains are quadratic and not negligible. Since the nonlinear electrostriction (see Eq. (5.141)) is not included in the constitutive laws $(4.86)_4$, the effect is not covered in the redefined problem for insulators and conductors as well.

The second step is to modify the problem according to the case of an insulator or conductor. Both cases are different from the physical point of view. In the framework of the Lekhnitskii and Stroh formalism, Hwu and Kuo [21] proposed a method which fulfil the condition of the interface impermeability by reducing the permittivity to a sufficiently small value when modelling an insulator or increasing to a very large value when considering a conductor. Its purpose was to be in agreement with authors in [85, 137, 141], who modelled the insulator/piezoelectric bi-material by prescribing $D_\theta^{\mathrm{insulator}}(0) = 0$ along the interface, and conductor/piezoelectric bi-material by prescribing $\phi^{\mathrm{conductor}}(0) = 0$ along the interface (the interface was defined coincident with x_1-axis, as in Fig. 5.22).

However, the condition for an insulator/piezoelectric interface is not physically exact. The assumption of zero electric displacement expresses an impermeable interface condition, i.e. the surfaces are free of charge. This effect is not violated, if one material has significantly higher permittivity than the second one, e.g. a piezoelectric ceramic in a contact with air [70], which is actually prescribed on the notch face. But this cannot be applicable to an insulator/piezoelectric

interface, because relative permittivity of insulators attains a wide range on values. Then, an insulator/piezoelectric bi-material notch can be modelled in the same way as a piezoelectric bi-material, but by prescribing zero piezoelectric constants and given permittivity, if they are known. Other notch face boundary conditions and their effects were reported in [142].

Electric intensity E inside a homogeneous conductor is zero. Thus, the electric potential ϕ is constant. An uncharged conductor in electrostatics can be regarded as a body with infinite permittivity ω [138]. Since the electric displacement D does not rely on the permittivity and it is finite in the entire body, it follows for the electric intensity that $E \to 0$ for $\omega \to \infty$, which is in accordance with properties of a conductor. Thus, the method of Hwu and Kuo in [21] for modelling the conductor/piezoelectric interface by setting a very large permittivity is in agreement with Landau and Lifshitz [138]. However, when zero electric intensity E is considered, it follows from Eq. $(4.81)_2$ that $\phi = \text{const}$ inside the conductor and on its surface, but Hwu and Kuo in [21] implicitly assumed $\phi = 0$. The resulting constant value of the asymptotic solution represented by the expanded LES formalism along the interface between the piezoelectric material and conductor is contingent upon the permittivity magnitude and boundary conditions of the FEM solution.

The above mentioned modifications of the piezoelectric bi-material problem is valid for a bi-material, where the non-piezoelectric material shows transversally orthotropic properties, i.e. the material matrices (5.96b) are not degenerate. However, most insulators and especially conductors have isotropic properties. By substituting the material parameters into the in-plane characteristic equation (5.101), triple complex conjugate roots $\mu_{1,2,3} = i$ are obtained. The formalism has to be then modified according to the redefinition introduced in section 5.1.8 by employing the Muskhelishvili complex potentials.

Due to the assumption of zero piezoelectric coefficients $\hat{\mathbf{g}}'$ (see Eq. $(4.107a)_4$), the structural and electrical constitutive equations are decoupled, as can be seen from (4.132b) and (4.136). Thus, the modification of the formalism discussed in the previous sections unifies the relations for pure isotropic elasticity introduced in section 5.1.8 with equations describing the electrostatic filed. The complex potentials of an isotropic media (marked with a star) have the same form as (5.80), i.e.

$$\mathbf{f}^\star(z) = \mathbf{f}(z) + (\overline{z} - z)\,\mathbf{Q}\,\frac{\mathrm{d}\mathbf{f}(z)}{\mathrm{d}z}, \tag{5.143}$$

where

$$\mathbf{Q} = \begin{bmatrix} 0 & 0 & 0 \\ 1 & 0 & 0 \\ 0 & 0 & 0 \end{bmatrix}.$$

The complex potentials $\mathbf{f}(z)$ are defined as

$$\mathbf{f}(z) = \begin{Bmatrix} \varphi(z) \\ \psi(z) \\ \varsigma(z) \end{Bmatrix}, \quad z = r\,(\cos\theta + i\sin\theta), \tag{5.144}$$

in which the first two complex functions are the Muskhelishvili complex potentials defined in (5.82) and $\varsigma(z)$ is

$$\varsigma(z) = z^\delta v_3. \tag{5.145}$$

The displacements and stress functions (5.7) have the form

$$\mathbf{u}^\star(z) = \mathbf{A}^\star \mathbf{Z}^{\star\delta} \mathbf{v} + \overline{\mathbf{A}^\star \mathbf{Z}^{\star\delta}}\,\mathbf{w}, \tag{5.146a}$$

$$\mathbf{T}^\star(z) = \mathbf{L}^\star \mathbf{Z}^{\star\delta} \mathbf{v} + \overline{\mathbf{L}^\star \mathbf{Z}^{\star\delta}}\,\mathbf{w}, \tag{5.146b}$$

where the matrices $\mathbf{A}^\star$ and $\mathbf{L}^\star$ are expressed by

$$\mathbf{A}^\star = \begin{bmatrix} \frac{1}{4Gi}\kappa i & -\frac{1}{4Gi}i & 0 \\ \frac{1}{4Gi}\kappa & \frac{1}{4Gi} & 0 \\ 0 & 0 & a_{44} \end{bmatrix}, \quad \mathbf{L}^\star = \frac{1}{2}\begin{bmatrix} i & -i & 0 \\ 1 & 1 & 0 \\ 0 & 0 & -1 \end{bmatrix} \tag{5.147}$$

with a_{44} is defined in (4.132b) and $\kappa = 3 - 4\nu$ for plane strain and $\kappa = (3 - \nu)/(1 + \nu)$ for plane stress. Since the available material data of insulators or conductors are provided in the same form as the piezoelectric ones, it follows for the isotropic parameters that

$$\nu = \frac{C_{12}^E}{2(C_{12}^E + C_{44}^E)}, \quad G = C_{44}^E. \tag{5.148}$$

The complex functions $\mathbf{Z}^{\star\delta}$ are

$$\mathbf{Z}^{\star\delta} = \begin{bmatrix} z^\delta & 0 & 0 \\ (\bar{z} - z)\,\delta z^{\delta-1} & z^\delta & 0 \\ 0 & 0 & z^\delta \end{bmatrix} = \begin{bmatrix} r^\delta\,\mathrm{e}^{i\delta\theta} & 0 & 0 \\ -2ir^\delta\delta\,\mathrm{e}^{i(\delta-1)\theta}\sin\theta & r^\delta\,\mathrm{e}^{i\delta\theta} & 0 \\ 0 & 0 & r^\delta\,\mathrm{e}^{i\delta\theta} \end{bmatrix}. \tag{5.149}$$

Note that the upper left 2×2 matrix is the same as in (5.87) for pure isotropic elasticity, while the third diagonal element describes the electric field. The simplified notation (5.13) can be implemented for the diagonal elements, because it follows for functions (5.14) and (5.15) that $R^2 = 1$ and $\Psi = \theta$ when $\mu_{1,2,3} = i$. Complex conjugation of the function (5.149) leads to

$$\overline{\mathbf{Z}}^{*\delta} = \begin{bmatrix} r^\delta\,\mathrm{e}^{-i\delta\theta} & 0 & 0 \\ 2ir^\delta\delta\,\mathrm{e}^{-i(\delta-1)\theta}\sin\theta & r^\delta\,\mathrm{e}^{-i\delta\theta} & 0 \\ 0 & 0 & r^\delta\,\mathrm{e}^{-i\delta\theta} \end{bmatrix}. \tag{5.150}$$

The eigenvalue problem for a bi-material notch composed of a piezoelectric material and a conductor or insulator is redefined in terms of the equations (5.7) and (5.146). A bi-material notch with the geometry in Fig. 5.2 is considered, where material 1 is the non-piezoelectric one defined by elastic constants C_{ij}^E and permittivities ω_{ij}^ε. Let us define the following identities:

$$\begin{aligned} \mathbf{A}^{\mathrm{I}} &= \mathbf{A}^\star, \quad \mathbf{L}^{\mathrm{I}} = \mathbf{L}^\star, \\ \mathbf{u}^{\mathrm{I}} &= \mathbf{u}^\star, \quad \mathbf{T}^{\mathrm{I}} = \mathbf{T}^\star, \\ \mathbf{Z}_1^{\mathrm{I}\delta} &= \mathbf{Z}_1^{\star\delta}, \quad \mathbf{Z}_0^{\mathrm{I}\delta} = \mathbf{Z}_0^{\star\delta}, \end{aligned} \tag{5.151}$$

while the corresponding relations for the region II remain unchanged. The eigenvalue problem is introduced by the boundary conditions (5.17) and (5.18). The system of eight homogeneous algebraic equations has the form (5.19). The identity of (5.20) is valid also for the isotropic material, i.e.

$$\mathbf{Z}_0^{\star\delta} = \mathbf{I}, \quad \overline{\mathbf{Z}}_0^{\star\delta} = \mathbf{I}. \tag{5.152}$$

The eigenvalue problem modifications (5.21)–(5.36) can be then employed. All the other procedures remain identical, i.e. normalization (5.41a) or (5.41b), shape function introduction (5.43) and the Ψ-integral (5.117)–(5.119) (the relations (5.47)–(5.69) expanded for the piezoelectric problem). The finite element model has the same properties and geometry, except for the material model of the material 1.

Definitions for the asymptotic stresses and electric displacements of the isotropic non-piezoelectric material have the form

$$\begin{aligned} \boldsymbol{\sigma}^{\star 1} &= H_1 r^{\delta_1-1}\tilde{\boldsymbol{\lambda}}_{1,x_2}^\star(\theta) + H_2 r^{\delta_2-1}\tilde{\boldsymbol{\lambda}}_{2,x_2}^\star(\theta) + H_3 r^{\delta_3-1}\tilde{\boldsymbol{\lambda}}_{3,x_2}^\star(\theta), \\ \boldsymbol{\sigma}^{\star 2} &= H_1 r^{\delta_1-1}\tilde{\boldsymbol{\lambda}}_{1,x_1}^\star(\theta) + H_2 r^{\delta_2-1}\tilde{\boldsymbol{\lambda}}_{2,x_1}^\star(\theta) + H_3 r^{\delta_3-1}\tilde{\boldsymbol{\lambda}}_{3,x_1}^\star(\theta), \end{aligned} \tag{5.153}$$

material constants		epoxy	polymer	Al$_2$O$_3$	SiC
C_{11}^E	$\times 10^{10}$ [Pa]	0.80	0.386	47.0804	49.9391
C_{12}^E	$\times 10^{10}$ [Pa]	0.44	0.257	14.4626	11.9433
C_{23}^E	$\times 10^{10}$ [Pa]	0.44	0.257	14.4626	11.9433
C_{22}^E	$\times 10^{10}$ [Pa]	0.80	0.386	47.0804	49.9391
C_{44}^E	$\times 10^{10}$ [Pa]	0.18	0.0645	16.3089	18.9979
e_{11}	[Cm^{-2}]	0	0	0	0
e_{12}	[Cm^{-2}]	0	0	0	0
e_{26}	[Cm^{-2}]	0	0	0	0
ω_{11}^ε	$\times 10^{-10}$ [C(Vm)$^{-1}$]	0.372	0.797	0.885	0.885
ω_{22}^ε	$\times 10^{-10}$ [C(Vm)$^{-1}$]	0.372	0.797	0.885	0.885

Tab. 5.15: Material properties of typical insulators [99].

where the derivatives of the shape functions are given by

$$\tilde{\boldsymbol{\lambda}}_{i,x_2}^*(\theta) = \mathbf{B}^*\delta_i\mathbf{Z}^{*\delta_i-1}(\theta)\mathbf{v}_i + \overline{\mathbf{B}}^*\delta_i\overline{\mathbf{Z}}^{*\delta_i-1}(\theta)\mathbf{w}_i, \quad i = 1,2,3, \tag{5.154a}$$

$$\tilde{\boldsymbol{\lambda}}_{i,x_i}^*(\theta) = \mathbf{L}^*\delta_i\mathbf{Z}^{*\delta_i-1}(\theta)\mathbf{v}_i + \overline{\mathbf{L}}^*\delta_i\overline{\mathbf{Z}}^{*\delta_i-1}(\theta)\mathbf{w}_i, \quad i = 1,2,3, \tag{5.154b}$$

where

$$\mathbf{B}^* = \frac{1}{2}\begin{bmatrix} 3 & -1 & 0 \\ i & -i & 0 \\ 0 & 0 & 2i \end{bmatrix} \tag{5.155}$$

and

$$\begin{aligned}
\mathbf{Z}^{\star\delta-1} = r^{\delta-1}\mathbf{Z}^{\star\delta-1}(\theta) &= r^{\delta-1}\begin{bmatrix} \delta\,\mathrm{e}^{i(\delta-1)\theta} & 0 & 0 \\ -2i\delta(\delta-1)\,\mathrm{e}^{i(\delta-2)\theta}\sin\theta & \delta\,\mathrm{e}^{i(\delta-1)\theta} & 0 \\ 0 & 0 & \delta\,\mathrm{e}^{i(\delta-1)\theta} \end{bmatrix}, \\
\overline{\mathbf{Z}}^{\star\delta-1} = r^{\delta-1}\overline{\mathbf{Z}}^{\star\delta-1}(\theta) &= r^{\delta-1}\begin{bmatrix} \delta\,\mathrm{e}^{-i(\delta-1)\theta} & 0 & 0 \\ 2i\delta(\delta-1)\,\mathrm{e}^{-i(\delta-2)\theta}\sin\theta & \delta\,\mathrm{e}^{-i(\delta-1)\theta} & 0 \\ 0 & 0 & \delta\,\mathrm{e}^{-i(\delta-1)\theta} \end{bmatrix}.
\end{aligned} \tag{5.156}$$

Subscripts $_{,x_1}$ and $_{,x_2}$ denote differentiation with respect to x_1, x_2 introduced in (5.78).

Example 13: Singularity exponents and electro-elastic field reconstruction of a non-piezoelectric/piezoelectric bi-material notch   Within the following studies, settings of all numerical procedures remain unchanged. For the sake of brevity, the Ψ-integral path independence and mesh density studies are not performed. A bi-material notch with the local geometry illustrated in Fig. 5.22 is considered. The material 1 is non-piezoelectric and material 2 has piezoelectric properties stated in Tab. 5.6.

Firstly, an insulator/piezoelectric bi-material notch is studied. Material parameters of four typical insulators are listed in Tab. 5.15. Dielectric constants of Al$_2$O$_3$ and SiC were not known, therefore they were set ten times higher than the vacuum permittivity. Consider two bi-material combinations – epoxy/PZT-4 and Al$_2$O$_3$/PZT-4. The first case is characterized by smaller elastic properties than the piezoelectric part, while the insulator in the latter case has higher elastic properties. Let the angle $\omega_2 = -180°$ be fixed. The dependence of the exponents
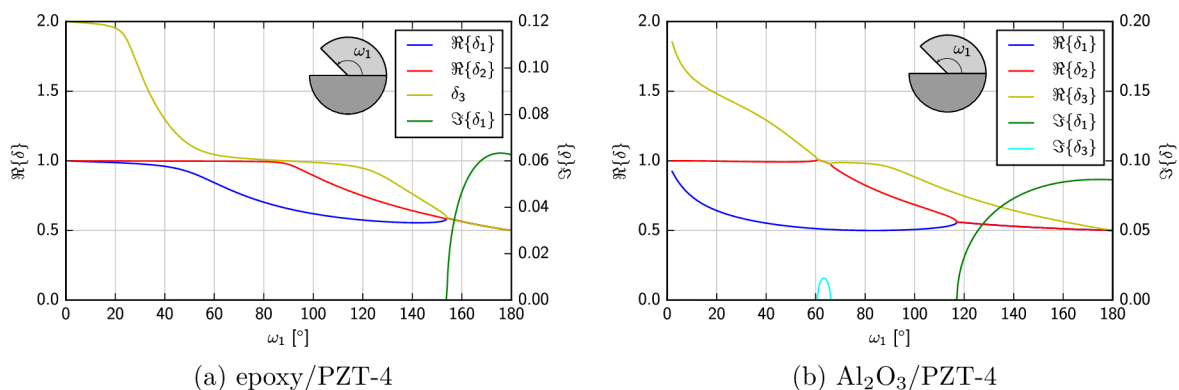
(a) epoxy/PZT-4   (b) Al_2O_3/PZT-4

Fig. 5.44: The exponent δ_i dependence on the notch angle ω_1 of the insulator/piezoelectric bi-material notch. The poling direction of the material 2 is $\alpha_2 = 90°$.

δ_i on the notch angle ω_1 for the bi-material combinations are shown in Figs. 5.44(a) and 5.44(b). The graphs have the typical character of the type A piezoelectric bi-materials described in Fig. 5.26(a), nevertheless there are some dissimilarities. Firstly, the roots δ_1 and δ_2 for epoxy/PZT-4 bi-material approach the limit value 1.0 asymptotically, just as $\delta_3 \to 2.0$. But, in the case of the Al_2O_3/PZT-4 bi-material, only δ_2 shows approximative behaviour. The close proximity to the pole in the 1.0 brings about numerical troubles in the root finding algorithm `findroot`, which has to be set properly. Additionally, in the latter bi-material combination there is a region between 60° and 70°, where roots δ_2 and δ_3 are complex conjugate. Finally, the regions where δ_1 and δ_2 are complex conjugate, are wider and the imaginary parts of the roots do not reach their maximal value for $\omega_2 = -180°$, as was typical for pure piezoelectric bi-materials.

Following the results in Ou and Wu [25] for a piezoelectric bi-material (Tabs. 5.8 and 5.9), Ou and Chen [99] investigated an insulator/piezoelectric interface crack in terms of the Hilbert problem. Since the studied non-piezoelectric materials had isotropic properties, they avoided the degenerate matrices by considering the isotropic material as a transversally isotropic piezoelectric material by assuming very small piezoelectric coefficients e_{11}, e_{12} and e_{26}. They found out that, similarly to the pure piezoelectric problem, the bi-material combinations can show either ε- or κ-class singularity. However, all investigated material combinations possessed only ε-type singularity, see Eq. 5.103. Tab. 5.16 summarizes the singular exponents δ_i obtained by the presented redefined eigenvalue problem for non-piezoelectric/piezoelectric interface crack of and their comparison with results reported by Ou and Chen [99]. The remaining exponent was always $\delta_3 = 0.5$. One can see that both approaches provide coincident eigenvalues. The introduction of a small perturbation in piezoelectric coefficients to avoid degeneracy was also reported in [20].

Let us consider a conductor/piezoelectric bi-material notch. Material properties of four typical conductors are summarized in Tab. 5.17. The dielectric constants are functions of the parameter p, which will be later determined according to the assumption of the infinite permittivity. The structure of the expanded LES formalism provides an elegant way to fulfil the infinite permittivity requirement. The only component in the material matrices $\mathbf{A}^\star$ and $\mathbf{L}^\star$ (see (5.147)) which depends on the dielectric coefficients, is the third diagonal element a_{44}. For the isotropic conductor properties, a_{44} is reduced to (see (4.132b))

$$a_{44} = \hat{\beta}'^\sigma_{22}/\mu_4. \tag{5.157}$$

Since the non-permittivity $\hat{\beta}'^\sigma_{22}$ is the inverse of ω^ε_{22}, it implies that $a_{44} \to 0$ for $\omega^\varepsilon_{22} \to \infty$.

bi-materials	δ_1	δ_2	oscillatory index ε	comparison with Ou and Chen [99]
epoxy/PZT-4[†]	$0.5 + 0.06260i$	$0.5 - 0.06260i$	0.06260	0.0626
epoxy/BaTiO$_3$	$0.5 + 0.06501i$	$0.5 - 0.06501i$	0.06501	0.0650
polymer/PZT-5H	$0.5 + 0.05021i$	$0.5 - 0.05021i$	0.05021	0.0502
Al$_2$O$_3$/PZT-4	$0.5 + 0.08639i$	$0.5 - 0.08639i$	0.08639	0.0864
Al$_2$O$_3$/PZT-6B	$0.5 + 0.04978i$	$0.5 - 0.04978i$	0.04978	0.0498
SiC/PZT-7A	$0.5 + 0.05652i$	$0.5 - 0.05652i$	0.05652	0.0565

[†] $\delta_{1,2} = 0.5 \pm 0.06258i$ computed by Hwu and Kuo [21] by using the expanded Stroh formalism

Tab. 5.16: Oscillatory indices of insulator/piezoelectric interface cracks and their comparison with results in [99].

material constants		copper	silver	lead	aluminium
C_{11}^E	$\times 10^{10}$ [Pa]	22.2852	14.0399	4.2992	9.19
C_{12}^E	$\times 10^{10}$ [Pa]	13.0882	8.6051	3.2433	4.53
C_{23}^E	$\times 10^{10}$ [Pa]	13.0882	8.6051	3.2433	4.53
C_{22}^E	$\times 10^{10}$ [Pa]	22.2852	14.0399	4.2992	9.19
C_{44}^E	$\times 10^{10}$ [Pa]	4.5985	2.7174	0.5280	2.33
e_{11}	[Cm^{-2}]	0	0	0	0
e_{12}	[Cm^{-2}]	0	0	0	0
e_{26}	[Cm^{-2}]	0	0	0	0
ω_{11}^ε	$\times 10^{-12}$ [C(Vm)$^{-1}$]	$8.854p$	$8.854p$	$8.854p$	$8.854p$
ω_{22}^ε	$\times 10^{-12}$ [C(Vm)$^{-1}$]	$8.854p$	$8.854p$	$8.854p$	$8.854p$

Tab. 5.17: Material properties of typical conductors [26].

The expanded LES formalism for modelling a conductor can be thereafter modified implicitly by setting $a_{44} = 0$. The knowledge of the dielectric constants is then not required. However, this cannot be applied to the finite element computations, because some commercial programs require the input in the form of permittivities ω_{22}^ε or ω_{22}^σ. For that purpose, a convergence study of the exponents δ_i on the multiplication parameter p was carried out. The results for three representative bi-materials are illustrated in Fig. 5.45. It can be seen that by increasing the parameter p, and so the permittivity of the material, the singularity exponents δ_i or oscillatory and non-oscillatory indices ε and κ converge to their limit values δ_i^∞, ε^∞ or κ^∞ determined by setting $a_{44} = 0$, which represents the infinite permittivity. On the secondary axis the absolute error is shown. For the subsequent comparative studies, $p = 10^8$ was chosen. The absolute error of the singularity exponents does not then exceed 2×10^{-6}.

A dependence of the exponents δ_i on the notch angle ω_1, while $\omega_2 = -180°$ is fixed, are shown in Figs. 5.46(a) and 5.46(b). The first graph has the character similar to the type B piezoelectric bi-material, which was typical for the most material combinations except for lead/PZT-6B bi-material combination, which shows the type A behaviour. Decreasing ω_1 causes that δ_1, δ_2 and δ_3 approaches 0.5, 1.0 and 1.5, respectively. Contrary to the previous examples, in the case of the lead/PZT-6B bi-material notch, the complex conjugate exponents are δ_2 and δ_3 for $175° < \omega_1 < 180°$, see Fig. 5.46(b).

Similarly to the study of the insulator/piezoelectric interface cracks in [99], Ou and Chen [26] investigated a conductor/piezoelectric interface crack in the terms of the Hilbert problem.
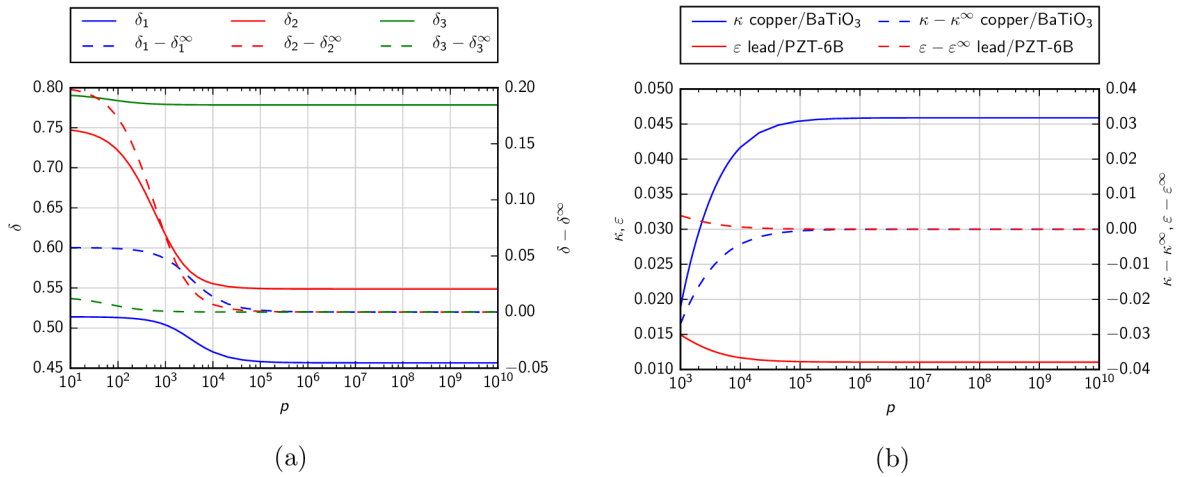
(a)

(b)

Fig. 5.45: Convergence study of the singularity exponents δ_i on the multiplicative parameter p introduced in Tab.5.17. (a) aluminium/PZT-4 bi-material notch, $\omega_1 = 120°$, $\omega_2 = -180°$, (b) interface cracks of copper/BaTiO$_3$ and lead/PZT-6H bi-materials.
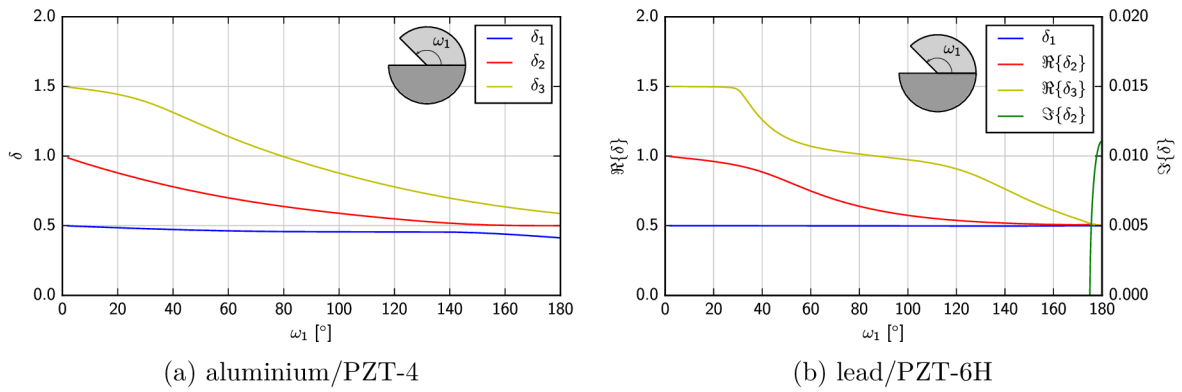

(a) aluminium/PZT-4

(b) lead/PZT-6H

Fig. 5.46: The exponent δ_i dependence on the notch angle ω_1 of the conductor/piezoelectric bi-material notch. Poling direction of the material 2 is $\alpha_2 = 90°$.

They avoided degenerate matrices due to the isotropic properties of the conductor by employing the same procedure, i.e. prescribing very small piezoelectric coefficients e_{11}, e_{12} and e_{26}. Tab. 5.18 summarizes singular exponents δ_i obtained by the redefined eigenvalue problem for the non-piezoelectric/piezoelectric interface crack. One can see that only lead/PZT-6B interface crack possess the ε-type singularity, all other bi-materials show κ-class singular exponents, which are evaluated Eq. (5.104). The resulting values and exponents reported in Ou and Chen [26] show a very good agreement.

The effects of the poling direction α_2 for an epoxy/PZT-4 and aluminium/PZT-4 interface crack are shown in Fig. 5.47. When considering a piezoelectric material coupled with an insulator or a conductor possessing isotropic material properties, the order of singularity does not depend on the fibre orientation of the material 2, which was also observed by pure isotropic/transversally isotropic material in Fig. 5.19. Let us consider an epoxy/PZT-4 interface crack with poling direction $\alpha_2 = 90°$ of the material 2. The boundary conditions illustrated in Fig. 5.32 remain identical, i.e. the upper side is loaded with applied stress $\sigma_2^{\mathrm{appl}} = 10\,\mathrm{kPa}$ and electric displace-

bi-materials	δ_1	δ_3	non-oscillatory index κ	comparison with Ou and Chen [26]
copper/PZT-4	0.39017	0.60983	0.10983	0.1098
silver/BaTiO$_3$	0.45764	0.542336	0.04236	0.0424
lead/PZT-5H	0.47193	0.52807	0.02807	0.0281
aluminium/PZT-4	0.41274	0.58726	0.08726	0.0873
copper/PZT-7A	0.43450	0.56550	0.06550	0.0655
	δ_2	δ_3	oscillatory index ε	
lead/PZT-6B	$0.5 + 0.01105i$	$0.5 - 0.01105i$	0.01105	0.0110

Tab. 5.18: Non-oscillatory and oscillatory indices of conductor/piezoelectric interface cracks and their comparison with results in [26].

(a) epoxy/PZT-4

(b) aluminium/PZT-4
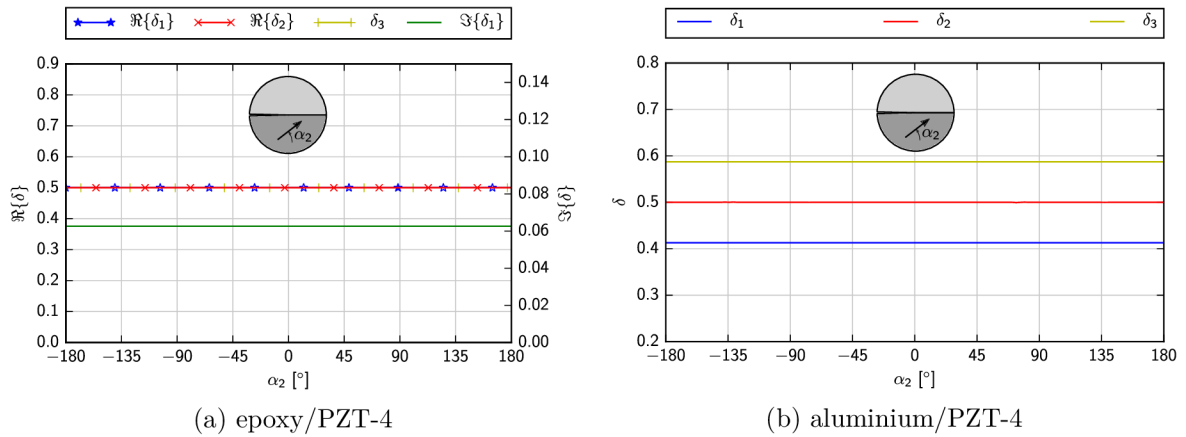
Fig. 5.47: The dependence of the interface crack exponents δ_i on the poling direction α_2.

ment $D_2^{\mathrm{appl}} = 0.01\,\mathrm{Cm}^{-2}$. The asymptotic stresses, electric displacements, displacements and electric potentials calculated along the circular path with radius $r = 0.001\,\mathrm{mm}$ encircling the notch tip together with results obtained by FEM are shown in Fig. 5.48. The superscripts H_i, $i = 1,2,3$ of plotted quantities listed in the legend indicate particular asymptotic terms in Eqs. (5.109a) and (5.153). The plots show a very good agreement of the asymptotic solution with the full-field FEM solution. The results computed along the circular path with radius $r = 2\,\mathrm{mm}$ are shown in Fig. 5.49. We can see that the correspondence is still very good. It can be also observed that the electric potential in the insulator is higher than in the piezoelectric part.

The stresses, electric displacements, displacements and electric potentials along the contours with radii $r = 0.001\,\mathrm{mm}$ and $r = 2\,\mathrm{mm}$ encircling the interface crack tip of the aluminium/PZT-4 bi-material notch are shown in Fig. 5.50 and 5.51, respectively. One can observe that the electric potential in the conductor is constant and very close to zero. The correspondence between the asymptotic and the FEM solution is very good for both radii.
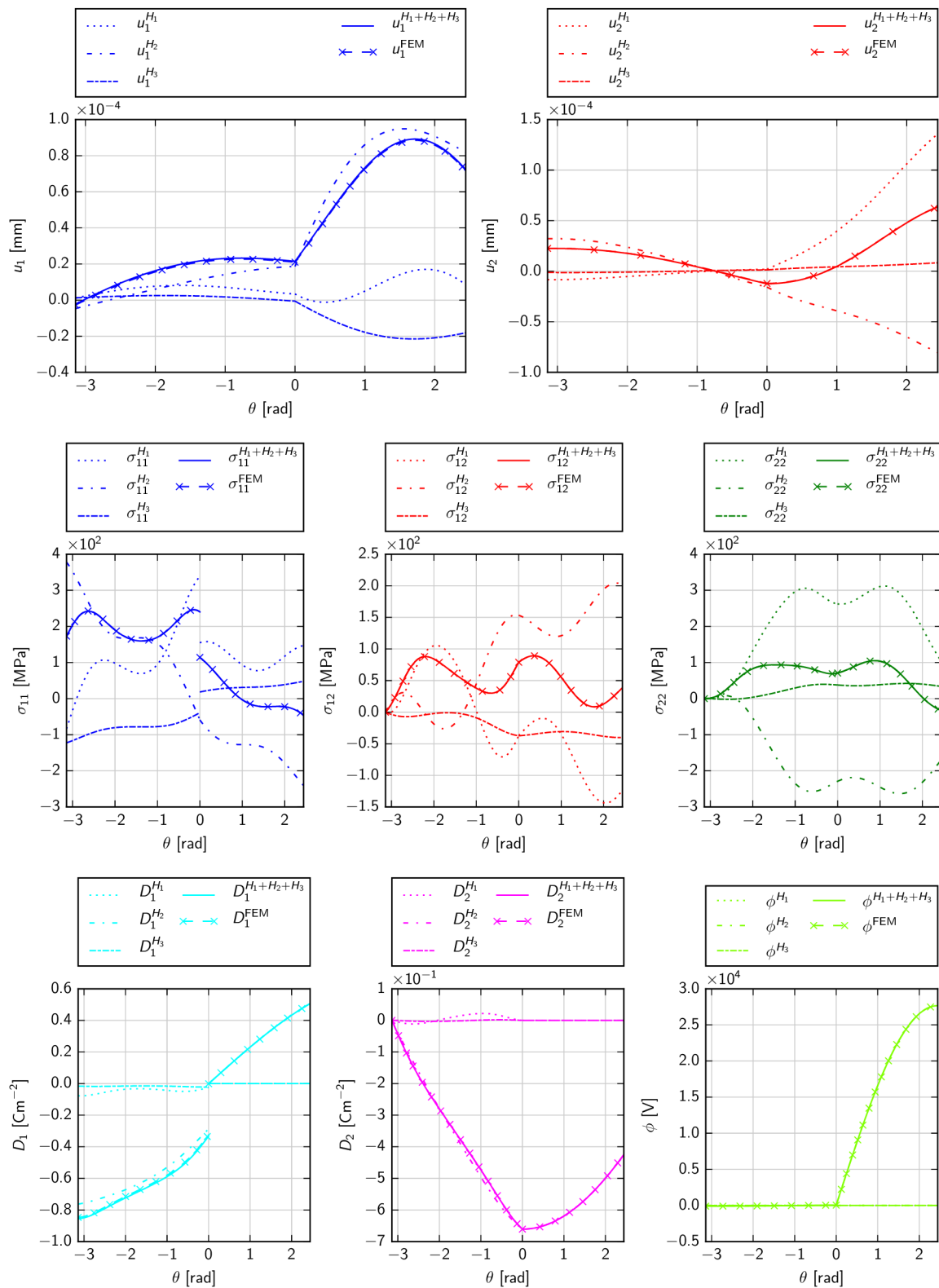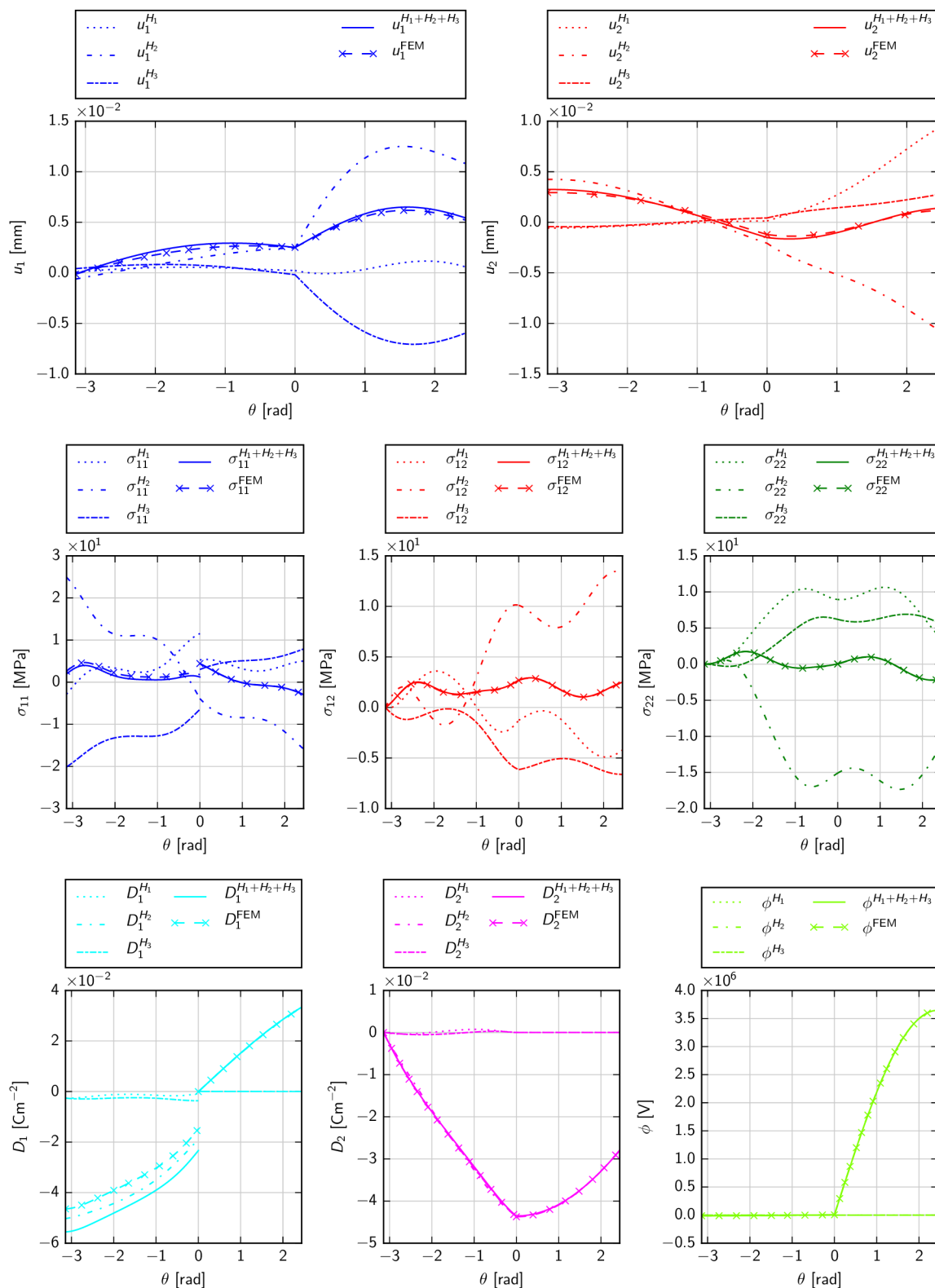
Fig. 5.48: The displacements, stress components, electric displacement components and electric potential of an epoxy/PZT-4 bi-material notch on the circular path $r = 0.001\,\mathrm{mm}$, $\omega_1 = 140°$, $\omega_2 = -180°$, the singularity exponents are $\delta_1 = 0.5557$, $\delta_2 = 0.6422$, $\delta_3 = 0.7624$.
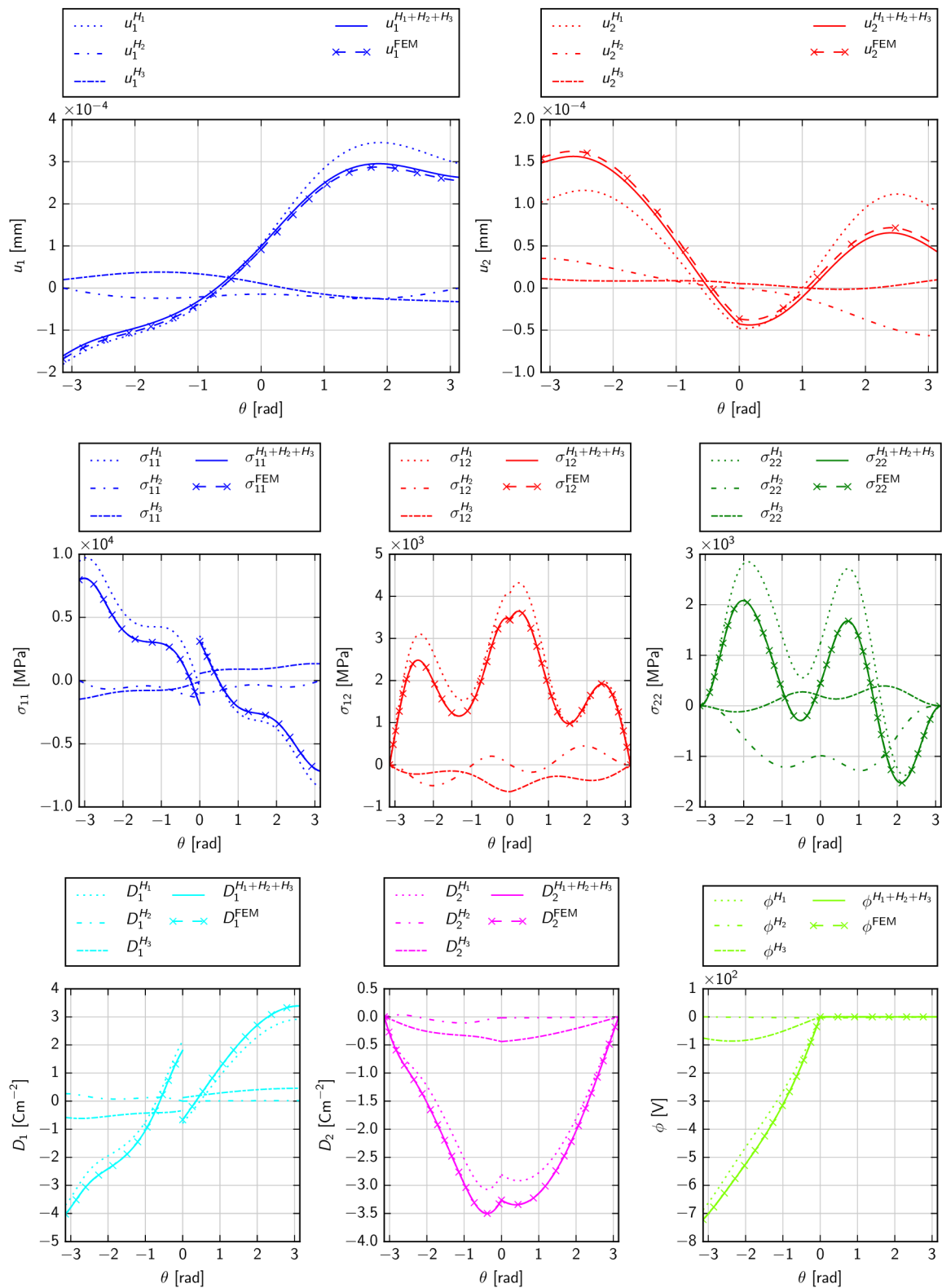
Fig. 5.49: The displacements, stress components, electric displacement components and electric potential of an epoxy/PZT-4 bi-material notch on the circular path $r = 2\,\mathrm{mm}$, $\omega_1 = 140°$, $\omega_2 = -180°$, the singularity exponents are $\delta_1 = 0.5557$, $\delta_2 = 0.6422$, $\delta_3 = 0.7624$.
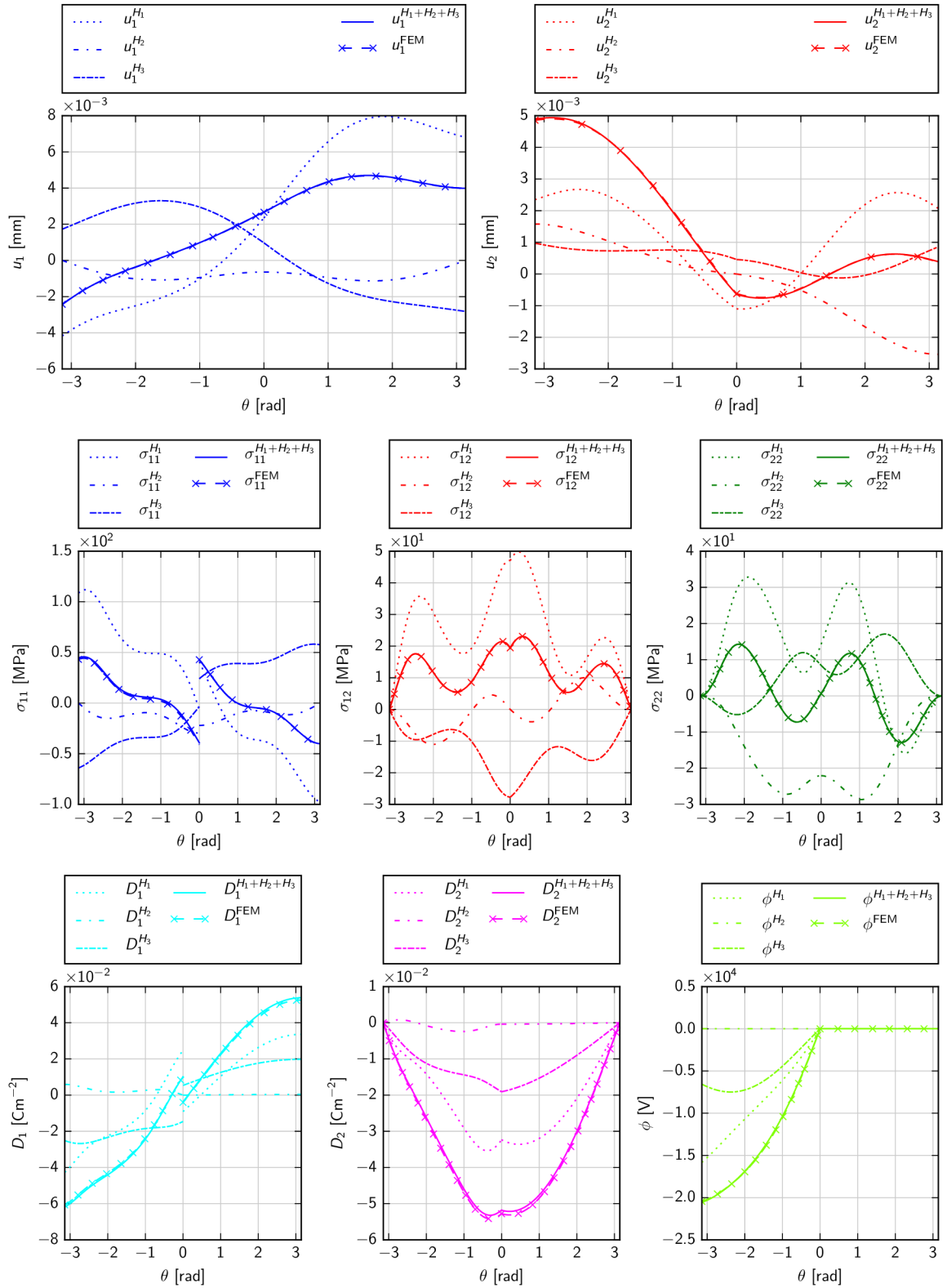
Fig. 5.50: The displacements, stress components, electric displacement components and electric potential of an aluminium/PZT-4 interface crack on the circular path $r = 0.001\,\text{mm}$, $\omega_1 = 180°$, $\omega_2 = -180°$, the singularity exponents are $\delta_1 = 0.4127$, $\delta_2 = 0.5$, $\delta_3 = 0.5873$.

Fig. 5.51: The displacements, stress components, electric displacement components and electric potential of an aluminium/PZT-4 interface crack on the circular path $r = 2\,\mathrm{mm}$, $\omega_1 = 180°$, $\omega_2 = -180°$, the singularity exponents are $\delta_1 = 0.4127$, $\delta_2 = 0.5$, $\delta_3 = 0.5873$.

6 Conclusion

The determination of the singular stress behaviour is one of the necessary steps for life evaluation of constructions containing compound materials. The expansion of the Lekhnitskii-Eshelby-Stroh formalism to piezoelectric materials firstly requires a deep investigation of pure anisotropic bi-material notches. The effect of the material and geometry and primarily the properties of the numerical procedures have to be studied. Many similarities between singular parameters of pure anisotropic and piezoelectric bi-material notches have been observed. However, mainly the numerical algorithms for finding roots of the characteristic and subsequent eigenvector extraction had to be enhanced. It was proved that the default settings of the advanced numerical procedures in `numpy` and `scipy` are inappropriate and have to be modified.

Firstly, a character of the singularity exponents as a function of the notch face angle ω_1 and fibre orientation α_1 was determined. Considering an in-plane problem and pure anisotropic material, there are two singularity exponents, which are both either real or complex-valued. The case of an interface crack is characterised by the oscillatory index. A HSV method was developed in order to easily identify roots of the eigenvalue problem. Then, an initial guess for the root finding algorithm can be estimated more precisely.

To achieve the most precise solution, the data extracted from the finite element analysis with a very fine mesh were interpolated, so that the adaptive Romberg's integration method can be implemented. After that, the path independence of the Ψ-integral was proved. A precision of all computed parameters was illustrated on the good coincidence of the asymptotic and FEM solutions on two representative circular paths enclosing the notch tip. The modification of the LES formalism in terms of the Muskhelishvili complex potentials enables a modelling of isotropic materials.

In the second step, the expanded Lekhnitskii-Eshelby-Stroh formalism for piezoelectric materials was applied to bi-material notches and interface crack problems. Although these two kinds of the stress concentrators are usually studied separately, especially in the case of the piezoelectric materials, the presented results showed that the used form of the expanded LES formalism and the eigenvalue problem captures acceptably both particular problems of the fracture mechanics. It was shown that the eigenvalue problem can be simply expanded, but the attention has to be paid to the eigenvector extraction due to the ill-conditioned matrices in the piezoelectric constitutive laws. The singularities of very closed bi-material notches, characterised by the complex valued exponents, were part of the discussion. Also arbitrary poling orientation of the piezoelectric materials in the $x_1 x_2$ plane was included into the considerations.

The generalization of the so-called ε and κ classification of the piezoelectric bi-materials was suggested. It was ascertained that the exponents of the singularity of the stresses, mechanical and electric displacements and electric potential are independent of the parallel poling orientation of the bi-material. Although in the case of the interface crack, the used eigenvalue procedure is not able to distinguish between the real and complex exponent form as does the Hilbert problem formulation presented in Ou and Wu [25]. It was shown that both methods give equivalent results. After that, the Ψ-integral path-independence was proved. Nevertheless, precision of the Ψ-integral evaluation method has to be significantly increased. The high accuracy of the GSIFs calculations was demonstrated by comparing the asymptotic solution with the full-field FEM solution obtained using a very fine mesh.

An insulator/piezoelectric and conductor/piezoelectric bi-material notches were modelled by implementing the Muskhelishvili complex potentials similarly to the pure anisotropic bi-material notches. As the piezoelectric coefficients were omitted, the elastic and electric fields are decoupled and the linear electrostriction is not considered. The effect of the quadratic electrostriction, which could be manifested under electrical loading, is not included in the constitutive law. It was

shown that the singularity exponents for the interface cracks agree with the ε and κ classification reported in Ou and Chen [99] and Ou and Chen [26].

The effect of the boundary conditions of a piezoelectric bi-material notch was also studied. It was observed that when one face was clamped, the characteristic equation has six roots. The relations for electro-elastic fields description were extended for all singular terms. A future research will focus on proposal of fracture criteria based on extending the Finite Fracture Mechanics concept [121] to piezoelectric bi-material notches.

References

[1] PAK, Y.E. Linear electro-elastic fracture mechanics of piezoelectric materials. *International Journal of Fracture*. 1992, vol. 54, no. 1, pp. 79–100. ISBN 0376-9429. ISSN 03769429. Available from DOI: 10.1007/BF00040857.

[2] POHANKA, R.C.; SMITH, P.L. Recent Advances in Piezoelectric Ceramics. In: LEVINSON, L.M. (ed.). *Electronic Ceramics: Properties: Devices, and Applications*. New York, 1988, chap. 2, p. 527. ISBN 0-8247-7761-1.

[3] MCHENRY, K.D.; KOEPKE, B.G. Electric field effects on subcritical crack growth in PZT. In: BRANDT, R.C.; EVANS, A.G.; HASSELMAN, D.P.H.; LANGE, F.F. (eds.). *Fracture mechanics of ceramics*. 6th ed. New York: Plenum Press, 1983, vol. 5, pp. 337–352. ISBN 0-306-41022-2.

[4] KOEPKE, B.G; MCHENRY, K.D.; SEIFRIED, L.M.; STOKES, R.J. Mechanical Integrity of Piezoelectric and Dielectric Ceramics. In: *IEEE 1986 Ultrasonics Symposium*. 1986, pp. 675–684. Available from DOI: 10.1109/ULTSYM.1986.198821.

[5] PARK, S.B.; SUN, C.T. Effect of electric field on fracture of piezoelectric ceramics. *International Journal of Fracture*. 1995, vol. 70, no. 3, pp. 203–216. ISSN 0376-9429. Available from DOI: 10.1007/BF00012935.

[6] LEKHNITSKII, S.G. *Theory of Elasticity of an Anisotropic Elastic Body*. First. San Francisco: Holden-Day, 1963.

[7] STROH, A.N. Dislocations and cracks in anisotropic elasticity. *Philosophical Magazine*. 1958. ISBN 1478-6435. ISSN 00318086. Available from DOI: 10.1080/14786435808565804.

[8] STROH, A.N. Steady State Problems in Anisotropic Elasticity. *J. Math. Phys.* 1962. ISSN 00971421. Available from DOI: 10.1002/sapm196241177.

[9] TING, T.C.T. *Anisotropic Elasticity : Theory and Applications*. New York: Oxford University Press, 1996. ISBN 1-280-52616-5.

[10] SUO, Z.; KUO, C.M.; BARNETT, D.M.; WILLIS, J.R. Fracture Mechanics for Piezoelectric Ceramics. *J. Mech. Phys. Solids*. 1992, vol. 40, no. 4, pp. 739–765.

[11] SOSA, Horacio; KHUTORYANSKY, Naum. New developments concerning piezoelectric materials with defects. *International Journal of Solids and Structures*. 1996, vol. 33, no. 23, pp. 3399–3414. ISSN 00207683. Available from DOI: 10.1016/0020-7683(95)00187-5.

[12] BANKS-SILLS, Leslie; MOTOLA, Yael; SHEMESH, Lucy. The M-integral for calculating intensity factors of an impermeable crack in a piezoelectric material. *Engineering Fracture Mechanics*. 2008, vol. 75, no. 5, pp. 901–925. ISSN 00137944. Available from DOI: 10.1016/j.engfracmech.2007.05.009.

[13] SINCLAIR, G. B. Logarithmic Stress Singularities Resulting From Various Boundary Conditions in Angular Corners of Plates Under Bending. *Journal of Applied Mechanics*. 2000, vol. 67, no. 1, pp. 219. ISSN 00218936. Available from DOI: 10.1115/1.321174.

[14] LABOSSIERE, Paul E.W.; DUNN, Martin L. Stress intensities at interface corners in anisotropic bimaterials. *Engineering Fracture Mechanics*. 1999, vol. 62, no. 6, pp. 555–576. ISSN 00137944. Available from DOI: 10.1016/S0013-7944(99)00005-3.

[15] CARPENTER, William C.; BYERS, Curtis. A path independent integral for computing stress intensities for V-notched cracks in a bi-material. *International Journal of Fracture*. 1987, vol. 35, no. 4, pp. 245–268. ISSN 03769429. Available from DOI: `10.1007/BF00276356`.

[16] SINCLAIR, G.B.; OKAJIMA, M.; GRIFFIN, J.H. Path independent integrals for computing stress intensity factors at sharp notches in elastic plates. *International Journal for Numerical Methods in Engineering*. 1984, vol. 20, pp. 999–1008. ISSN 10970207. Available from DOI: `10.1002/nme.1620200603`.

[17] HWU, Chyanbin. *Anisotropic Elastic Plates*. 1st ed. New York: Springer US, 2010. ISBN 978-1-4419-5914-0.

[18] BROBERG, Bertram K. *Cracks and fracture*. San Diego: Academic Press, 1999. ISBN 01-213-4130-5. Available from DOI: `10.1016/B978-012134130-5/50020-9`.

[19] PROFANT, T.; KLUSÁK, J.; ŠEVEČEK, O.; HRSTKA, M.; KOTOUL, M. An energetic criterion for a micro-crack of finite length initiated in orthotropic bi-material notches. *Engineering Fracture Mechanics*. 2013, vol. 110, pp. 396–409. ISSN 00137944. Available from DOI: `10.1016/j.engfracmech.2013.08.014`.

[20] HWU, Chyanbin. Some explicit expressions of extended Stroh formalism for two-dimensional piezoelectric anisotropic elasticity. *International Journal of Solids and Structures*. 2008, vol. 45, no. 16, pp. 4460–4473. ISSN 00207683. Available from DOI: `10.1016/j.ijsolstr.2008.03.025`.

[21] HWU, Chyanbin; KUO, T.L. Interface corners in piezoelectric materials. *Acta Mechanica*. 2010, vol. 214, pp. 95–110. Available from DOI: `10.1007/s00707-010-0318-5`.

[22] HWU, Chyanbin; IKEDA, T. Electromechanical fracture analysis for corners and cracks in piezoelectric materials. *International Journal of Solids and Structures*. 2008, vol. 45, no. 22-23, pp. 5744–5764. ISSN 00207683. Available from DOI: `10.1016/j.ijsolstr.2008.06.011`.

[23] HIRAI, H.; CHIBA, M.; ABE, M.; IKEDA, T.; MIYAZAKI, N. Stress intensity factor analysis of an interfacial corner between piezoelectric bimaterials using the H-integral method. *Engineering Fracture Mechanics*. 2012, vol. 82, pp. 60–72. ISBN 9780791844618. ISSN 00137944. Available from DOI: `10.1016/j.engfracmech.2011.11.023`.

[24] ABE, M.; IKEDA, T.; KOGANEMARU, M.; MIYAZAKI, N. Stress intensity factor analysis of a three-dimensional interfacial corner between anisotropic piezoelectric multi-materials under several boundary conditions on the corner surfaces. *Engineering Fracture Mechanics*. 2017, vol. 171, pp. 1–21. ISSN 00137944. Available from DOI: `10.1016/j.engfracmech.2016.12.009`.

[25] OU, Z.C.; WU, Xijia. On the crack-tip stress singularity of interfacial cracks in transversely isotropic piezoelectric bimaterials. *International Journal of Solids and Structures*. 2003, vol. 40, no. 26, pp. 7499–7511. ISSN 00207683. Available from DOI: `10.1016/j.ijsolstr.2003.08.021`.

[26] OU, Z.C; CHEN, Y.H. Near-tip stress fields and intensity factors for an interface crack in metal/piezoelectric bimaterials. *International Journal of Engineering Science*. 2004, vol. 42, no. 13-14, pp. 1407–1438. ISSN 0020-7225. Available from DOI: `10.1016/J.IJENGSCI.2004.01.008`.

[27] ANDERSON, T.L. *Fracture mechanics*. Third. Boca Raton: CRC Press, 2005. ISBN 0-8493-1656-1.

[28] WESTERGAARD, H.M. *Journal of Applied Mechanics*. Bearing pressures and cracks. 1939. ISBN 9780874216561.

[29] WILLIAMS, M.L. On the stress distribution at the base of stationary crack. *Journal of Applied Mechanics*. 1957, vol. 24, pp. 109. Available from DOI: 10.1115/1.3640470.

[30] GROSS, Dietmar; SEELIG, Thomas. *Fracture mechanics : With an introduction to micromechanics*. 4th. New York: Springer, 2006. ISBN 9788578110796. ISSN 1098-6596. Available from DOI: 10.1017/CBO9781107415324.004.

[31] KIM, J.H.; MOON, H.J.; EARMME, Y.Y. Inplane and antiplane T-stresses for an interface crack in anisotropic bimaterial. *Mechanics of Materials*. 2001, vol. 33, no. 1, pp. 21–32. ISSN 01676636. Available from DOI: 10.1016/S0167-6636(00)00034-X.

[32] PROFANT, T.; ŠEVEČEK, O.; KOTOUL, M. Calculation of K-factor and T-stress for cracks in anisotropic bimaterials. *Engineering Fracture Mechanics*. 2008, vol. 75, no. 12, pp. 3707–3726. ISSN 00137944. Available from DOI: 10.1016/j.engfracmech.2007.08.003.

[33] ŠEVEČEK, Oldřich; BERMEJO, Raul; PROFANT, Tomáš; KOTOUL, Michal. Influence of the T-stress on the Crack Bifurcation Phenomenon in Ceramic Laminates. *Procedia Materials Science*. 2014, vol. 3, pp. 1062–1067. ISSN 22118128. Available from DOI: 10.1016/j.mspro.2014.06.173.

[34] KNÉSL, Zdeněk; KLUSÁK, Jan; NÁHLÍK, Luboš. Crack Initiation Criteria for Singular Stress Concentrations Part I : A Universal Assessment of Singular. 2007, vol. 14, no. 6, pp. 399–408.

[35] KLUSÁK, Jan; KNÉSL, Zdeněk; NÁHLÍK, Luboš. Crack Initiation Criteria for Singular Stress Concentrations Part II : Stability of Sharp and Bi-Material Notches. 2007, vol. 14, no. 6, pp. 409–422.

[36] NÁHLÍK, Luboš; ŠTEGNEROVÁ, Kateřina; HUTAŘ, Pavel. Estimation of critical applied stress for crack initiation from a sharp V-notch. *Theoretical and Applied Fracture Mechanics*. 2018, vol. 93, no. June 2017, pp. 247–262. ISSN 01678442. Available from DOI: 10.1016/j.tafmec.2017.09.002.

[37] NÁHLÍK, Luboš; KNÉSL, Zdeněk; KLUSÁK, Jan. Crack Initiation Criteria for Singular Stress Concentrations Part III : Applications To Fracture Of Coated Structures. 2008, vol. 15, no. 4, pp. 263–270.

[38] ERDOGAN, F.; SIH, G.C. On the Crack Extension in Plates Under Plane Loading and Transverse Shear. *Journal of Basic Engineering*. 1963, pp. 519–525. ISBN 0098-2202. ISSN 00219223. Available from DOI: 10.1115/1.3656897.

[39] KLUSÁK, Jan; PROFANT, Tomáš; KNÉSL, Zdeněk; KOTOUL, Michal. The influence of discontinuity and orthotropy of fracture toughness on conditions of fracture initiation in singular stress concentrators. *Engineering Fracture Mechanics*. 2013, vol. 110, pp. 438–447. ISSN 00137944. Available from DOI: 10.1016/j.engfracmech.2013.05.002.

[40] SIH, G.C. Strain-energy-density factor applied to mixed mode crack problems. *International Journal of Fracture*. 1974, vol. 10, no. 3, pp. 305–321. ISBN 0376-9429. ISSN 03769429. Available from DOI: 10.1007/BF00035493.

[41] HRSTKA, Miroslav; PROFANT, Tomáš; KLUSÁK, Jan; ŠEVEČEK, Oldřich; KOTOUL, Michal. A Stability Criterion of an Orthotropic Bi-material Notch Based on the Strain Energy Density. *In Engineering Mechanics 2014*. 2014, vol. 1, pp. 232–235. ISBN 978-80-214-4871-1.

[42]   MUSKHELISHVILI, N.I. *Some basic problems of the mathematical theory of elasticity.* Gröningen: Noordhoff, 1953.

[43]   BARBER, J.R.; TING, T.C.T. Three-dimensional solutions for general anisotropy. *Journal of the Mechanics and Physics of Solids.* 2007, vol. 55, no. 9, pp. 1993–2006. ISSN 00225096. Available from DOI: 10.1016/j.jmps.2007.02.002.

[44]   SUO, Zhigang. Singularities, interfaces and cracks in dissimilar anisotropic media. *Proceedings of the Royal Society A: Mathematical, Physical and Engineering Sciences.* 1990, pp. 331–358. ISSN 1364-5021. Available from DOI: 10.1098/rspa.1990.0016.

[45]   BELOKOPYTOVA, L.V.; FIL'SHTINSKII, L.A. Two-dimensional boundary value problem of electroelasticity for a piezoelectric medium with cuts. *J. Appl. Math. Mech.* 1979, vol. 43, pp. 147–153.

[46]   SOSA, Horacio. Plane problems in piezoelectric media with defects. *Int. J. Solids Structures.* 1991, vol. 28, no. 4, pp. 491–505. ISBN 0020-7683. ISSN 02534827.

[47]   CHEN, T.; LAI, D.S. An exact correspondence between plane piezoelectricity and generalized plane strain in elasticity. *Proc. R. Soc. Lond.* 1997, vol. 453, pp. 2689–2713.

[48]   CHEN, Tungyang; YEN, Wen Jin. Piezoelectric analogy of generalized torsion in anisotropic elasticity. *Journal of Elasticity.* 1997, vol. 49, no. 3, pp. 239–256. ISSN 03743535. Available from DOI: 10.1023/A:1007426225271.

[49]   CHEN, T. Further correspondences between plane piezoelectricity and generalized plane strain in elasticity. *Proceedings of the Royal Society A: Mathematical, Physical and Engineering Sciences.* 1998, vol. 454, no. 1971, pp. 873–884. ISSN 1364-5021. Available from DOI: 10.1098/rspa.1998.0190.

[50]   GAO, Cun-Fa; YU, Jian-Hang. Two-dimensional analysis of a semi-infinite crack in piezoelectric media. *Mechanics Research Communications.* 1998, vol. 25, no. 6, pp. 695–700. ISSN 0093-6413. Available from DOI: 10.1016/S0093-6413(98)00089-5.

[51]   XU, X.-L.; RAJAPAKSE, R.K.N.D. Analytical solution for an arbitrarily oriented void/crack and fracture of piezoceramics. *Acta Materialia.* 1999, vol. 47, no. 6, pp. 1735–1747. ISSN 13596454. Available from DOI: 10.1016/S1359-6454(99)00075-0.

[52]   HUANG, Zhenyu; KUANG, Zhen-Bang. Explicit expression of the A and B matrices for piezoelectric media. *Mechanics Research Communications.* 2000, vol. 27, no. 5, pp. 575–581. ISSN 0093-6413. Available from DOI: 10.1016/S0093-6413(00)00132-4.

[53]   CHUE, Ching-Hwei; CHEN, Chung-De. Decoupled formulation of piezoelectric elasticity under generalized plane deformation and its application to wedge problems. *International Journal of Solids and Structures.* 2002, vol. 39, no. 12, pp. 3131–3158. ISSN 0020-7683. Available from DOI: 10.1016/S0020-7683(02)00247-0.

[54]   OWEN, D.R.J.; FAWKES, A.J. *Engineering Fracture Mechanics: Numerical Methods and Applications.* Swansea: Pineridge Press Ltd, 1983.

[55]   HILTON, P.D.; SIH, G.C. Applications of the finite element method to the cal- culations of stress intensity factors. In: *Mechanics of Fracture - Methods of analysis and solutions of crack problems.* Leyden: Noordhoff International Publishing, 1973, pp. 426–477.

[56]   KLUSÁK, Jan; PROFANT, Tomáš; KOTOUL, Michal. Study of the Stress Distribution Around an Orthotropic Bi-Material Notch Tip. *Key Engineering Materials.* 2009, vol. 417-418, pp. 385–388. ISSN 1662-9795. Available from DOI: 10.4028/www.scientific.net/KEM.417-418.385.

[57] CHOI, S.T.; SHIN, H.; EARMME, Y.Y. On the unified approach to anisotropic and isotropic elasticity for singularity, interface and crack in dissimilar media. *International Journal of Solids and Structures*. 2003, vol. 40, no. 6, pp. 1411–1431. ISSN 00207683. Available from DOI: `10.1016/S0020-7683(02)00671-6`.

[58] HWU, Chyanbin; OMIYA, Masaki; KISHIMOTO, Kikuo. A Key matrix N for the Stress Singularity of the Anisotropic Elastic Composite Wedges. *JSME International Journal*. 2003, vol. 46, no. 1, pp. 40–50.

[59] HWU, Chyanbin; KUO, T.L. A unified definition for stress intensity factors of interface corners and cracks. *International Journal of Solids and Structures*. 2007, vol. 44, no. 18-19, pp. 6340–6359. ISSN 00207683. Available from DOI: `10.1016/j.ijsolstr.2007.02.031`.

[60] HWU, Chyanbin. Correspondence realations betweem amisotropic and isotropic elasticity. *The Chines Journal of Mechanics*. 1996, vol. 12, no. 4, pp. 483–493.

[61] TING, T.C.T. Generalized Dundurs constants for anisotropic bimaterials. *International Journal of Solids and Structures*. 1995, vol. 32, no. 3-4, pp. 483–500. ISSN 0020-7683. Available from DOI: `10.1016/0020-7683(94)00113-B`.

[62] TING, T.C.T. A modified Lekhnitskii formalism à la Stroh for anisotropic elasticity and classifications of the 6×6 matrix N. *Proceedings of the Royal Society of London*. 1999, vol. 455, no. 1981, pp. 69–89. ISSN 1364-5021. Available from DOI: `10.1098/rspa.1999.0303`.

[63] ESHELBY, J.D.; READ, W.T.; SHOCKLEY, W. Anisotropic elasticity with applications to dislocation theory. *Acta Metallurgica*. 1953. ISBN 0001-6160. ISSN 00016160. Available from DOI: `10.1016/0001-6160(53)90099-6`.

[64] SOSA, H.; CASTRO, M. On concentrated loads at the boundary of a piezoelectric half-plane. *Journal of the Mechanics and Physics of Solids*. 1994, vol. 42, no. 7, pp. 1105–1122. ISSN 00225096. Available from DOI: `10.1016/0022-5096(94)90062-0`.

[65] DEVONSHIRE, A.F. Theory of ferroelectrics. *Advances in Physics*. 1954, vol. 3, no. 10, pp. 85–130. Available from DOI: `10.1080/00018739400101505`.

[66] FANG, Dai-ning; LIU, Jin-xi. *Fracture Mechanics of Piezoelectric and Ferroelectric Solids*. Beijing: Tsinghua University Press, 2013. ISBN 978-3-642-30087-5.

[67] DINEVA, P.; GROSS, D.; MÜLLER, R.; RANGELOV, T. *Dynamic Fracture of Piezoelectric Materials, Solutions of Time-Harmonic Problems via BIEM*. 212th ed. New York: Springer, 2014. ISBN 978-3-319-03961-9. Available from DOI: `10.1007/978-3-319-03961-9`.

[68] FORSBERGH, P.W. Piezoelectricity, Electrostriction and Ferroelectricity. In: *Encyclopedia of Physics*. 16th ed. Berlin: Springer, 1956, p. 405. ISBN 978-3-642-4.

[69] MILNE, I.; RITCHIE, R.O.; KARIHALOO, B. *Comprehensive Structural Integrity: Fracture of Materials from Nano to Macro*. Elsevier Science, 2003. ISBN 0-08-043749-4.

[70] QIN, Qing-Hua. *Advanced Mechanics of Piezoelectricity*. Beijing: Higher Education Press, 2013. ISBN 978-7-04-034497- 4.

[71] BALMES, E.; DERAEMAEKER, A. *Modeling structures with piezoelectric materials, Theory and STD Tutorial*. Paris: SDTools, 2001. Available also from: `http://www.sdtools.com`.

[72] TIERSEN, H.F. *Linear Piezoelectric Plate Vibrations*. 1st. New York: Plenum Press, 1969. ISBN 978-1-4899-6453-3.

[73] YANG, J. *Special Topics in the Theory of Piezoelectricity.* New York: Springer Science+Business Media, 2009. ISBN 978-0-387-89497-3. Available from DOI: `10.1007/978-0-387-89498-0`.

[74] ROGACHEVA, N.N. *The Theory of Piezoelectric Shells and Plates.* Boca Raton: CRC Press, 1994.

[75] SAHA, G.C.; KALAMKAROV, A.L.; GEORGIADES, A.V. Micromechanical analysis of effective piezoelastic properties of smart composite sandwich shells made of generally orthotropic materials. *Smart Materials and Structures.* 2007, vol. 16, no. 3, pp. 866–883. ISSN 09641726. Available from DOI: `10.1088/0964-1726/16/3/037`.

[76] NYE, J.F. *Physical Propeties of Crystals, They Representation by Tensors and Matrices.* Oxford: Oxford University Press, 1985. ISBN 0-19-851165-5.

[77] BARNETT, D.M.; LOTHE, J. Dislocation and line charges in anisotropic piezoelectric insulators. *Physical Status Solidi (b).* 1975, vol. 67, pp. 105–111. Available from DOI: `10.1002/pssb.2220670108`.

[78] PAK, Y.E. Crack Extension Force in a Piezoelectric Material. *Journal of Applied Mechanics.* 1990, vol. 57, no. 3, pp. 647. ISBN 0021-8936. ISSN 00218936. Available from DOI: `10.1115/1.2897071`.

[79] KUO, C.M.; BARNETT, D.M. Stress Singularities of Interfacial Cracks in Bonded Piezoelectric Half-Spaces. In: WU, J.J.; TING, T.C.T.; BARNETT, D.M. (eds.). *Modern Theory of Anisotropic Elasticity and Applications.* Philadelphia: Siam, 1991, pp. 33–50. ISBN 0-89871-289-0.

[80] LIANG, Y.C.; HWU, Chyanbin. Electromechanical analysis of defects in piezoelectric materials. *Smart Materials and Structures.* 1996, vol. 5, no. 3, pp. 314–320. ISSN 09641726. Available from DOI: `10.1088/0964-1726/5/3/009`.

[81] CHUNG, M.Y.; TING, T.C.T. Piezoelectric solid with an elliptic inclusion or hole. *International Journal of Solids and Structures.* 1996, vol. 33, no. 23, pp. 3343–3361. ISSN 00207683. Available from DOI: `10.1016/0020-7683(95)00189-1`.

[82] OU, Z.C.; CHEN, Y.H. Explicit expressions of eigenvalues and eigenvectors for transversely isotropic piezoelectric materials. *Acta Mechanica.* 2003, vol. 162, no. 1-4, pp. 213–219. ISSN 00015970. Available from DOI: `10.1007/s00707-002-1010-1`.

[83] HWU, Chyanbin; KUO, T.L. Interface Cracks/Corners in Anisotropic/Piezoelectric materials. *3rd International Conference on Integrity, Reliability and Failure, Porto/Portugal 20-24 July 2009.* 2009, no. July, pp. 20–24.

[84] HWU, Chyanbin. A Unified Definition of Stress Intensity Factors for Cracks/Corners/Interface Cracks/Interface Corners in Anisotropic/Piezoelectric/Viscoelastic Materials. *Procedia Materials Science.* 2014, vol. 3, pp. 257–263. ISSN 22118128. Available from DOI: `10.1016/j.mspro.2014.06.045`.

[85] XU, X.-L.; RAJAPAKSE, R.K.N.D. On singularities in composite piezoelectric wedges and junctions. *International Journal of Solids and Structures.* 2000, vol. 37, no. 23, pp. 3253–3275. ISSN 00207683. Available from DOI: `10.1016/S0020-7683(99)00143-2`.

[86] CHEN, Chung-De. On the singularities of the thermo-electro-elastic fields near the apex of a piezoelectric bonded wedge. *International Journal of Solids and Structures.* 2006, vol. 43, no. 5, pp. 957–981. ISSN 0020-7683. Available from DOI: `10.1016/J.IJSOLSTR.2005.03.011`.

[87] XU, C.H.; ZHOU, Z.H.; XU, X.S.; LEUNG, A.Y.T. Electroelastic singularities and intensity factors for an interface crack in piezoelectric-elastic bimaterials. *Applied Mathematical Modelling*. 2015, vol. 39, no. 9, pp. 2721–2739. ISSN 0307904X. Available from DOI: `10.1016/j.apm.2014.10.061`.

[88] SASAKI, Toru; KONDO, Toshimi; TANE, Takeshi. Analogy of Stress Singularities Analysis between Piezoelectric Materials and Anisotropic Materials. *Procedia Materials Science*. 2014, vol. 3, pp. 1767–1772. ISSN 2211-8128. Available from DOI: `10.1016/J.MSPRO.2014.06.285`.

[89] KAH SOH, Ai; LIU, Jin-xi; FANG, Dai-ning. Explicit expressions of the generalized Barnett–Lothe tensors for anisotropic piezoelectric materials. *International Journal of Engineering Science*. 2001, vol. 39, no. 16, pp. 1803–1814. ISSN 00207225. Available from DOI: `10.1016/S0020-7225(01)00018-0`.

[90] LIOU, J.Y.; SUNG, J.C. On the generalized Barnett–Lothe tensors for monoclinic piezoelectric materials. *International Journal of Solids and Structures*. 2007, vol. 44, no. 16, pp. 5208–5221. ISSN 00207683. Available from DOI: `10.1016/j.ijsolstr.2006.12.031`.

[91] ZHAO, M.H.; SHEN, Y.P.; LIU, Y.J.; LIU, G.N. Isolated crack in three-dimensional piezoelectric solid. Part II: Stress intensity factors for circular crack. *Theoretical and Applied Fracture Mechanics*. 1997, vol. 26, no. 2, pp. 141–149. ISSN 01678442. Available from DOI: `10.1016/S0167-8442(96)00042-0`.

[92] KUNA, Meinhard. Fracture mechanics of piezoelectric materials – Where are we right now? *Engineering Fracture Mechanics*. 2010, vol. 77, no. 2, pp. 309–326. ISSN 0013-7944. Available from DOI: `10.1016/J.ENGFRACMECH.2009.03.016`.

[93] CAO, Changyong; YU, Aibing; QIN, Qing-hua. A new hybrid finite element approach for plane piezoelectricity with defects. 2013, vol. 61, pp. 41–61. Available from DOI: `10.1007/s00707-012-0741-x`.

[94] BREBIA, C.A. *The Boundary Element Method for Engineers*. 2nd. Plymouth: Pentech Press, 1984. ISBN 0-7273-0205-1.

[95] LI, Chao; MAN, Hou; SONG, Chongmin; GAO, Wei. Analysis of cracks and notches in piezoelectric composites using scaled boundary finite element method. *Composite Structures*. 2013, vol. 101, pp. 191–203. ISSN 02638223. Available from DOI: `10.1016/j.compstruct.2013.02.009`.

[96] QIN, Qing-Hua; YU, Shou-Wen. An arbitrarily-oriented plane crack terminating at the interface between dissimilar piezoelectric materials. *International Journal of Solids and Structures*. 1997, vol. 34, no. 5, pp. 581–590. ISSN 00207683. Available from DOI: `10.1016/S0020-7683(96)00040-6`.

[97] TIAN, Wen-Ye; CHEN, Yi-Heng. Interaction between an interface crack and subinterface microcracks in metal/piezoelectric bimaterials. *International Journal of Solids and Structures*. 2000, vol. 37, no. 52, pp. 7743–7757. ISSN 0020-7683. Available from DOI: `10.1016/S0020-7683(00)00110-4`.

[98] OU, Z.C.; CHEN, Y.H. Interface crack-tip generalized stress field and stress intensity factors in transversely isotropic piezoelectric bimaterials. *Mechanics Research Communications*. 2004, vol. 31, no. 4, pp. 421–428. ISSN 0093-6413. Available from DOI: `10.1016/J.MECHRESCOM.2003.08.004`.

[99] OU, Zhuo Cheng; CHEN, Yi Heng. Interface crack problem in elastic dielectric/piezoelectric bimaterials. *International Journal of Fracture*. 2004, vol. 130, no. 1, pp. 427–454. ISSN 03769429. Available from DOI: `10.1023/B:FRAC.0000049502.54417.1c`.

[100] SLÁDEK, J.; SLÁDEK, V.; WÜNSCHE, M.; ZHANG, Ch. Analysis of an interface crack between two dissimilar piezoelectric solids. *Engineering Fracture Mechanics*. 2012, vol. 89, pp. 114–127. ISSN 0013-7944. Available from DOI: `10.1016/J.ENGFRACMECH.2012.04.032`.

[101] LEUGERING, G.; NAZAROV, S.A. The Eshelby Theorem and its Variants for Piezoelectric Media. 2015, vol. 215, pp. 707–739.

[102] HWU, C.; TING, T.C.T. Solutions for the anisotropic elastic wedge at critical wedge angles. *Journal of Elasticity*. 1990, vol. 24, no. 1-3, pp. 1–20.

[103] TING, T.C.T. Recent developments in anisotropic elasticity. *International Journal of Solids and Structures*. 2000, vol. 37, no. 1-2, pp. 401–409. ISSN 00207683. Available from DOI: `10.1016/S0020-7683(99)00102-X`.

[104] LEE, V.-G. The extension of stroh formalism to three-dimensional anisotropic elasticity. *Journal of Mechanics*. 2003, vol. 19, no. 1, pp. 61–68.

[105] BARROSO, A.; MANTIČ, V.; PARÍS, F. Singularity parameter determination in adhesively bonded lap joints for use in failure criteria. *Composites Science and Technology*. 2008, vol. 68, no. 13, pp. 2671–2677. ISSN 02663538. Available from DOI: `10.1016/j.compscitech.2008.04.035`.

[106] BARROSO, A.; MANTIČ, V.; PARÍS, F. Computing stress singularities in transversely isotropic multimaterial corners by means of explicit expressions of the orthonormalized Stroh-eigenvectors. *Engineering Fracture Mechanics*. 2009, vol. 76, no. 2, pp. 250–268. ISSN 00137944. Available from DOI: `10.1016/j.engfracmech.2008.10.006`.

[107] CHEN, C.-H.; HSU, J. The stress intensity factors of regularly perturbed-interface cracks of anisotropic bimaterials. *International Journal of Solids and Structures*. 1997, vol. 34, no. 10, pp. 1235–1253. ISSN 00207683.

[108] CHOI, S.T.; EARMME, Y.Y. Elastic study on singularities interacting with interfaces using alternating technique. *International Journal of Solids and Structures*. 2002, vol. 39, no. 5, pp. 1199–1211. ISSN 00207683. Available from DOI: `10.1016/S0020-7683(01)00231-1`.

[109] DUNDURS, J. Discussion: Edge-Bonded Dissimilar Orthogonal Elastic Wedges Under Normal and Shear Loading. *Journal of Applied Mechanics*. 1969. ISBN 9781607614289. ISSN 00218936. Available from DOI: `10.1115/1.3564739`.

[110] DESMORAT, R.; LECKIE, F.A. Singularities in bi-materials: parametric study of an isotropic/anisotropic joint. *European Journal of Mechanics - A/Solids*. 1998, vol. 17, no. 1, pp. 33–52. ISSN 09977538. Available from DOI: `10.1016/S0997-7538(98)80062-4`.

[111] TING, T.C.T.; CHOU, S.C. Edge Singularities in Anisotropic Composites. *Int. J. Solids Structures*. 1981, vol. 17, no. 11, pp. 1057–1068.

[112] ŠEVEČEK, Oldřich. *Solution of general stress concentrators in anisotropic media by combination of FEM and the complex potential theory*. 2009. Doctoral thesis. Brno University of Technology.

[113] PAPADAKIS, Panagiotis J.; BABUSKA, Ivo. A numerical procedure for the determination of certain quantities related to the stress intensity factors in two-dimensional elasticity. *Computer Methods in Applied Mechanics and Engineering*. 1995, vol. 122, no. 1-2, pp. 69–92. ISSN 0045-7825. Available from DOI: `10.1016/0045-7825(94)00748-C`.

[114] KIUSALAAS, Jaan. *Numerical Methods in Engineering with Python 3*. New York: Cambridge University Press, 2013. ISBN 978-1-107-03385-6.

[115] CHEN, Hua-Peng. Stress singularities in anisotropic multi-material wedges and junctions. *International Journal of Solids and Structures*. 1998, vol. 35, no. 11, pp. 1057–1073. ISSN 0020-7683. Available from DOI: `10.1016/S0020-7683(97)00108-X`.

[116] SINCLAIR, G.B.; OKAJIMA, M.; GRIFFIN, J.H. Path independent integrals for computing stress intensity factors at sharp notches in elastic plates. *International Journal for Numerical Methods in Engineering*. 1984, vol. 20, no. 6, pp. 999–1008. ISSN 10970207. Available from DOI: `10.1002/nme.1620200603`.

[117] VU-QUOC, Loc; TRAN, Van Xuan. Singularity analysis and fracture energy-release rate for composites: Piecewise homogeneous-anisotropic materials. *Computer Methods in Applied Mechanics and Engineering*. 2006, vol. 195, no. 37-40, pp. 5162–5197. ISBN 0045-7825. ISSN 00457825. Available from DOI: `10.1016/j.cma.2005.11.009`.

[118] SOKOLNIKOFF, I.S. *Mathematical Theory of Elasticity*. New York: Tata McGraw-Hill, 1956.

[119] RICE, J.R. A Path Independent Integral and the Approximate Analysis of Strain Concentration by Notches and Cracks. *Journal of Applied Mechanics*. 1968, vol. 35, no. 2, pp. 379. ISBN 0021-8936. ISSN 00218936. Available from DOI: `10.1115/1.3601206`.

[120] *ANSYS® Academic Research Mechanical, Release 18.1*.

[121] LEGUILLON, Dominique. Strength or toughness? A criterion for crack onset at a notch. *European Journal of Mechanics - A/Solids*. 2002, vol. 21, no. 1, pp. 61–72. ISSN 09977538. Available from DOI: `10.1016/S0997-7538(01)01184-6`.

[122] KLUSÁK, Jan; HRSTKA, Miroslav; PROFANT, Tomáš; KREPL, Odnřej; ŠEVEČEK, Oldřich; KOTOUL, Michal. The influence of the first non-singular stress terms on crack initiation direction in an orthotropic bi-material plate. *Theoretical and Applied Fracture Mechanics*. 2014, vol. 71, pp. 67–75. ISSN 01678442. Available from DOI: `10.1016/j.tafmec.2014.05.008`.

[123] SHIN, Kum Cheol; KIM, Won Seock; LEE, Jung Ju. Application of stress intensity to design of anisotropic/isotropic bi-materials with a wedge. *International Journal of Solids and Structures*. 2007, vol. 44, no. 24, pp. 7748–7766. ISSN 00207683. Available from DOI: `10.1016/j.ijsolstr.2007.05.014`.

[124] ŠEVEČEK, Oldřich; KOTOUL, Michal; PROFANT, Tomáš. Effect of higher order asymptotic terms on the competition between crack penetration and debond at a bimaterial interface between aligned orthotropic materials. *Engineering Fracture Mechanics*. 2012, vol. 80, pp. 28–51. ISSN 0013-7944. Available from DOI: `10.1016/J.ENGFRACMECH.2011.11.006`.

[125] BARROSO, A.; MANTIČ, V.; PARÍS, F. Singularity analysis of anisotropic multimaterial corners. *International Journal of Fracture*. 2003, vol. 119, no. 1, pp. 1–23.

[126] FAN, Hui. Decay Rates in a Piezoelectric Strip. *International Journal of Engineering Science*. 1995, vol. 33, no. 8, pp. 1095–1103. Available from DOI: `10.1016/0020-7225(94)00126-5`.

[127] ZIKUNG, Wang; BAILIN, Zheng. The general solution of three-dimensional problems in piezoelectric media. *International Journal of Solids and Structures*. 1995, vol. 32, no. 1, pp. 105–115. ISSN 00207683. Available from DOI: `10.1016/0020-7683(94)00101-2`.

[128] CHUE, C.H.; CHEN, C.D. Antiplane stress singularities in a bonded bimaterial piezoelectric wedge. *Archive of Applied Mechanics (Ingenieur Archiv)*. 2003, vol. 72, no. 9, pp. 673–685. ISSN 09391533. Available from DOI: `10.1007/s00419-002-0241-x`.

[129] CHEN, Chung De; CHUE, Ching Hwei. Singular electro-mechanical fields near the apex of a piezoelectric bonded wedge under antiplane shear. *International Journal of Solids and Structures*. 2003, vol. 40, no. 23, pp. 6513–6526. ISSN 0020-7683. Available from DOI: `10.1016/S0020-7683(03)00415-3`.

[130] WANG, B.L.; SUN, Y.G. Out-of-plane interface cracks in dissimilar piezoelectric materials. *Archive of Applied Mechanics*. 2004, vol. 74, no. 1-2, pp. 2–15. ISSN 09391533. Available from DOI: `10.1007/s00419-003-0286-5`.

[131] CHENG, Changzheng; CHENG, Xiang; NIU, Zhongrong; RECHO, Naman. Singularity characteristic analyses for magneto-electro-elastic V-notches. *European Journal of Mechanics - A/Solids*. 2016, vol. 57, pp. 59–70. ISSN 0997-7538. Available from DOI: `10.1016/J.EUROMECHSOL.2015.12.005`.

[132] WANG, Xu; ZHOU, Kun. Twelve-dimensional Stroh-like formalism for Kirchhoff anisotropic piezoelectric thin plates. *International Journal of Engineering Science*. 2013, vol. 71, pp. 111–136. ISSN 00207225. Available from DOI: `10.1016/j.ijengsci.2013.06.004`.

[133] CHEN, Y.I.Heng; HASEBE, Norio. Current understanding on fracture behaviors of ferroelectric/piezoelectric materials. *Journal of Intelligent Material Systems and Structures*. 2005, vol. 16, no. 7-8, pp. 673–687. ISBN 1045-389X. ISSN 1045389X. Available from DOI: `10.1177/1045389X05054330`.

[134] SOH, Ai Kah; FANG, Dai-Ning; LUN LEE, Kwok. Fracture analysis of piezoelectric materials with defects using energy density theory. *International Journal of Solids and Structures*. 2001, vol. 38, no. 46-47, pp. 8331–8344. ISSN 00207683. Available from DOI: `10.1016/S0020-7683(01)00080-4`.

[135] QUN, Li; YIHENG, Chen. Analysis of crack-tip singularities for an interfacial permeable crack in metal/piezoelectric bimaterials. *Acta Mechanica Solida Sinica*. 2007, vol. 20, no. 3, pp. 247–257. ISBN 0894-9166. ISSN 08949166. Available from DOI: `10.1007/s10338-007-0729-6`.

[136] HUANG, C.S.; HU, C.N. Three-dimensional analyses of stress singularities at the vertex of a piezoelectric wedge. *Applied Mathematical Modelling*. 2013, vol. 37, no. 6, pp. 4517–4537. ISSN 0307-904X. Available from DOI: `10.1016/J.APM.2012.09.021`.

[137] WENG, S.-M.; CHUE, C.-H. The stress singularities at the apex of composite piezoelectric junctions. *Archive of Applied Mechanics (Ingenieur Archiv)*. 2004, vol. 73, no. 9-10, pp. 638–649. ISBN 0041900303136. ISSN 0939-1533. Available from DOI: `10.1007/s00419-003-0313-6`.

[138] LANDAU, L.D.; LIFSHITZ, E.M. *Electrodynamics of Continuous Media*. Second. Oxford: Pergamon Press Ltd, 1984. ISBN 0-08-030276-9.

[139] PILGRIM, S.M.; REVATHI, S. Electrostrictive Ceramics for Sonar Projectors. In: *Encyclopedia of Materials: Science and Technology*. 2001, pp. 2738–2743. Available from DOI: `10.1016/b978-0-12-803581-8.01716-1`.

[140] STAKHIN, N.A. Electrostriction in Dielectrics and Metals. *Russian Physics Journal*. 1998, vol. 41, no. 11, pp. 1107–1111.

[141] CHEN, M.C; ZHU, J.J.; SZE, K.Y. Electroelastic singularities in piezoelectric-elastic wedges and junctions. *Engineering Fracture Mechanics*. 2006, vol. 73, no. 7, pp. 855–868. ISSN 00137944. Available from DOI: `10.1016/j.engfracmech.2005.11.004`.

[142] MOTOLA, Yael; BANKS-SILLS, Leslie; FOURMAN, Victor. *International Journal of Fracture*. Vol. 159, On fracture testing of piezoelectric ceramics. 2009. No. 2. ISBN 9723640813. ISSN 03769429. Available from DOI: `10.1007/s10704-009-9392-x`.

[143] KREPL, Ondřej; KLUSÁK, Jan. The influence of non-singular terms on the precision of stress description near a sharp material inclusion tip. *Theoretical and Applied Fracture Mechanics*. 2017, vol. 90, pp. 85–99. ISSN 01678442. Available from DOI: `10.1016/j.tafmec.2017.03.007`.

[144] MAILETT, E. Sur les lignes de décroissance maxima des modules et les équations algébraiques ou transcendantes. *J. de l'Éc.* 1903, vol. 8, pp. 75–95.

[145] REIMERDES, O. *Die Niveau- und Fallinien auf Flächen insbesondere auf Modulflächen analytischer Funktionen*. 1911. Inaugural Dissertation. Christian-Albrechts-Universität zu Kiel.

[146] JAHNKE, E.; EMDE, F. Funktionentafeln mit Formeln und Kurven. *B. G. Teubner*. 1933, vol. 2.

[147] ULLRICH, E. Betragsächen mit ausgezeichnetem Kräummungsverhalten. *Math. Zeitschr.* 1951, vol. 54, pp. 297–328.

[148] WEGERT, Elias. *Visual Complex Functions: An Introduction with Phase Portraits*. Visual complex functions: An introduction with phase portraits. 2012. ISBN 978-3-0348-0180-5. ISSN 1098-6596. Available from DOI: `10.1007/978-3-0348-0180-5_1`.

[149] DAVIS, John E. *Complex Domain Coloring Using Fztopng* [online]. 2017 [visited on 2017-01-01]. Available from: `http://www.jedsoft.org/fun/complex/fztopng.html`.

[150] DAWRIGHT. *Visualizing Complex Functions* [online]. 2010 [visited on 2017-08-23]. Available from: `https://www.codeproject.com/Articles/80641/Visualizing-Complex-Functions`.

Nomenclature

$C_{ij}, \hat{C}_{ij}$	Elastic stiffness, reduced elastic stiffness
C_{ij}^E	Elastic stiffness at constant electric field
$\hat{C}_{ij}^E$	Reduced elastic stiffness at constant electric field for generalized plane strain and short circuit
D_i	Electric displacement
D_i^{appl}	Applied electric displacement
E_i	Electric intensity
H_i	Generalized stress intensity factors
$\mathbf{K}$	Transformation matrix 6×6 describing in-plane rotation
$K_{\mathrm{I}}, K_{\mathrm{II}}, K_{\mathrm{IV}}$	Stress intensity factors
$S_{ij}, \hat{S}_{ij}$	Elastic compliance, reduced elastic compliance
S_{ij}^D	Elastic compliance at constant electric displacement
$\hat{S}_{ij}^D$	Reduced elastic compliance at constant electric displacement for generalized plane strain and short circuit
$\mathbf{T}$	Stress functions
$\mathbf{Z}^\delta$	Complex potentials
a, b	FEM model dimensions
$e_{ij}, d_{ij}, h_{ij}, g_{ij}$	Piezoelectric coefficients
e_{ij}^0	Reduced piezoelectric coefficients
$\mathbf{f}(z)$	Complex function vector
$\hat{g}_{ij}'$	Reduced piezoelectric coefficients
i	Imaginary unit
ℓ	Length parameter
$\mathbf{n}$	Normal vector
q	Electric charge
r, θ	Polar coordinates
r_c	Radius of the integration contour
$\mathbf{T}$	Tractions
$\mathbf{t}^{\mathrm{FEM}}$	Vector of tractions computed by FEM
$\mathbf{A}, \mathbf{L}, \mathbf{B}$	Material matrices
$\mathbf{u}$	Displacements
$\mathbf{u}^{\mathrm{FEM}}$	Vector of displacements computed by FEM
$\mathbf{v}_i, \mathbf{w}_i$	Eigenvectors
x_i	Cartesian coordinates
z	Complex variable
$\boldsymbol{\Omega}$	Transformation matrix 3×3 describing in-plane rotation

$\Psi\left(\mathbf{u},\hat{\mathbf{u}}\right)$	Ψ-integral
α_1,α_2	Fibre orientations or poling directions
β_{ij}^σ	Dielectric non-permittivity at constant stress
$\hat{\beta}_{ij}^{\prime\sigma}$	Reduced dielectric non-permittivity at constant stress for generalized plane strain and short circuit
δ_i	Singularity exponent
ε	Oscillatory index
ε_{ij}	Strain tensor
$\boldsymbol{\eta}_i$	Shape function vector for displacements
φ,ψ,ξ	Lekhnitskii's stress functions
κ	Non-oscillatory index
λ,μ	Lamé constants
$\boldsymbol{\lambda}_i$	Shape function vector for stresses
μ_i	Material eigenvalues
ν	Poisson's ratio
$\nu_{LT},\nu_{TT'}$	Poisson's ratio in the principal material directions L,T,T'
ω_1,ω_2	Notch face angles
ω_{ij}^ε	Dielectric permittivity at constant strain
$\hat{\omega}_{ij}^{\prime\varepsilon}$	Reduced dielectric permittivity at constant strain for generalized plane strain and short circuit
ϕ	Electric potential
σ_{ij}	Stress tensor
$\sigma_{ij}^{\mathrm{appl}}$	Applied stress
FEM	Finite element method
GSIF	Generalized stress intensity factor
GSSC	Generalized stress singular concentrator
LES	Lekhnitskii-Eshelby-Stroh formalism
SEDF	Strain energy density factor

A HSV algorithm for visualizing a complex function

One of the crucial tasks in problems of bi-material notches is finding of the roots δ_i of the transcendental function (5.36). When the roots are real numbers, a root finding algorithm can be constructed easily, e.g. by using the Newton's method [114]. But there are special cases, such as orthotropic interface cracks [110] or isotropic interface corners studied in [143], which have complex-valued roots. In such cases, it is suitable to depict the transcendental function in order to quantify the roots visually. Additionally, the initial guess for the Python global search algorithm `findroot` can be set more precisely.

The problem of depicting a complex function lies in its definition. Several methods were introduced in [144, 145, 146, 147] and their subsequent research work, such as analytic landscape depicting.

The complex function is described by its modulus $|f(z)|$ and argument $\arg f(z)$ (in the literature also known as a phase). The modulus $|f(z)|$ and the argument $\arg f(z)$ can be described by one-colour surface and certain colour space, respectively. The way, how both descriptions can be displayed in one 2D graph, explains the following appendix via the so-called HSV algorithm.

A.1 Domain colouring

For purposes of the present study, the HSV method for depicting a complex function was developed [148], which is based on recomputing a complex number to hue (H), saturation (S) and value (V). A complex function $f(z) : \mathbb{C} \to \mathbb{C}$ lives in four real dimensions, which brings about difficulties in depicting such a structure, because a human imagination is used to perceive only in a 3D space.

It is suitable to express a complex number z in the eulerian form, i.e.

$$z = x_1 + ix_2 = |z|\,\mathrm{e}^{i\varphi}, \tag{A.1}$$

where x_1, x_2 are Cartesian coordinates, $|z|$ is called the module and φ the phase. They can be encoded to a HSV colour space.

A HSV colour model is a cylindrical-coordinate representation of a standard RGB colour model. In the literature, there are many relations how to recalculate a module and a phase to hue, saturation and value, such as [149, 150] by using logarithmic or goniometric functions.

A complex number in the eulerian form A.1 is recalculated to hue H, saturation S and value V by the following prescription:

$$H = \left(\frac{\varphi}{2\pi} + 1\right) \bmod 1, \tag{A.2a}$$

$$S = \mathrm{const} \tag{A.2b}$$

$$V = 1 - \frac{1}{1 + |z|}. \tag{A.2c}$$

Then, hue represents a colour and value a brightness (opacity of the black colour). Saturation defines a colour intensity with respect to an individual character of the studied function. It holds for hue and value that $H \in \langle 0,2\pi \rangle$ and $V \in \langle 0,1 \rangle$. The function A.2c represents a morphism (or a mapping function) that transforms the absolute value of z to the interval $\langle 0,1 \rangle$. Its development is depicted in Fig. A.2. Data for the phase plot are obtained by transforming the HSV colour model to the RGB colour model by using the Python library `hsv_to_rgb`.
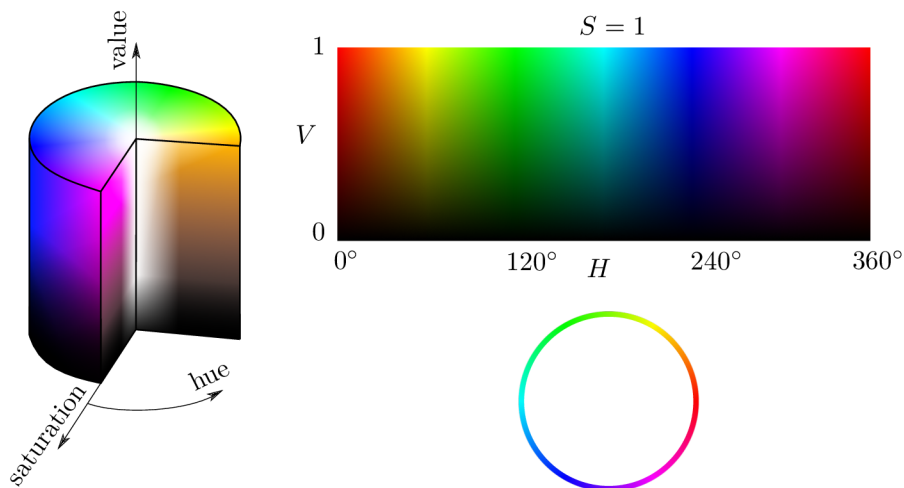
Fig. A.1: Cut-away 3D model of the HSV colour space. On the right there is a circumferential cut by $S = 1$ and below the unit circle.

A.2 Phase portrait

Many common functions can be depicted by using the above described procedure. However, fracture mechanics of singular stress concentrators, especially piezoelectric bi-material notches, deals with numbers of various orders, which brings about difficulties with the value V. For example, the elements of the compliance matrix (see Eq. (4.107a)) are in the order of 10^{-11} MPa. In the denominator of A.2c, there is a summation of 1 and a lower order number $|z|$, which causes problem for the floating point arithmetic. Substitution of sufficiently small $|z|$ into (A.2c) leads to 1. The contribution of the small number is lost and value V equals to 0. The phase plot is then destroyed by black colour ($V \cong 0$, as can be seen in Fig. A.3).

For root identification purposes, we can forget about the modulus completely and depict only the phase encoded to the hue. The lost information still makes possible to identify root of the investigated functions. Let us illustrate it on an example adopted from [148]. The phase portrait of a complex function

$$f(z) = \frac{z - 1}{z^2 + z + 1} \tag{A.3}$$

is depicted in Fig. A.4. Hue remains defined by (A.2a), saturation and value were set to $S = 1$ and $V = 1$.

A.3 Zero and pole identification

Three exceptional points where all colours come together are highlighted in Fig. A.4. These points are characterised as zeros, $f(z) = 0$, and poles, $f(z) = \infty$. Zeros and poles can be distinguished by ordering of colours in their neighbourhood. If we travel on a circle in the vicinity of the point in the clockwise direction, then a zero has the same orientation (same colour ordering) as on the unit circle (see Fig. A.1), a pole has a reversed orientation. The order of a zero or a pole can be determined as a number of isochromatic rays of one arbitrarily chosen colour, which goes to that point. Then, the phase φ rotates with n-times at the point z if the function $f(z)$ has a power n as follows from the eulerian form (A.1). With this knowledge we can then say that the points 1 and 2 are poles of order one and the point 3 is a zero also of order one [148].
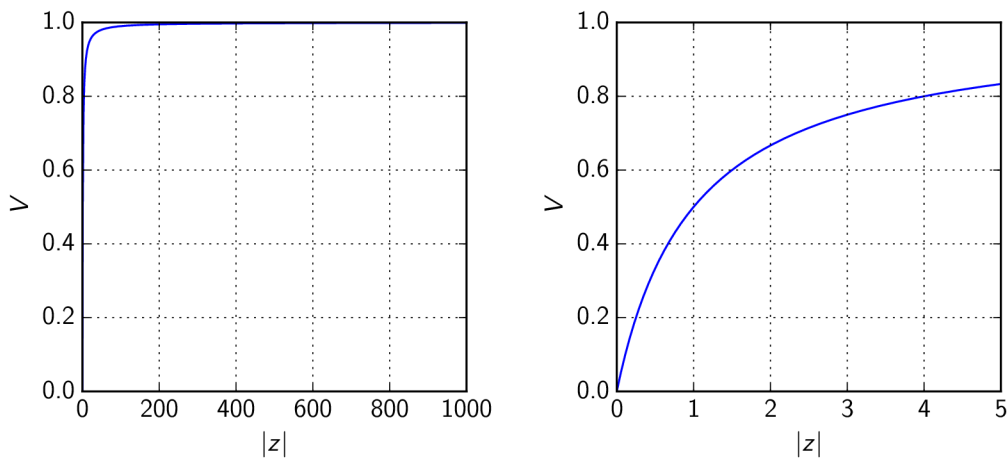
Fig. A.2: Mapping function A.2c in the range $|z| \in (0,10^3)$ (left) and zoomed in for $|z| \in (0,5)$ (right).
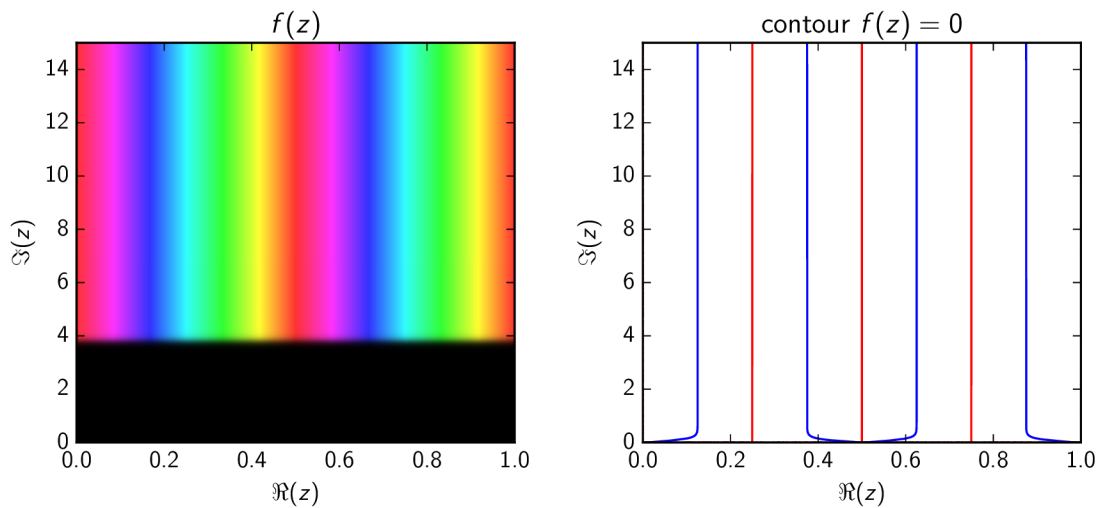

Fig. A.3: Phase plot of the determinant (5.22) by using the mapping function A.2c. The reduction (B.6) causes destruction of the whole domain by black colour.
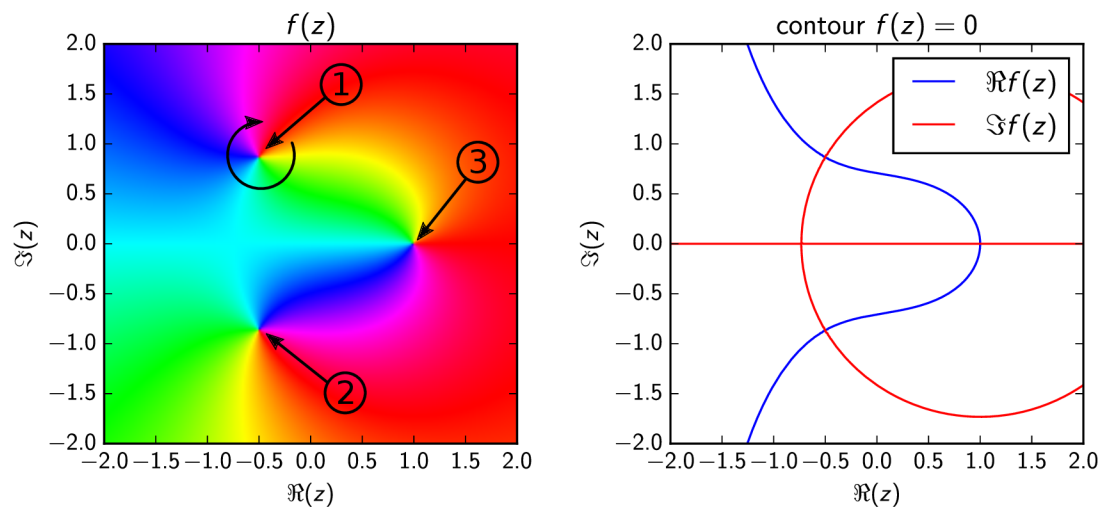
Fig. A.4: The HSV phase portrait of the complex function $f(z) = (z - 1)/(z^2 + z + 1)$ and the contour plot for $f(z) = 0$. The intersection of the blue and red line identifies the zeros or poles.

B Reduction of the linear equation system

The system (5.22) can be reduced to a system of two equations by using the following algebraic operations. If the first row of (5.22) is multiplied by inverse of $\overline{\mathbf{X}}_1^{\mathrm{I}}$ from the left, we get

$$\left(\overline{\mathbf{X}}_1^{\mathrm{I}}\right)^{-1}\mathbf{X}_1^{\mathrm{I}}\mathbf{L}^{\mathrm{I}}\mathbf{v}^{\mathrm{I}} + \overline{\mathbf{L}}^{\mathrm{I}}\mathbf{w}^{\mathrm{I}} = \mathbf{Y}_1^{\mathrm{I}}\mathbf{L}^{\mathrm{I}}\mathbf{v}^{\mathrm{I}} + \overline{\mathbf{L}}^{\mathrm{I}}\mathbf{w}^{\mathrm{I}} = \mathbf{0}. \tag{B.1a}$$

An analogous equation can be obtained from the second row of (5.22):

$$\left(\overline{\mathbf{X}}_2^{\mathrm{II}}\right)^{-1}\mathbf{X}_2^{\mathrm{II}}\mathbf{L}^{\mathrm{I}}\mathbf{v}^{\mathrm{II}} + \overline{\mathbf{L}}^{\mathrm{II}}\mathbf{w}^{\mathrm{II}} = \mathbf{Y}_2^{\mathrm{II}}\mathbf{L}^{\mathrm{II}}\mathbf{v}^{\mathrm{II}} + \overline{\mathbf{L}}^{\mathrm{II}}\mathbf{w}^{\mathrm{II}} = \mathbf{0}. \tag{B.1b}$$

The combination of the relations (B.1a) and (B.1b) leads to the relations between eigenvectors $\mathbf{v}$ and $\mathbf{w}$, which

$$\overline{\mathbf{L}}^{\mathrm{I}}\mathbf{w}^{\mathrm{I}} = -\mathbf{Y}_1^{\mathrm{I}}\mathbf{L}^{\mathrm{I}}\mathbf{v}^{\mathrm{I}}, \tag{B.2a}$$

$$\overline{\mathbf{L}}^{\mathrm{II}}\mathbf{w}^{\mathrm{II}} = -\mathbf{Y}_2^{\mathrm{II}}\mathbf{L}^{\mathrm{II}}\mathbf{v}^{\mathrm{II}}. \tag{B.2b}$$

By substituting (B.2) to the third row of (5.22), one gets:

$$\begin{aligned}
\mathbf{B}_0^{\mathrm{I}}\mathbf{L}^{\mathrm{I}}\mathbf{v}^{\mathrm{I}} + \overline{\mathbf{B}}_0^{\mathrm{I}}\mathbf{Y}_1^{\mathrm{I}}\mathbf{L}^{\mathrm{I}}\mathbf{v}^{\mathrm{I}} - \mathbf{B}_0^{\mathrm{II}}\mathbf{L}^{\mathrm{II}}\mathbf{v}^{\mathrm{II}} - \overline{\mathbf{B}}_0^{\mathrm{II}}\mathbf{Y}_2^{\mathrm{II}}\mathbf{L}^{\mathrm{II}}\mathbf{v}^{\mathrm{II}} = \\
= \left(\mathbf{B}_0^{\mathrm{I}} + \overline{\mathbf{B}}_0^{\mathrm{I}}\mathbf{Y}_1^{\mathrm{I}}\right)\mathbf{L}^{\mathrm{I}}\mathbf{v}^{\mathrm{I}} - \left(\mathbf{B}_0^{\mathrm{II}} + \overline{\mathbf{B}}_0^{\mathrm{II}}\mathbf{Y}_2^{\mathrm{II}}\right)\mathbf{L}^{\mathrm{II}}\mathbf{v}^{\mathrm{II}} = \mathbf{0}.
\end{aligned} \tag{B.3}$$

From the fourth row of (5.22) we get:

$$\begin{aligned}
\mathbf{L}^{\mathrm{I}}\mathbf{v}^{\mathrm{I}} + \overline{\mathbf{L}}^{\mathrm{I}}\mathbf{w}^{\mathrm{I}} - \mathbf{L}^{\mathrm{II}}\mathbf{v}^{\mathrm{II}} - \overline{\mathbf{L}}^{\mathrm{II}}\mathbf{w}^{\mathrm{II}} = \\
= \mathbf{L}^{\mathrm{I}}\mathbf{v}^{\mathrm{I}} - \mathbf{Y}_1^{\mathrm{I}}\mathbf{L}^{\mathrm{I}}\mathbf{v}^{\mathrm{I}} - \mathbf{L}^{\mathrm{II}}\mathbf{v}^{\mathrm{II}} + \mathbf{Y}_2^{\mathrm{II}}\mathbf{L}^{\mathrm{II}}\mathbf{v}^{\mathrm{II}} = \\
= \left(\mathbf{I} - \mathbf{Y}_1^{\mathrm{I}}\right)\mathbf{L}^{\mathrm{I}}\mathbf{v}^{\mathrm{I}} - \left(\mathbf{I} - \mathbf{Y}_2^{\mathrm{II}}\right)\mathbf{L}^{\mathrm{II}}\mathbf{v}^{\mathrm{II}} = \mathbf{0},
\end{aligned} \tag{B.4}$$

from which we express the following relation:

$$\mathbf{L}^{\mathrm{II}}\mathbf{v}^{\mathrm{II}} = \left(\mathbf{I} - \mathbf{Y}_2^{\mathrm{II}}\right)^{-1}\left(\mathbf{I} - \mathbf{Y}_1^{\mathrm{I}}\right)\mathbf{L}^{\mathrm{I}}\mathbf{v}^{\mathrm{I}}. \tag{B.5}$$

Substituting (B.5) into (B.3), the resulting reduced system of two equations is obtained:

$$\left[\mathbf{B}_0^{\mathrm{I}} + \overline{\mathbf{B}}_0^{\mathrm{I}}\mathbf{Y}_1^{\mathrm{I}} - \left(\mathbf{B}_0^{\mathrm{II}} + \overline{\mathbf{B}}_0^{\mathrm{II}}\mathbf{Y}_2^{\mathrm{II}}\right)\left(\mathbf{I} - \mathbf{Y}_2^{\mathrm{II}}\right)^{-1}\left(\mathbf{I} - \mathbf{Y}_1^{\mathrm{I}}\right)\right]\mathbf{L}^{\mathrm{I}}\mathbf{v}^{\mathrm{I}} = \mathbf{0}. \tag{B.6}$$

C Additional results for a transversally isotropic bi-material notch
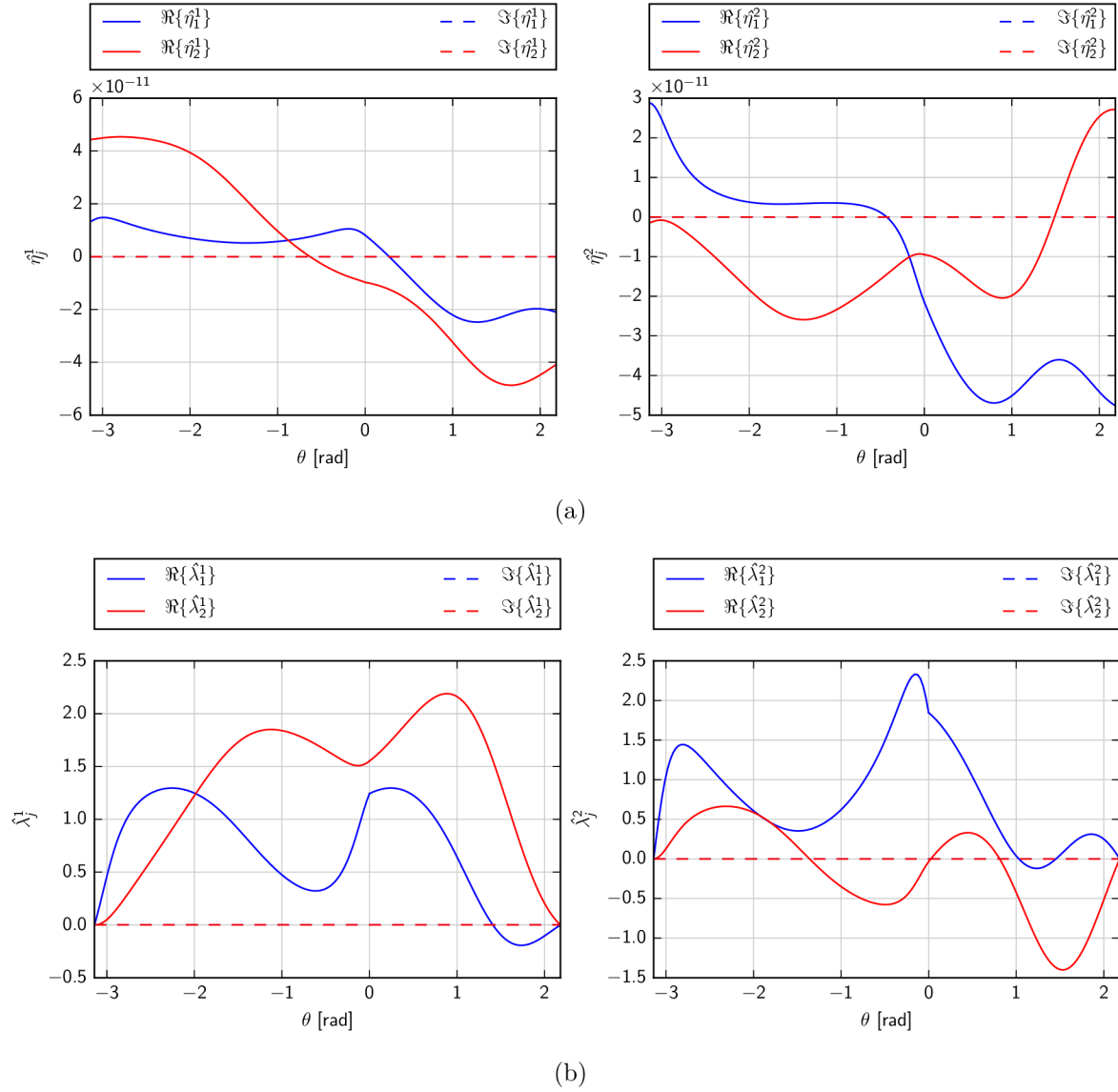
C.1 Auxiliary shape functions

(a)

(b)

Fig. C.1: Components of the auxiliary shape function vectors (a) $\hat{\boldsymbol{\eta}}_1$, $\hat{\boldsymbol{\eta}}_2$ and (b) $\hat{\boldsymbol{\lambda}}_1$, $\hat{\boldsymbol{\lambda}}_2$ for a bi-material notch $\omega_1 = 125°$, $\omega_2 = -180°$ (materials are defined in Tab. 5.1).
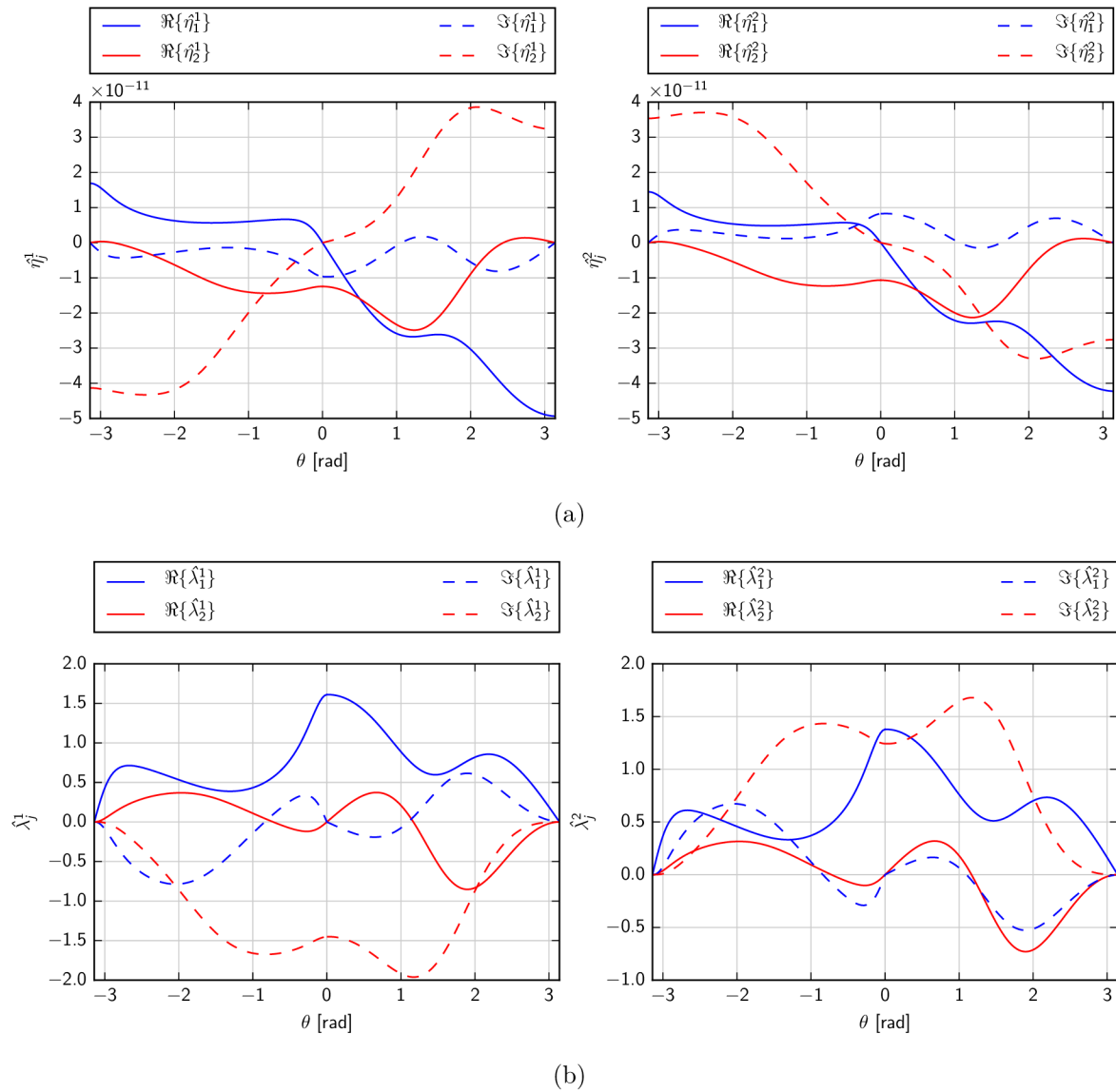
(a)

(b)

Fig. C.2: Components of the auxiliary shape function vectors (a) $\hat{\boldsymbol{\eta}}_1$, $\hat{\boldsymbol{\eta}}_2$ and (b) $\hat{\boldsymbol{\lambda}}_1$, $\hat{\boldsymbol{\lambda}}_2$ for an interface crack $\omega_1 = 180°$, $\omega_2 = -180°$ (materials are defined in Tab. 5.1).

C.2 Displacement and stress development with imaginary parts depicted
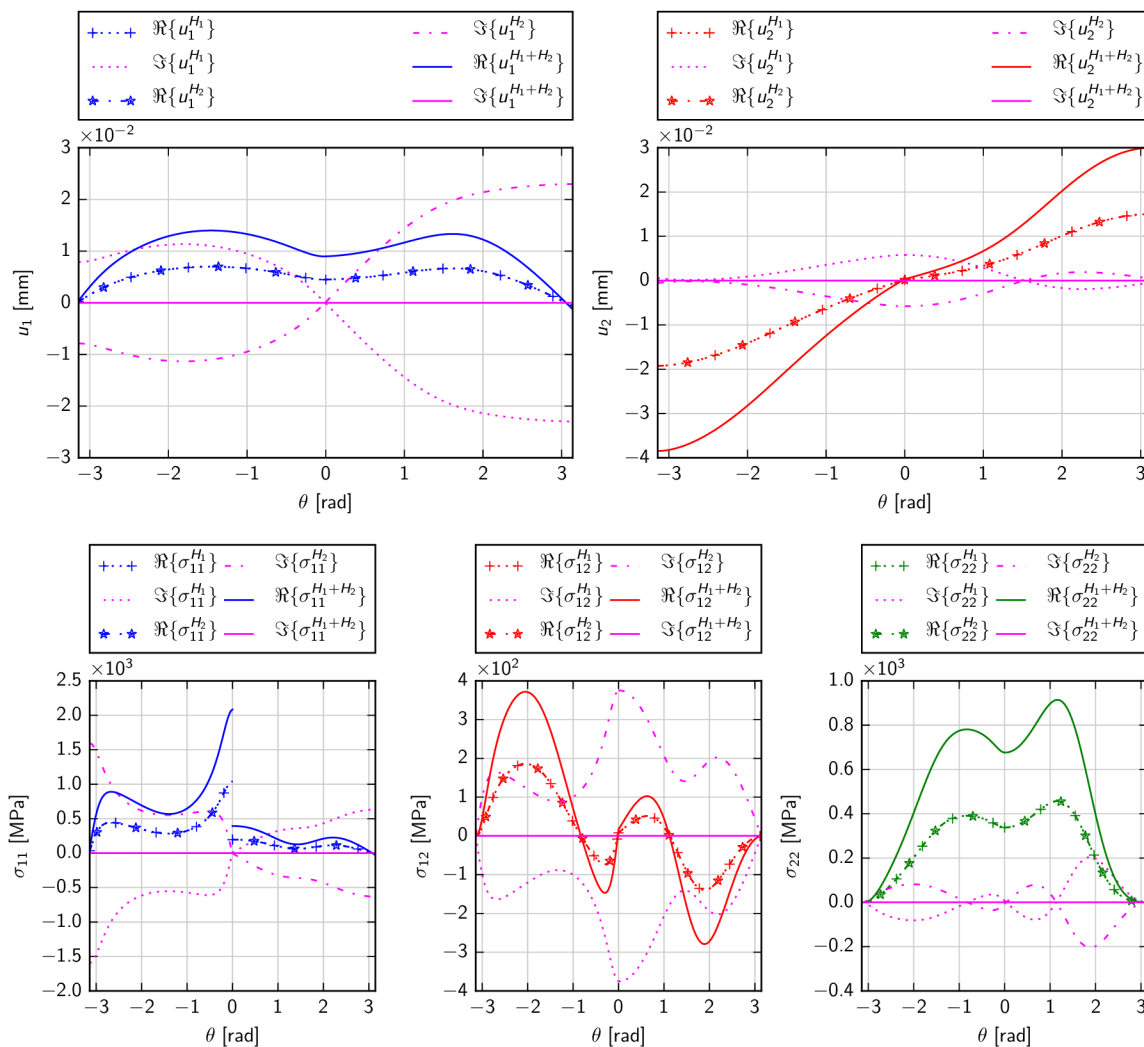
Fig. C.3: Real and imaginary parts of displacement and stress components evaluated on the circular path with radius $r = 1\,\mathrm{mm}$ enclosing the interface crack tip.

C.3 Displacement and stress development with non-coincident fibre orientation
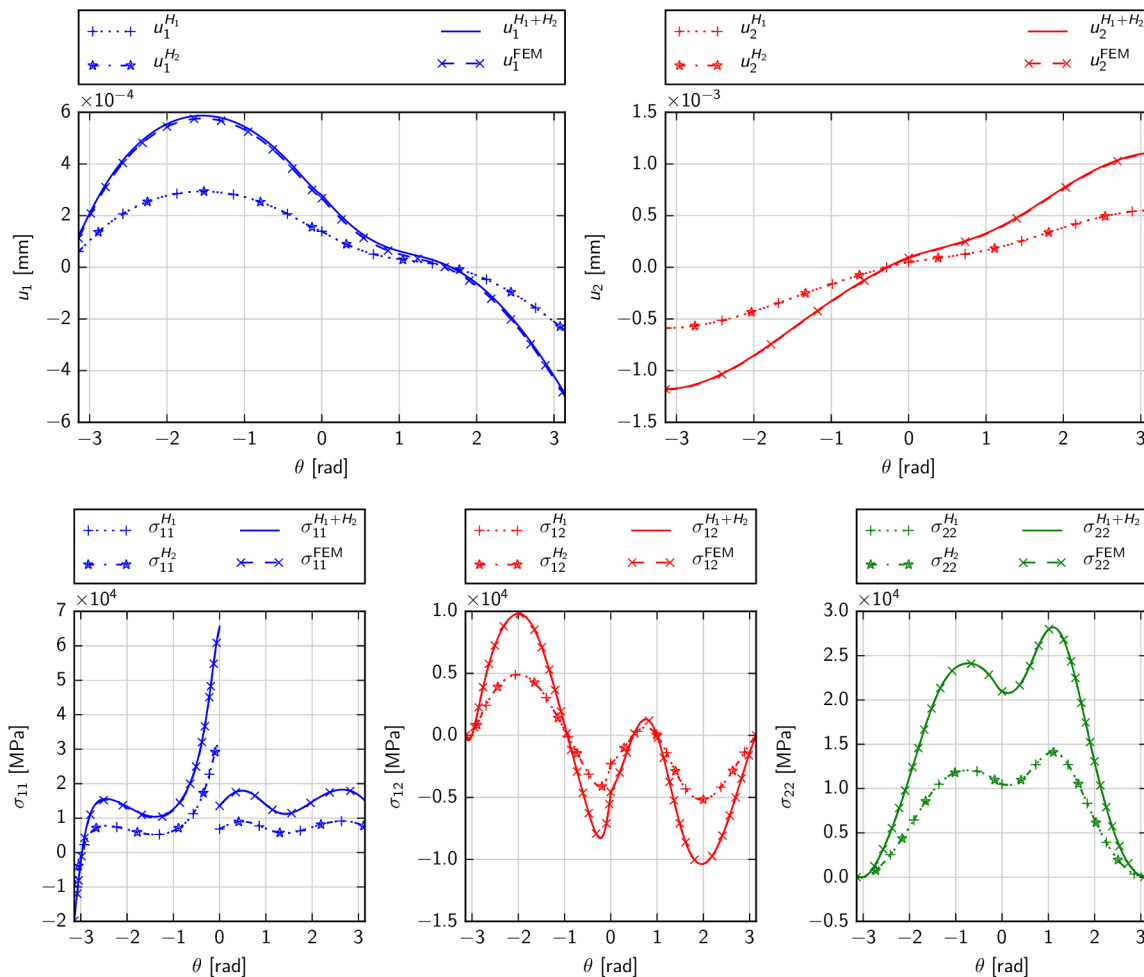
Fig. C.4: The displacement and stress components on the circular path $r = 0.001\,\text{mm}$ of an interface crack $\omega_1 = 180°$, $\omega_2 = -180°$ and material 1 fibre orientation $\alpha_1 = 50°$. Materials are defined in Tab. 5.1, singularity exponents are $\delta_1 = 0.5092 + 0.02512i$, $\delta_2 = 0.5092 - 0.02512i$.

D Additional results for a piezoelectric bi-material notch
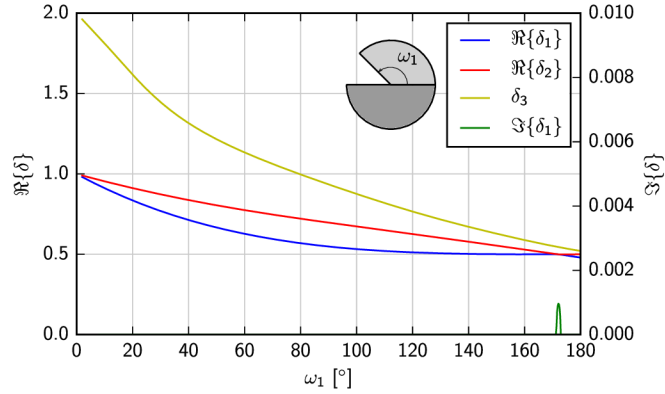
Fig. D.1: The exponent δ_i dependence on the PZT-7A/BaTiO$_3$ bi-material notch geometry ω_1. Poling directions are $\alpha_1 = 90°$, $\alpha_2 = 90°$.

(a) PZT-5H/BaTiO$_3$
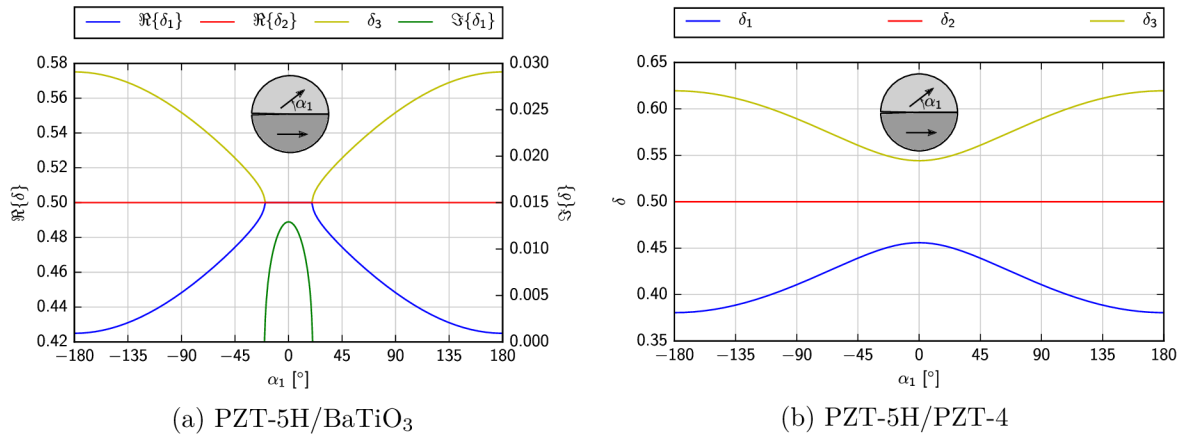
(b) PZT-5H/PZT-4

Fig. D.2: The dependence of the interface crack exponents δ_i on the poling direction α_1. The poling direction $\alpha_2 = 0°$.
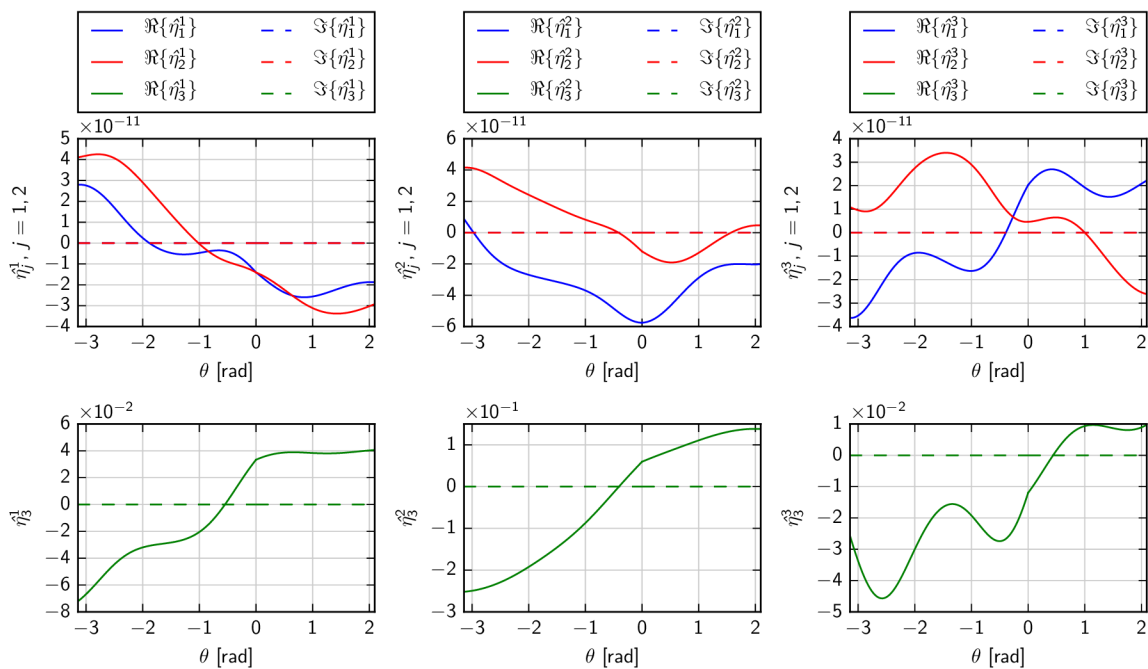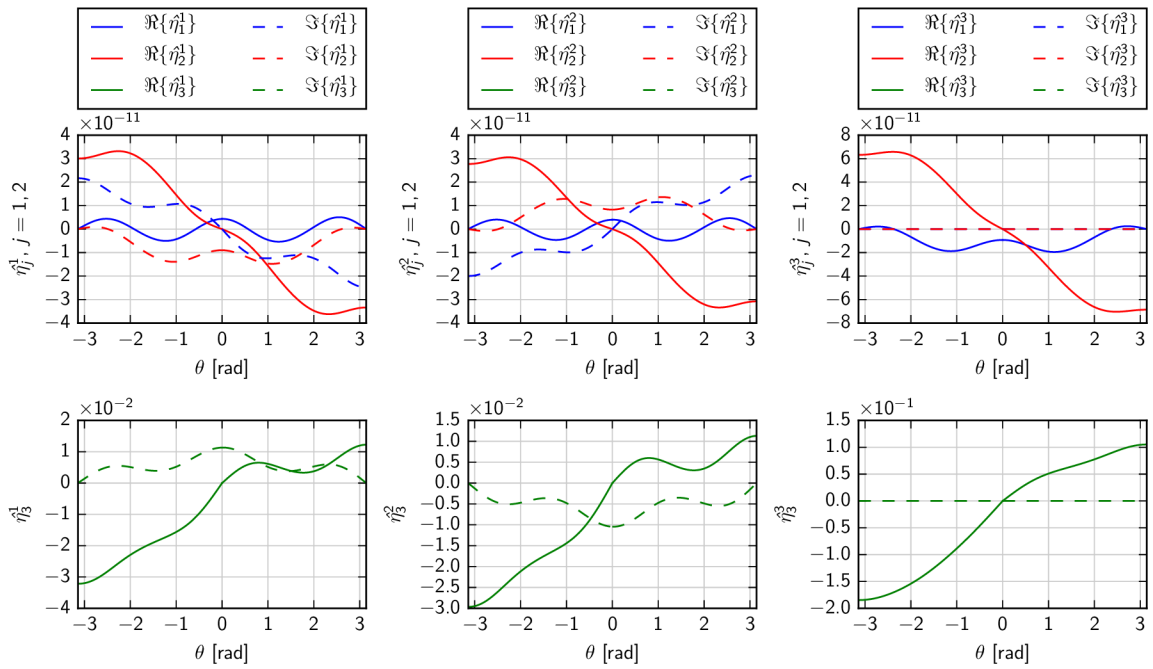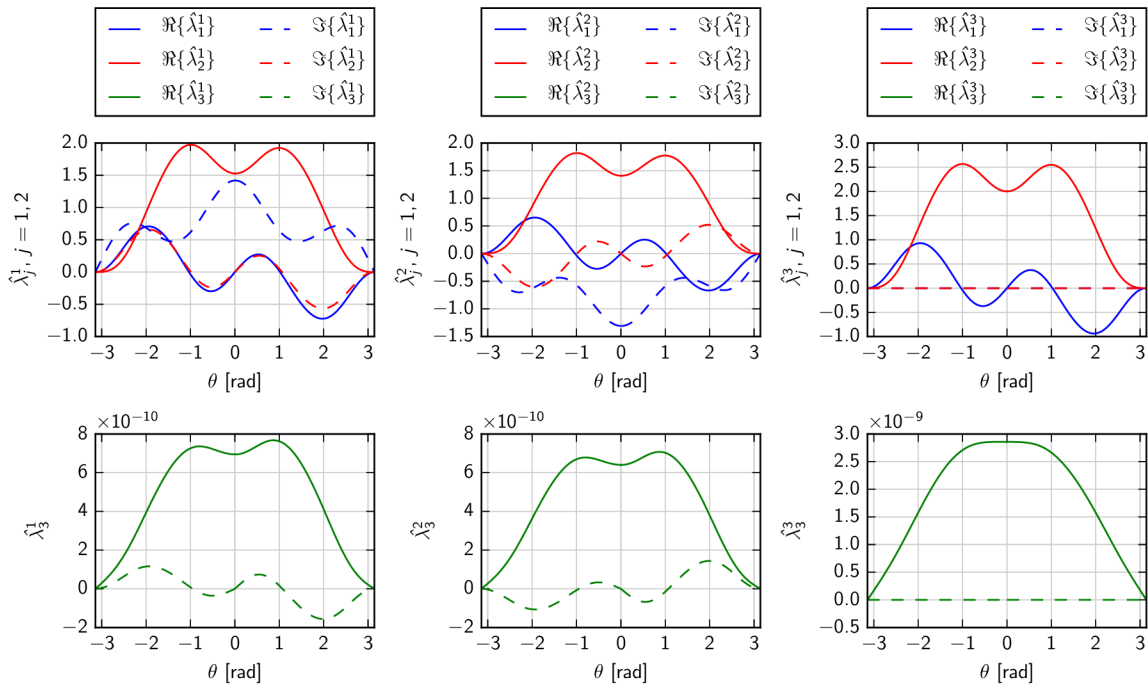
D.1 Auxiliary shape functions

(a)

(b)
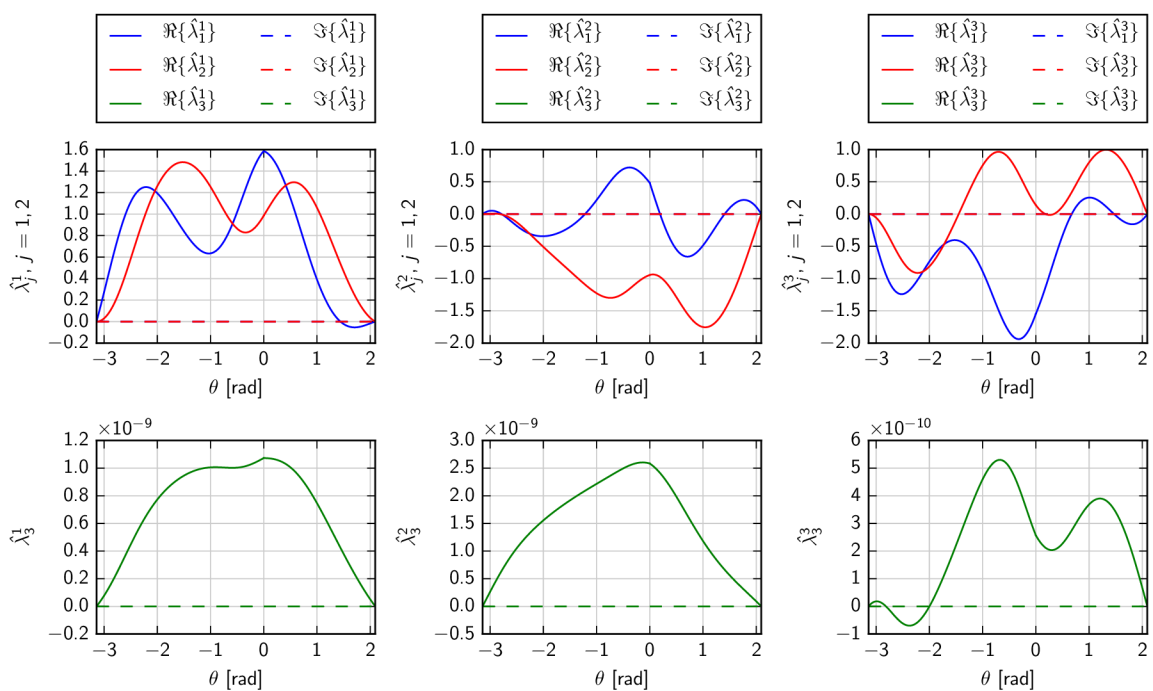
Fig. D.3: Components of the auxiliary shape function vectors (a) $\hat{\boldsymbol{\eta}}_1$, $\hat{\boldsymbol{\eta}}_2$, $\hat{\boldsymbol{\eta}}_3$ and (b) $\hat{\boldsymbol{\lambda}}_1$, $\hat{\boldsymbol{\lambda}}_2$, $\hat{\boldsymbol{\lambda}}_3$ for a PZT-5H/PZT-4 bi-material notch defined by $\omega_1 = 120°$.

Fig. D.4: Components of the auxiliary shape function vectors (a) $\hat{\boldsymbol{\eta}}_1$, $\hat{\boldsymbol{\eta}}_2$, $\hat{\boldsymbol{\eta}}_3$ and (b) $\hat{\boldsymbol{\lambda}}_1$, $\hat{\boldsymbol{\lambda}}_2$, $\hat{\boldsymbol{\lambda}}_3$ for an interface crack of PZT-5H/BaTiO$_3$ bi-material.

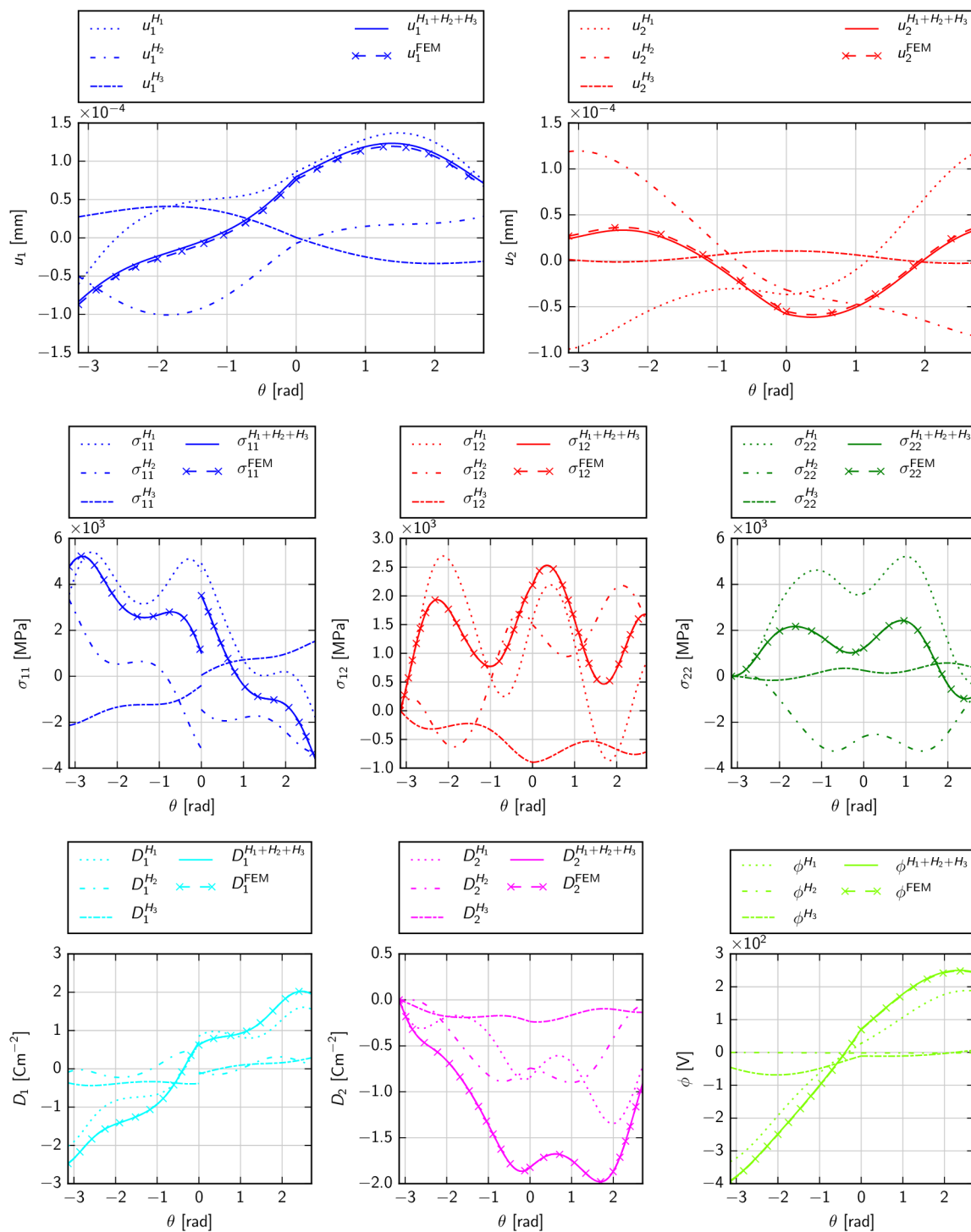## D.2 Mechanical and electrical fields of a bi-material with nonco-incident poling orientation

Fig. D.5: The displacements, stress components, electric displacement components and electric potential of a PZT-5H/PZT-4 bi-material notch on the circular path $r = 0.001\,\mathrm{mm}$, $\omega_1 = 155°$, $\omega_2 = -180°$. Poling directions are $\alpha_1 = 40°$ and $\alpha_2 = 90°$, the singularity exponents are $\delta_1 = 0.4647$, $\delta_2 = 0.5271$, $\delta_3 = 0.6174$.
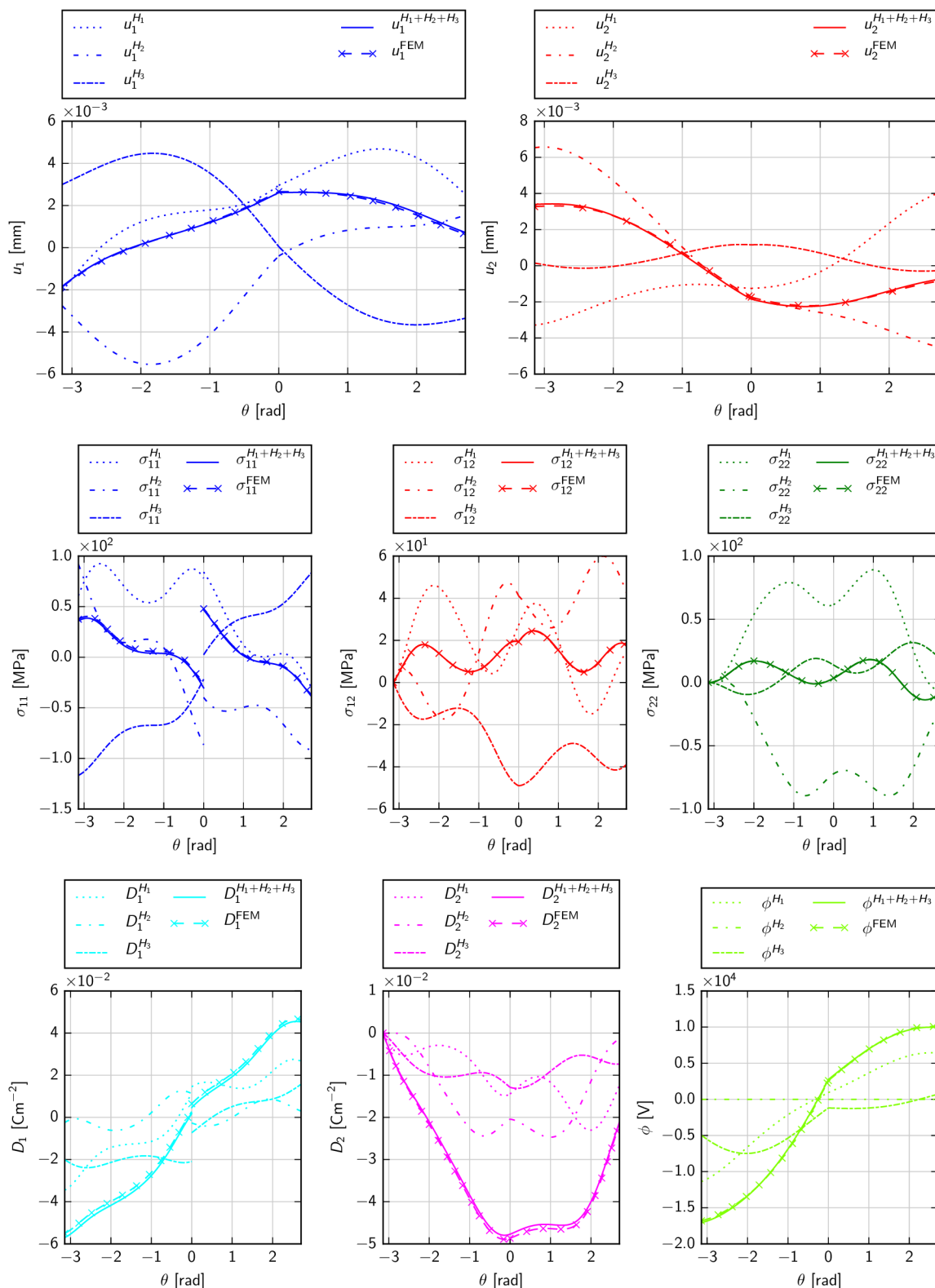
Fig. D.6: The displacements, stress components, electric displacement components and electric potential of a PZT-5H/PZT-4 bi-material notch on the circular path $r = 2\,\mathrm{mm}$, $\omega_1 = 155°$, $\omega_2 = -180°$. Poling directions are $\alpha_1 = 40°$ and $\alpha_2 = 90°$, the singularity exponents are $\delta_1 = 0.4647$, $\delta_2 = 0.5271$, $\delta_3 = 0.6174$.

E Attached scripts

The attached CD contains scripts for evaluating the fracture-mechanical parameters for determination of the stress intensity in the vicinity of an anisotropic and piezoelectric bi-material notch. The first group are the APDL macros executable by ANSYS software (within the dissertation ANSYS v18.1 was used). Input data are the material parameters, notch geometry and the line division parameter Δ_c. The output files contain nodal data of electro-elastic fields. Below, the macros for evaluation of the displacement, electric potential, stress and electric displacement finite element fields are listed.

`Notch_AA_v3.mac`	Anisotropic bi-material notch with the free-free notch faces.
`Notch_AI_v3.mac`	Isotropic/anisotropic bi-material notch with the free-free notch faces.
`Notch_AA_v3_CF.mac`	Anisotropic bi-material notch with the free-clamped notch faces.
`Notch_PP_v3.mac`	Piezoelectric bi-material notch with the free-free notch faces.
`Notch_PI_v3.mac`	Isotropic/piezoelectric bi-material notch with the free-free notch faces.
`Notch_PP_v3_CF.mac`	Piezoelectric bi-material notch with the free-clamped notch faces.
`sqmesh.mac`	Macro controlling the mesh structure.

The second group is represented by Python scripts (Anaconda Python 2.7) for evaluating the electro-elastic fields. The input parameters are the material data including the orientation of the principal material directions (or poling), the notch geometry and the initial guess for the `mpmath.findroot` algorithm. The result files from the FEM analysis described above are also imported. Below, scripts for evaluation of the singularity exponents, generalized stress intensity factors and displacements, electric potentials, stresses and electric displacements computed along the circular paths around the notch tip are listed.

`LES_AA_v3.mac`	Anisotropic bi-material notch with the free-free notch faces.
`LES_AI_v3.mac`	Isotropic/anisotropic bi-material notch with the free-free notch faces.
`LES_AA_v3_CF.mac`	Anisotropic bi-material notch with the free-clamped notch faces.
`LES_PP_v3.mac`	Piezoelectric bi-material notch with the free-free notch faces.
`LES_PI_v3.mac`	Isotropic/piezoelectric bi-material notch with the free-free notch faces.
`LES_PA_v3.mac`	Anisotropic/piezoelectric bi-material notch with the free-free notch faces.
`LES_PP_v3_CF.mac`	Piezoelectric bi-material notch with the free-clamped notch faces.
`mod_HSV_v4.mac`	Module for depicting the phase portrait of the characteristic function.

F Author's outputs and activities

Papers in scientific journals with IF

- PROFANT, T.; KLUSÁK, J.; ŠEVEČEK, O.; HRSTKA, M.; KOTOUL, M. An energetic criterion for a micro-crack of finite length initiated in orthotropic bi-material notches. *Engineering Fracture Mechanics*, 2013, vol. 110, no. 2013, p. 396–409. ISSN: 0013-7944. [IF = 1.662]

- KLUSÁK, J.; HRSTKA, M.; PROFANT, T.; KREPL, O.; ŠEVEČEK, O.; KOTOUL, M. The influence of the first non-singular stress terms on crack initiation direction in an orthotropic bi-material plate. *Theoretical and Applied Fracture Mechanics*, 2014, vol. 71, no. 2014, p. 67–75. ISSN: 0167-8442. [IF = 1.262]

- HRSTKA, M.; PROFANT, T.; KOTOUL, M. Electro-mechanical singularities of piezoelectric bi-material notches and cracks. In *Engineering Fracture Mechanics*. Manuscript under review. [IF = 2.580]

Conference proceedings and papers in SCOPUS

- HRSTKA, M.; PROFANT, T.; KLUSÁK, J.; ŠEVEČEK, O.; KOTOUL, M. A Stability Criterion of an Orthotropic Bi-Material Notch Based on the Strain Energy Density. In *Engineering Mechanics 2014*. 1. Svratka: BUT, 2014. p. 232–235. ISBN: 978-80-214-4871-1.

- PROFANT, T.; KLUSÁK, J.; ŠEVEČEK, O.; KOTOUL, M.; HRSTKA, M.; MARCIÁN, P. An effect of the first non-singular term of the Williams asymptotic expansion to the stability of the bi-material orthotropic notch. *In Materials Structure & Micromechanics of Fracture VII. Key Engineering Materials (print)*. Switzerland: Trans Tech Publications, 2014. p. 745–748. ISSN: 1013-9826.

Other papers in scientific journals with IF

- PROFANT, T.; HRSTKA, M.; KLUSÁK, J. An asymptotic analysis of crack initiation from an interfacial zone surrounding the circular inclusion. *COMPOSITE STRUCTURES*, 2019, vol. 208, no. 1, p. 479–497. ISSN: 0263-8223. [IF = 4.101]

- VOJTEK, T.; HRSTKA, M. Why standard methods fail to predict monotonic and cyclic plastic zones of shear-mode fatigue cracks? *Theoretical and Applied Fracture Mechanics*. Manuscript under review. [IF = 2.215]

Other conference proceedings and papers in SCOPUS

- MARCIÁN, P.; VALÁŠEK, J.; HRSTKA, M.; MAJER, Z.; ŠEVEČEK, O.; PROFANT, T.; DLOUHÝ, I.; FLORIAN, Z. Computational Modeling of Porous Ceramics with Bioactive Layer. In *MATERIALS STRUCTURE & MICROMECHANICS OF FRACTURE VII. Key Engineering Materials (print)*. Switzerland: Trans Tech Publications, 2014. p. 378–381. ISBN: 978-3-03785-934-6. ISSN: 1013-9826.

- SVATOŠ, V.; NEUŽIL, P.; HRSTKA, M.; HUBÁLEK, J. Effective simulation approach for study of carbon nanotube mechanical properties. In *Proceedings of abstracts*. Ostrava: Tanger, 2015. p. 1–6. ISBN: 978-80-87294-59-8.

- PROFANT, T.; HRSTKA, M.; KLUSÁK, J.; KERŠNER, Z. On the Energy Release Rate of the Crack Emanating from the Inclusion Interphase. In *ENGINEERING MECHANICS 2017. Engineering mechanics 2017.* Dolejškova 5, Prague 8, 182 00, Czech Republic: ACAD SCI CZECH REPUBLIC, INST THERMOMECHANICS, 2017. p. 806–809. ISBN: 978-80-214-5497-2. ISSN: 1805-8248.

- HRSTKA, M.; ŽÁK, S.; VOJTEK, T. Large plastic zones and extensive influence of notch under near-threshold mode II and mode III loading of fatigue cracks. *Procedia Structural Integrity*, 2018, vol. 13, no. special, p. 1123–1128. ISSN: 2452-3216. (ECF22, Belgrade, Serbia, 2018)

- HRSTKA, M.; ŽÁK, S.; VOJTEK, T. On the Non-Validity of Routinely Used Formulae for Stress Intensity Factors and Plastic Zone Sizes of Mode II and Mode III Fatigue Cracks. (ICSMA18, Columbus, OH, USA, 2018)

- PROFANT, T.; HRSTKA, M.; KLUSÁK, J. Microcrack interaction with circular inclusion and interfacial zone. *Frattura ed Integrita Strutturale*, 2019, vol. 1, no. 48, p. 503–512. ISSN: 1971-8993. (CP2018, Verona, Italy, 2018)

Research internships

- TU Darmstadt, Fachbereich der Strukturmechanik (FSM), Germany, September 1st 2014 – February 27th 2015. Supervisor: Prof. Wilfried Becker.

- TU Darmstadt, Fachbereich der Strukturmechanik (FSM), Germany, October 19th – 25th 2015. Supervisor: Prof. Wilfried Becker.

Teaching experience

- Kinematics (3 semesters)

- Theses supervisor: diploma (1), bachelor (2)